CROSS-SCALE MODEL VALIDATION WITH ALEATORY AND EPISTEMIC UNCERTAINTY

A Thesis
Presented to
The Academic Faculty

by

Joel Blumer

In Partial Fulfillment
of the Requirements for the Degree
Master of Science in the
School of Mechanical Engineering

Georgia Institute of Technology
April 2015

CROSS-SCALE MODEL VALIDATION WITH ALEATORY AND EPISTEMIC UNCERTAINTY

Approved by:

Dr. Yan Wang, Co-Advisor
School of Mechanical Engineering
Georgia Institute of Technology

Dr. David McDowell, Co-Advisor
School of Mechanical Engineering
Georgia Institute of Technology

Dr. Laura Swiler
Sandia National Laboratories

Date Approved: 2 April, 2015

This thesis is dedicated to Emily and Adam. Thank you for the joy you bring to my life. This would have been impossible without your support and encouragement.

.

ACKNOWLEDGEMENTS

I would like to thank my committee members for their time and effort spent on the development of this thesis and research. Dr. Yan Wang in particular spent many hours proofing and editing, not to mention his guidance in developing the techniques used and in finding the necessary resources to guide my research. Dr. Swiler and Dr. McDowell provided much-needed perspective on the research both in its preliminary and final stages. Each of these committee members provided essential encouragement and positive feedback at critical moments during the research process.

My fellow student Aaron Tallman contributed much to this work. We shared many discussions on the interpretation and applications of GIBR, and his work in providing the materials simulations data and in finding the experimental data that were used to generate and update the probabilities found in this thesis was indispensable.

The research detailed in this thesis was largely funded by a Nuclear Energy University Programs project through the U.S. Department of Energy's Office of Nuclear Energy, for which support I am very grateful.

TABLE OF CONTENTS

LIST OF TABLES

Page

LIST OF FIGURES

Page

LIST OF SYMBOLS AND ABBREVIATIONS

θ		a set of parameters used to run a simulation
ρ	$\Omega \bullet cm \times 10^{-26}$	electrical resistivity
n	e^{-}/cm^{2}	number of defects (Frenkel Pairs)
σ	barns	total displacement cross-section
T	eV	transferred energy (recoil energy; simulation input)
T_d	eV	damage threshold (energy required to induce damage)
T_m	eV	maximum transmitted energy (energy of incident particle)
l		length
P(event)		Probability of an event
P(event)		Probability of an event expressed as an interval

SUMMARY

Nearly every decision must be made with a degree of uncertainty regarding the outcome. Decision making based on modeling and simulation predictions needs to incorporate and aggregate uncertain evidence. To validate multiscale simulation models, it may be necessary to consider evidence collected at a length scale that is different from the one at which a model predicts. In addition, traditional methods of uncertainty analysis do not distinguish between two types of uncertainty: uncertainty due to inherently random inputs, and uncertainty due to lack of information about the inputs. This thesis examines and applies a Bayesian approach for model parameter validation that uses generalized interval probability to separate these two types of uncertainty. A generalized interval Bayes' rule (GIBR) is used to combine the evidence and update belief in the validity of parameters. The sensitivity of completeness and soundness for interval range estimation in GIBR is investigated. Several approaches to represent complete ignorance of probabilities' values are tested. The result from the GIBR method is verified using Monte Carlo simulations. The method is first applied to validate the parameter set for a molecular dynamics simulation of defect formation due to radiation. Evidence is supplied by the comparison with physical experiments. Because the simulation includes variables whose effects are not directly observable, an expanded form of GIBR is implemented to incorporate the uncertainty associated with measurement in belief update. In a second example, the proposed method is applied to combining the evidence from two models of crystal plasticity at different length scales.

CHAPTER 1: INTRODUCTION

1.1: Aleatory and Epistemic Uncertainty

Uncertainty is an inevitable component of almost every decision. When uncertainty can be measured and documented, decisions can be made with a better understanding of the risks and benefits. With a better record of what was understood beforehand, the second-guessing effects of "20/20 hindsight" can also be reduced. Many methods exist for uncertainty quantification. A recent development uses generalized interval probabilities to simultaneously represent both aleatory and epistemic uncertainty. This thesis focuses on using an expanded form of Generalized Interval Bayes' Rule to combine and update generalized interval probabilities.

Aleatory and epistemic uncertainty represent two very different causes of uncertainty. Uncertainty is described as aleatory when it is due to random variations—that is, no amount of careful measurement, of further study, or of increased data collection could decrease the amount of uncertainty. Radioactive decay of an atom is one example of a process with obvious aleatory uncertainty. No matter how much information is gathered on an atom, the only prediction that can be made of its decay will be probabilistic and uncertain.

On the other hand, uncertainty is described as epistemic when it is due to a lack of knowledge. When different methods of measurement lead to different values and it is not known which one is more accurate, that is epistemic uncertainty.

To a certain extent, the delineation of aleatory versus epistemic uncertainty can be dependent on the scope of the research at hand. For instance, if a study is looking at the entire population of humpback whales, then the current weight of whales in the study will be represented by a range of weights. This uncertainty is aleatory, because variations due to individual eating habits, genetics, and other conditions lead to differences in the actual

weight from whale to whale. On the other hand, if another study has a scope limited to a single, specific whale, then that whale has one true value for its weight at any given time. The whale's weight may still be represented by a range, but this is because of inherent difficulties in putting a humpback whale on a scale. In this case, the uncertainty of the whale's weight is epistemic, because gathering more information about the whale could reduce the uncertainty.

Modeling and simulation is a field in which sources of epistemic uncertainty abound. The very essence of modeling is approximation for the sake of efficiency, but every approximation made corresponds to a loss of information and an increase in epistemic uncertainty. Nonlinear relationships that are linearized, structures that are simplified, and physical laws that are idealized are some broad categories of epistemic uncertainty sources present in models. Without these approximations, models may become impractical to use, but the uncertainty should be identified and quantified for the models to be used responsibly.

Problems can arise when aleatory and epistemic uncertainty are left unseparated. For instance, if the variation within a system is aleatory but is mistakenly categorized as epistemic, time and money may be wasted trying to reduce irreducible error. On the other hand, if a process is designed to accommodate a huge range of inputs where a much smaller range would have sufficed if only further study had been done, it is again a waste of resources. Understanding the sources of uncertainty allows for more informed decision making, and for better allocation of time, money, and other resources.

1.2: Problem Statement

Epistemic uncertainty may arise when there are multiple versions of models available that describe the same phenomenon, several calculation paths that lead to the estimation of the same quantity, or different beliefs about the same subject from experts. Without further evidence, there is no way to judge which model/path/belief is more

correct. Of course, it is rare to have values and relationships that are absolutely certain within any model or calculation path, and so each model or path will lead not to a definitive value, but rather to a probability. This represents the aleatory uncertainty of the calculation.

Traditionally, sensitivity analysis is performed to assess the impact of epistemic uncertainty for modeling and simulation. By changing the input parameters of a model, the variation of the output is obtained. Various methods such as statistical global sensitivity analysis, local sensitivity analysis, Monte Carlo sampling, etc. have been developed. However, extensive computations are required in these methods. This prohibits the wide applications in large-scale simulations where each run of simulation is already costly, and repetitive runs of simulation with different combinations of input parameters should be avoided.

In order to find efficient alternatives to sensitivity analysis to quantify epistemic uncertainty, in this thesis, generalized interval probabilities are used to represent the two components of uncertainty. Experimental results are used to update the simulation results in a generalized interval formulation of Bayes' Rule. Where the experimental results and the simulation results are on different scales of measurement, Generalized Interval Bayes' Rule is expanded to incorporate intermediate links between the prior probability and the updating information. This result is then verified with Monte Carlo simulations. This gives a better understanding of the completeness and soundness of the Generalized Interval Bayes' Rule.

Uncertainty quantification is significant in any scientific field, where complete certainty is the exception rather than the rule. This thesis examines uncertainty quantification in the face of extremely high levels of uncertainty in the context of materials science problems, including material degradation under radiation and material property prediction based on crystalline orientation. The principles demonstrated can be applied in any field that must make calculations in spite of uncertain input.

Manufacturing applications are an ideal venue for interval analysis, as tolerances provide a natural interval. The expanded form of Generalized Interval Bayes' Rule follows the same form as a Generalized Hidden Markov Model, further increasing the potential applicability of this method by allowing the interval approach to be used in fields where measurable results are not directly available for the forces that create them.

Determining the intervals to use in generalized interval probability theory requires both careful calculation of the probability ranges and careful consideration of interval modality (proper vs. improper intervals). The assignment of interval modality requires the application of domain-specific knowledge, and is based on the rules of logical interpretation: intervals whose epistemic uncertainty is critical to the analysis will typically be considered *focal* and given a proper modality, whereas less critical intervals may be considered non-focal and given an improper modality. It will be demonstrated that the choice of modality can greatly affect the result of a GIBR update. Despite the caution needed in those steps, the computational expense is considerably very low compared with many other methods. GIBR has not previously been verified by comparison with other methods; this thesis aims to verify examples of GIBR using Monte Carlo simulations, thus allowing future researchers to better know how to employ this new, efficient approach.

1.3: Research Approach

Problems have been selected from the intersection of materials science and mechanical engineering. The examples used in Chapter 4 and Chapter 5 are from the field of computational materials design; in these examples, predictions based on computational material models are updated based on their comparison with physical experiments. GIBR was applied in the simplest form when possible. When the model results and the experimental results were in different domains of scale or were otherwise initially incompatible, an expanded form of GIBR was employed to allow them to link.

Mathematically, Bayes' Rule predicts a conditional probability ($P(A|B)$) based on the independent probabilities of the input events ($P(A)$ and $P(B)$) and on the reversed conditional probability ($P(B|A)$). Practically, Bayes' Rule is a method of combining evidence to update one's belief from a prior probability or likelihood based on the addition of new information or evidence. The intent of Generalized Interval Bayes' Rule is to predict a range for the conditional probability when the precise value of the input probabilities is unknown. It does not assume any distribution or specific value of the quantities represented by each interval; it simply states that the true value should be somewhere within the bounds of the interval.

1.4: Generalized Intervals

Interval analysis (Sainz, et al., 2014) stems from what are now referred to as "classical intervals." A classical interval represents a set of real numbers with a pair of lower and upper bounds. They may be used whenever it is impractical or impossible to do so with a single real number, including:

- When truncation errors prevent the representation of the precise number,
- When an exact value is unknown, but bounding values can be determined, and
- When an exact value may vary during the context of the problem.

Classical interval analysis focuses on providing what may be termed a "worst-case" analysis of a problem: if two inputs, each with an upper and lower bound, are combined by some operation, classical interval analysis represents the full range of possible results—in other words, classical intervals provide a complete solution. A further description of the arithmetic used in this analysis is given in §2.2.1. Intervals can be used to simultaneously represent and separate aleatory and epistemic uncertainty in a compact, readable form. When an interval is populated with probabilities, it is termed an "imprecise probability." An arbitrary example is the interval $[0.50,0.75]$. The epistemic

uncertainty is represented by the width of the interval, or $0.75 - 0.50 = 0.25$. The aleatory uncertainty is represented by the values of the interval endpoints, as both 0.50 and 0.75. Using this interval, there is anywhere from a 50% chance to a 75% chance of the event described by this interval occurring. Further study may lead to a reduction in epistemic uncertainty: just a few more measurements may give the interval $[0.68,0.75]$, and a nearly infinite number of further measurements may lead to the point interval $[0.72,0.72]$ and the elimination of all epistemic uncertainty.

Generalized intervals are not designed to provide the same *complete* solution that classical intervals give. Rather, generalized intervals are intended to give a *sound* solution to an interval problem—while the calculated interval may not cover all possible combinations of real values from the input intervals, all the real values within the bounds of the calculated interval should be obtainable by some combination of real values from within the input intervals.

Generalized intervals differ from traditional intervals primarily in that they allow the upper bound to precede the lower bound within the interval. This, in turn, allows for simpler mathematical operations that are reversible. For instance, traditional intervals allow the interval $[2,3]$ but not the interval $[3,2]$. Both are acceptable as generalized intervals. According to traditional interval analysis, $[2,3] + [3,4] = [5,7]$, but $[5,7] - [3,4] \neq [2,3]$. Instead, $[5,7] - [3,4] = [1,4]$. Generalized intervals introduce the *dual* operator in order to make mathematical operations reversible. The *dual* operator simply switches the location of the upper and lower bounds of an interval—thus $dual[\underline{x}, \overline{x}] = [\overline{x}, \underline{x}]$, and $dual[\overline{x}, \underline{x}] = [\underline{x}, \overline{x}]$. Using generalized intervals, $[2,3] + [3,4] = [5,7]$ is still true, as is $[5,7] - dual[3,4] = [2,3]$. A more complete description of mathematical operators for generalized intervals is given in §3.2.2.

Other methods of quantifying epistemic uncertainty have been developed. Perhaps the most common method is to view epistemic uncertainty probabilistically and to work

with it indistinguishably from aleatory uncertainty. Dempster-Shafer theory was developed to separate the two types of uncertainty, and also uses an interval—in this case, one bound of the interval is given by the evidence for an event (the *belief* in the event), while the other bound is given by one minus the evidence against an event (the *plausibility* of the even); and the width of the interval is the ambiguity that remains given the current evidence. More methods are discussed in §2.1.

1.5: New Contributions

This thesis is the first to make extensive use of Monte Carlo simulations in an attempt to verify the completeness and soundness of Generalized Interval Bayes' Rule. Because interval analysis is a natural choice when uncertainty is large, there are often instances of great uncertainty, including complete ignorance, present in GIBR equations. This thesis demonstrates how the Logic Coherence Constraint should be used when enough information is present, but demonstrates that if the LCC is enforced in a total ignorance situation, the result is far from a complete answer. For instance, the decision to represent an even of unknown probability as [0,1] or as [1,0] can significantly affect the posterior probability, but in many instances it is a subjective choice. Moreover, when more than two mutually disjoint events are subject to complete ignorance, choosing [0,1] for one event and [1,0] for the second event forces all remaining events to have a probability of [0,0] when the LCC is employed. This misleadingly implies perfect knowledge that the event is impossible. In response to these challenges, this thesis introduces a convention for dealing with complete uncertainty by selectively ignoring the LCC. This allows researchers to avoid making subjective decisions that may greatly affect the outcome of the analysis.

This thesis represents the first application of the Generalized Interval Bayes' Rule to cross-scale validation. The approach is demonstrated in Chapter 4 with interval-valued equations, but the intervals may be narrowed until they reach real values, and thus the

cross-scale validation approach demonstrated may be applied to the real-valued Bayes' Rule as well.

This thesis also employs a new approach to model aggregation: using Generalized Interval Bayes' Rule to update the belief obtained from one model with the evidence from another model. This, too, is equally applicable to a real-valued Bayesian update when the intervals are degenerated into real-valued probabilities. A model validation and comparison scheme based on Kullback-Leibler divergence is developed with interval probability.

In the course of working with large equations that use intervals, it became necessary to find a more compact method of writing the equations. This thesis employs a matrix-based method of representing large interval calculations (first shown in §3.5.2). The matrix method not only makes the equations more compact, but it also makes it easier to recognize when intervals representing mutually disjoint events do or do not conform to the Logic Coherence Constraint.

CHAPTER 2: LITERATURE REVIEW

2.1: Uncertainty Quantification Methods

Many methods have been devised to measure and predict uncertainty in analyses. Indeed, one perspective is that the term "uncertainty quantification" could actually encompass the whole field of statistics (O'Hagan, 2013). As such, one of the most familiar forms of uncertainty quantification is simply the expression of the probability of an event. However, many other methods have been devised to measure, express, and predict uncertainty.

2.1.1: Sensitivity Analysis

In a general sense, uncertainty quantification seeks to find the degree to which a system output is uncertain based on the uncertainty of all of its inputs. Sensitivity analysis may be seen as a more specific form of this study, as it seeks to determine the degree to which the uncertainty in a system output is dependent on the uncertainty in each specific input (Helton, Johnson, Sallaberry, & Storlie, 2006). Many sensitivity analysis methods are based on the derivative of one variable with respect to another; this is perhaps the most basic definition of sensitivity, but the technique only provides a useful measurement of the sensitivity at the point where the derivative is taken. Extrapolation around this point is possible, but only for linear systems, and thus this type of sensitivity analysis may be referred to as *local sensitivity analysis* (Saltelli, et al., 2008). Systems with large amounts of uncertainty, however, cannot be properly analyzed with local sensitivity analysis techniques, and so global techniques should be employed. Global sensitivity analysis (Weirs, et al., 2012) identifies or assumes distributions and ranges for each of the inputs, samples repeatedly from the inputs, and records and compares the corresponding outputs. It can be computationally expensive, and methods are sought to decrease the required sampling.

Adjoint sensitivity analysis (Errico, 1997) is, in some sense, the reverse of typical sensitivity analysis (Sandu, Daescu, & Carmichael, 2003). Traditional sensitivity analysis varies a single input parameter at a single point by use of a derivative, and must be done repeatedly in different locations and for different input parameters in order to have a good general idea of the model behavior, but it can be effective if the number of inputs is relatively few. By contrast, adjoint sensitivity analysis perturbs multiple inputs at once by use of a gradient, and can reveal the sensitivity of the output to various inputs relative to one another. It is particularly advantageous when a few outputs are influenced by a large number of inputs (Cao, Li, Petzold, & Serban, 2003).

2.1.2: Bayesian Model Averaging

Bayesian Model Averaging (Hoeting, Madigan, Raftery, & Volinsky, 1999) (Chick, 1999) eliminates or reduces model form uncertainty by combining multiple models. A classical approach commonly underestimates the uncertainty about which distribution is correct, does not quantify the probability that a chosen distribution actually is the best fit, and it does not provide any guidance as to which model to select when several may work. These challenges are eliminated by Bayesian Model Averaging. Rather than forcing the analyst to pick any specific "best fit" model, all of the models that can fit the data are identified, and then it combines the outcomes of the models using a form of Bayes' rule. Through this process, Bayesian Model Averaging provides both a better prediction of system behavior and a better idea of the existing uncertainty than any single model could. Prior and posterior probability distributions must be calculated for each model, making BMA not only computationally expensive, but also potentially very difficult from a reasoning and record-keeping standpoint. While reducing model form uncertainty does take out a major source of epistemic uncertainty, Bayesian Model Averaging does not separate aleatory and epistemic uncertainty in any explicit manner.

2.1.3: Robust Bayesian Analysis

Uncertainty quantification is applied to Bayes' Rule in yet another form in Robust Bayesian Analysis (Berger J. O., 1994) (Pericchi & Walley, 1991) (Walley, 1991). This interval-based method used in one of two ways: either with an interval expanded from a single point or with a broader interval when no more specific data about the prior probabilities is available. The first circumstance reveals how sensitive the Bayes' Rule output is to uncertain inputs—whether or not the Bayesian calculation is robust to variation. The second circumstance is termed "near-ignorance" for obvious reasons. Robust Bayesian Analysis builds on the foundation of providing actual and specific distributions for the prior probability inputs, and improves on that foundation by providing enough variety in the inputs to encompass the unknown true value of the prior distribution. This is necessary because the so-called "noninformative prior" distribution is actually a precise distribution, often a uniform distribution, that seeks to convey the lack of knowledge about the actual distribution. Unfortunately, the noninformative prior tends to be too informative, biasing the later results.

One common method for performing sensitivity analysis on prior is ε-contamination (Moreno & Pericchi, 1993) (Berger & Berliner, 1986), wherein the base prior π_0 is combined with some contamination q by an error ε. The distribution of priors is thus described as $\Gamma = (1 - \varepsilon)\pi_0 + \varepsilon \cdot q$. As q is a member of some class of priors, the choice of q allows the ε-contamination method to be used for both extremely wide and extremely narrow implementations of Robust Bayesian Analysis.

2.1.4: Design-of-Experiments (DOE)

Carefully designed experiments (Lawson & Erjavec, 2001) allow the effects and interactions of several input variables to be measured in an efficient, repeatable manner that avoids bias and should expose or minimize the effects of hidden variables. It seeks an efficient method of forming a response surface based on varying levels of the inputs.

Repeating experimental runs can give a good idea of aleatory uncertainty, but epistemic uncertainty is not typically part of the analysis. DOE can also be used as a form of sensitivity analysis, based on the way that the inputs are chosen.

2.1.5: Resampling

Sampling-based methods are often used for analysis and prediction. Where a sufficient quantity of data is not available for analysis, resampling (Barton & Schruben, Resampling methods, 2001) can be used to analyze the distribution generated and improve prediction. Three methods considered are:

- Direct resampling, which requires taking new data for each analysis,
- Bootstrapping (Babu & Rao, 1993), which samples with replacement from the original data sample, and
- Randomizing EDFs, which involves randomly changing the increments of the empirical distribution function (EDF) for resampling (Barton & Schruben, Uniform and bootstrap resampling, 1993).

These methods can provide good descriptive and predictive results with plentiful data, but they can fall short when high uncertainty is present, i.e. with missing or conflicting data.

An older method is jackknife resampling (Efron, 1982). This method provides an estimate of the bias of a statistic by repeatedly calculating the statistic with one observation removed from the total sample. These repeated statistics are compared to the same statistic for the total population, and the average of these comparisons converges toward the bias. A similar method may be employed to estimate the variance. The jackknife method can be applied to many situations, but is typically not the most efficient method for most situations.

2.1.6: Monte Carlo simulations

Monte Carlo simulation may be used to show the aleatory uncertainty of a system with a known distribution. However, if the distribution form is known, but the exact parameters are not, then second-order Monte Carlo simulation (Swiler, Paez, Mayes, & Eldred, 2009) can be used to find both the aleatory and the epistemic uncertainty of the system. The lack of knowledge about the nature of the distribution is reflected in the range of values sampled for the distribution parameters—the outer loop of the Monte Carlo simulation. For each outer loop of the Monte Carlo simulation, an inner loop simulation is run, giving an output distribution and showing the aleatory uncertainty of the system, just as in first-order Monte Carlo simulation. When all of the resulting distributions are plotted together, the separation between them shows the epistemic uncertainty of the system output.

2.1.7: Polynomial Chaos

Polynomial chaos (O'Hagan, 2013) (Ghanem & Spanos, 2003) (Xiu & Karniadakis, 2002) approximates a distribution by a multi-step process: a polynomial is created to approximate the cumulative distribution function's inverse transform. Then another polynomial (or set of polynomials) is used to generate numbers that can be fed into that mapping function. Polynomial chaos is thus a 'stochastic' version of a surrogate model, whose purpose is to predict behavior of an otherwise unmeasurable output.

2.1.8: Dempster-Shafer Theory

A long-standing method of measuring and expressing epistemic uncertainty is Dempster-Shafer theory (Dempster, 1967) (Shafer, 1976). Evidence for a proposition is bounded by a *belief* and a *plausibility*, where *belief* is defined as all of the evidence in support of the proposition, and *plausibility* is defined as one minus all of the evidence contrary to that proposition. Belief is always less than (or equal to) plausibility. Dempster-Shafer theory gives a clear way to organize all of the evidence related to a

subject under study. It is a basic building block upon which many other methods of dealing with uncertainty are founded.

2.1.9: Fuzzy Sets and Clouds

A set is a group defined by some sort of inclusion criteria. A random set (Molchanov, 2005), as the name implies, is a set whose inclusion criteria is based upon one or more random variables. A group of random sets may be used to examine some behavior because the family of all sets is typically too large for examination. In the classical sense a number must be either completely included or completely excluded from a set, but a fuzzy set (Möller & Beer, 2004) allows values to be included by degrees. The degree of inclusion is determined by an inclusion criterion in the form of a function whose output may be any value between zero and one, where one represents full inclusion and zero represents complete exclusion. A cloud (Neumaier, 2004), on the other hand, takes on the form of an envelope of probability distributions that encompass the unknown actual distribution. Its structure is more complex than a generalized interval probability, and it sits between a precise distribution and a fuzzy set in terms of information contained.

2.1.10: Interval Probability Methods

Interval probability may be regarded as an attempt to generalize classical probabilities (Weichselberger, 2000). As such, classical probabilities should be consistent with interval probabilities and should be expressible as a special case of interval probability. Weichselberger described three axioms of interval probability that correspond to Kolmogorov's three axioms of classical probability. Intervals that follow Weichselberger's first two axioms were termed R-probabilities, while intervals that also followed the third axiom were termed F-probabilities.

The probability box (or p-box) (Ferson, Kreinovich, Ginzburg, Myers, & Sentz, 2002) consists of a pair of non-decreasing functions that envelope the actual probability

distribution, much like a cloud. The enveloping functions can be smooth or discretized. A line parallel to the cumulative probability axis on a plotted p-box can be used to find an interval of probabilities associated with an event. Lines plotted perpendicular to the cumulative probability axis can be used to generate a Dempster-Shafer structure that represents the Dempster-Shafer theory interpretation of the p-box data. Interval probabilities are a special case of p-boxes.

A credal network (Cozman, 2000) (de Cooman, Hermans, Antonucci, & Zaffalon, 2010) is a visual model that combines a Bayesian network with imprecise probability. It uses a multiple input/multiple output directed tree to update beliefs according to a specific algorithm. While most credal networks are based on strong independence between each set within the network, credal networks based on epistemic irrelevance allow for much weaker connection between sets, and can better express greater amounts of uncertainty.

2.2: Generalized Interval Probabilities

Generalized intervals are an outgrowth of classical intervals. Imprecise probabilities are one specific application of generalized intervals.

2.2.1: Classical Intervals

In the classical sense, an interval (Moore, 1966) is the set of real numbers bounded by an upper and a lower bound. Classical interval arithmetic is simply defined as:

$$[a, b] * [c, d] = \{x * y | a \leq x \leq b, c \leq y \leq d\}$$

where the symbol * represents one of the four standard arithmetic symbols for addition, subtraction, multiplication, and division. One necessary caveat is that if $0 \in [c, d]$, then $[a, b]/[c, d]$ is undefined.

2.2.2: Generalized Intervals

Classical intervals (as discussed in §1.4) are fairly well-known, but generalized intervals are not as commonly used. The mathematics of generalized intervals were first defined in (Kaucher, 1980), where generalized intervals were described as occupying the "extended interval space $\mathbb{IR}$." Many notations exist for representing generalized intervals: (Wang, Generalized interval form, 2008) refers to the generalized interval space as $\mathbb{KR}$, with $\mathbb{IR}$ containing proper intervals and $\overline{\mathbb{IR}}$ containing improper intervals, while (Shary, Algebraic approach, 1996) refers to classical intervals as $\mathrm{I}\mathbb{R}$ and to generalized intervals as $\mathbb{IR}$. Other naming conventions are also used. Within this thesis, all intervals used are generalized intervals.

While a classical interval refers to a *set* of real numbers, a generalized interval is defined by two bounding numbers, with no assumptions about numbers occupying the space between them. In a proper generalized interval, the lesser of the two bounds precedes the greater, whereas for an improper interval this is reversed. $[1,2]$, $[-2,1]$, and $[-e,\pi]$ are all proper intervals, while $[2,1]$, $[-2,-3]$, and $\left[\frac{1}{2},\frac{1}{3}\right]$ are all improper intervals. In classical intervals, improper intervals are invalid and cannot be used. Because the terms *lower bound* and *upper bound* (frequently used to delineate the two bounds in classical intervals) imply a *less than* or *greater than* relationship, they cannot be used to delineate the first or second bounding number of a generalized interval. Instead, the under-bar and over-bar accent marks are used: a generalized interval $\boldsymbol{x}$ has the bounds $\left[\underline{x},\overline{x}\right]$, where $\underline{x} \leq \overline{x}$ for a proper interval and $\underline{x} \geq \overline{x}$ for an improper interval. For notation in this thesis, a bolded term refers to an interval.

The modality of an interval (proper versus improper) has an effect on the interpretation of the interval as well (Börner, Bulatov, Jeavons, & Krokhin, 2003) (Hu & Wang, Sensitivity analysis, 2013) (Batarseh, 2010). Proper intervals are associated with the *for all* (∀) quantifier, whereas improper intervals are associated with the *existential*

(∃) quantifier. For instance, the equation $[1,2] + [3,2] = [4,4]$ may be interpreted as, "for all values within the interval $[1,2]$, there exists a value within the interval $[3,2]$ such that the result is within the interval $[4,4]$ (or equal to 4)." A point interval, such as $[4,4]$, is considered both proper and improper. Within the context of Generalized Interval Bayes' Rule, intervals that are critical to the analysis are typically associated with the *for all* quantifier, and thus will be proper. They may also be termed *focal*. Other intervals that are deemed less important may be associated with the *existential* quantifier, and are thus improper or *non-focal*.

This ability to use intervals with reversed bounds leads to the necessity of several operators that deal specifically with forcing certain behaviors from the bounds of an interval. Using the interval $\boldsymbol{x} = [\underline{x}, \overline{x}]$ as an example, they include:

$$pro(\boldsymbol{x}) = \left[\min\left(\underline{x}, \overline{x}\right), \max\left(\underline{x}, \overline{x}\right)\right]$$

$$imp(\boldsymbol{x}) = \left[\max\left(\underline{x}, \overline{x}\right), \min\left(\underline{x}, \overline{x}\right)\right]$$

$$dual(\boldsymbol{x}) = [\overline{x}, \underline{x}]$$

For the sake of comparing intervals, the following relationships are also defined for the generalized intervals $\boldsymbol{x} = [\underline{x}, \overline{x}]$ and $\boldsymbol{y} = [\underline{y}, \overline{y}]$:

$$\boldsymbol{x} < \boldsymbol{y} \Leftrightarrow \left(\underline{x} < \underline{y}\right) \wedge \left(\overline{x} < \underline{y}\right) \wedge (\overline{x} < \overline{y})$$

$$\boldsymbol{x} \prec \boldsymbol{y} \Leftrightarrow \left(\underline{x} < \underline{y}\right) \wedge \left(\overline{x} > \underline{y}\right) \wedge (\overline{x} < \overline{y})$$

$$\boldsymbol{x} \subset \boldsymbol{y} \Leftrightarrow \left(\underline{x} > \underline{y}\right) \wedge (\overline{x} < \overline{y})$$

The $>$, $\succ$, and $\supset$ relationships easily follow from these. Other operators have been developed for use with generalized intervals, but as not all are used in the scope of this thesis, they are not detailed here. More comprehensive lists of operators and relationships can be found in (Dimitrova, Markov, & Popova, 1992) and (Gardeñes, et al., 2001). Generalized intervals use the Kaucher arithmetic as defined in (Kaucher, 1980). It is important to note that Kaucher used the symbol $\overline{\boldsymbol{x}}$ to indicate switching the bounds of a

generalized interval, while this thesis uses $dual(\boldsymbol{x})$ for the same purpose; in this thesis, the symbol $\overline{x}$ indicates the second bounding number of the interval $\boldsymbol{x}$.

The power of the Kaucher arithmetic is demonstrated by the completeness of equations already mentioned in Chapter 1—specifically, if generalized intervals $\boldsymbol{a} + \boldsymbol{b} = \boldsymbol{c}$, then $\boldsymbol{c} - dual(\boldsymbol{b}) = \boldsymbol{a}$.

(Gardeñes, et al., 2001) points out that real numbers, as a system, have a significant shortcoming: there is no way to properly represent their infinite precision with the finite capabilities of a computer. Classical intervals are a natural method for overcoming that, because while a specific number may not be able to be definitively stored in a system, values greater than and less than the number can be identified and stored. The shortcomings of the classical interval system come when the existence and the "for all" proposition are confused—the two have very different meanings. Another shortcoming comes when an interval is subjected to "inner rounding" (rounding up the lower value and rounding down the greater value), which may result in an improper interval. Gardeñes proposes that this be solved by the use of modal intervals, which allow improper intervals and which specify the existence versus "for all" qualifiers.

2.2.3: Intervals as Imprecise Probabilities

Interval analysis has some important characteristics where high uncertainties are involved. Consider the following case: an independent variable is known to be distributed between an upper and lower bound, but the actual distribution is unknown. Traditional analysis methods often assume a uniform distribution in this instance. If this is done, then as subsequent information is added to the model, the model approaches the true distribution asymptotically. The original guess of a uniform distribution continues to influence the model and pull it away from the true value. If the cumulative distribution function of the initial assumption, the subsequent updates, and the true value are plotted together as in Figure 1, the bias introduced by the initial assumption becomes apparent. It

causes low probabilities to be overestimated, and high probabilities to be underestimated. This is reasonable, but the effects can persist through many updates.

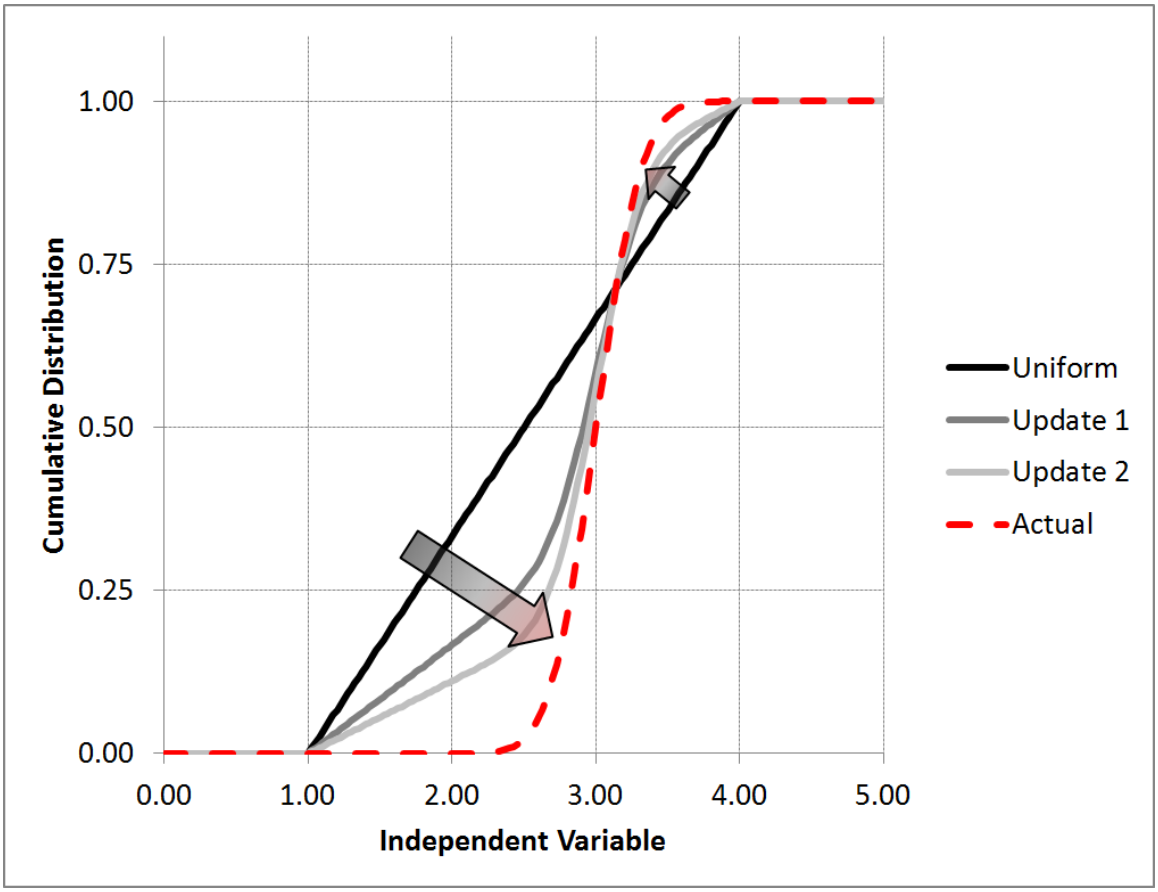

Figure 1: The initial assumption of a uniform distribution where no distribution is known heavily influences later updates.

If the lack of knowledge is represented with an interval, then as subsequent information is added to the model, the model can be incrementally narrowed around the actual distribution. The interval can approach the data asymptotically, but can do so from both sides, and the increasingly specific intervals should always contain the actual distribution. This is illustrated with the cumulative distribution functions shown in Figure 2. While the traditional approach of assuming a uniform distribution introduces a strong bias to further analysis, an interval approach avoids a bias by allowing any and all values within the interval to be included in the analysis.

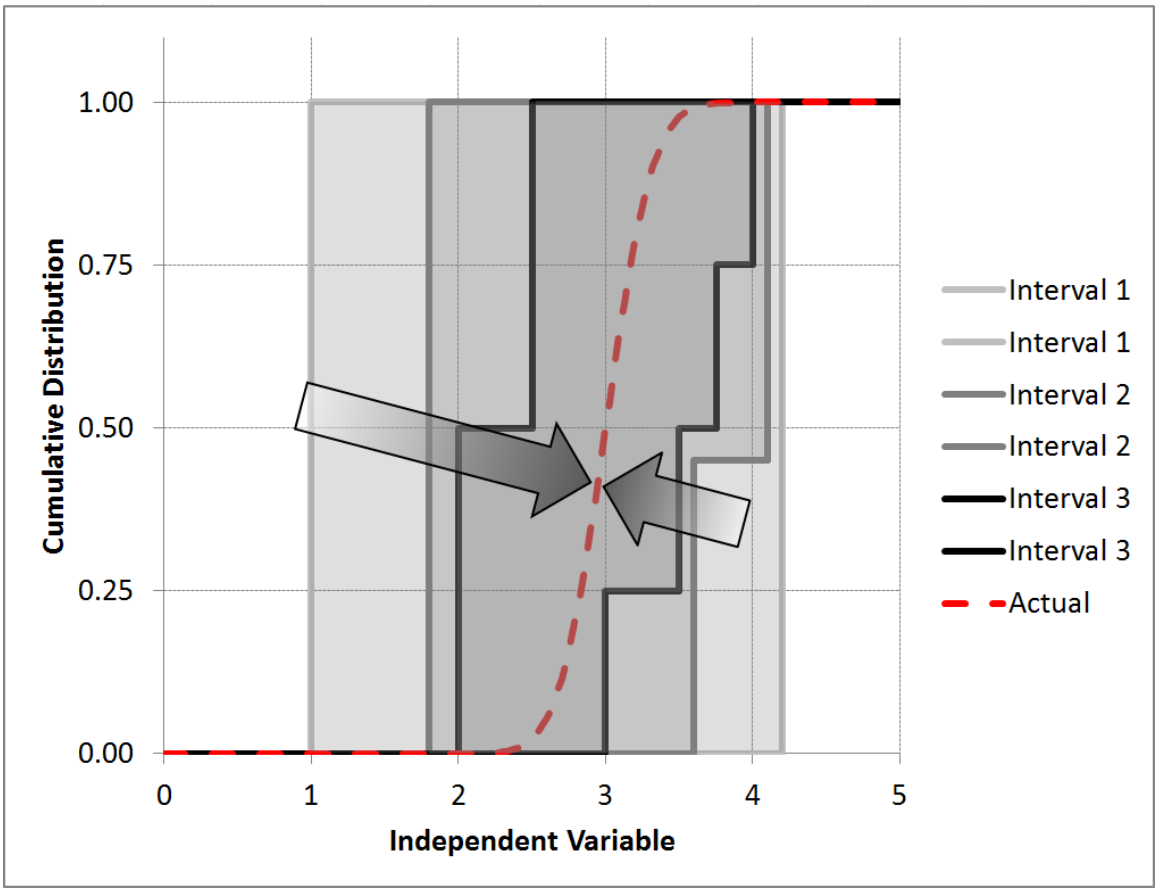

Figure 2: When no distribution is known, an interval can represent the lack of knowledge without introducing bias. Further information updates serve to draw the interval closer to the true value.

Many things can contribute to a lack of knowledge in modeling and simulation situations. Data may be missing to inform parameters or other model inputs. Data from different sources may conflict, forcing researchers to choose one data set over another and thus lose information. When hard numbers are not available, expert elicitation may likewise lead to conflicting values, but in this case the conflict is not in data but in the beliefs or opinions of different experts. Models are constructed based on available data, but experiments often examine only one or two variables, leaving dependency and interaction between parameters unknown. And as with all data, errors in measurement and errors due to round-off and truncation can be sources of epistemic uncertainty. These sources of epistemic uncertainty are discussed greater detail in (Walley, 1991).

CHAPTER 3: GENERAL METHODOLOGY

3.1: Generalized Interval Probability

General Interval Probability uses intervals to simultaneously represent two types of uncertainty in a compact form. Uncertainty due to random variations, herein referred to as aleatory uncertainty, is represented by the numeric value of the upper and lower bounds of the interval. Uncertainty due to missing information, or epistemic uncertainty, is represented by the width of the interval. For instance, the chance of rain in the forecast may be represented by the interval [0.40,0.50], meaning "a 40 to 50% chance of rain." Here, the epistemic uncertainty is 10%—the width of the interval. As more weather-related information becomes available, the epistemic uncertainty may be reduced, and the interval may become a point interval, such as [0.42,0.42]. However, no amount of added information will change the inherent randomness of the weather (aleatory uncertainty), and thus the prediction cannot be made more certain than 42% until the weather actually arrives.

To a certain extent, categorizing error as aleatory or epistemic may be dependent upon the scope of work. The height of a stand of trees may be between five and six meters, and if the scope of work must include the whole stand, then a variable representing tree height will be have a large component of aleatory uncertainty. However, if the scope of work involves only a single tree, then any uncertainty about its height is due to a lack of knowledge about that specific tree and may therefore be regarded as epistemic uncertainty. As can be observed in this example, a major source of epistemic uncertainty is measurement error. As such, one of the primary methods for reducing epistemic uncertainty is improving measurement techniques. Changing the scope of one's work, on the other hand, can result in the re-categorization of one type of uncertainty to

the other type. In every case, the researcher must determine if the relative cost is worth the reduction of uncertainty.

3.2: Arithmetic Conventions

3.2.1: Classical Interval Arithmetic

In order to realize the "worst-case" range of possible results with varying inputs, classical intervals use the following arithmetic rules:

For two intervals $\boldsymbol{x} = [x_1, x_2]$ and $\boldsymbol{y} = [y_1, y_2]$, where $x_1 \leq x_2$ and $y_1 \leq y_2$,

$$\boldsymbol{x} + \boldsymbol{y} = [x_1 + y_1, x_2 + y_2]$$

$$\boldsymbol{x} - \boldsymbol{y} = [x_1 - y_2, x_2 - y_1]$$

$$\boldsymbol{x} \times \boldsymbol{y} = [\min(x_1y_1, x_1y_2, x_2y_1, x_2y_2), \max(x_1y_1, x_1y_2, x_2y_1, x_2y_2)]$$

$$\boldsymbol{x} \div \boldsymbol{y} = \left[\min\left(\frac{x_1}{y_1}, \frac{x_1}{y_2}, \frac{x_2}{y_1}, \frac{x_2}{y_2}\right), \max\left(\frac{x_1}{y_1}, \frac{x_1}{y_2}, \frac{x_2}{y_1}, \frac{x_2}{y_2}\right)\right], 0 \notin \boldsymbol{y}$$

These relationships are the backbone of interval analysis, but they have several shortcomings. One major drawback is that operations are not reversible. If $\boldsymbol{a} + \boldsymbol{b} = \boldsymbol{c}$, then unless $\boldsymbol{b} = [0,0]$, $\boldsymbol{c} - \boldsymbol{b} \neq \boldsymbol{a}$. Similar examples can be made for other operations. Another major drawback is that many algebraic formulations have no solution. Unless $\boldsymbol{a} = [0,0]$, there is no interval $\boldsymbol{x}$ for which $\boldsymbol{a} + \boldsymbol{x} = [0,0]$. Many other examples can be given for any of the four basic algebraic operations listed.

A further drawback is not as easily seen and so may prove to be more insidious. Sainz et al., in the first chapter of *Modal Interval Analysis*, point out the dangers of trying to simply switch from a real-valued equation to an interval valued equation (Sainz, et al., 2014). Specifically, three formulations of an equation are presented, all of which produce an identical result for simple, real inputs. When the values are replaced with intervals, the equations do not produce the same results, and none of the three actually predicts the full potential interval that may be found in the results.

3.2.2: Generalized Interval Arithmetic

The Kaucher arithmetic is repeated here for completeness, as shown in (Gardeñes, et al., 2001). For two intervals $\boldsymbol{x} = \left[\underline{x}, \overline{x}\right]$ and $\boldsymbol{y} = \left[\underline{y}, \overline{y}\right]$:

$$\boldsymbol{x} + \boldsymbol{y} = \left[\underline{x} + \underline{y}, \overline{x} + \overline{y}\right]$$

$$\boldsymbol{x} - \boldsymbol{y} = \left[\underline{x} - \overline{y}, \overline{x} - \underline{y}\right]$$

$$\boldsymbol{x} \times \boldsymbol{y} = \left\{ \begin{array}{ll} \text{if } \underline{x} \geq 0, \overline{x} \geq 0, \underline{y} \geq 0, \overline{y} \geq 0, & \text{then } \left[\underline{x}\underline{y}, \bar{x}\bar{y}\right] \\ \text{if } \underline{x} \geq 0, \overline{x} \geq 0, \underline{y} \geq 0, \overline{y} < 0, & \text{then } \left[\underline{x}\underline{y}, \underline{x}\overline{y}\right] \\ \text{if } \underline{x} \geq 0, \overline{x} \geq 0, \underline{y} < 0, \overline{y} \geq 0, & \text{then } \left[\overline{x}\underline{y}, \overline{x}\overline{y}\right] \\ \text{if } \underline{x} \geq 0, \overline{x} \geq 0, \underline{y} < 0, \overline{y} < 0, & \text{then } \left[\overline{x}\underline{y}, \underline{x}\overline{y}\right] \\ \text{if } \underline{x} \geq 0, \overline{x} < 0, \underline{y} \geq 0, \overline{y} \geq 0, & \text{then } \left[\underline{x}\underline{y}, \overline{x}\underline{y}\right] \\ \text{if } \underline{x} \geq 0, \overline{x} < 0, \underline{y} \geq 0, \overline{y} < 0, & \text{then } \left[\max\left(\overline{x}\overline{y}, \underline{x}\underline{y}\right), \min\left(\overline{x}\underline{y}, \underline{x}\overline{y}\right)\right] \\ \text{if } \underline{x} \geq 0, \overline{x} < 0, \underline{y} < 0, \overline{y} \geq 0, & \text{then } [0,0] \\ \text{if } \underline{x} \geq 0, \overline{x} < 0, \underline{y} < 0, \overline{y} < 0, & \text{then } \left[\overline{x}\overline{y}, \underline{x}\overline{y}\right] \\ \text{if } \underline{x} < 0, \overline{x} \geq 0, \underline{y} \geq 0, \overline{y} \geq 0, & \text{then } \left[\underline{x}\overline{y}, \overline{x}\overline{y}\right] \\ \text{if } \underline{x} < 0, \overline{x} \geq 0, \underline{y} \geq 0, \overline{y} < 0, & \text{then } [0,0] \\ \text{if } \underline{x} < 0, \overline{x} \geq 0, \underline{y} < 0, \overline{y} \geq 0, & \text{then } \left[\max\left(\underline{x}\overline{y}, \overline{x}\underline{y}\right), \min\left(\underline{x}\underline{y}, \overline{x}\overline{y}\right)\right] \\ \text{if } \underline{x} < 0, \overline{x} \geq 0, \underline{y} < 0, \overline{y} < 0, & \text{then } \left[\overline{x}\underline{y}, \underline{x}\underline{y}\right] \\ \text{if } \underline{x} < 0, \overline{x} < 0, \underline{y} \geq 0, \overline{y} \geq 0, & \text{then } \left[\underline{x}\overline{y}, \overline{x}\underline{y}\right] \\ \text{if } \underline{x} < 0, \overline{x} < 0, \underline{y} \geq 0, \overline{y} < 0, & \text{then } \left[\overline{x}\overline{y}, \overline{x}\underline{y}\right] \\ \text{if } \underline{x} < 0, \overline{x} < 0, \underline{y} < 0, \overline{y} \geq 0, & \text{then } \left[\underline{x}\overline{y}, \underline{x}\underline{y}\right] \\ \text{if } \underline{x} < 0, \overline{x} < 0, \underline{y} < 0, \overline{y} < 0, & \text{then } \left[\overline{x}\overline{y}, \underline{x}\underline{y}\right] \end{array} \right\}$$

$$\frac{\boldsymbol{x}}{\boldsymbol{y}} = \left\{ \begin{array}{ll} \text{if } \underline{x} \geq 0, \overline{x} \geq 0, \underline{y} > 0, \overline{y} > 0, & \text{then } \left[\underline{x}/\overline{y}, \overline{x}/\underline{y} \right] \\ \text{if } \underline{x} \geq 0, \overline{x} \geq 0, \underline{y} < 0, \overline{y} < 0, & \text{then } \left[\overline{x}/\overline{y}, \underline{x}/\underline{y} \right] \\ \text{if } \underline{x} \geq 0, \overline{x} < 0, \underline{y} > 0, \overline{y} > 0, & \text{then } \left[\underline{x}/\overline{y}, \overline{x}/\overline{y} \right] \\ \text{if } \underline{x} \geq 0, \overline{x} < 0, \underline{y} < 0, \overline{y} < 0, & \text{then } \left[\overline{x}/\underline{y}, \underline{x}/\underline{y} \right] \\ \text{if } \underline{x} < 0, \overline{x} \geq 0, \underline{y} > 0, \overline{y} > 0, & \text{then } \left[\underline{x}/\underline{y}, \overline{x}/\underline{y} \right] \\ \text{if } \underline{x} < 0, \overline{x} \geq 0, \underline{y} < 0, \overline{y} < 0, & \text{then } \left[\overline{x}/\overline{y}, \underline{x}/\overline{y} \right] \\ \text{if } \underline{x} < 0, \overline{x} < 0, \underline{y} > 0, \overline{y} > 0, & \text{then } \left[\underline{x}/\underline{y}, \overline{x}/\overline{y} \right] \\ \text{if } \underline{x} < 0, \overline{x} < 0, \underline{y} < 0, \overline{y} < 0, & \text{then } \left[\overline{x}/\underline{y}, \underline{x}/\overline{y} \right] \end{array} \right\}$$

As with classical interval analysis, $\boldsymbol{x}/\boldsymbol{y}$ is undefined when 0 is between the bounds of $\boldsymbol{y}$.

When dealing with imprecise probabilities expressed as intervals, all interval values are between zero and one, greatly simplifying calculations. The Kaucher arithmetic for this special case is simply:

$$\boldsymbol{x} + \boldsymbol{y} = \left[\underline{x} + \underline{y}, \overline{x} + \overline{y} \right], \qquad \boldsymbol{x} \times \boldsymbol{y} = \left[\underline{x}\underline{y}, \overline{x}\overline{y} \right]$$

$$\boldsymbol{x} - \boldsymbol{y} = \left[\underline{x} - \overline{y}, \overline{x} - \underline{y} \right], \qquad \frac{\boldsymbol{x}}{\boldsymbol{y}} = \left[\underline{x}/\overline{y}, \overline{x}/\underline{y} \right]$$

With the Kaucher arithmetic, completeness of expression is only available through the use of the *dual* operator, as was discussed in Chapter 1. However, this completeness can be expressed in multiple ways. Four equations demonstrate this for the case of addition and subtraction:

$$\boldsymbol{a} - \boldsymbol{b} = \boldsymbol{c} \qquad \boldsymbol{a} = \boldsymbol{c} + dual(\boldsymbol{b})$$
$$\boldsymbol{a} - dual(\boldsymbol{b}) = \boldsymbol{c}' \qquad \boldsymbol{a} = \boldsymbol{c}' + \boldsymbol{b}$$

Similarly, for multiplication and division:

$$\frac{\boldsymbol{x}}{\boldsymbol{y}} = \boldsymbol{z} \qquad \boldsymbol{x} = \boldsymbol{z} \times dual(\boldsymbol{y})$$
$$\frac{\boldsymbol{x}}{dual(\boldsymbol{y})} = \boldsymbol{z}' \qquad \boldsymbol{x} = \boldsymbol{z}' \times \boldsymbol{y}$$

In either case, the arithmetic is complete. For the formulations of GIBR given in this thesis, the *dual* operator has been applied whenever division or subtraction is enacted—the reasons for this are discussed in §3.3. When following this convention, the Kaucher arithmetic can be expressed as:

$$\boldsymbol{x} + \boldsymbol{y} = \left[\underline{x} + \underline{y}, \overline{x} + \overline{y}\right], \qquad \boldsymbol{x} \times \boldsymbol{y} = \left[\underline{x}\underline{y}, \overline{x}\overline{y}\right]$$

$$\boldsymbol{x} - dual(\boldsymbol{y}) = \left[\underline{x} - \underline{y}, \overline{x} - \overline{y}\right], \qquad \frac{\boldsymbol{x}}{dual(\boldsymbol{y})} = \left[\underline{x}/\underline{y}, \overline{x}/\overline{y}\right]$$

By following this convention, the arithmetic is greatly simplified. Indeed, every formula can simply be broken up into two real-valued versions of itself: one using all of the bounds $\underline{x}$, and the other using all of the other bounds $\overline{x}$.

3.3: Bayesian Updating

Bayes' Rule (Bayes & Price, 1763) is well-known, and forms the basis for a large body of probability theory, including Dempster-Shafer theory (see §2.1.8), Jeffrey's Rule of Conditioning (Diaconis & Zabell, 1986), Bayesian Model Averaging (§2.1.2), and Robust Bayesian Analysis(§2.1.3). Bayes' Rule may be simply represented by the following equation:

$$P(E|A) = \frac{P(A|E) \cdot P(E)}{P(A)}$$

It is tempting to change this to a generalized interval equation simply by replacing each quantity with an interval, giving the equation:

$$\boldsymbol{P}(E|A) = \frac{\boldsymbol{P}(A|E) \cdot \boldsymbol{P}(E)}{\boldsymbol{P}(A)}$$

When the bounds of the intervals in question are between 0 and 1, both classical interval arithmetic and the Kaucher arithmetic calculate the results of this equation identically: the lower bound in this case is calculated as $\underline{\boldsymbol{P}}(E|A) = \frac{\underline{P}(A|E) \cdot \underline{P}(E)}{\overline{P}(A)}$, and the upper bound is calculated as $\overline{\boldsymbol{P}}(E|A) = \frac{\overline{P}(A|E) \cdot \overline{P}(E)}{\underline{P}(A)}$. This gives a true "worst-case" analysis, meaning that any for any real values within the intervals $\boldsymbol{P}(A|E)$, $\boldsymbol{P}(E)$, and $\boldsymbol{P}(A)$, the real value of the fraction $\frac{P(A|E) \cdot P(E)}{P(A)}$ will be within the interval $\boldsymbol{P}(E|A)$. This may also be referred to as a "complete solution." However, this worst-case analysis gives intervals that are far too wide to be useful, and frequently provides an upper bound with an impossible probability greater than 100%.

A more useful version of Bayes' theorem for intervals can be derived by returning to the derivation of Bayes' theorem, which starts with the statement that $P(E|A) \cdot P(A) = P(A|E) \cdot P(E)$. If the real-valued probabilities are replaced with generalized intervals at this step, then solving for $\boldsymbol{P}(E|A)$ gives the formulas:

$$\boldsymbol{P}(E|A) \cdot \boldsymbol{P}(A) = \boldsymbol{P}(A|E) \cdot \boldsymbol{P}(E)$$

$$\boldsymbol{P}(E|A) = \frac{\boldsymbol{P}(A|E) \cdot \boldsymbol{P}(E)}{dual\big(\boldsymbol{P}(A)\big)}$$

The advantageous formulation of the second equation allows the calculation of the updated interval to be done as two separate real-valued calculations, because $\underline{\boldsymbol{P}}(E|A) = \frac{\underline{P}(A|E) \cdot \underline{P}(E)}{\underline{P}(A)}$, and $\overline{\boldsymbol{P}}(E|A) = \frac{\overline{P}(A|E) \cdot \overline{P}(E)}{\overline{P}(A)}$. De-coupling the bounds of each interval for calculation greatly increases the computational simplicity because most computational tools are set up to use real values rather than intervals, and any of these may then be used for posterior probability calculation. By its very definition, this equation should not be expected to provide a posterior probability that encompasses all

the results that may be produced by the full range of values within the input intervals—it will not give a complete solution. However, it should always provide a "sound" solution, meaning that all values within the posterior interval may be obtained by a combination of some values within the input intervals. It is desirable for this sound solution to provide a good idea of the location of the likely results of a real-valued equation, either by being centered within the complete solution's boundaries, or by containing a high proportion of the results that might occur using the range of inputs offered in the equation.

If E_i is one of a set of n mutually disjoint events such that $\sum_{j=1}^{n} P(E_j) = 1$, then the real-valued denominator can be generalized as $P(A) = \sum_{j=1}^{n} P(A|E_j) \cdot P(E_j)$. This may be familiar as a form of Jeffrey's Rule (Diaconis & Zabell, 1986), which is yet another expansion of Bayes' Rule. Applying this to the interval-valued Bayesian update, if E_i is one of a set of n mutually disjoint events such that $\sum_{j=1}^{n} \boldsymbol{P}(E_j) = [1,1]$, then the equation becomes:

$$\boldsymbol{P}(E_i|A) = \frac{\boldsymbol{P}(A|E_i) \cdot \boldsymbol{P}(E_i)}{\sum_{j=1}^{n} dual\left(\boldsymbol{P}(A|E_j)\right) \cdot dual\left(\boldsymbol{P}(E_j)\right)} \quad (1)$$

Equation (1) is hereafter referred to as Generalized Interval Bayes' Rule, or GIBR. The requirement that a set of interval-valued mutually disjoint events should add up to [1,1] is referred to as the Logic Coherence Constraint, or LCC.

3.4: Expanding GIBR for cross-scale work.

In multiscale modeling, evidence used for validation may well be found in a different scale than that of the model's output. As such, it is necessary to have an approach that allows evidence to be applied across scales. An equation that allows this to take place is derived here, starting with a basic rule of conditional probability:

$$P(E|A) \cdot P(A) = P(A|E) \cdot P(E)$$

In this case, let E represent the focal event, and let A represent the evidence that can be gathered to validate E. In order to incorporate the multiple scales that may be

found in a model or in its related evidence, the event E is replaced with the combination of events $(B \cap C)$. C is considered to be the new focal event, while B is some link between the scales of A and C:

$$P(B \cap C|A) \cdot P(A) = P(A|B \cap C) \cdot P(B \cap C)$$

Another basic rule of probability, $P(B \cap C) = P(B|C) \cdot P(C)$, can be applied:

$$P(B \cap C|A) \cdot P(A) = P(A|B \cap C) \cdot P(B|C) \cdot P(C)$$

Assuming conditional independence of A and C based on B, the equation becomes:

$$P(B \cap C|A) \cdot P(A) = P(A|B) \cdot P(B|C) \cdot P(C)$$

Assuming conditional independence of B and C based on A further changes the equation to:

$$P(B|A) \cdot P(C|A) \cdot P(A) = P(A|B) \cdot P(B|C) \cdot P(C)$$

From Bayes' Rule, $P(B|A) = \frac{P(A|B) \cdot P(B)}{P(A)}$. Substituting this in gives:

$$\frac{P(A|B) \cdot P(B)}{P(A)} \cdot P(C|A) \cdot P(A) = P(A|B) \cdot P(B|C) \cdot P(C)$$

This can then be simplified to:

$$P(C|A) \cdot P(A|B) \cdot P(B) = P(A|B) \cdot P(B|C) \cdot P(C)$$

If all possible values of C are considered, then $P(B)$ can be related to $P(B|C) \cdot P(C)$. Specifically, $P(B) = \int \big(P(B|C) \cdot P(C)\big) dC$. This allows the equation to be re-written as:

$$P(C|A) \cdot P(A|B) \cdot \int \big(P(B|C) \cdot P(C)\big) dC = P(A|B) \cdot P(B|C) \cdot P(C)$$

Without a loss of generality, both sides of the equation can be integrated over all possible values of B. This is necessary because B represents a hidden link between A and C, and the desired outcome is the relationship between A and C, rather than the link between B and either A or C. That integration gives the following equation:

$$\int \left(P(C|A) \cdot P(A|B) \cdot \int \left(P(B|C) \cdot P(C) \right) dC \right) dB = \int \left(P(A|B) \cdot P(B|C) \cdot P(C) \right) dB$$

Some rearrangement of the terms in the equation gives the following useful form:

$$P(C|A) = \frac{\int P(A|B) \cdot P(B|C) dB \cdot P(C)}{\int \int P(A|B) \cdot P(B|C) \cdot P(C) dB \, dC}$$

This "probability chain" form may be used when the prior probability and the update cannot be directly connected. If one of the links in the chain represents a hidden variable, then this form may be used to represent a Hidden Markov Model (MacDonald & Zucchini, 1997). The steps of the previous derivation can be expanded to incorporate further degrees of separation between the model and the evidence, resulting in what can be thought of as a longer "chain" of probabilities:

$$P(D|A) = \frac{\int \int P(A|B) \cdot P(B|C) \cdot P(C|D) dB \, dC \cdot P(D)}{\int \int \int P(A|B) \cdot P(B|C) \cdot P(C|D) \cdot P(D) dB \, dC \, dD} \quad (2)$$

In either case, converting the equations for use with generalized intervals is a simple matter, involving applying the dual operator to the denominator and denoting that the probabilities are each intervals. The generalized interval versions of the previous equations can be used to represent a Generalized Hidden Markov Model (Wang, Multiscale uncertainty quantification, 2011), and are given as equations (3) and (4):

$$\boldsymbol{P}(C|A) = \frac{\int \boldsymbol{P}(A|B) \cdot \boldsymbol{P}(B|C) dB \cdot \boldsymbol{P}(C)}{dual(\int \int \boldsymbol{P}(A|B) \cdot \boldsymbol{P}(B|C) \cdot \boldsymbol{P}(C) dB \, dC)} \quad (3)$$

$$\boldsymbol{P}(D|A) = \frac{\int \int \boldsymbol{P}(A|B) \cdot \boldsymbol{P}(B|C) \cdot \boldsymbol{P}(C|D) dB \, dC \cdot \boldsymbol{P}(D)}{dual(\int \int \int \boldsymbol{P}(A|B) \cdot \boldsymbol{P}(B|C) \cdot \boldsymbol{P}(C|D) \cdot \boldsymbol{P}(D) dB \, dC \, dD)} \quad (4)$$

3.5: A numerical example of the method

3.5.1: An example of integration by summation

For illustrative purposes, a purely mathematical example is given here without regard for a specific physical meaning. For this first example, the variables α, β, δ, and γ

are used, where γ represents some model that is being validated, α represents evidence related to the model, and β and δ are the links between them. The equation that is employed is:

$$\boldsymbol{P}(\gamma|\alpha) = \frac{\int\int \boldsymbol{P}(\alpha|\beta)\cdot\boldsymbol{P}(\beta|\delta)\cdot\boldsymbol{P}(\delta|\gamma)d\delta\, d\beta\cdot\boldsymbol{P}(\gamma)}{dual\int\int\int \boldsymbol{P}(\alpha|\beta)\cdot\boldsymbol{P}(\beta|\delta)\cdot\boldsymbol{P}(\delta|\gamma)\cdot\boldsymbol{P}(\gamma)d\delta\, d\beta\, d\gamma} \quad (5)$$

True integration is often infeasible or even impossible for many applications, but an approximation of integration can be achieved with a summation. If equation (5) is integrated by breaking it up into a summation of all possible values of δ, and if δ can take on only two values, then the equation can be expressed as:

$$\boldsymbol{P}(\gamma|\alpha) = \frac{\int\begin{bmatrix}\boldsymbol{P}(\alpha|\beta)\cdot\boldsymbol{P}(\beta|\delta_1)\cdot\boldsymbol{P}(\delta_1|\gamma)\ldots \\ \ldots+\boldsymbol{P}(\alpha|\beta)\cdot\boldsymbol{P}(\beta|\delta_2)\cdot\boldsymbol{P}(\delta_2|\gamma)\end{bmatrix}d\beta\cdot\boldsymbol{P}(\gamma)}{dual\int\int\begin{bmatrix}\boldsymbol{P}(\alpha|\beta)\cdot\boldsymbol{P}(\beta|\delta_1)\cdot\boldsymbol{P}(\delta_1|\gamma)\cdot\boldsymbol{P}(\gamma)\ldots \\ \ldots+\boldsymbol{P}(\alpha|\beta)\cdot\boldsymbol{P}(\beta|\delta_2)\cdot\boldsymbol{P}(\delta_2|\gamma)\cdot\boldsymbol{P}(\gamma)\end{bmatrix}d\beta\, d\gamma}$$

This assumes that δ_1 and δ_2 are mutually disjoint events. Next, the integration over all values of β further expands the equation. As with δ, only two values of β are considered. That simple case is shown here:

$$\boldsymbol{P}(\gamma|\alpha) = \frac{\begin{bmatrix}\boldsymbol{P}(\alpha|\beta_1)\cdot\boldsymbol{P}(\beta_1|\delta_1)\cdot\boldsymbol{P}(\delta_1|\gamma)\ldots \\ \ldots+\boldsymbol{P}(\alpha|\beta_2)\cdot\boldsymbol{P}(\beta_2|\delta_1)\cdot\boldsymbol{P}(\delta_1|\gamma)\ldots \\ \ldots+\boldsymbol{P}(\alpha|\beta_1)\cdot\boldsymbol{P}(\beta_1|\delta_2)\cdot\boldsymbol{P}(\delta_2|\gamma)\ldots \\ \ldots+\boldsymbol{P}(\alpha|\beta_2)\cdot\boldsymbol{P}(\beta_2|\delta_2)\cdot\boldsymbol{P}(\delta_2|\gamma)\end{bmatrix}\cdot\boldsymbol{P}(\gamma)}{dual\int\begin{bmatrix}\boldsymbol{P}(\alpha|\beta_1)\cdot\boldsymbol{P}(\beta_1|\delta_1)\cdot\boldsymbol{P}(\delta_1|\gamma)\cdot\boldsymbol{P}(\gamma)\ldots \\ \ldots+\boldsymbol{P}(\alpha|\beta_2)\cdot\boldsymbol{P}(\beta_2|\delta_1)\cdot\boldsymbol{P}(\delta_1|\gamma)\cdot\boldsymbol{P}(\gamma)\ldots \\ \ldots+\boldsymbol{P}(\alpha|\beta_1)\cdot\boldsymbol{P}(\beta_1|\delta_2)\cdot\boldsymbol{P}(\delta_2|\gamma)\cdot\boldsymbol{P}(\gamma)\ldots \\ \ldots+\boldsymbol{P}(\alpha|\beta_2)\cdot\boldsymbol{P}(\beta_2|\delta_2)\cdot\boldsymbol{P}(\delta_2|\gamma)\cdot\boldsymbol{P}(\gamma)\end{bmatrix}d\gamma}$$

Again, this assumes that β_1 and β_2 are mutually disjoint events. If, on the other hand, β can take on other values, then this additional information can also be incorporated, as long as all of them together form a set of mutually disjoint events. A set of three mutually disjoint events for β is shown in the following version of equation (5):

$$\boldsymbol{P}(\gamma|\alpha) = \frac{\begin{bmatrix} \boldsymbol{P}(\alpha|\beta_1)\cdot\boldsymbol{P}(\beta_1|\delta_1)\cdot\boldsymbol{P}(\delta_1|\gamma)\ldots \\ \ldots+\boldsymbol{P}(\alpha|\beta_2)\cdot\boldsymbol{P}(\beta_2|\delta_1)\cdot\boldsymbol{P}(\delta_1|\gamma)\ldots \\ \ldots+\boldsymbol{P}(\alpha|\beta_3)\cdot\boldsymbol{P}(\beta_3|\delta_1)\cdot\boldsymbol{P}(\delta_1|\gamma)\ldots \\ \ldots+\boldsymbol{P}(\alpha|\beta_1)\cdot\boldsymbol{P}(\beta_1|\delta_2)\cdot\boldsymbol{P}(\delta_2|\gamma)\ldots \\ \ldots+\boldsymbol{P}(\alpha|\beta_2)\cdot\boldsymbol{P}(\beta_2|\delta_2)\cdot\boldsymbol{P}(\delta_2|\gamma)\ldots \\ \ldots+\boldsymbol{P}(\alpha|\beta_3)\cdot\boldsymbol{P}(\beta_3|\delta_2)\cdot\boldsymbol{P}(\delta_2|\gamma) \end{bmatrix}\cdot\boldsymbol{P}(\gamma)}{dual\int\begin{bmatrix} \boldsymbol{P}(\alpha|\beta_1)\cdot\boldsymbol{P}(\beta_1|\delta_1)\cdot\boldsymbol{P}(\delta_1|\gamma)\cdot\boldsymbol{P}(\gamma)\ldots \\ \ldots+\boldsymbol{P}(\alpha|\beta_2)\cdot\boldsymbol{P}(\beta_2|\delta_1)\cdot\boldsymbol{P}(\delta_1|\gamma)\cdot\boldsymbol{P}(\gamma)\ldots \\ \ldots+\boldsymbol{P}(\alpha|\beta_3)\cdot\boldsymbol{P}(\beta_3|\delta_1)\cdot\boldsymbol{P}(\delta_1|\gamma)\cdot\boldsymbol{P}(\gamma)\ldots \\ \ldots+\boldsymbol{P}(\alpha|\beta_1)\cdot\boldsymbol{P}(\beta_1|\delta_2)\cdot\boldsymbol{P}(\delta_2|\gamma)\cdot\boldsymbol{P}(\gamma)\ldots \\ \ldots+\boldsymbol{P}(\alpha|\beta_2)\cdot\boldsymbol{P}(\beta_2|\delta_2)\cdot\boldsymbol{P}(\delta_2|\gamma)\cdot\boldsymbol{P}(\gamma)\ldots \\ \ldots+\boldsymbol{P}(\alpha|\beta_3)\cdot\boldsymbol{P}(\beta_3|\delta_2)\cdot\boldsymbol{P}(\delta_2|\gamma)\cdot\boldsymbol{P}(\gamma) \end{bmatrix}d\gamma}$$

This leaves only one integration to be performed in the denominator of the equation. Assuming that the model γ can only take on two values (represented as γ and γ^C), the equation becomes:

$$\boldsymbol{P}(\gamma|\alpha) = \frac{\begin{bmatrix} \boldsymbol{P}(\alpha|\beta_1)\cdot\boldsymbol{P}(\beta_1|\delta_1)\cdot\boldsymbol{P}(\delta_1|\gamma)\ldots \\ \ldots+\boldsymbol{P}(\alpha|\beta_2)\cdot\boldsymbol{P}(\beta_2|\delta_1)\cdot\boldsymbol{P}(\delta_1|\gamma)\ldots \\ \ldots+\boldsymbol{P}(\alpha|\beta_3)\cdot\boldsymbol{P}(\beta_3|\delta_1)\cdot\boldsymbol{P}(\delta_1|\gamma)\ldots \\ \ldots+\boldsymbol{P}(\alpha|\beta_1)\cdot\boldsymbol{P}(\beta_1|\delta_2)\cdot\boldsymbol{P}(\delta_2|\gamma)\ldots \\ \ldots+\boldsymbol{P}(\alpha|\beta_2)\cdot\boldsymbol{P}(\beta_2|\delta_2)\cdot\boldsymbol{P}(\delta_2|\gamma)\ldots \\ \ldots+\boldsymbol{P}(\alpha|\beta_3)\cdot\boldsymbol{P}(\beta_3|\delta_2)\cdot\boldsymbol{P}(\delta_2|\gamma) \end{bmatrix}\cdot\boldsymbol{P}(\gamma)}{dual\begin{bmatrix} \boldsymbol{P}(\alpha|\beta_1)\cdot\boldsymbol{P}(\beta_1|\delta_1)\cdot\boldsymbol{P}(\delta_1|\gamma)\cdot\boldsymbol{P}(\gamma)\ldots \\ \ldots+\boldsymbol{P}(\alpha|\beta_2)\cdot\boldsymbol{P}(\beta_2|\delta_1)\cdot\boldsymbol{P}(\delta_1|\gamma)\cdot\boldsymbol{P}(\gamma)\ldots \\ \ldots+\boldsymbol{P}(\alpha|\beta_3)\cdot\boldsymbol{P}(\beta_3|\delta_1)\cdot\boldsymbol{P}(\delta_1|\gamma)\cdot\boldsymbol{P}(\gamma)\ldots \\ \ldots+\boldsymbol{P}(\alpha|\beta_1)\cdot\boldsymbol{P}(\beta_1|\delta_2)\cdot\boldsymbol{P}(\delta_2|\gamma)\cdot\boldsymbol{P}(\gamma)\ldots \\ \ldots+\boldsymbol{P}(\alpha|\beta_2)\cdot\boldsymbol{P}(\beta_2|\delta_2)\cdot\boldsymbol{P}(\delta_2|\gamma)\cdot\boldsymbol{P}(\gamma)\ldots \\ \ldots+\boldsymbol{P}(\alpha|\beta_3)\cdot\boldsymbol{P}(\beta_3|\delta_2)\cdot\boldsymbol{P}(\delta_2|\gamma)\cdot\boldsymbol{P}(\gamma)\ldots \\ \ldots+\boldsymbol{P}(\alpha|\beta_1)\cdot\boldsymbol{P}(\beta_1|\delta_1)\cdot\boldsymbol{P}(\delta_1|\gamma^C)\cdot\boldsymbol{P}(\gamma^C)\ldots \\ \ldots+\boldsymbol{P}(\alpha|\beta_2)\cdot\boldsymbol{P}(\beta_2|\delta_1)\cdot\boldsymbol{P}(\delta_1|\gamma^C)\cdot\boldsymbol{P}(\gamma^C)\ldots \\ \ldots+\boldsymbol{P}(\alpha|\beta_3)\cdot\boldsymbol{P}(\beta_3|\delta_1)\cdot\boldsymbol{P}(\delta_1|\gamma^C)\cdot\boldsymbol{P}(\gamma^C)\ldots \\ \ldots+\boldsymbol{P}(\alpha|\beta_1)\cdot\boldsymbol{P}(\beta_1|\delta_2)\cdot\boldsymbol{P}(\delta_2|\gamma^C)\cdot\boldsymbol{P}(\gamma^C)\ldots \\ \ldots+\boldsymbol{P}(\alpha|\beta_2)\cdot\boldsymbol{P}(\beta_2|\delta_2)\cdot\boldsymbol{P}(\delta_2|\gamma^C)\cdot\boldsymbol{P}(\gamma^C)\ldots \\ \ldots+\boldsymbol{P}(\alpha|\beta_3)\cdot\boldsymbol{P}(\beta_3|\delta_2)\cdot\boldsymbol{P}(\delta_2|\gamma^C)\cdot\boldsymbol{P}(\gamma^C) \end{bmatrix}} \quad (6)$$

3.5.2: Matrix decomposition of integrated equations

Equation (6) is closer to yielding a numerical result than was equation (5), but it is unwieldy and repetitive. Examination of the pattern of terms within the equation

reveals that the long combination of summed multiplications can more easily be represented by the multiplication of matrices; decomposing the numerator into two matrices gives the following result:

$$\boldsymbol{P}(\gamma|\alpha) = \frac{[\boldsymbol{P}(\alpha|\beta_1) \quad \boldsymbol{P}(\alpha|\beta_2) \quad \boldsymbol{P}(\alpha|\beta_3)] \begin{bmatrix} \boldsymbol{P}(\beta_1|\delta_1)\cdot\boldsymbol{P}(\delta_1|\gamma) + \boldsymbol{P}(\beta_1|\delta_2)\cdot\boldsymbol{P}(\delta_2|\gamma) \\ \boldsymbol{P}(\beta_2|\delta_1)\cdot\boldsymbol{P}(\delta_1|\gamma) + \boldsymbol{P}(\beta_2|\delta_2)\cdot\boldsymbol{P}(\delta_2|\gamma) \\ \boldsymbol{P}(\beta_3|\delta_1)\cdot\boldsymbol{P}(\delta_1|\gamma) + \boldsymbol{P}(\beta_3|\delta_2)\cdot\boldsymbol{P}(\delta_2|\gamma) \end{bmatrix} \cdot \boldsymbol{P}(\gamma)}{dual \begin{bmatrix} \boldsymbol{P}(\alpha|\beta_1)\cdot\boldsymbol{P}(\beta_1|\delta_1)\cdot\boldsymbol{P}(\delta_1|\gamma)\cdot\boldsymbol{P}(\gamma)\ldots \\ \ldots + \boldsymbol{P}(\alpha|\beta_2)\cdot\boldsymbol{P}(\beta_2|\delta_1)\cdot\boldsymbol{P}(\delta_1|\gamma)\cdot\boldsymbol{P}(\gamma)\ldots \\ \ldots + \boldsymbol{P}(\alpha|\beta_3)\cdot\boldsymbol{P}(\beta_3|\delta_1)\cdot\boldsymbol{P}(\delta_1|\gamma)\cdot\boldsymbol{P}(\gamma)\ldots \\ \ldots + \boldsymbol{P}(\alpha|\beta_1)\cdot\boldsymbol{P}(\beta_1|\delta_2)\cdot\boldsymbol{P}(\delta_2|\gamma)\cdot\boldsymbol{P}(\gamma)\ldots \\ \ldots + \boldsymbol{P}(\alpha|\beta_2)\cdot\boldsymbol{P}(\beta_2|\delta_2)\cdot\boldsymbol{P}(\delta_2|\gamma)\cdot\boldsymbol{P}(\gamma)\ldots \\ \ldots + \boldsymbol{P}(\alpha|\beta_3)\cdot\boldsymbol{P}(\beta_3|\delta_2)\cdot\boldsymbol{P}(\delta_2|\gamma)\cdot\boldsymbol{P}(\gamma)\ldots \\ \ldots + \boldsymbol{P}(\alpha|\beta_1)\cdot\boldsymbol{P}(\beta_1|\delta_1)\cdot\boldsymbol{P}(\delta_1|\gamma^C)\cdot\boldsymbol{P}(\gamma^C)\ldots \\ \ldots + \boldsymbol{P}(\alpha|\beta_2)\cdot\boldsymbol{P}(\beta_2|\delta_1)\cdot\boldsymbol{P}(\delta_1|\gamma^C)\cdot\boldsymbol{P}(\gamma^C)\ldots \\ \ldots + \boldsymbol{P}(\alpha|\beta_3)\cdot\boldsymbol{P}(\beta_3|\delta_1)\cdot\boldsymbol{P}(\delta_1|\gamma^C)\cdot\boldsymbol{P}(\gamma^C)\ldots \\ \ldots + \boldsymbol{P}(\alpha|\beta_1)\cdot\boldsymbol{P}(\beta_1|\delta_2)\cdot\boldsymbol{P}(\delta_2|\gamma^C)\cdot\boldsymbol{P}(\gamma^C)\ldots \\ \ldots + \boldsymbol{P}(\alpha|\beta_2)\cdot\boldsymbol{P}(\beta_2|\delta_2)\cdot\boldsymbol{P}(\delta_2|\gamma^C)\cdot\boldsymbol{P}(\gamma^C)\ldots \\ \ldots + \boldsymbol{P}(\alpha|\beta_3)\cdot\boldsymbol{P}(\beta_3|\delta_2)\cdot\boldsymbol{P}(\delta_2|\gamma^C)\cdot\boldsymbol{P}(\gamma^C) \end{bmatrix}}$$

Carrying the matrix decomposition one step further onto three matrices gives the most compact representation of the numerator, with:

$$\boldsymbol{P}(\gamma|\alpha) = \frac{[\boldsymbol{P}(\alpha|\beta_1) \quad \boldsymbol{P}(\alpha|\beta_2) \quad \boldsymbol{P}(\alpha|\beta_3)] \begin{bmatrix} \boldsymbol{P}(\beta_1|\delta_1) & \boldsymbol{P}(\beta_1|\delta_2) \\ \boldsymbol{P}(\beta_2|\delta_1) & \boldsymbol{P}(\beta_2|\delta_2) \\ \boldsymbol{P}(\beta_3|\delta_1) & \boldsymbol{P}(\beta_3|\delta_2) \end{bmatrix} \begin{bmatrix} \boldsymbol{P}(\delta_1|\gamma) \\ \boldsymbol{P}(\delta_2|\gamma) \end{bmatrix} \cdot \boldsymbol{P}(\gamma)}{dual \begin{bmatrix} \boldsymbol{P}(\alpha|\beta_1)\cdot\boldsymbol{P}(\beta_1|\delta_1)\cdot\boldsymbol{P}(\delta_1|\gamma)\cdot\boldsymbol{P}(\gamma)\ldots \\ \ldots + \boldsymbol{P}(\alpha|\beta_2)\cdot\boldsymbol{P}(\beta_2|\delta_1)\cdot\boldsymbol{P}(\delta_1|\gamma)\cdot\boldsymbol{P}(\gamma)\ldots \\ \ldots + \boldsymbol{P}(\alpha|\beta_3)\cdot\boldsymbol{P}(\beta_3|\delta_1)\cdot\boldsymbol{P}(\delta_1|\gamma)\cdot\boldsymbol{P}(\gamma)\ldots \\ \ldots + \boldsymbol{P}(\alpha|\beta_1)\cdot\boldsymbol{P}(\beta_1|\delta_2)\cdot\boldsymbol{P}(\delta_2|\gamma)\cdot\boldsymbol{P}(\gamma)\ldots \\ \ldots + \boldsymbol{P}(\alpha|\beta_2)\cdot\boldsymbol{P}(\beta_2|\delta_2)\cdot\boldsymbol{P}(\delta_2|\gamma)\cdot\boldsymbol{P}(\gamma)\ldots \\ \ldots + \boldsymbol{P}(\alpha|\beta_3)\cdot\boldsymbol{P}(\beta_3|\delta_2)\cdot\boldsymbol{P}(\delta_2|\gamma)\cdot\boldsymbol{P}(\gamma)\ldots \\ \ldots + \boldsymbol{P}(\alpha|\beta_1)\cdot\boldsymbol{P}(\beta_1|\delta_1)\cdot\boldsymbol{P}(\delta_1|\gamma^C)\cdot\boldsymbol{P}(\gamma^C)\ldots \\ \ldots + \boldsymbol{P}(\alpha|\beta_2)\cdot\boldsymbol{P}(\beta_2|\delta_1)\cdot\boldsymbol{P}(\delta_1|\gamma^C)\cdot\boldsymbol{P}(\gamma^C)\ldots \\ \ldots + \boldsymbol{P}(\alpha|\beta_3)\cdot\boldsymbol{P}(\beta_3|\delta_1)\cdot\boldsymbol{P}(\delta_1|\gamma^C)\cdot\boldsymbol{P}(\gamma^C)\ldots \\ \ldots + \boldsymbol{P}(\alpha|\beta_1)\cdot\boldsymbol{P}(\beta_1|\delta_2)\cdot\boldsymbol{P}(\delta_2|\gamma^C)\cdot\boldsymbol{P}(\gamma^C)\ldots \\ \ldots + \boldsymbol{P}(\alpha|\beta_2)\cdot\boldsymbol{P}(\beta_2|\delta_2)\cdot\boldsymbol{P}(\delta_2|\gamma^C)\cdot\boldsymbol{P}(\gamma^C)\ldots \\ \ldots + \boldsymbol{P}(\alpha|\beta_3)\cdot\boldsymbol{P}(\beta_3|\delta_2)\cdot\boldsymbol{P}(\delta_2|\gamma^C)\cdot\boldsymbol{P}(\gamma^C) \end{bmatrix}}$$

As with the numerator, the denominator can be decomposed into the result of the multiplication of matrices. With this matrix decomposition carried out, the fully integrated and decomposed form of equation (5) is:

$$\boldsymbol{P}(\gamma|\alpha) = \frac{[\boldsymbol{P}(\alpha|\beta_1) \quad \boldsymbol{P}(\alpha|\beta_2) \quad \boldsymbol{P}(\alpha|\beta_3)] \begin{bmatrix} \boldsymbol{P}(\beta_1|\delta_1) & \boldsymbol{P}(\beta_1|\delta_2) \\ \boldsymbol{P}(\beta_2|\delta_1) & \boldsymbol{P}(\beta_2|\delta_2) \\ \boldsymbol{P}(\beta_3|\delta_1) & \boldsymbol{P}(\beta_3|\delta_2) \end{bmatrix} \begin{bmatrix} \boldsymbol{P}(\delta_1|\gamma) \\ \boldsymbol{P}(\delta_2|\gamma) \end{bmatrix} \cdot \boldsymbol{P}(\gamma)}{dual\left([\boldsymbol{P}(\alpha|\beta_1) \quad \boldsymbol{P}(\alpha|\beta_2) \quad \boldsymbol{P}(\alpha|\beta_3)] \begin{bmatrix} \boldsymbol{P}(\beta_1|\delta_1) & \boldsymbol{P}(\beta_1|\delta_2) \\ \boldsymbol{P}(\beta_2|\delta_1) & \boldsymbol{P}(\beta_2|\delta_2) \\ \boldsymbol{P}(\beta_3|\delta_1) & \boldsymbol{P}(\beta_3|\delta_2) \end{bmatrix} \begin{bmatrix} \boldsymbol{P}(\delta_1|\gamma) & \boldsymbol{P}(\delta_1|\gamma^C) \\ \boldsymbol{P}(\delta_2|\gamma) & \boldsymbol{P}(\delta_2|\gamma^C) \end{bmatrix} \begin{bmatrix} \boldsymbol{P}(\gamma) \\ \boldsymbol{P}(\gamma^C) \end{bmatrix} \right)} \quad (7)$$

This form is not only beneficial for its relative compactness, but also for its ease of error-checking. For instance, in every matrix with more than a single row, the columns represent a set of mutually disjoint events, and the intervals in them must sum to [1,1]. In the case of a single-valued rather than interval-valued equation, the entries in any multi-rowed column must sum to 1. This property is due to the imposition of the Logic Coherence Constraint in the case of generalized intervals, which is analogous to the definition of mutually disjoint events for the single-valued case. Rows with more than one column (e.g. $[\boldsymbol{P}(\alpha|\beta_1) \quad \boldsymbol{P}(\alpha|\beta_2) \quad \boldsymbol{P}(\alpha|\beta_3)]$)are not numerically related. The simplified format also makes it easier to keep track of variable names and decreases repetition, simplifying the process of performing or of programming the calculations. Matrices must be arranged such that the result of the final multiplication is a single interval, or, in the case of a non-interval equation, a scalar.

In addition, when the pattern of matrix decomposition is recognized, it becomes a simple matter to change the number of terms that each link in the chain contains, or to change the number of links in the chain. For instance, if the GIBR equation is used to link model γ with evidence α using only the link β, then the relevant integration is:

$$\boldsymbol{P}(\gamma|\alpha) = \frac{\int \boldsymbol{P}(\alpha|\beta) \cdot \boldsymbol{P}(\beta|\gamma) d\beta \cdot \boldsymbol{P}(\gamma)}{dual \int \int \boldsymbol{P}(\alpha|\beta) \cdot \boldsymbol{P}(\beta|\gamma) \cdot \boldsymbol{P}(\gamma) d\beta \, d\gamma}$$

This can easily be broken up into a very simple case of only two terms for each parameter. For the sake of compactness in representation, a shorthand is employed; each term represents a probability, and the subscript represents the condition upon which the probability depends. For instance, $\beta 1_\gamma$ is used to represent $\boldsymbol{P}(\beta_1|\gamma)$. Using the shorthand notation, this simple case is represented as:

$$\boldsymbol{P}(\gamma|\alpha) = \frac{[\alpha_{\beta 1} \quad \alpha_{\beta 2}] \begin{bmatrix} \beta 1_{\gamma} \\ \beta 2_{\gamma} \end{bmatrix} \cdot \gamma}{dual\left([\alpha_{\beta 1} \quad \alpha_{\beta 2}] \begin{bmatrix} \beta 1_{\gamma} & \beta 1_{\gamma^C} \\ \beta 2_{\gamma} & \beta 2_{\gamma^C} \end{bmatrix} \begin{bmatrix} \gamma \\ \gamma^C \end{bmatrix} \right)}$$

The same integration can just as easily be broken up into a very complex case of four terms each for both α and β:

$$\boldsymbol{P}(\gamma|\alpha) = \frac{[\alpha_{\beta 1} \quad \alpha_{\beta 2} \quad \alpha_{\beta 3} \quad \alpha_{\beta 4}] \begin{bmatrix} \beta 1_{\gamma} \\ \beta 2_{\gamma} \\ \beta 3_{\gamma} \\ \beta 4_{\gamma} \end{bmatrix} \cdot \gamma}{dual\left([\alpha_{\beta 1} \quad \alpha_{\beta 2} \quad \alpha_{\beta 3} \quad \alpha_{\beta 4}] \begin{bmatrix} \beta 1_{\gamma} & \beta 1_{\gamma^C} \\ \beta 2_{\gamma} & \beta 2_{\gamma^C} \\ \beta 3_{\gamma} & \beta 3_{\gamma^C} \\ \beta 4_{\gamma} & \beta 4_{\gamma^C} \end{bmatrix} \begin{bmatrix} \gamma \\ \gamma^C \end{bmatrix} \right)}$$

In the case of more links in the chain, the GIBR equation might look like this:

$$\boldsymbol{P}(\gamma|\alpha) = \frac{\int\int\int \boldsymbol{P}(\alpha|\beta) \cdot \boldsymbol{P}(\beta|\delta) \cdot \boldsymbol{P}(\delta|\epsilon) \cdot \boldsymbol{P}(\epsilon|\gamma) d\epsilon \, d\delta \, d\beta \cdot \boldsymbol{P}(\gamma)}{dual \int\int\int\int \boldsymbol{P}(\alpha|\beta) \cdot \boldsymbol{P}(\beta|\delta) \cdot \boldsymbol{P}(\delta|\epsilon) \cdot \boldsymbol{P}(\epsilon|\gamma) \cdot \boldsymbol{P}(\gamma) \, d\epsilon \, d\delta \, d\beta d\gamma}$$

And it could be decomposed into this:

$$\boldsymbol{P}(\gamma|\alpha) = \frac{[\alpha_{\beta 1} \quad \alpha_{\beta 2}] \begin{bmatrix} \beta 1_{\delta 1} & \beta 1_{\delta 2} \\ \beta 2_{\delta 1} & \beta 2_{\delta 2} \end{bmatrix} \begin{bmatrix} \delta 1_{\epsilon 1} & \delta 1_{\epsilon 2} \\ \delta 2_{\epsilon 1} & \delta 2_{\epsilon 2} \end{bmatrix} \begin{bmatrix} \epsilon 1_{\gamma} \\ \epsilon 2_{\gamma} \end{bmatrix} \cdot \gamma}{dual\left([\alpha_{\beta 1} \quad \alpha_{\beta 2}] \begin{bmatrix} \beta 1_{\delta 1} & \beta 1_{\delta 2} \\ \beta 2_{\delta 1} & \beta 2_{\delta 2} \end{bmatrix} \begin{bmatrix} \delta 1_{\epsilon 1} & \delta 1_{\epsilon 2} \\ \delta 2_{\epsilon 1} & \delta 2_{\epsilon 2} \end{bmatrix} \begin{bmatrix} \epsilon 1_{\gamma} & \epsilon 1_{\gamma^C} \\ \epsilon 2_{\gamma} & \epsilon 2_{\gamma^C} \end{bmatrix} \begin{bmatrix} \gamma \\ \gamma^C \end{bmatrix} \right)}$$

Or, almost as easily, into this:

$$\boldsymbol{P}(\gamma|\alpha) = \frac{[\alpha_{\beta 1} \quad \alpha_{\beta 2}] \begin{bmatrix} \beta 1_{\delta 1} & \beta 1_{\delta 2} & \beta 1_{\delta 3} \\ \beta 2_{\delta 1} & \beta 2_{\delta 2} & \beta 2_{\delta 3} \end{bmatrix} \begin{bmatrix} \delta 1_{\epsilon 1} & \delta 1_{\epsilon 2} & \delta 1_{\epsilon 3} & \delta 1_{\epsilon 4} \\ \delta 2_{\epsilon 1} & \delta 2_{\epsilon 2} & \delta 2_{\epsilon 3} & \delta 2_{\epsilon 4} \\ \delta 3_{\epsilon 1} & \delta 3_{\epsilon 2} & \delta 3_{\epsilon 3} & \delta 3_{\epsilon 4} \end{bmatrix} \begin{bmatrix} \epsilon 1_{\gamma} \\ \epsilon 2_{\gamma} \\ \epsilon 3_{\gamma} \\ \epsilon 4_{\gamma} \end{bmatrix} \cdot \gamma}{dual\left([\alpha_{\beta 1} \quad \alpha_{\beta 2}] \begin{bmatrix} \beta 1_{\delta 1} & \beta 1_{\delta 2} & \beta 1_{\delta 3} \\ \beta 2_{\delta 1} & \beta 2_{\delta 2} & \beta 2_{\delta 3} \end{bmatrix} \begin{bmatrix} \delta 1_{\epsilon 1} & \delta 1_{\epsilon 2} & \delta 1_{\epsilon 3} & \delta 1_{\epsilon 4} \\ \delta 2_{\epsilon 1} & \delta 2_{\epsilon 2} & \delta 2_{\epsilon 3} & \delta 2_{\epsilon 4} \\ \delta 3_{\epsilon 1} & \delta 3_{\epsilon 2} & \delta 3_{\epsilon 3} & \delta 3_{\epsilon 4} \end{bmatrix} \begin{bmatrix} \epsilon 1_{\gamma} & \epsilon 1_{\gamma^C} \\ \epsilon 2_{\gamma} & \epsilon 2_{\gamma^C} \\ \epsilon 3_{\gamma} & \epsilon 3_{\gamma^C} \\ \epsilon 4_{\gamma} & \epsilon 4_{\gamma^C} \end{bmatrix} \begin{bmatrix} \gamma \\ \gamma^C \end{bmatrix} \right)}$$

There is no theoretical limit on the number of links in the expanded GIBR chain, nor on the number of mutually disjoint events that may be used in the discretization of the integrals. There is, however, a practical limitation: too many links or too many levels of

discretization will cause the equations to become large and unwieldy, even with matrix decomposition. The analysis may be further limited in practice by the amount of information available to populate the likelihoods that connect the evidence to the model.

3.5.3: Verification through Monte Carlo Simulations

Generalized Interval Bayes' Rule attempts to predict the interval in which a result will lie given the intervals for each of the inputs. For the sake of illustration, the following equation is used:

$$\boldsymbol{P}(\gamma|\alpha) = \frac{[\alpha_{\beta1} \quad \alpha_{\beta2} \quad \alpha_{\beta3} \quad \alpha_{\beta4}]\begin{bmatrix}\beta1_\gamma \\ \beta2_\gamma \\ \beta3_\gamma \\ \beta4_\gamma\end{bmatrix}\cdot\gamma}{dual\left([\alpha_{\beta1} \quad \alpha_{\beta2} \quad \alpha_{\beta3} \quad \alpha_{\beta4}]\begin{bmatrix}\beta1_\gamma & \beta1_{\gamma^C} \\ \beta2_\gamma & \beta2_{\gamma^C} \\ \beta3_\gamma & \beta3_{\gamma^C} \\ \beta4_\gamma & \beta4_{\gamma^C}\end{bmatrix}\begin{bmatrix}\gamma \\ \gamma^C\end{bmatrix}\right)} \quad (8)$$

Intervals were arbitrarily assigned to each of the probabilities in equation (8). These are shown in Table 1:

Table 1: Assigned probability intervals for an example problem.

Symbol	Probability	Interval	Notes
$\alpha_{\beta1}$	$\boldsymbol{P}(\alpha\|\beta1)$	[0.3880,0.9973]	Arbitrarily Assigned Note that the assigned intervals are all proper intervals. Only where the Logic Coherence Constraint is used to generate an interval value does the value become an improper interval (e.g. $\beta4_\gamma$, $\beta4_{\gamma^C}$, and γ^C).
$\alpha_{\beta2}$	$\boldsymbol{P}(\alpha\|\beta2)$	[0.7415,0.9024]	
$\alpha_{\beta3}$	$\boldsymbol{P}(\alpha\|\beta3)$	[0.3667,0.8688]	
$\alpha_{\beta4}$	$\boldsymbol{P}(\alpha\|\beta4)$	[0.1655,0.4140]	
$\beta1_\gamma$	$\boldsymbol{P}(\beta1\|\gamma)$	[0.1197,0.1826]	
$\beta2_\gamma$	$\boldsymbol{P}(\beta2\|\gamma)$	[0.1662,0.3080]	
$\beta3_\gamma$	$\boldsymbol{P}(\beta3\|\gamma)$	[0.3587,0.4603]	
$\beta4_\gamma$	$\boldsymbol{P}(\beta4\|\gamma)$	[0.3554,0.0491]	$\beta4_\gamma = 1 - dual\left(\beta1_\gamma + \beta2_\gamma + \beta3_\gamma\right)$
$\beta1_{\gamma^C}$	$\boldsymbol{P}(\beta1\|\gamma^C)$	[0.0410,0.1930]	Arbitrarily Assigned
$\beta2_{\gamma^C}$	$\boldsymbol{P}(\beta2\|\gamma^C)$	[0.1527,0.1772]	
$\beta3_{\gamma^C}$	$\boldsymbol{P}(\beta3\|\gamma^C)$	[0.3683,0.4682]	
$\beta4_{\gamma^C}$	$\boldsymbol{P}(\beta4\|\gamma^C)$	[0.4380,0.1616]	$\beta4_{\gamma^C} = 1 - dual\left(\beta1_{\gamma^C} + \beta2_{\gamma^C} + \beta3_{\gamma^C}\right)$
γ	$\boldsymbol{P}(\gamma)$	[0.3000,0.4500]	Arbitrarily Assigned
γ^C	$\boldsymbol{P}(\gamma^C)$	[0.7000,0.5500]	$\gamma^C = 1 - dual(\gamma)$

Once the interval values are substituted into equation (8), the resulting equation is as shown in equation (9). The $[\alpha_\beta]$ matrix has been transposed only for the sake of compactness in representation:

$$\boldsymbol{P}(\gamma|\alpha) = \frac{\begin{bmatrix}[0.3880,0.9973]\\[0.7415,0.9024]\\[0.3667,0.8688]\\[0.1655,0.4140]\end{bmatrix}^T \begin{bmatrix}[0.1197,0.1826]\\[0.1662,0.3080]\\[0.3587,0.4603]\\[0.3554,0.0491]\end{bmatrix} \cdot [0.3000,0.4500]}{dual\left(\begin{bmatrix}[0.3880,0.9973]\\[0.7415,0.9024]\\[0.3667,0.8688]\\[0.1655,0.4140]\end{bmatrix}^T \begin{bmatrix}[0.1197,0.1826] & [0.0410,0.1930]\\[0.1662,0.3080] & [0.1527,0.1772]\\[0.3587,0.4603] & [0.3683,0.4682]\\[0.3554,0.0491] & [0.4380,0.1616]\end{bmatrix} \begin{bmatrix}[0.3000,0.4500]\\[0.7000,0.5500]\end{bmatrix}\right)} \quad (9)$$

The lower bound of the posterior probability $\underline{\boldsymbol{P}}(\gamma|\alpha) = 0.3143$ is calculated by using the lower bounds of each of the input intervals, as follows:

$$\underline{\boldsymbol{P}}(\gamma|\alpha) = \frac{\begin{bmatrix}0.3880 & 0.7415 & 0.3667 & 0.1655\end{bmatrix} \begin{bmatrix}0.1197\\0.1662\\0.3587\\0.3554\end{bmatrix} \cdot 0.3000}{dual\left(\begin{bmatrix}0.3880 & 0.7415 & 0.3667 & 0.1655\end{bmatrix} \begin{bmatrix}0.1197 & 0.0410\\0.1662 & 0.1527\\0.3587 & 0.3683\\0.3554 & 0.4380\end{bmatrix} \begin{bmatrix}0.3000\\0.7000\end{bmatrix}\right)}$$

Similarly, the upper bound $\overline{\boldsymbol{P}}(\gamma|\alpha) = 0.4658$ is calculated by using the upper bound of each of the input intervals:

$$\overline{\boldsymbol{P}}(\gamma|\alpha) = \frac{\begin{bmatrix}0.9973 & 0.9024 & 0.8688 & 0.4140\end{bmatrix} \begin{bmatrix}0.1826\\0.3080\\0.4603\\0.0491\end{bmatrix} \cdot 0.4500}{dual\left(\begin{bmatrix}0.9973 & 0.9024 & 0.8688 & 0.4140\end{bmatrix} \begin{bmatrix}0.1826 & 0.1930\\0.3080 & 0.1772\\0.4603 & 0.4682\\0.0491 & 0.1616\end{bmatrix} \begin{bmatrix}0.4500\\0.5500\end{bmatrix}\right)}$$

A single counter-example can clearly demonstrate the lack of completeness in the GIBR solution: a real-valued equation in the form of equation (8) that has inputs within the given intervals, and an output beyond the range of the output interval. One such counter-example is $P(\gamma|\alpha) = 0.4901$.

$$P(\gamma|\alpha) = \frac{\begin{bmatrix}0.8094 & 0.8026 & 0.7881 & 0.2634\end{bmatrix}\begin{bmatrix}0.1346\\0.2921\\0.4435\\0.1298\end{bmatrix}.}{dual\left(\begin{bmatrix}0.8094 & 0.8026 & 0.7881 & 0.2634\end{bmatrix}\begin{bmatrix}0.1346 & 0.0624\\0.2921 & 0.1542\\0.4435 & 0.3712\\0.1298 & 0.4123\end{bmatrix}\begin{bmatrix}0.4321\\0.2679\end{bmatrix}\right)}$$

Despite the fact that every value in the right-hand side of the given equation is within the intervals prescribed, the resulting posterior probability of 0.4901 is outside of the predicted interval of [0.3143,0.4658]. Obviously the GIBR solution is not complete, but there is still much that can be learned about its soundness by repeated testing of the equation outputs and the distribution of results.

In its purest interpretation, a generalized interval neither represents nor implies any particular distribution of values within its limits. The actual result could be single value somewhere within or even on the limits, or it could be any distribution contained within the limits, as demonstrated in Figure 3.

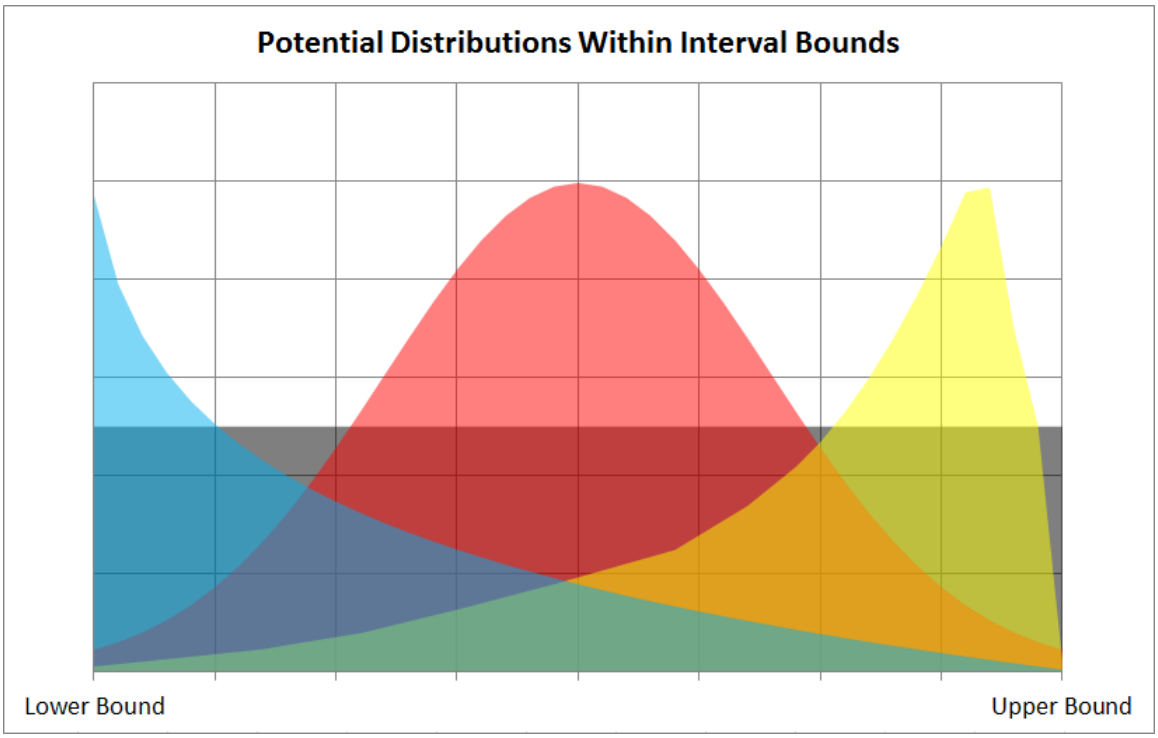

Figure 3: Some of the many distributions that could be represented by an interval.

For something like a normal distribution, the limits could be said to reasonably represent the distribution if they contained it only to a certain level, such as ±3σ. As such, the distribution of values that are obtained from multiple examples provides a valuable insight into the usefulness of GIBR. This leads directly to the use of Monte Carlo simulation to verify GIBR. As an example Monte Carlo simulation, equation (9) was used to calculate a posterior probability interval. Each input interval within the equation was replaced with a real value randomly generated to conform to the boundaries of the interval, thus allowing a single real-valued output to be obtained as a posterior probability.

3.5.3.1: Uniform Input Monte Carlo Simulation

For the first Monte Carlo verification simulation, the assigned input intervals in equation(9) were replaced with uniformly distributed random values within their bounds; the value for the complementary intervals (i.e. $\beta 4_{\gamma}$, $\beta 4_{\gamma^c}$, and γ^C) was determined by subtraction in order to comply with the Logic Coherence Constraint. Assuming a distribution goes against the nature of generalized intervals, but is necessary for the sake of obtaining an observable, understandable verification result. The resulting real-valued equation was then used to calculate a posterior probability. This process was repeated 1,000,000 times, using pseudo-random numbers generated by Microsoft Excel's "rand()" function. A histogram and the corresponding count of the results is shown in Figure 4. The bin size of the histogram was intentionally selected so that twenty bins would completely cover the proposed posterior probability of [0.3143,0.4658].

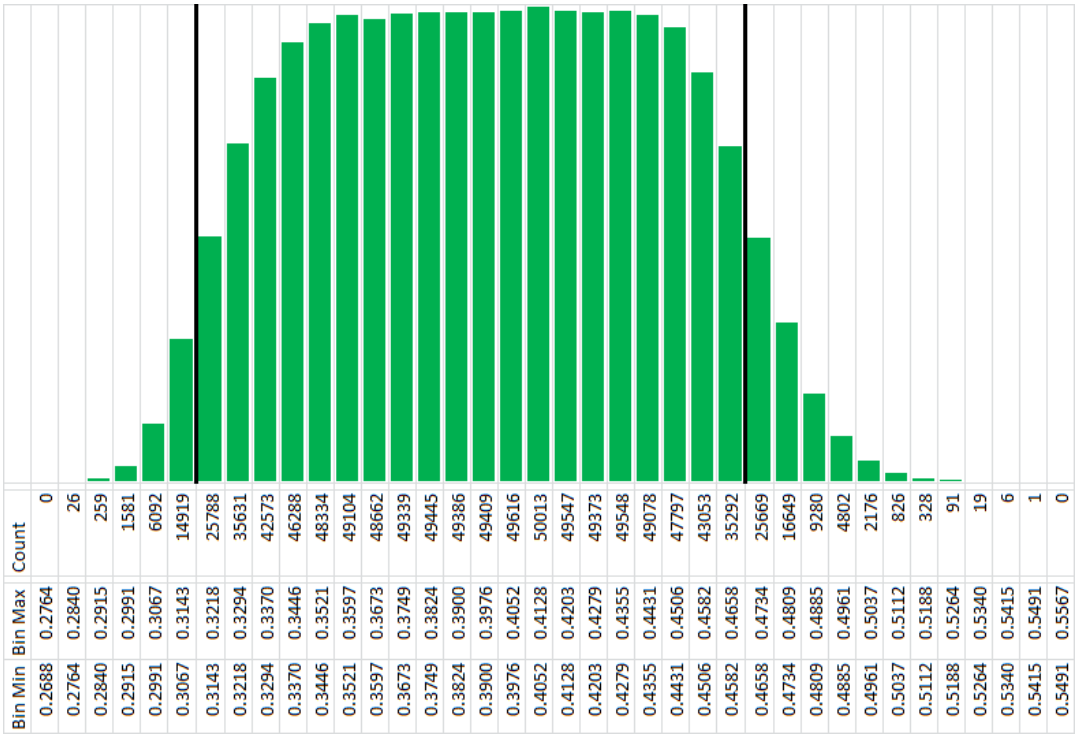

Bin Min	Bin Max	Count
0.2688	0.2764	0
0.2764	0.2840	26
0.2840	0.2915	259
0.2915	0.2991	1581
0.2991	0.3067	6092
0.3067	0.3143	14919
0.3143	0.3218	25788
0.3218	0.3294	35631
0.3294	0.3370	42573
0.3370	0.3446	46288
0.3446	0.3521	48334
0.3521	0.3597	49104
0.3597	0.3673	48662
0.3673	0.3749	49339
0.3749	0.3824	49445
0.3824	0.3900	49386
0.3900	0.3976	49409
0.3976	0.4052	49616
0.4052	0.4128	50013
0.4128	0.4203	49547
0.4203	0.4279	49373
0.4279	0.4355	49548
0.4355	0.4431	49078
0.4431	0.4506	47797
0.4506	0.4582	43053
0.4582	0.4658	35292
0.4658	0.4734	25669
0.4734	0.4809	16649
0.4809	0.4885	9280
0.4885	0.4961	4802
0.4961	0.5037	2176
0.5037	0.5112	826
0.5112	0.5188	328
0.5188	0.5264	91
0.5264	0.5340	19
0.5340	0.5415	6
0.5415	0.5491	1
0.5491	0.5567	0

Figure 4: Histogram of a 1,000,000 run Monte Carlo simulation with uniform inputs. The heavy black vertical bars represent the limits of the posterior probability as predicted by GIBR. The height of each bar represents the relative frequency, or count, of the Monte Carlo simulation's output falling within the bin denoted beneath the bar. The bins are inclusive of their respective lower bounds and exclusive of their upper bounds. For instance, $0.3143 \leq \boldsymbol{P}(\boldsymbol{\gamma}|\boldsymbol{\alpha}) < 0.3218$ **defines one of the bins; the simulation result fell in this bin 25,788 times.**

Aside from the obvious fact that the Monte Carlo simulation results exceed the interval limits at both the upper and lower bounds, there are other relevant measurements that can be gained from these results. The proposed interval of [0.3143,0.4658] is 57.19% of the width of the extreme limits of the Monte Carlo simulation, which were [0.2777,0.5426]. Of the million runs, however, 91.73% did fall within the [0.3143,0.4658] limits. Despite the lack of completeness, the proposed interval is at least sound. In this case, *soundness* denotes a solution that does not include any impossible values, whereas *completeness* denotes a solution that does not exclude any possible values. It is also worth noting that, with uniform input intervals, the distribution of the Monte Carlo simulation falls off sharply near the borders of the predicted posterior probability interval.

In an ideal situation, the wide intervals of an initial calculation should gradually be narrowed as more information is gained. In order to simulate this, the intervals in

Table 1 were replaced with intervals of half the width and the simulation was run again. The process was repeated with intervals one-quarter the width of the original, and finally with a real-valued equation. The intervals used are shown below in Table 2, and the results of the simulation are shown in Figure 5 and Figure 6.

Table 2: Assigned probability intervals that are narrower than the originally assigned intervals, and centered on the original intervals. The three rows shown in italics ($\beta 4_{\gamma}$, $\beta 4_{\gamma^C}$, and γ^C) were calculated using the Logic Coherence Constraint; all others were simply calculated as a proportion of the original arbitrary interval. The posterior probabilities are also shown and are each compared with the results of million-run MC simulations.

Symbol/Probability		Original Interval	Half-Width Interval	Quarter-Width Interval	Centered Real Value
$\alpha_{\beta 1}$	$\boldsymbol{P}(\alpha\|\beta 1)$	[0.3880,0.9973]	[0.5403,0.8450]	[0.6165,0.7688]	0.6927
$\alpha_{\beta 2}$	$\boldsymbol{P}(\alpha\|\beta 2)$	[0.7415,0.9024]	[0.7817,0.8622]	[0.8018,0.8421]	0.8220
$\alpha_{\beta 3}$	$\boldsymbol{P}(\alpha\|\beta 3)$	[0.3667,0.8688]	[0.4922,0.7433]	[0.5550,0.6805]	0.6178
$\alpha_{\beta 4}$	$\boldsymbol{P}(\alpha\|\beta 4)$	[0.1655,0.4140]	[0.2276,0.3519]	[0.2587,0.3208]	0.2898
$\beta 1_{\gamma}$	$\boldsymbol{P}(\beta 1\|\gamma)$	[0.1197,0.1826]	[0.1354,0.1669]	[0.1433,0.1590]	0.1512
$\beta 2_{\gamma}$	$\boldsymbol{P}(\beta 2\|\gamma)$	[0.1662,0.3080]	[0.2017,0.2726]	[0.2194,0.2548]	0.2371
$\beta 3_{\gamma}$	$\boldsymbol{P}(\beta 3\|\gamma)$	[0.3587,0.4603]	[0.3841,0.4349]	[0.3968,0.4222]	0.4095
$\beta 4_{\gamma}$	$\boldsymbol{P}(\beta 4\|\gamma)$	*[0.3554,0.0491]*	*[0.2788,0.1257]*	*[0.2405,0.1640]*	*0.2023*
$\beta 1_{\gamma^C}$	$\boldsymbol{P}(\beta 1\|\gamma^C)$	[0.0410,0.1930]	[0.0790,0.1550]	[0.0980,0.1360]	0.1170
$\beta 2_{\gamma^C}$	$\boldsymbol{P}(\beta 2\|\gamma^C)$	[0.1527,0.1772]	[0.1588,0.1711]	[0.1619,0.1680]	0.1650
$\beta 3_{\gamma^C}$	$\boldsymbol{P}(\beta 3\|\gamma^C)$	[0.3683,0.4682]	[0.3933,0.4432]	[0.4058,0.4307]	0.4183
$\beta 4_{\gamma^C}$	$\boldsymbol{P}(\beta 4\|\gamma^C)$	*[0.4380,0.1616]*	*[0.3689,0.2307]*	*[0.3344,0.2653]*	*0.2998*
γ	$\boldsymbol{P}(\gamma)$	[0.3000,0.4500]	[0.3375,0.4125]	[0.3563,0.3938]	0.3750
γ^C	$\boldsymbol{P}(\gamma^C)$	*[0.7000,0.5500]*	*[0.6625,0.5875]*	*[0.6438,0.6063]*	*0.6250*
Results					
Posterior: $\boldsymbol{P}(\gamma\|\alpha)$		[0.3143,0.4658]	[0.3565,0.4310]	[0.3761,0.4132]	0.3949
% of M.C. runs within output interval		91.73%	91.24%	91.05%	NA
Extreme values of M.C. simulation		[0.2777,0.5426]	[0.3352,0.4621]	[0.3655,0.4283]	NA
$\frac{\boldsymbol{P}(\gamma\|\alpha)}{M.C.Range}$%		57.19%	58.72%	59.06%	NA

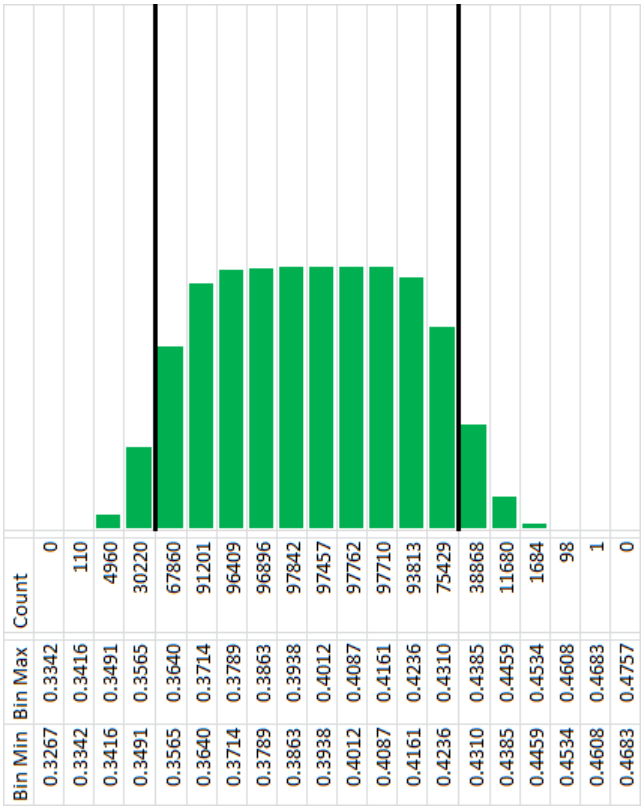

Bin Min	Bin Max	Count
0.3267	0.3342	0
0.3342	0.3416	110
0.3416	0.3491	4960
0.3491	0.3565	30220
0.3565	0.3640	67860
0.3640	0.3714	91201
0.3714	0.3789	96409
0.3789	0.3863	96896
0.3863	0.3938	97842
0.3938	0.4012	97457
0.4012	0.4087	97762
0.4087	0.4161	97710
0.4161	0.4236	93813
0.4236	0.4310	75429
0.4310	0.4385	38868
0.4385	0.4459	11680
0.4459	0.4534	1684
0.4534	0.4608	98
0.4608	0.4683	1
0.4683	0.4757	0

Figure 5: Histogram of 1,000,000 run Monte Carlo simulation with half-width interval inputs. The height of the data bars has been scaled to be consistent with Figure 6.

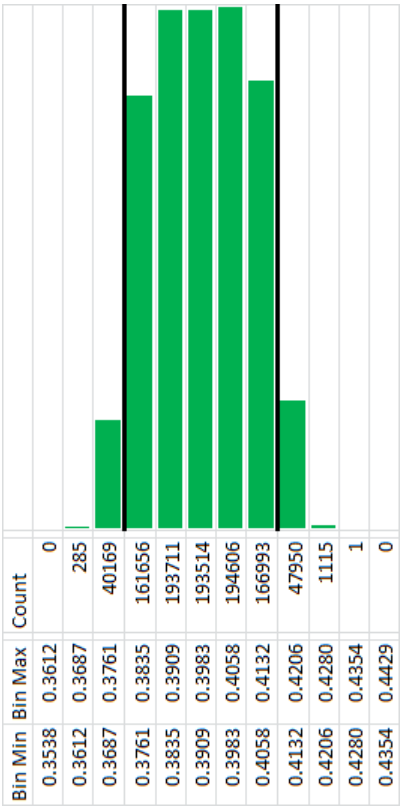

Bin Min	Bin Max	Count
0.3538	0.3612	0
0.3612	0.3687	285
0.3687	0.3761	40169
0.3761	0.3835	161656
0.3835	0.3909	193711
0.3909	0.3983	193514
0.3983	0.4058	194606
0.4058	0.4132	166993
0.4132	0.4206	47950
0.4206	0.4280	1115
0.4280	0.4354	1
0.4354	0.4429	0

Figure 6: Histogram of a 1,000,000 run Monte Carlo simulation with quarter-width inputs.

When the input intervals are narrowed about their respective centers, the output interval predictably does the same. The calculated real-valued posterior probability of 0.3949 is almost centered in each of the calculate interval posterior probabilities. All three simulations contained a similar percentage of the Monte Carlo simulation runs, and the comparison of Monte Carlo extreme values versus posterior probability interval was almost the same for all three cases, suggesting that the equation's predictive capability is scale independent. More importantly, it demonstrates that GIBR converges to classical Bayes' rule as the interval widths reduce. As the interval widths reduce, the completeness of interval range estimation also improves.

3.5.3.2: Normal Input Monte Carlo Simulation

For the second Monte Carlo verification simulation, the assigned input intervals in equation(9) were replaced with normally distributed random values based on their

bounds; the value for the complementary intervals was again determined by subtraction in order to comply with the Logic Coherence Constraint. The bounds of the assigned intervals were assumed to represent the ±3σ limits of a distribution centered at the average of the upper and lower bounds. As before, the resulting real-valued equation was then used to calculate a posterior probability. This process was repeated 1,000,000 times, using pseudo-random numbers generated by Microsoft Excel's "norm.inv()" function, with the "rand()" function as one of its inputs. A histogram and the corresponding count of the results is shown in Figure 7.

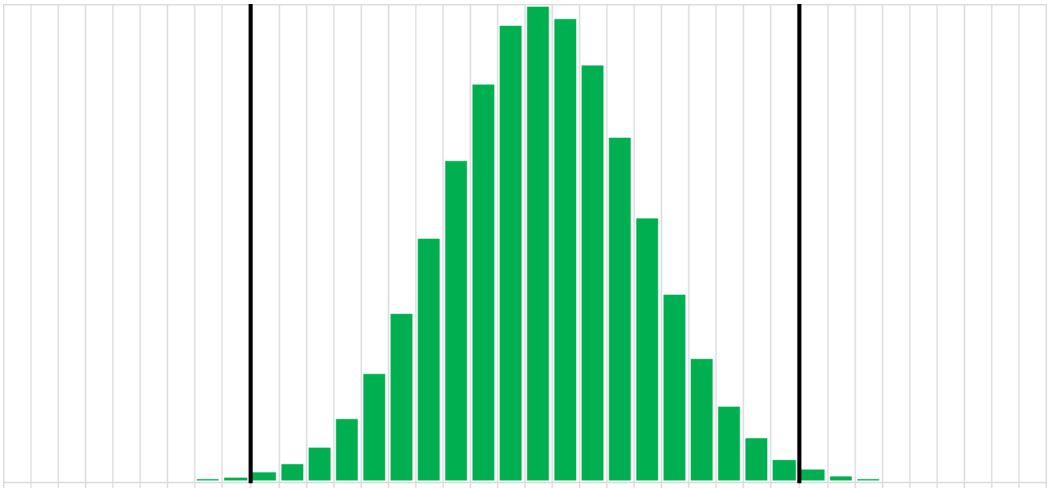

Bin Min	Bin Max	Count
0.2537	0.2612	0
0.2612	0.2688	2
0.2688	0.2764	1
0.2764	0.2840	6
0.2840	0.2915	41
0.2915	0.2991	108
0.2991	0.3067	321
0.3067	0.3143	785
0.3143	0.3218	1901
0.3218	0.3294	3993
0.3294	0.3370	7814
0.3370	0.3446	14537
0.3446	0.3521	25178
0.3521	0.3597	39401
0.3597	0.3673	57043
0.3673	0.3749	75653
0.3749	0.3824	93506
0.3824	0.3900	107623
0.3900	0.3976	112029
0.3976	0.4052	109276
0.4052	0.4128	98253
0.4128	0.4203	81169
0.4203	0.4279	62138
0.4279	0.4355	43919
0.4355	0.4431	28841
0.4431	0.4506	17461
0.4506	0.4582	9869
0.4582	0.4658	4945
0.4658	0.4734	2453
0.4734	0.4809	1104
0.4809	0.4885	403
0.4885	0.4961	150
0.4961	0.5037	52
0.5037	0.5112	15
0.5112	0.5188	9
0.5188	0.5264	1
0.5264	0.5340	0

Figure 7: Histogram of a 1,000,000 run Monte Carlo simulation with normal inputs. The bins are inclusive of their respective lower bounds and exclusive of their upper bounds.

As with the uniform input simulation, the results of the normal input simulation indicate that the proposed interval is sound but not complete. In this case, 99.45% of the million runs fell within the bounds of [0.3143,0.4658], and the proposed interval was 58.23% of the width of the extreme limits of the situation, which ranged from 0.2636 to an 0.5238. For this example, GIBR does provide a very good idea of where the results will be concentrated, both with uniformly distributed inputs and with normally distributed

inputs, which is the general goal of sensitivity analysis. It should be noticed that classical sensitivity analysis methods do not guarantee the completeness of range estimation either.

CHAPTER 4: AN APPLICATION OF THE METHOD IN SIMULATING DEFECT FORMATION

This chapter demonstrates an application of the method described in Chapter 3. A model, including the input parameters and other model characteristics, is referred to as θ. The model θ simulates the firing of an atom at BCC iron. It transfers some energy T during impact, where $T=T_m$ for a direct hit, or $T< T_m$ for a glancing blow. A defect (specifically a Frenkel Pair) may be formed due to this transfer of energy. The actual formation of a defect is probabilistic and dependent on several parameters and conditions. The purpose of the model θ is to simulate the formation of a defect. Physical evidence used to validate the model θ comes in the form of experiments measuring the resistivity change per defect, $\frac{\Delta\rho}{n}$, and the links between the two are the energy T_m of the incident particles and the damage threshold energy T_d.

This chapter focuses on the calculation of a posterior probability $\boldsymbol{P}\left(\theta\middle|\frac{\Delta\rho}{n}\right)$, where the prior probability that the model θ is correct ($\boldsymbol{P}(\theta)$) is updated using the physical evidence of experiments that measure $\frac{\Delta\rho}{n}$. Several obstacles make calculating the posterior probability difficult, and lead directly to the expanded form of GIBR. While the simulation looks at a single atom impacting a crystalline lattice, physical experiments must work on a larger scale—for example, a continual stream of atoms bombarding a polycrystalline sample. Because the original simulation looked at a single defect, evidence used to validate the simulation must be normalized by dividing by the number of defects. Scale discrepancies necessitate the use intermediate links in the probability updated and thus an expanded form of GIBR.

Atomic level defects (a single displaced atom and the void it leaves behind) are not directly measurable. However, the effects of a large number of defects are

measurable. For instance, as the number of defects (n) increases, the electrical resistivity ρ of the material increases by some amount Δρ. Similarly, as n increases, so does the volume of the material (the material actually expands as it is subject to radiation). This increase in volume is more easily measured in one dimension as an increase in length (Δℓ), and is rendered unitless by dividing by the original length (Δℓ/ℓ). Multiple calculation paths exist to bridge this gap of measurable versus simulated quantities, though, which leads to the use of interval probabilities.

4.1: Constructing the applied equation

Having derived the basic form of a GIBR equation, the next step is to translate it into an application. The starting point, equation (4), is repeated here for clarity:

$$P(D|A) = \frac{\int\int P(A|B)\cdot P(B|C)\cdot P(C|D)dB\,dC\cdot P(D)}{\int\int\int P(A|B)\cdot P(B|C)\cdot P(C|D)\cdot P(D)dB\,dC\,dD}$$

The goal of this equation development is to update a belief that the model θ accurately reflects reality given the information from experiments that measure a resistivity change per defect (Frenkel pair) in BCC iron. The actual parameters and variables that are applied to the equation are shown simply in Table 3.

Table 3: Parameters and variables used in the GIBR example.

Symbol	Explanation
$\boldsymbol{P}\left(\theta\middle\vert\frac{\Delta\rho}{n}\right)$	The calculated result: the probability that the model θ accurately represents reality, given the physical evidence of experiments measuring (Δρ/n).
$\boldsymbol{P}(\theta)$	The probability that the model θ accurately represents reality, given no other evidence.
$\boldsymbol{P}(T_d\vert\theta)$	The probability of finding a specific damage threshold T_d, given the model θ.
$\boldsymbol{P}(T_m\vert T_d)$	The probability of having a specific maximum possible level of transferred energy T_m (or of being struck by an incident electron having a specific energy) given a damage threshold T_d.
$\boldsymbol{P}\left(\frac{\Delta\rho}{n}\middle\vert T_m\right)$	The probability that damage causing a resistivity change Δρ/n occurs, given that incident particles have energy level T_m.

Once these terms are assembled into a cohesive equation, the result is as seen in equation (10). The calculation of the input interval values in this equation are given in the next section.

$$\boldsymbol{P}\left(\theta\middle|\frac{\Delta\rho}{\mathrm{n}}\right)=\frac{\int\int\left[\boldsymbol{P}\left(\frac{\Delta\rho}{\mathrm{n}}\middle|\mathrm{T_m}\right)\cdot\boldsymbol{P}(\mathrm{T_m}|\mathrm{T_d})\cdot\boldsymbol{P}(\mathrm{T_d}|\theta)\right]\mathrm{dT_d}\mathrm{dT_m}\cdot\boldsymbol{P}(\theta)}{dual\int\int\int\left[\boldsymbol{P}\left(\frac{\Delta\rho}{\mathrm{n}}\middle|\mathrm{T_m}\right)\cdot\boldsymbol{P}(\mathrm{T_m}|\mathrm{T_d})\cdot\boldsymbol{P}(\mathrm{T_d}|\theta)\cdot\boldsymbol{P}(\theta)\right]\mathrm{dT_d}\mathrm{dT_m}\mathrm{d}\theta} \qquad (10)$$

4.1.1: Calculations and assumptions for the input intervals

In assembling the probability chain used in the GIBR equation, the first "link" is the probability that the model θ accurately reflects reality. The shorthand used to represent this is $P(\theta)$ for a single value, or $\boldsymbol{P}(\theta)$ for an interval-valued probability. For this chapter's example, $\boldsymbol{P}(\theta)=[0.4,0.5]$ was used. The interval was based purely on intuition rather than on any mathematical derivation or numerical evidence. For the denominator of the GIBR, a set of mutually disjoint events is required, and so the Logic Coherence Constraint was used to find $\boldsymbol{P}(\theta^C)$, or the probability that the model θ does not accurately reflect reality. Quite simply, $\boldsymbol{P}(\theta^C)=1-dual\boldsymbol{P}(\theta)=[0.6,0.5]$.

A major simplification occurs with the introduction of a damage threshold $\mathrm{T_d}$. It is assumed that if the transferred energy is less than $\mathrm{T_d}$, then no damage occurs. Similarly, if the transferred energy is greater than or equal to $\mathrm{T_d}$, then damage occurs. $\mathrm{T_d}$ is found by interpreting the damage function ν of the transfer/ recoil energy T as a cumulative distribution function, or CDF. A smoothing algorithm is applied to the damage function to ensure that it is non-decreasing over its domain. This algorithm allows the generation of two limiting curves on the CDF, which in turn allows for interval-valued probabilities based on the chart.

To generate conditional probability $\boldsymbol{P}(\mathrm{T_d}|\theta)$, the value $\mathrm{T_d}$=70 eV was arbitrarily chosen. Using the CDF of the damage function of T, the upper and lower limits of the damage function then correspond to the upper and lower limits of the probability $\boldsymbol{P}(\mathrm{T_d}\leq 70|\theta)$; they are [0.7923,1.000]. The Logic Coherence Constraint again easily

allows the calculation of $\boldsymbol{P}(\mathrm{T_d} \geq 70|\theta)$, which is $[0.2077,0.000]$. This is also referred to as $\boldsymbol{P}(\mathrm{T_d^C}|\theta)$.

$\boldsymbol{P}(\mathrm{T_d}|\theta^{\mathrm{C}})$ is the probability of $\mathrm{T_d}$ taking some value when the model θ is not consulted. Of necessity this represents complete ignorance. The first choice for this probability is the interval $[0,1]$. Employing the Logic Coherence Constraint then gives $\boldsymbol{P}(\mathrm{T_d^C}|\theta^{\mathrm{C}}) = [1,0]$.

$\boldsymbol{P}(\mathrm{T_m}|\mathrm{T_d})$ is a more difficult example of complete ignorance. The subscript "m" stands for "maximum;" $\mathrm{T_m}$ is the maximum possible energy that can be transferred during a collision. It is also the energy of the incident particle striking the iron crystal in the simulation. The actual damage threshold should have no bearing on the energy of the incident particle, and so the intervals related to $\boldsymbol{P}(\mathrm{T_m}|\mathrm{T_d})$ should represent complete ignorance. The values used for $\boldsymbol{P}(\mathrm{T_m}|\mathrm{T_d})$ within this thesis are the same as those previously published for this application in (Tallman, Blumer, Wang, & McDowell, 2014); they represent the result of a misunderstanding of the meaning of the probabilities within the equation, and are preserved here only for the sake of consistency with the earlier published account. Rather than representing $\boldsymbol{P}(\mathrm{T_m}|\mathrm{T_d})$, the calculated probabilities are more correctly rendered as $\boldsymbol{P}(\mathrm{Damage}|\mathrm{T_m}, \mathrm{T_d})$, but the original notation is preserved here. Damage is impossible when the damage threshold is greater than the maximum possible transferred energy, and thus $\boldsymbol{P}(\mathrm{T_m} = 70|\mathrm{T_d} > 70) = [0,0]$. When the damage threshold is less than or equal to the maximum transferred energy, damage is possible but not certain, and thus $\boldsymbol{P}(\mathrm{T_m} = 70|\mathrm{T_d} \leq 70) = [0,1]$. When the maximum transferred energy is unknown but complementary (i.e. $\mathrm{T_m} \neq 70, \mathrm{T_m} \neq 100$), the probability of damage could be anywhere in the interval $[0,1]$, but the related probabilities were designated as non-focal because their conditions were complementary to the conditions where more was understood, and thus $\boldsymbol{P}(\mathrm{T_m} \neq 70, \mathrm{T_m} \neq 100|\mathrm{T_d} \leq 70) = [1,0]$ and $\boldsymbol{P}(\mathrm{T_m} \neq 70, T_m \neq 100|\mathrm{T_d} > 70) = [1,0]$. With these four probabilities in place, the

Logic Coherence Constraint dictated the final two probability intervals: $\boldsymbol{P}(\mathrm{T_m} = 100|\mathrm{T_d} \leq 70) = [0,0]$, and $\boldsymbol{P}(\mathrm{T_m} = 100|\mathrm{T_d} > 70) = [0,1]$. Calculating the $\boldsymbol{P}(\mathrm{T_m} = 100|\mathrm{T_d})$ intervals by subtraction with the LCC while designating the $\boldsymbol{P}(\mathrm{T_m} \neq 70, \mathrm{T_m} \neq 100|\mathrm{T_d})$ as non-focal and thus improper represents significantly flawed logic, and is only preserved here for consistency with the previously published account of this application. Once these errors in logic and in notation were found and understood, these probabilities were replaced with various improved representations of complete ignorance.

$\boldsymbol{P}\left(\frac{\Delta\rho}{\mathrm{n}}\middle|\mathrm{T_m}\right)$ is based on a physical experiment reported in (Vajda, 1977). Figure 26 of that paper shows the increases in both resistivity and displacement cross-section of radiation-damaged BCC iron in three directions. The <111> direction was selected for further analysis. By using the pixel-counting capabilities of Plot Digitizer 2.6.4 on an image of Figure 26, the data points shown in Table 4 were found. Using the curves' values at $\mathrm{T_m}$=20, 30, 45, 60, 70, 80, 100, and 130 eV to correlate between the graphs for σ and $\frac{\Delta\rho}{\mathrm{n}}$, a least-squares fit linear relationship between σ and $\frac{\Delta\rho}{\mathrm{n}}$ was calculated and is shown in equation (11). Using this equation, eight points on the calculated line were generated; these are shown in Table 5. For each of the eight values of $\mathrm{T_m}$ used to generate the line, the distance between the calculated and the actual values of σ and $\frac{\Delta\rho}{\mathrm{n}}$ was calculated. The average of these distances, 0.1536, was assumed to represent the possible error in the $\frac{\Delta\rho}{\mathrm{n}}$ measurements; the values of $\frac{\Delta\rho}{\mathrm{n}}$ found in Figure 26a were assumed to be the center of a uniform distribution of values with the range $\frac{\Delta\rho}{\mathrm{n}} \pm 0.1536$.

Table 4: Corresponding values of T_m, σ, and $\frac{\Delta\rho}{n}$ from Figure 26 in (Vajda, 1977).

T_m, eV	20	30	45	60	70	80	100	130
σ, barns	0.8667	9.605	17.63	24.21	29.08	33.29	39.21	46.32
$\frac{\Delta\rho}{n}$, $\frac{\Omega\cdot cm\times 10^{-26}}{e^-/cm^2}$	0.4082	2.897	5.794	7.857	9.405	10.91	13.02	15.75

$$\frac{\Delta\rho}{n} = 0.3370\sigma - 0.1775 \qquad (11)$$

Table 5: Values for σ and $\frac{\Delta\rho}{n}$ based on a least-squares linear fit, with corresponding values for T_m.

T_m, eV	20	30	45	60	70	80	100	130
σ, barns	0.9555	9.556	17.64	24.17	29.01	33.25	39.20	46.41
$\frac{\Delta\rho}{n}$, $\frac{\Omega\cdot cm\times 10^{-26}}{e^-/cm^2}$	0.1444	3.043	5.767	7.968	9.599	11.03	13.03	15.46

Table 6: Range of values for $\frac{\Delta\rho}{n}$ based the average error of the measured versus calculated values.

1	T_m, eV	20	30	45	60	70	80	100	130
2	$\frac{\Delta\rho}{n}$, min	0.2546	2.743	5.640	7.704	9.251	10.76	12.86	15.60
3	$\frac{\Delta\rho}{n}$, max	0.5618	3.050	5.947	8.011	9.558	11.07	13.17	15.91
4	$\boldsymbol{P}\left(\frac{\Delta\rho}{n} \le 9.4048 \middle\vert T_m\right)$, assuming a uniform distribution	[1,1]	[1,1]	[1,1]	[1,1]	[0.5,0.5]	[0,0]	[0,0]	[0,0]
5	standard deviation of $\frac{\Delta\rho}{n}$,	0.1831	0.3535	1.159	0.2248	0.5850	0.5072	0.9281	1.150
6	$\boldsymbol{P}\left(\frac{\Delta\rho}{n} \le 9.4048 \middle\vert T_m\right)$, assuming either of two normal distributions centered at the min (line 2) or the max (line 3), with standard deviation from line 5.	[1.000, 1.000]	[1.000, 1.000]	[0.9986, 0.9994]	[1.000, 1.000]	[0.3965, 0.6036]	[0.0005, 0.0038]	[0.0000, 0.0001]	[0.0000, 0.0000]

Once a distribution was assumed for each value of $\frac{\Delta\rho}{n}$, the calculation of an interval for $\boldsymbol{P}\left(\frac{\Delta\rho}{n}\middle|T_m\right)$ was relatively straightforward. 9.4048 (Ω•cm×10^{-26})/(e^{-}/cm^2) was chosen for comparison because it is the measured value for $\frac{\Delta\rho}{n}$ corresponding to $T_m = 70eV$, and therefore falls at the halfway point for the range of $\frac{\Delta\rho}{n}$ for that value of T_m. As such, the interval for $\boldsymbol{P}\left(\frac{\Delta\rho}{n} \leq 9.4048\middle|T_m = 70\right) = [0.5,0.5]$. The range of values for $\frac{\Delta\rho}{n}$ corresponding to $T_m = 100eV$ is 12.8623 to 13.1695; 9.4048 is below the lower bound of this range, and so $\boldsymbol{P}\left(\frac{\Delta\rho}{n} \leq 9.4048\middle|T_m = 100\right) = [0,0]$. This method, while simple, only calculates a single value and results in zero-width intervals. The probabilities for $\frac{\Delta\rho}{n}$ given each level of T_m using this method are shown in line 4 of Table 6.

A different method was used to calculate the value of $\boldsymbol{P}\left(\frac{\Delta\rho}{n} \leq 9.4048\middle|\begin{matrix}T_m \neq 70\\T_m \neq 100\end{matrix}\right)$. While the purest interpretation of the method would likely express this probability as pure ignorance with $[0,1]$, it was desired that a narrower interval be obtained for the sake of testing the capabilities of the equations. At this point, it was realized that Figure 26a from (Vajda, 1977) was generated using measurements that were clearly delineated in Figure 1c of (Maury, Biget, Vajda, Lucasson, & Lucasson, 1976). Using Plot Digitizer 2.6.4 on an image of Figure 1c, the values of each discrete measurement of $\frac{\Delta\rho}{n}$ at the stratified values of T_m were measured, giving a standard deviation for $\frac{\Delta\rho}{n}$ at each level of T_m; these appear in line 5 of Table 6. In order to obtain intervals wider than a single point, two distributions were assumed for each value of T_m: one was normally distributed with a mean at the minimum level of $\frac{\Delta\rho}{n}$ (line 2 of Table 6), and the other was normally distributed with a mean at the maximum level of $\frac{\Delta\rho}{n}$ (line 3 of

the same table). Using these two distributions, it was possible to generate an interval for $\boldsymbol{P}\left(\frac{\Delta\rho}{n} \leq 9.4048 \middle| T_m\right)$; this is shown in line 6 of Table 6.

Even with these interval probabilities, further assumptions were necessary to generate an interval value for $\boldsymbol{P}\left(\frac{\Delta\rho}{n} \leq 9.4048 \middle| \begin{matrix} T_m \neq 70 \\ T_m \neq 100 \end{matrix}\right)$. This probability can be more properly written as $\boldsymbol{P}\left(\frac{\Delta\rho}{n} \leq 9.4048 \middle| \begin{matrix} T_m \neq 70 \ldots \\ \cap\, T_m \neq 100 \end{matrix}\right)$, and using the fact that $P(A|B) = \frac{P(A \cap B)}{P(B)}$, it can also be expressed as:

$$\boldsymbol{P}\left(\frac{\Delta\rho}{n} \leq 9.4048 \middle| \begin{matrix} T_m \neq 70 \\ T_m \neq 100 \end{matrix}\right) = \frac{\boldsymbol{P}\left(\frac{\Delta\rho}{n} \leq 9.4048 \cap \left(\begin{matrix} T_m \neq 70 \ldots \\ \cap\, T_m \neq 100 \end{matrix}\right)\right)}{dual\boldsymbol{P}\left(\begin{matrix} T_m \neq 70 \ldots \\ \cap\, T_m \neq 100 \end{matrix}\right)}$$

As this derivation progresses, $\left(\frac{\Delta\rho}{n} \leq 9.4048\right)$ will be replaced with $\frac{\Delta\rho}{\mathrm{n}}$ for the sake of compactness. It was assumed that T_m could only take on one of the eight values at which the figures in (Vajda, 1977) and (Maury, Biget, Vajda, Lucasson, & Lucasson, 1976) had been measured. This is reasonable only because T_m is specified as an input to the model θ and values occur without variability. Because of this assumption, $\boldsymbol{P}\left(\frac{\Delta\rho}{n} \middle| \begin{matrix} T_m \neq 70 \\ T_m \neq 100 \end{matrix}\right)$ can also be expressed as:

$$\boldsymbol{P}\left(\frac{\Delta\rho}{\mathrm{n}} \middle| \begin{matrix} T_m \neq 70 \\ T_m \neq 100 \end{matrix}\right) = \frac{\boldsymbol{P}\left(\frac{\Delta\rho}{\mathrm{n}} \cap \left(\begin{matrix} T_m = 20 \cup T_m = 30 \cup T_m = 45 \ldots \\ \ldots \cup T_m = 60 \cup T_m = 80 \cup T_m = 130 \end{matrix}\right)\right)}{dual\boldsymbol{P}\left(\begin{matrix} T_m = 20 \cup T_m = 30 \cup T_m = 45 \ldots \\ \ldots \cup T_m = 60 \cup T_m = 80 \cup T_m = 130 \end{matrix}\right)}$$

Each value of T_m is mutually exclusive of the other values, and so the equation can be further re-written as:

$$\boldsymbol{P}\left(\frac{\Delta\rho}{\mathrm{n}}\middle|\begin{matrix}T_m\neq 70\\ T_m\neq 100\end{matrix}\right)=\frac{\begin{pmatrix}\boldsymbol{P}\left(\frac{\Delta\rho}{\mathrm{n}}\cap T_m=20\right)+\boldsymbol{P}\left(\frac{\Delta\rho}{\mathrm{n}}\cap T_m=30\right)\ldots\\ \ldots+\boldsymbol{P}\left(\frac{\Delta\rho}{\mathrm{n}}\cap T_m=45\right)+\boldsymbol{P}\left(\frac{\Delta\rho}{\mathrm{n}}\cap T_m=60\right)\ldots\\ \ldots+\boldsymbol{P}\left(\frac{\Delta\rho}{\mathrm{n}}\cap T_m=80\right)+\boldsymbol{P}\left(\frac{\Delta\rho}{\mathrm{n}}\cap T_m=130\right)\end{pmatrix}}{dual\begin{pmatrix}\boldsymbol{P}(T_m=20)+\boldsymbol{P}(T_m=30)+\boldsymbol{P}(T_m=45)\ldots\\ \ldots+\boldsymbol{P}(T_m=60)+\boldsymbol{P}(T_m=80)+\boldsymbol{P}(T_m=130)\end{pmatrix}}$$

Because $P(A\cap B)=P(A|B)P(B)$, the equation can then be expressed as:

$$\boldsymbol{P}\left(\frac{\Delta\rho}{\mathrm{n}}\middle|\begin{matrix}T_m\neq 70\\ T_m\neq 100\end{matrix}\right)=\frac{\begin{pmatrix}\boldsymbol{P}\left(\frac{\Delta\rho}{\mathrm{n}}\middle|T_m=20\right)\boldsymbol{P}(T_m=20)\ldots\\ +\boldsymbol{P}\left(\frac{\Delta\rho}{\mathrm{n}}\middle|T_m=30\right)\boldsymbol{P}(T_m=30)\ldots\\ +\boldsymbol{P}\left(\frac{\Delta\rho}{\mathrm{n}}\middle|T_m=45\right)\boldsymbol{P}(T_m=45)\ldots\\ +\boldsymbol{P}\left(\frac{\Delta\rho}{\mathrm{n}}\middle|T_m=60\right)\boldsymbol{P}(T_m=60)\ldots\\ +\boldsymbol{P}\left(\frac{\Delta\rho}{\mathrm{n}}\middle|T_m=80\right)\boldsymbol{P}(T_m=80)\ldots\\ +\boldsymbol{P}\left(\frac{\Delta\rho}{\mathrm{n}}\middle|T_m=130\right)\boldsymbol{P}(T_m=130)\end{pmatrix}}{dual\begin{pmatrix}\boldsymbol{P}(T_m=20)+\boldsymbol{P}(T_m=30)+\boldsymbol{P}(T_m=45)\ldots\\ \ldots+\boldsymbol{P}(T_m=60)+\boldsymbol{P}(T_m=80)+\boldsymbol{P}(T_m=130)\end{pmatrix}}$$

A further assumption was made that $\mathrm{T_m}$ would be uniformly distributed among the eight possible values, and so $\boldsymbol{P}(T_m)=\left[\frac{1}{8},\frac{1}{8}\right]\forall T_m$. Because this is a zero-width interval, it can also be given as a single value with no loss of information, and the *dual* operator can be left out of the denominator. This assumption simplifies the equation to:

$$\boldsymbol{P}\left(\frac{\Delta\rho}{\mathrm{n}}\middle|\begin{matrix}T_m\neq 70\\ T_m\neq 100\end{matrix}\right)=\frac{\begin{pmatrix}\boldsymbol{P}\left(\frac{\Delta\rho}{\mathrm{n}}\middle|T_m=20\right)\cdot\frac{1}{8}+\boldsymbol{P}\left(\frac{\Delta\rho}{\mathrm{n}}\middle|T_m=30\right)\cdot\frac{1}{8}\ldots\\ \ldots+\boldsymbol{P}\left(\frac{\Delta\rho}{\mathrm{n}}\middle|T_m=45\right)\cdot\frac{1}{8}+\boldsymbol{P}\left(\frac{\Delta\rho}{\mathrm{n}}\middle|T_m=60\right)\cdot\frac{1}{8}\ldots\\ \ldots+\boldsymbol{P}\left(\frac{\Delta\rho}{\mathrm{n}}\middle|T_m=80\right)\cdot\frac{1}{8}+\boldsymbol{P}\left(\frac{\Delta\rho}{\mathrm{n}}\middle|T_m=130\right)\cdot\frac{1}{8}\end{pmatrix}}{\frac{1}{8}+\frac{1}{8}+\frac{1}{8}+\frac{1}{8}+\frac{1}{8}+\frac{1}{8}}$$

$$\boldsymbol{P}\left(\frac{\Delta\rho}{\mathrm{n}}\middle|\begin{matrix}T_m \neq 70\\ T_m \neq 100\end{matrix}\right)=\frac{1}{6}\begin{pmatrix}\boldsymbol{P}\left(\frac{\Delta\rho}{\mathrm{n}}\middle|T_m=20\right)+\boldsymbol{P}\left(\frac{\Delta\rho}{\mathrm{n}}\middle|T_m=30\right)\ldots\\ \ldots+\boldsymbol{P}\left(\frac{\Delta\rho}{\mathrm{n}}\middle|T_m=45\right)+\boldsymbol{P}\left(\frac{\Delta\rho}{\mathrm{n}}\middle|T_m=60\right)\ldots\\ \ldots+\boldsymbol{P}\left(\frac{\Delta\rho}{\mathrm{n}}\middle|T_m=80\right)+\boldsymbol{P}\left(\frac{\Delta\rho}{\mathrm{n}}\middle|T_m=130\right)\end{pmatrix}$$

This formulation is equal to an average of the six probabilities calculated above, and is permissible only with the given assumptions. Finally, using the values for each of these probabilities that are given in line 6 of Table 6, $\boldsymbol{P}\left(\frac{\Delta\rho}{\mathrm{n}}\middle|\begin{matrix}T_m \neq 70\\ T_m \neq 100\end{matrix}\right)$ can be calculated as [0.6665,0.6672].

4.1.2: Updating to find a posterior probability

Because of the lengthy nature of the GIBR equations, it is necessary to employ a shorthand notation in order to fit a fully developed equation in a standard-sized document. This shorthand is explained in Table 7. Table 7 also contains a summary of the values of the input intervals.

Table 7: Explanation of shorthand symbols.

Symbol	Interval Value	Explanation
$\boldsymbol{P}\left(\theta\middle\|\frac{\Delta\rho}{\mathrm{n}}\right)$	[0.4,0.5]	The calculated result: the probability that the model θ accurately represents reality, given the physical evidence of experiments measuring (Δρ/n).
ρ_{Tm1}	[0.5,0.5]	The probability that $\Delta\rho/n \leq 9.4048\ \Omega\cdot cm\times10^{-26}/(e^-/cm^2)$ given that T_m=70eV.
ρ_{Tm2}	[0,0]	The probability that $\Delta\rho/n \leq 9.4048\ \Omega\cdot cm\times10^{-26}/(e^-/cm^2)$ given that T_m=100eV.
ρ_{Tm3}	[0.6665,0.6672]	The probability that $\Delta\rho/n \leq 9.4048\ \Omega\cdot cm\times10^{-26}/(e^-/cm^2)$ given that T_m is neither 70eV nor 100eV.
$Tm1_{Td}$	[0,1]	The probability that the maximum possible transferred energy (or energy of the incident particle) T_m=70eV, given that the damage threshold $T_d \leq$70eV.
$Tm2_{Td}$	[0,0]	The probability that the maximum possible transferred energy (or energy of the incident particle) T_m=100eV, given that the damage threshold $T_d \leq$70eV.

Symbol	Interval Value	Explanation
$Tm3_{Td}$	[1,0]	The probability that the maximum possible transferred energy (or energy of the incident particle) T_m is neither 70eV nor 100eV, given that the damage threshold T_d ≤70eV.
$Tm1_{Td^c}$	[0,0]	The probability that the maximum possible transferred energy (or energy of the incident particle) T_m=70eV, given that the damage threshold T_d >70eV.
$Tm2_{Td^c}$	[0,1]	The probability that the maximum possible transferred energy (or energy of the incident particle) T_m=100eV, given that the damage threshold T_d >70eV.
$Tm3_{Td^c}$	[1,0]	The probability that the maximum possible transferred energy (or energy of the incident particle) T_m is neither 70eV nor 100eV, given that the damage threshold T_d >70eV.
Td_θ	[0.7923,1]	The probability that the damage threshold T_d ≤70eV, given that the model θ is accurate.
Td_θ^c	[0.2077,0]	The probability that the damage threshold T_d >70eV, given that the model θ is accurate.
Td_{θ^c}	[0,1]	The probability that the damage threshold T_d≤70eV, given that the model θ is *not* accurate.
$Td_{\theta^c}^c$	[1,0]	The probability that the damage threshold T_d >70eV, given that the model θ is *not* accurate.
θ	[0.4,0.5]	The initial probability that the model θ accurately represents reality, given no other evidence.
θ^c	[0.6,0.5]	The initial probability that the model θ *does not* accurately represent reality, given no other evidence.

Using the shorthand notation, equation (10) becomes:

$$\boldsymbol{P}\left(\theta\middle|\frac{\Delta\rho}{n}\right)=\frac{[\rho_{Tm1}\quad\rho_{Tm2}\quad\rho_{Tm3}]\begin{bmatrix}Tm1_{Td} & Tm1_{Td^c}\\ Tm2_{Td} & Tm2_{Td^c}\\ Tm3_{Td} & Tm3_{Td^c}\end{bmatrix}\begin{bmatrix}Td_\theta\\ Td_\theta^c\end{bmatrix}\theta}{dual\left([\rho_{Tm1}\quad\rho_{Tm2}\quad\rho_{Tm3}]\begin{bmatrix}Tm1_{Td} & Tm1_{Td^c}\\ Tm2_{Td} & Tm2_{Td^c}\\ Tm3_{Td} & Tm3_{Td^c}\end{bmatrix}\begin{bmatrix}Td_\theta & Td_{\theta^c}\\ Td_\theta^c & Td_{\theta^c}^c\end{bmatrix}\begin{bmatrix}\theta\\ \theta^c\end{bmatrix}\right)} \qquad (12)$$

For the sake of completeness in explanation, the posterior probability calculation is explicitly shown here. First, the intervals are substituted in for their respective variable names in equation (12), resulting in equation (13).

$$\boldsymbol{P}\left(\theta\middle|\frac{\Delta\rho}{\mathrm{n}}\right)=\frac{[[0.5,0.5]\quad[0,0]\quad[0.6665,0.6672]]\begin{bmatrix}[0,1] & [0,0]\\ [0,0] & [0,1]\\ [1,0] & [1,0]\end{bmatrix}\begin{bmatrix}[0.7923,1]\\ [0.2077,0]\end{bmatrix}[0.4,0.5]}{dual\left([[0.5,0.5]\quad[0,0]\quad[0.6665,0.6672]]\begin{bmatrix}[0,1] & [0,0]\\ [0,0] & [0,1]\\ [1,0] & [1,0]\end{bmatrix}\begin{bmatrix}[0.7923,1] & [0,1]\\ [0.2077,0] & [1,0]\end{bmatrix}\begin{bmatrix}[0.4,0.5]\\ [0.6,0.5]\end{bmatrix}\right)} \quad (13)$$

The lower bound of the posterior probability is calculated by using the lower bound of each input interval, as shown in the following equation:

$$\underline{\boldsymbol{P}}\left(\theta\middle|\frac{\Delta\rho}{\mathrm{n}}\right)=\frac{[0.5\quad 0\quad 0.6665]\begin{bmatrix}0 & 0\\ 0 & 0\\ 1 & 1\end{bmatrix}\begin{bmatrix}0.7923\\ 0.2077\end{bmatrix}0.4}{[0.5\quad 0\quad 0.6665]\begin{bmatrix}0 & 0\\ 0 & 0\\ 1 & 1\end{bmatrix}\begin{bmatrix}0.7923 & 0\\ 0.2077 & 1\end{bmatrix}\begin{bmatrix}0.4\\ 0.6\end{bmatrix}}=0.4$$

Likewise, the upper bound of the posterior probability is calculated by using the upper bound of each input interval, as follows:

$$\overline{\boldsymbol{P}}\left(\theta\middle|\frac{\Delta\rho}{\mathrm{n}}\right)=\frac{[0.5\quad 0\quad 0.6672]\begin{bmatrix}1 & 0\\ 0 & 1\\ 0 & 0\end{bmatrix}\begin{bmatrix}1\\ 0\end{bmatrix}0.5}{[0.5\quad 0\quad 0.6672]\begin{bmatrix}1 & 0\\ 0 & 1\\ 0 & 0\end{bmatrix}\begin{bmatrix}1 & 1\\ 0 & 0\end{bmatrix}\begin{bmatrix}0.5\\ 0.5\end{bmatrix}}=0.5$$

Thus, the posterior probability interval is [0.4,0.5]. This value is identical to the prior probability, and is a result of the representation of complete ignorance found in the $(Tm|Td)$ terms. As equation (12) represents a chain of probabilities, ignorance in the middle terms can be thought of as a missing link. When the connection between levels of information is missing, no evidence can get through to update the posterior probability. While this thesis endeavors to find a method for expressing complete ignorance that allows some information updating to occur, researchers would do well to be cautious when using GIBR in cases where complete ignorance is present. This is no surprise, as total ignorance is a challenge in all forms of probability analysis. More important, though, is the negative impact of applying the Logic Coherence Constraint in the presence of complete ignorance, which forces the presence of one proper interval [0,1],

one improper interval $[1,0]$, and one point interval $[0,0]$. This will be further examined in §4.4.2 and in §4.5.

4.2: Incorporating Multiple Sources of Information

A large part of the value of Bayesian updating is the ability to incorporate information from multiple sources. In this case, experimental results were also obtained for change in length per defect in BCC iron. Because both changes are used to update a belief in the same model θ, equation (10) can be modified to incorporate both the information for change in resistivity and the information for change in length:

$$\boldsymbol{P}\left(\theta\middle|\frac{\Delta\rho}{\mathrm{n}}\cap\frac{\Delta\ell/\ell}{n}\right)=\frac{\int\int\left[\boldsymbol{P}\left(\frac{\Delta\rho}{\mathrm{n}}\cap\frac{\Delta\ell/\ell}{n}\middle|\mathrm{T_m}\right)\cdot\boldsymbol{P}(\mathrm{T_m}|\mathrm{T_d})\cdot\boldsymbol{P}(\mathrm{T_d}|\theta)\right]\mathrm{dT_d}\,\mathrm{dT_m}\cdot\boldsymbol{P}(\theta)}{dual\int\int\int\left[\boldsymbol{P}\left(\frac{\Delta\rho}{\mathrm{n}}\cap\frac{\Delta\ell/\ell}{n}\middle|\mathrm{T_m}\right)\cdot\boldsymbol{P}(\mathrm{T_m}|\mathrm{T_d})\cdot\boldsymbol{P}(\mathrm{T_d}|\theta)\cdot\boldsymbol{P}(\theta)\right]\mathrm{dT_d}\,\mathrm{dT_m}\,\mathrm{d}\theta} \qquad (14)$$

The measurements for length change are not coupled from the measurements for resistivity change; indeed, it would be extremely difficult to measure these simultaneously. Because of this, it can be assumed that $\boldsymbol{P}\left(\frac{\Delta\rho}{\mathrm{n}}\middle|T_m\right)$ and $\boldsymbol{P}\left(\frac{\Delta\ell/\ell}{n}\middle|T_m\right)$ are independent. Incorporating this assumption into equation (14) gives the following:

$$\boldsymbol{P}\left(\theta\middle|\frac{\Delta\rho}{\mathrm{n}}\cap\frac{\Delta\ell/\ell}{n}\right)=\frac{\int\int\left[\boldsymbol{P}\left(\frac{\Delta\rho}{\mathrm{n}}\middle|\mathrm{T_m}\right)\cdot\boldsymbol{P}\left(\frac{\Delta\ell/\ell}{n}\middle|\mathrm{T_m}\right)\cdot\boldsymbol{P}(\mathrm{T_m}|\mathrm{T_d})\cdot\boldsymbol{P}(\mathrm{T_d}|\theta)\right]\mathrm{dT_d}\,\mathrm{dT_m}\cdot\boldsymbol{P}(\theta)}{dual\int\int\int\left[\boldsymbol{P}\left(\frac{\Delta\rho}{\mathrm{n}}\middle|\mathrm{T_m}\right)\cdot\boldsymbol{P}\left(\frac{\Delta\ell/\ell}{n}\middle|\mathrm{T_m}\right)\cdot\boldsymbol{P}(\mathrm{T_m}|\mathrm{T_d})\cdot\boldsymbol{P}(\mathrm{T_d}|\theta)\cdot\boldsymbol{P}(\theta)\right]\mathrm{dT_d}\,\mathrm{dT_m}\,\mathrm{d}\theta} \qquad (15)$$

Integrating this equation and decomposing it into a multiplied-matrix format gives:

$$\boldsymbol{P}\left(\theta\middle|\frac{\Delta\rho}{\mathrm{n}}\cap\frac{\Delta\ell/\ell}{n}\right)=\frac{\begin{bmatrix}\ell_{Tm1}\cdot\rho_{Tm1}\\ \ell_{Tm2}\cdot\rho_{Tm2}\\ \ell_{Tm3}\cdot\rho_{Tm3}\end{bmatrix}^{T}\begin{bmatrix}Tm1_{Td} & Tm1_{Td^c}\\ Tm2_{Td} & Tm2_{Td^c}\\ Tm3_{Td} & Tm3_{Td^c}\end{bmatrix}\begin{bmatrix}Td_\theta\\ Td_\theta^c\end{bmatrix}\theta}{dual\left(\begin{bmatrix}\ell_{Tm1}\cdot\rho_{Tm1}\\ \ell_{Tm2}\cdot\rho_{Tm2}\\ \ell_{Tm3}\cdot\rho_{Tm3}\end{bmatrix}^{T}\begin{bmatrix}Tm1_{Td} & Tm1_{Td^c}\\ Tm2_{Td} & Tm2_{Td^c}\\ Tm3_{Td} & Tm3_{Td^c}\end{bmatrix}\begin{bmatrix}Td_\theta & Td_{\theta^c}\\ Td_\theta^c & Td_{\theta^c}^c\end{bmatrix}\begin{bmatrix}\theta\\ \theta^c\end{bmatrix}\right)} \qquad (16)$$

The leading matrix has been transposed in both the numerator and the denominator of the equation in order to conserve space. Note that equation (16) only differs from equation (12) in that each ρ term has been multiplied by an ℓ term.

Without any shorthand, the three intervals that must be determined are $\boldsymbol{P}\left(\frac{\Delta\ell/\ell}{n} \leq 15 \middle| T_m = 70\right)$, $\boldsymbol{P}\left(\frac{\Delta\ell/\ell}{n} \leq 15 \middle| T_m = 100\right)$, and $\boldsymbol{P}\left(\frac{\Delta\ell/\ell}{n} \leq 15 \middle| \begin{matrix} T_m \neq 70 \\ T_m \neq 100 \end{matrix}\right)$, where T_m is measured in eV, $\Delta\ell/\ell$ is unitless, and n is measured in e^-/cm^2. The comparison point of $\frac{\Delta\ell/\ell}{n} \leq 15\,\frac{cm^2\times10^{-2}}{e^-}$ was chosen arbitrarily.

To demonstrate the process, the calculation of the interval for $\boldsymbol{P}\left(\frac{\Delta\ell/\ell}{n} \leq 15 \middle| T_m = 70\right)$ is shown. (Dunlop & Lesueur, 1989) determined a Frenkel Pair Formation Volume for iron (ν_{Fe}) of 1.35 ± 0.25; the value is found both in the abstract an in Table IV on page 347 of that paper. Equation (2) of the same paper notes that for isotropic crystals (including BCC iron), Frenkel Pair Formation Volume is related to changing length by $\nu = \frac{3(\Delta\ell/\ell)}{c}$, where c is the defect concentration or number of defects (the same as n in (Vajda, 1977)). Substituting in 1.35 ± 0.25 for ν in that equation and solving for the length change to defect concentration ratio gives $\frac{(\Delta\ell/\ell)}{c} = \frac{1.35\pm0.25}{3}$ (units $\frac{1}{e^-}$) or [0.367,0.533] as a range for $\frac{(\Delta\ell/\ell)}{c}$. In order to phrase this value in terms that are compatible with the GIBR equation, a relationship between length change and energy level T_m must be determined.

Radiation-induced swelling is based on the number of defects formed, which, in turn, is based on the displacement cross section. Displacement cross section is not based alone on the material being irradiated, but upon the material and the energy level of the incident radiation. As such, the displacement cross section is the necessary link between $\frac{(\Delta\ell/\ell)}{c}$ and T_m. Examining the <111> line on Figure 26b of (Vajda, 1977) gives a

displacement cross section of σ=29.08 barns ($cm^2 \times 10^{-24}$) when $T_m = 70eV$. From there, a simple multiplication gives a range of possible values for $\frac{(\Delta\ell/\ell)}{n}$:

$$\left([0.367,0.533]\frac{1}{e^-}\right) \times (29.08cm^2 \times 10^{-24}) = [10.66,15.51]\frac{cm^2 \times 10^{-24}}{e^-}$$

The bounds $[10.66,15.51]$ were assumed to represent the upper and lower limits of a 95% confidence interval for a normal distribution, which means that the distribution has a standard deviation of 1.24 and a mean of 13.09. Given this normal distribution, $P\left(\frac{\Delta\ell/\ell}{n} \leq 15 \middle| T_m = 70\right) = 94\%$. This is one of the bounds of $\boldsymbol{P}\left(\frac{\Delta\ell/\ell}{n} \leq 15 \middle| T_m = 70\right)$; whether this is the upper or the lower bound depends on the value for $P\left(\frac{\Delta\ell/\ell}{n} \leq 15 \middle| T_m = 70\right)$ that is found through another calculation path.

For the second probability, Figure 26a of (Vajda, 1977), was consulted. $T_m = 70eV$ on that figure corresponds to a value of $\frac{\Delta\rho}{n} = 9.40\frac{\Omega \cdot cm \times 10^{-26}}{e^-/cm^2}$. Table IV on page 347 of (Dunlop & Lesueur, 1989) gives the range $260 \pm 30\frac{1}{\Omega \cdot cm}$ (or [230,290]) for the ratio $\left(\frac{\Delta\ell/\ell}{\Delta\rho}\right)$. However, Figure 26 also resulted in $\rho_F = 30\Omega \cdot cm \cdot 10^{-4}$, whereas (Dunlop & Lesueur, 1989) used $\rho_F = 1700\Omega \cdot cm \cdot 10^{-6}$. A scaling change must be used in order to make the results compatible. For the sake of consistency, $30\Omega \cdot cm \cdot 10^{-4}$ is instead rendered as $3000\Omega \cdot cm \cdot 10^{-6}$, and the entire equation conversion is multiplied by 1 in the form of $\frac{0.01 \times 10^{-24}}{10^{-26}}$. Combining all of this results in the following equation.

$$\left(9.40\frac{\Omega \cdot cm \times 10^{-26}}{e^-/cm^2}\right) \times \left([230,290]\frac{1}{\Omega \cdot cm}\right) \times \frac{\left(1700\frac{\Omega \cdot cm \cdot 10^{-6}}{Frenkel\ Pair}\right)}{\left(3000\frac{\Omega \cdot cm \cdot 10^{-6}}{Frenkel\ Pair}\right)} \times \left(\frac{0.01 \times 10^{-24}}{10^{-26}}\right)$$

$$= [12.25,15.46]\frac{cm^2 \times 10^{-24}}{e^-}$$

15.46 and 12.25 are taken to represent the upper and lower limits of a 95% confidence interval for a normal distribution, meaning that the distribution has a standard

deviation of 0.82 and a mean of 13.86. Given the normal distribution generated, $P\left(\frac{\Delta\ell/\ell}{n} \leq 15 \middle| T_m = 70\right) = 92\%$. Because this is less than the formerly calculated $P\left(\frac{\Delta\ell/\ell}{n} \leq 15 \middle| T_m = 70\right)$, it will become the lower bound of the interval probability. Thus, $\boldsymbol{P}\left(\frac{\Delta\ell/\ell}{n} \leq 15 \middle| T_m = 70\right) = [0.92,0.94]$.

This process was repeated for each of eight values found, using the same assumptions and conversion factors each time. A summary of the eight calculations is found in Table 8.

Table 8: Values used in the calculations of $\boldsymbol{P}\left(\frac{\Delta\ell/\ell}{n} \leq 15 \middle| T_m\right)$, based on Figure 26 of (Vajda, 1977).

T_m (eV)	σ(barns)	95% confidence interval of $\frac{\Delta\ell/\ell}{n}$ based on σ	$\frac{\Delta\rho}{n}\left(\frac{\Omega\cdot cm\times 10^{-26}}{e^-/cm^2}\right)$	95% confidence interval of $\frac{\Delta\ell/\ell}{n}$ based on $\frac{\Delta\rho}{n}$	$\boldsymbol{P}\left(\frac{\Delta\ell/\ell}{n} \leq 15 \middle| T_m\right)$
20	0.8667	[0.3178,0.4622]	0.4082	[0.5320,0.6707]	[1.00,1.00]
30	9.605	[3.522,5.123]	2.897	[3.776,4.760]	[1.00,1.00]
45	17.63	[6.465,9.404]	5.794	[7.551,9.521]	[1.00,1.00]
60	24.21	[8.877,12.91]	7.857	[10.24,12.91]	[1.00,1.00]
70	29.08	[10.66,15.51]	9.405	[12.26,15.46]	[0.92,0.94]
80	33.29	[12.21,17.75]	10.91	[14.22,17.93]	[0.13,0.51]
100	39.21	[14.38,20.91]	13.02	[16.96,21.39]	[0.01,0.06]
130	46.32	[16.98,24.70]	15.75	[20.53,25.89]	[0.00,0.00]

In order to find the complementary probability $\boldsymbol{P}\left(\frac{\Delta\ell/\ell}{n} \leq 15 \middle| \begin{matrix} T_m \neq 70 \\ T_m \neq 100 \end{matrix}\right)$, the same assumptions were made as were made to determine $\boldsymbol{P}\left(\frac{\Delta\rho}{n} \leq 9.4048 \middle| \begin{matrix} T_m \neq 70 \\ T_m \neq 100 \end{matrix}\right)$, namely: the eight values of T_m given in Table 8 form a set of mutually disjoint events, all eight of which are equally likely to occur. This allows the formation of the following equation:

$$\boldsymbol{P}\left(\frac{\Delta\ell/\ell}{n} \middle| \begin{matrix} T_m \neq 70 \\ T_m \neq 100 \end{matrix}\right) = \frac{1}{6}\left(\begin{matrix} \boldsymbol{P}\left(\frac{\Delta\ell/\ell}{n} \middle| T_m = 20\right) + \boldsymbol{P}\left(\frac{\Delta\ell/\ell}{n} \middle| T_m = 30\right) \ldots \\ \ldots + \boldsymbol{P}\left(\frac{\Delta\ell/\ell}{n} \middle| T_m = 45\right) + \boldsymbol{P}\left(\frac{\Delta\ell/\ell}{n} \middle| T_m = 60\right) \ldots \\ \ldots + \boldsymbol{P}\left(\frac{\Delta\ell/\ell}{n} \middle| T_m = 80\right) + \boldsymbol{P}\left(\frac{\Delta\ell/\ell}{n} \middle| T_m = 130\right) \end{matrix}\right)$$

Using this equation, the value for $\boldsymbol{P}\left(\frac{\Delta\ell/\ell}{n} \leq 15 \middle| \begin{matrix} T_m \neq 70 \\ T_m \neq 100 \end{matrix}\right)$ shown in Table 9 is obtained.

Table 9: Explanation of shorthand symbols.

Probability	Symbol	Interval Value	Explanation
$\boldsymbol{P}\left(\frac{\Delta\ell/\ell}{n} \leq 15 \middle\| T_m = 70\right)$	ℓ_{Tm1}	[0.9200,0.9400]	The probability that (Δℓ/ℓ)/n≤15 $cm^2 \times 10^{-2}$/(e⁻) given that T_m=70eV.
$\boldsymbol{P}\left(\frac{\Delta\ell/\ell}{n} \leq 15 \middle\| T_m = 100\right)$	ℓ_{Tm2}	[0.0000,0.0556]	The probability that (Δℓ/ℓ)/n≤15 $cm^2 \times 10^{-2}$/(e⁻) given that T_m=100eV.
$\boldsymbol{P}\left(\frac{\Delta\ell/\ell}{n} \leq 15 \middle\| \begin{matrix} T_m \neq 70 \\ T_m \neq 100 \end{matrix}\right)$	ℓ_{Tm3}	[0.6879,0.7512]	The probability that (Δℓ/ℓ)/n≤15 $cm^2 \times 10^{-2}$/(e⁻) given that T_m is neither 70eV nor 100eV.

With these three probabilities determined, equation (16) can finally be evaluated. With the intervals in place, the equation becomes:

$$\boldsymbol{P}\left(\theta \middle| \frac{\Delta\rho}{n} \cap \frac{\Delta\ell/\ell}{n}\right) = \frac{\begin{bmatrix} [0.9200,0.9400]\cdot[0.5,0.5] \\ [0.0000,0.0556]\cdot[0,0] \\ [0.6879,0.7512]\cdot[0.6665,0.6672] \end{bmatrix}^T \begin{bmatrix} [0,1] & [0,0] \\ [0,0] & [0,1] \\ [1,0] & [1,0] \end{bmatrix} \begin{bmatrix} [0.7923,1] \\ [0.2077,0] \end{bmatrix} [0.4,0.5]}{dual\left(\begin{bmatrix} [0.9200,0.9400]\cdot[0.5,0.5] \\ [0.0000,0.0556]\cdot[0,0] \\ [0.6879,0.7512]\cdot[0.6665,0.6672] \end{bmatrix}^T \begin{bmatrix} [0,1] & [0,0] \\ [0,0] & [0,1] \\ [1,0] & [1,0] \end{bmatrix} \begin{bmatrix} [0.7923,1] & [0,1] \\ [0.2077,0] & [1,0] \end{bmatrix} \begin{bmatrix} [0.4,0.5] \\ [0.6,0.5] \end{bmatrix}\right)} \quad (17)$$

The result of this interval update is [0.4,0.5]—identical to the result of equation (13), and identical to the prior probability. Unfortunately, the expressions of complete ignorance in the $(Tm|Td)$ matrix prevent the passage of updating information through the equation. An analysis of the treatment of ignorance appears in §4.4.2, and alternative methods of expressing ignorance are presented in §4.4.2.1 and §4.5. However, because the added experimental information of $\frac{\Delta\ell/\ell}{n}$ in equations (16) and (17) does not affect the posterior probability in the current formulation of the GIBR update, equations (12) and (13) will be used for further analysis and verification within this chapter.

4.3: Verification through Monte Carlo simulation

Generalized Interval Bayes' Rule predicts that, if each of the inputs on the right hand side of equation (12) is within its given interval as shown in Table 7, then the

output on the left hand side should be within the calculated interval shown on the same table. What follows is an attempt at verifying this application of GIBR through Monte Carlo simulations.

4.3.1: Monte Carlo Verification with Uniformly Distributed Inputs

As in the example from §3.5.3.1, the input intervals in equation (13) were replaced with uniformly distributed random values within their bounds, and the resulting real-valued equation was then used to calculate a posterior probability. The results of one million calculations are shown in Figure 8.

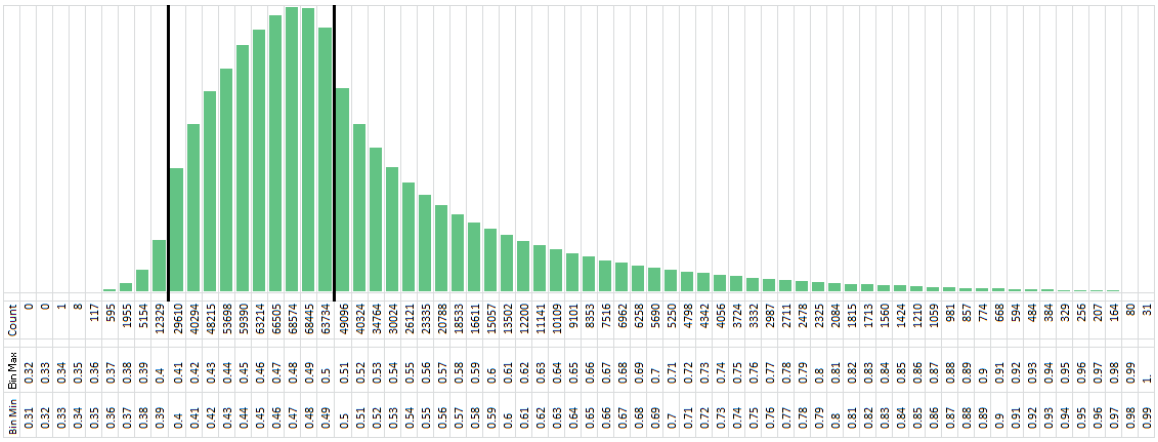

Figure 8: Histogram of a 1,000,000 run Monte Carlo simulation with uniform inputs. Each bin is inclusive of its lower limit and exclusive of its upper limit.

Similar to the examples in §3.5.3, the proposed posterior probability interval is sound, but not complete. The proposed interval of [0.4.0.5] is only 15.19% of the width of the extreme limits of the Monte Carlo simulation, which were [0.3390,0.9974]. Of the million runs, however, 56.17% did fall within the [0.4,0.5] limits. For this example, GIBR does provide a good idea of where the results will be the most concentrated, but it does severely underestimate the range of possible results.

4.3.2: Monte Carlo Verification with Normally Distributed Inputs

For the second verification Monte Carlo simulation, the input intervals in equation (13) were replaced with normally distributed random values within their bounds. The bounds were assumed to represent the ±3σ limits of a distribution centered between the

bounds. As before, the resulting real-valued equation was then used to calculate a posterior probability. This process was repeated 1,000,000 times. The results of this simulation are shown in Figure 9 and Table 10.

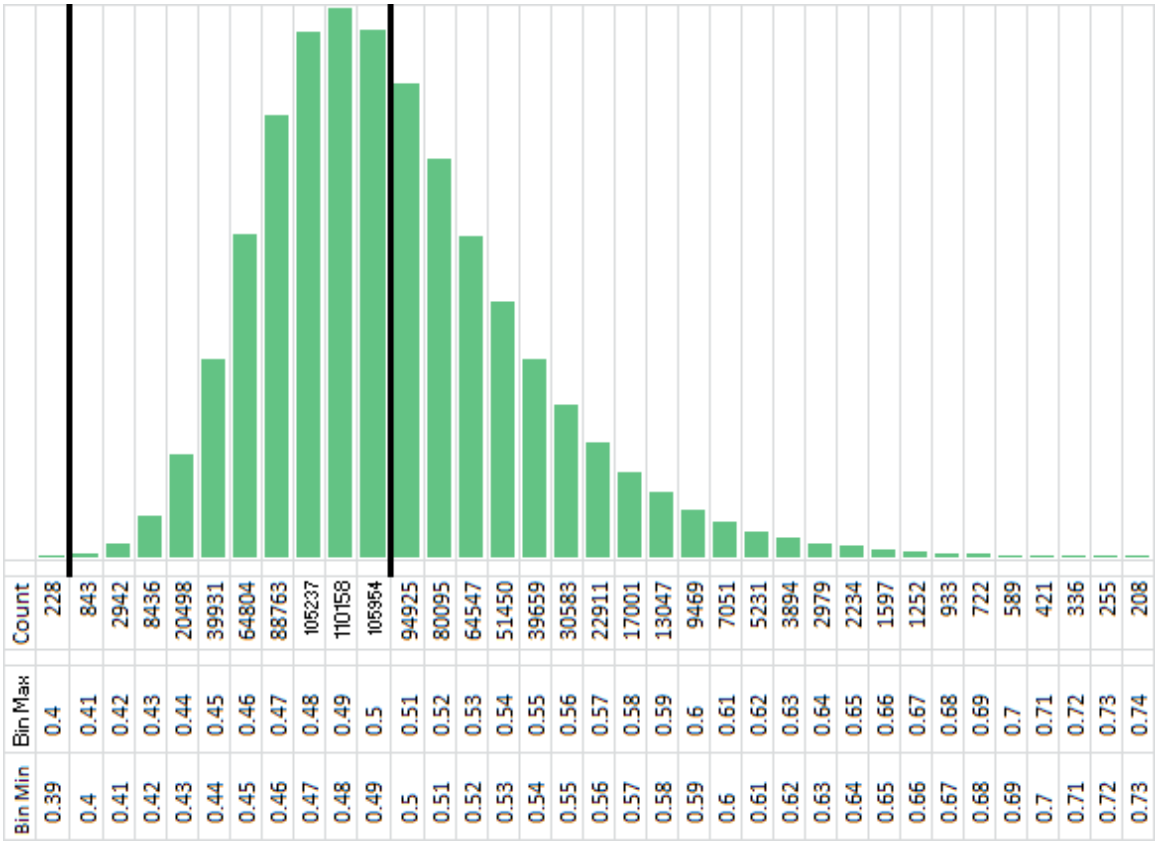

Bin Min	Bin Max	Count
0.39	0.4	228
0.4	0.41	843
0.41	0.42	2942
0.42	0.43	8436
0.43	0.44	20498
0.44	0.45	39931
0.45	0.46	64804
0.46	0.47	88763
0.47	0.48	105237
0.48	0.49	110158
0.49	0.5	105954
0.5	0.51	94925
0.51	0.52	80095
0.52	0.53	64547
0.53	0.54	51450
0.54	0.55	39659
0.55	0.56	30583
0.56	0.57	22911
0.57	0.58	17001
0.58	0.59	13047
0.59	0.6	9469
0.6	0.61	7051
0.61	0.62	5231
0.62	0.63	3894
0.63	0.64	2979
0.64	0.65	2234
0.65	0.66	1597
0.66	0.67	1252
0.67	0.68	933
0.68	0.69	722
0.69	0.7	589
0.7	0.71	421
0.71	0.72	336
0.72	0.73	255
0.73	0.74	208

Figure 9: Histogram of a 1,000,000 run Monte Carlo simulation with inputs normally distributed to ±3σ within the input interval bounds. This figure is trimmed at both the upper and lower ends, because the visual representation of the count became invisible beyond the limits shown here. Again, each bin is inclusive of its lower limit and exclusive of its upper limit.

Table 10: Count of posterior probability calculations that fell within each bin for the 1,000,000 run Monte Carlo simulation with normally distributed inputs.

Bin	Count
0.36 ≤ P < 0.37	2
0.37 ≤ P < 0.38	16
0.38 ≤ P < 0.39	57
0.39 ≤ P < 0.40	228
0.40 ≤ P < 0.41	843
0.41 ≤ P < 0.42	2942
0.42 ≤ P < 0.43	8436
0.43 ≤ P < 0.44	20498
0.44 ≤ P < 0.45	39931
0.45 ≤ P < 0.46	64804
0.46 ≤ P < 0.47	88763
0.47 ≤ P < 0.48	105237
0.48 ≤ P < 0.49	110158
0.49 ≤ P < 0.50	105954
0.50 ≤ P < 0.51	94925
0.51 ≤ P < 0.52	80095
0.52 ≤ P < 0.53	64547
0.53 ≤ P < 0.54	51450
0.54 ≤ P < 0.55	39659
0.55 ≤ P < 0.56	30583
0.56 ≤ P < 0.57	22911
0.57 ≤ P < 0.58	17001
0.58 ≤ P < 0.59	13047
0.59 ≤ P < 0.60	9469
0.60 ≤ P < 0.61	7051
0.61 ≤ P < 0.62	5231
0.62 ≤ P < 0.63	3894
0.63 ≤ P < 0.64	2979
0.64 ≤ P < 0.65	2234

Bin	Count
0.65 ≤ P < 0.66	1597
0.66 ≤ P < 0.67	1252
0.67 ≤ P < 0.68	933
0.68 ≤ P < 0.69	722
0.69 ≤ P < 0.70	589
0.70 ≤ P < 0.71	421
0.71 ≤ P < 0.72	336
0.72 ≤ P < 0.73	255
0.73 ≤ P < 0.74	208
0.74 ≤ P < 0.75	151
0.75 ≤ P < 0.76	130
0.76 ≤ P < 0.77	95
0.77 ≤ P < 0.78	75
0.78 ≤ P < 0.79	48
0.79 ≤ P < 0.80	37
0.80 ≤ P < 0.81	31
0.81 ≤ P < 0.82	27
0.82 ≤ P < 0.83	27
0.83 ≤ P < 0.84	21
0.84 ≤ P < 0.85	12
0.85 ≤ P < 0.86	11
0.86 ≤ P < 0.87	17
0.87 ≤ P < 0.88	7
0.88 ≤ P < 0.89	4
0.89 ≤ P < 0.90	5
0.90 ≤ P < 0.91	6
0.91 ≤ P < 0.92	8
0.92 ≤ P < 0.93	5
0.93 ≤ P < 0.94	1

Bin	Count
0.94 ≤ P < 0.95	4
0.95 ≤ P < 0.96	1
0.96 ≤ P < 0.97	2
0.97 ≤ P < 0.98	1
0.98 ≤ P < 0.99	2
0.99 ≤ P < 1.00	2
1.00 ≤ P < 1.01	1
1.01 ≤ P < 1.02	0
1.02 ≤ P < 1.03	1
1.03 ≤ P < 1.04	0
1.04 ≤ P < 1.05	0
1.05 ≤ P < 1.06	0
1.06 ≤ P < 1.07	1
1.07 ≤ P < 1.08	0
1.08 ≤ P < 1.09	0
1.09 ≤ P < 1.10	2
1.10 ≤ P < 1.11	2
1.11 ≤ P < 1.12	0
1.12 ≤ P < 1.13	0
1.13 ≤ P < 1.14	1
1.14 ≤ P < 1.15	0
1.15 ≤ P < 1.16	2
1.16 ≤ P < 1.17	1
1.17 ≤ P < 1.18	0
1.18 ≤ P < 1.19	0
1.19 ≤ P < 1.20	0
1.20 ≤ P < 1.21	1

As with the uniform input simulation, the results of the normal input simulation indicate that the proposed interval is sound but not complete. In this case, 54.76% of the million runs fell within the bounds of [0.4,0.5], and the proposed interval was only 11.92% of the width of the extreme limits of the simulation, which ranged from 0.3619 to an impossible 1.2006. In twelve instances the calculated posterior probability exceeded 1; this is due to the fact that, as is expected with a normal distribution, in some cases the

randomly generated real values of the inputs fell outside of their respective ±3σ boundaries. If these values are instead replaced with a probability of 1. then the proposed interval range covers 15.67% of the width of the extreme limits of the simulation. While over half of the simulation results are within the proposed posterior probability interval, a large skew means that the center of their distribution is close to the edge of the interval.

4.4: Analyzing the sensitivity of the GIBR with respect to likelihoods

4.4.1: Proper versus Improper Input Intervals

Some attention to which input intervals are proper or improper is due. A generalized interval with two bounds $\underline{x}$ and $\overline{x}$ where $\underline{x} \leq \overline{x}$ can be represented as either $[\underline{x}, \overline{x}]$ or $[\overline{x}, \underline{x}]$. In both cases, the range of values represented by the interval is the same, but the mathematical outcome of equations using the interval may be quite different. As a reminder, the intervals used in the simulations of equation (12) §4.3.1 and §4.3.2 are shown below in equation (18), along with the output of that calculation.

$$\boldsymbol{P}\left(\theta \middle| \frac{\Delta\rho}{n}\right) = \frac{[[0.5,0.5] \quad [0,0] \quad [0.6665,0.6672]] \begin{bmatrix} [0,1] & [0,0] \\ [0,0] & [0,1] \\ [1,0] & [1,0] \end{bmatrix} \begin{bmatrix} [0.7923,1] \\ [0.2077,0] \end{bmatrix} [0.4,0.5]}{dual\left([[0.5,0.5] \quad [0,0] \quad [0.6665,0.6672]] \begin{bmatrix} [0,1] & [0,0] \\ [0,0] & [0,1] \\ [1,0] & [1,0] \end{bmatrix} \begin{bmatrix} [0.7923,1] & [0,1] \\ [0.2077,0] & [1,0] \end{bmatrix} \begin{bmatrix} [0.4,0.5] \\ [0.6,0.5] \end{bmatrix} \right)} \quad (18)$$

$$= [0.4,0.5]$$

The change with the most obvious result is switching the bounds for the prior probability θ. This directly carries through the equation and switches the bounds for the posterior probability, as seen in equation (19), where the intervals whose bounds have been switched are indicated in bold:

$$\boldsymbol{P}\left(\theta\middle|\frac{\Delta\rho}{n}\right)$$

$$= \frac{[[0.5,0.5] \quad [0,0] \quad [0.6665,0.6672]]\begin{bmatrix}[0,1] & [0,0]\\ [0,0] & [0,1]\\ [1,0] & [1,0]\end{bmatrix}\begin{bmatrix}[0.7923,1]\\ [0.2077,0]\end{bmatrix}[\mathbf{0.5},\mathbf{0.4}]}{dual\left([[0.5,0.5] \quad [0,0] \quad [0.6665,0.6672]]\begin{bmatrix}[0,1] & [0,0]\\ [0,0] & [0,1]\\ [1,0] & [1,0]\end{bmatrix}\begin{bmatrix}[0.7923,1] & [0,1]\\ [0.2077,0] & [1,0]\end{bmatrix}\begin{bmatrix}[\mathbf{0.5},\mathbf{0.4}]\\ [\mathbf{0.5},\mathbf{0.6}]\end{bmatrix}\right)} \quad (19)$$

$= [0.5,0.4]$

A more dramatic change can be observed by switching the bounds for Td_θ and, to comply with the Logic Coherence Constraint, Td_θ^C. This results in a dramatic narrowing of the posterior probability interval, as seen in equation (20):

$$\boldsymbol{P}\left(\theta\middle|\frac{\Delta\rho}{n}\right) = \frac{[[0.5,0.5] \quad [0,0] \quad [0.6665,0.6672]]\begin{bmatrix}[0,1] & [0,0]\\ [0,0] & [0,1]\\ [1,0] & [1,0]\end{bmatrix}\begin{bmatrix}[\mathbf{1},\mathbf{0.7923}]\\ [\mathbf{0},\mathbf{0.2077}]\end{bmatrix}[0.4,0.5]}{dual\left([[0.5,0.5] \quad [0,0] \quad [0.6665,0.6672]]\begin{bmatrix}[0,1] & [0,0]\\ [0,0] & [0,1]\\ [1,0] & [1,0]\end{bmatrix}\begin{bmatrix}[\mathbf{1},\mathbf{0.7923}] & [0,1]\\ [\mathbf{0},\mathbf{0.2077}] & [1,0]\end{bmatrix}\begin{bmatrix}[0.4,0.5]\\ [0.6,0.5]\end{bmatrix}\right)} \quad (20)$$

$= [0.4,0.4421]$

On the other hand, a dramatic widening of the interval occurs if the "complete ignorance" probabilities of Td_{θ^c} and $Td_{\theta^c}^C$ are reversed, as seen in equation(21):

$$\boldsymbol{P}\left(\theta\middle|\frac{\Delta\rho}{n}\right) = \frac{[[0.5,0.5] \quad [0,0] \quad [0.6665,0.6672]]\begin{bmatrix}[0,1] & [0,0]\\ [0,0] & [0,1]\\ [1,0] & [1,0]\end{bmatrix}\begin{bmatrix}[0.7923,1]\\ [0.2077,0]\end{bmatrix}[0.4,0.5]}{dual\left([[0.5,0.5] \quad [0,0] \quad [0.6665,0.6672]]\begin{bmatrix}[0,1] & [0,0]\\ [0,0] & [0,1]\\ [1,0] & [1,0]\end{bmatrix}\begin{bmatrix}[0.7923,1] & [\mathbf{1},\mathbf{0}]\\ [0.2077,0] & [\mathbf{0},\mathbf{1}]\end{bmatrix}\begin{bmatrix}[0.4,0.5]\\ [0.6,0.5]\end{bmatrix}\right)} \quad (21)$$

$= [0.4,1]$

Other significant changes can be observed by switching the bounds of some of the other complete ignorance intervals, such as $Tm1_{Td}$ and $Tm3_{Td}$ in equation (22) or $Tm2_{Td}^C$ and $Tm3_{Td}^C$ in equation (23). A more in-depth examination of the treatment of complete ignorance will be given in §4.4.2.

$$\boldsymbol{P}\left(\theta\middle|\frac{\Delta\rho}{n}\right) = \frac{[[0.5,0.5] \quad [0,0] \quad [0.6665,0.6672]]\begin{bmatrix}[\mathbf{1},\mathbf{0}] & [0,0]\\ [0,0] & [0,1]\\ [\mathbf{0},\mathbf{1}] & [1,0]\end{bmatrix}\begin{bmatrix}[0.7923,1]\\ [0.2077,0]\end{bmatrix}[0.4,0.5]}{dual\left([[0.5,0.5] \quad [0,0] \quad [0.6665,0.6672]]\begin{bmatrix}[\mathbf{1},\mathbf{0}] & [0,0]\\ [0,0] & [0,1]\\ [\mathbf{0},\mathbf{1}] & [1,0]\end{bmatrix}\begin{bmatrix}[0.7923,1] & [0,1]\\ [0.2077,0] & [1,0]\end{bmatrix}\begin{bmatrix}[0.4,0.5]\\ [0.6,0.5]\end{bmatrix}\right)} \quad (22)$$

$= [0.3484,0.5]$

$$\boldsymbol{P}\left(\theta\middle|\frac{\Delta\rho}{\mathrm{n}}\right)=\frac{[[0.5,0.5]\quad[0,0]\quad[0.6665,0.6672]]\begin{bmatrix}[0,1] & [0,0]\\ [0,0] & [\mathbf{1},\mathbf{0}]\\ [1,0] & [\mathbf{0},\mathbf{1}]\end{bmatrix}\begin{bmatrix}[0.7923,1]\\ [0.2077,0]\end{bmatrix}[0.4,0.5]}{dual\left([[0.5,0.5]\quad[0,0]\quad[0.6665,0.6672]]\begin{bmatrix}[0,1] & [0,0]\\ [0,0] & [\mathbf{1},\mathbf{0}]\\ [1,0] & [\mathbf{0},\mathbf{1}]\end{bmatrix}\begin{bmatrix}[0.7923,1] & [0,1]\\ [0.2077,0] & [1,0]\end{bmatrix}\begin{bmatrix}[0.4,0.5]\\ [0.6,0.5]\end{bmatrix}\right)}\quad(23)$$

$$=[1,0.5]$$

Examining the changes that can occur due to an arbitrary reversal of the order of the limits of intervals within GIBR equations demands a convention for why certain intervals may be expressed as proper or improper within the context of GIBR.

Intervals not subject to the Logic Coherence Constraint should always be represented as proper intervals. Examples of this are ρ_{Tm1}, ρ_{Tm2}, and ρ_{Tm3}. It is worth noting that the limits of these intervals are obtained from experimental measurements, suggesting a further convention: *when an interval has been determined by analysis of simulation or experimental results, it should be represented as a proper interval*. The companion rule is that *when an interval has been determined simply by its subjection to the Logic Coherence Constraint, it may then be represented by an improper interval*. Finally, *the prior probability receiving the update should be represented as a proper interval*. In the case of equation (12), these three conventions lock down the order of all but the intervals representing complete ignorance. However, other situations may arise that require further conventions. For instance, in this case Td_θ was determined by examining simulation results in the form of a cumulative distribution function, whereas Td_θ^C was determined by applying the Logic Coherence Constraint to Td_θ. A situation could arise wherein both Td_θ^C and Td_θ are determined by examining simulation or experimental results; which one should be proper in that case? Or, if two or more intervals that should be subject to the Logic Coherence Constraint have values that are determined from simulation/experimental results and the evidence for them conflicts, how can the conflicting results be reconciled? These questions have yet to be answered.

4.4.2: Challenges Due to the Representation of Complete Ignorance

In further examining the initial inputs of equation (12), it becomes apparent that some of the input intervals were too restrictive for the amount of information available. For instance, $Tm1_{Td}$, $Tm2_{Td}$, and $Tm3_{Td}$ were respectively assigned intervals of [0,1], [0,0], and [1,0]. This was an attempt to represent complete ignorance, as seen in the two full-width intervals of $Tm1_{Td}$ and $Tm3_{Td}$. However, once these were assigned, the Logic Coherence Constraint forced the value of $Tm2_{Td}$ to an overly restrictive [0,0]. This strong assumption exerted undue influence on the outcome of both equation (12) and the simulations based upon it. Another method for expressing ignorance is desired.

4.4.2.1: Equal Weighting to Represent Complete Ignorance

A more traditional approach would weight all three mutually disjoint events equally; expressed as intervals, their values would all be [⅓,⅓]. Other mutually disjoint events that attempt to show complete ignorance should similarly be equally weighted: $Tm1_{Td^C}$, $Tm2_{Td^C}$, and $Tm3_{Td^C}$ would each be assigned the interval [⅓,⅓], and Td_{θ^C} and $Td_{\theta^C}^{C}$ would each be assigned the interval [½,½]. Putting the interval values into equation (12) gives:

$$\boldsymbol{P}\left(\theta\middle|\frac{\Delta\rho}{n}\right) = \frac{[[0.5,0.5] \quad [0,0] \quad [0.6665,0.6672]] \begin{bmatrix} [\frac{1}{3},\frac{1}{3}] & [\frac{1}{3},\frac{1}{3}] \\ [\frac{1}{3},\frac{1}{3}] & [\frac{1}{3},\frac{1}{3}] \\ [\frac{1}{3},\frac{1}{3}] & [\frac{1}{3},\frac{1}{3}] \end{bmatrix} \begin{bmatrix} [0.7923,1] \\ [0.2077,0] \end{bmatrix} [0.4,0.5]}{dual\left([[0.5,0.5] \quad [0,0] \quad [0.6665,0.6672]] \begin{bmatrix} [\frac{1}{3},\frac{1}{3}] & [\frac{1}{3},\frac{1}{3}] \\ [\frac{1}{3},\frac{1}{3}] & [\frac{1}{3},\frac{1}{3}] \\ [\frac{1}{3},\frac{1}{3}] & [\frac{1}{3},\frac{1}{3}] \end{bmatrix} \begin{bmatrix} [0.7923,1] & [\frac{1}{2},\frac{1}{2}] \\ [0.2077,0] & [\frac{1}{2},\frac{1}{2}] \end{bmatrix} \begin{bmatrix} [0.4,0.5] \\ [0.6,0.5] \end{bmatrix} \right)} \qquad (24)$$

In effect, this is a hybrid model, combining the traditional approach of equally weighting fully unknown quantities with the nontraditional approach of representing other probabilities with intervals. Combining these two approaches has several shortcomings. For instance, in the context of generalized interval probability, a zero-width interval represents the removal of all epistemic uncertainty. Equally weighted intervals subject to the Logic Coherence Constraint are of necessity zero-width intervals,

incorrectly implying a complete lack of epistemic uncertainty when in fact epistemic uncertainty is at its maximum. A more serious drawback, though, is that none of the information actually gathered can affect the posterior probability while these equal weightings are used. This can be seen demonstrated by calculating either one of the bounds of the posterior probability; in this case, the lower bound is used:

$$\underline{\boldsymbol{P}}\left(\theta\middle|\frac{\Delta\rho}{n}\right)=\frac{[0.5\quad 0\quad 0.6665]\begin{bmatrix}\frac{1}{3}&\frac{1}{3}\\ \frac{1}{3}&\frac{1}{3}\\ \frac{1}{3}&\frac{1}{3}\end{bmatrix}\begin{bmatrix}0.7923\\ 0.2077\end{bmatrix}\cdot 0.4}{[0.5\quad 0\quad 0.6665]\begin{bmatrix}\frac{1}{3}&\frac{1}{3}\\ \frac{1}{3}&\frac{1}{3}\\ \frac{1}{3}&\frac{1}{3}\end{bmatrix}\begin{bmatrix}0.7923&\frac{1}{2}\\ 0.2077&\frac{1}{2}\end{bmatrix}\begin{bmatrix}0.4\\ 0.6\end{bmatrix}}$$

For illustrative purposes, the prior probability's lower bound, 0.4, is separated from the rest of the fraction. Additionally, the scalar ⅓ is factored out of the second matrix:

$$\underline{\boldsymbol{P}}\left(\theta\middle|\frac{\Delta\rho}{n}\right)=\frac{\frac{1}{3}\cdot[0.5\quad 0\quad 0.6665]\begin{bmatrix}1&1\\ 1&1\\ 1&1\end{bmatrix}\begin{bmatrix}0.7923\\ 0.2077\end{bmatrix}}{\frac{1}{3}\cdot[0.5\quad 0\quad 0.6665]\begin{bmatrix}1&1\\ 1&1\\ 1&1\end{bmatrix}\begin{bmatrix}0.7923&\frac{1}{2}\\ 0.2077&\frac{1}{2}\end{bmatrix}\begin{bmatrix}0.4\\ 0.6\end{bmatrix}}\cdot 0.4$$

The value ⅓ can be cancelled from the equation as the first two matrices in both the numerator and denominator are multiplied:

$$\underline{\boldsymbol{P}}\left(\theta\middle|\frac{\Delta\rho}{n}\right)=\frac{[1.1665\quad 1.1665]\begin{bmatrix}0.7923\\ 0.2077\end{bmatrix}}{[1.1665\quad 1.1665]\begin{bmatrix}0.7923&\frac{1}{2}\\ 0.2077&\frac{1}{2}\end{bmatrix}\begin{bmatrix}0.4\\ 0.6\end{bmatrix}}\cdot 0.4$$

The value 1.1665 can then be factored out of the leading matrix and cancelled, leaving:

$$\underline{\boldsymbol{P}}\left(\theta\middle|\frac{\Delta\rho}{n}\right)=\frac{\begin{bmatrix}1 & 1\end{bmatrix}\begin{bmatrix}0.7923\\0.2077\end{bmatrix}}{\begin{bmatrix}1 & 1\end{bmatrix}\begin{bmatrix}0.7923 & \frac{1}{2}\\0.2077 & \frac{1}{2}\end{bmatrix}\begin{bmatrix}0.4\\0.6\end{bmatrix}}\cdot 0.4$$

From here the Logic Coherence Constraint takes over, and all remaining multiplications result in matrices filled with ones. Continuing to multiply matrices left-to-right gives:

$$\underline{\boldsymbol{P}}\left(\theta\middle|\frac{\Delta\rho}{n}\right)=\frac{1}{\begin{bmatrix}1 & 1\end{bmatrix}\begin{bmatrix}0.4\\0.6\end{bmatrix}}\cdot 0.4$$

$$\underline{\boldsymbol{P}}\left(\theta\middle|\frac{\Delta\rho}{n}\right)=\frac{1}{1}\cdot 0.4$$

$$\underline{\boldsymbol{P}}\left(\theta\middle|\frac{\Delta\rho}{n}\right)=0.4$$

A similar pattern of multiplication, factorization, and cancellation can be observed when calculating $\overline{\boldsymbol{P}}\left(\theta\middle|\frac{\Delta\rho}{n}\right)=0.5$. In essence, combining a traditional equal-weighting approach with an interval approach nullifies both approaches, removing any variability except what is present in the prior probability—the result of a Monte Carlo simulation is simply input distribution chosen for the prior, as illustrated in Figure 10 and Figure 11. Yet another method is needed to quantify complete ignorance using Generalized Interval Bayes' Rule.

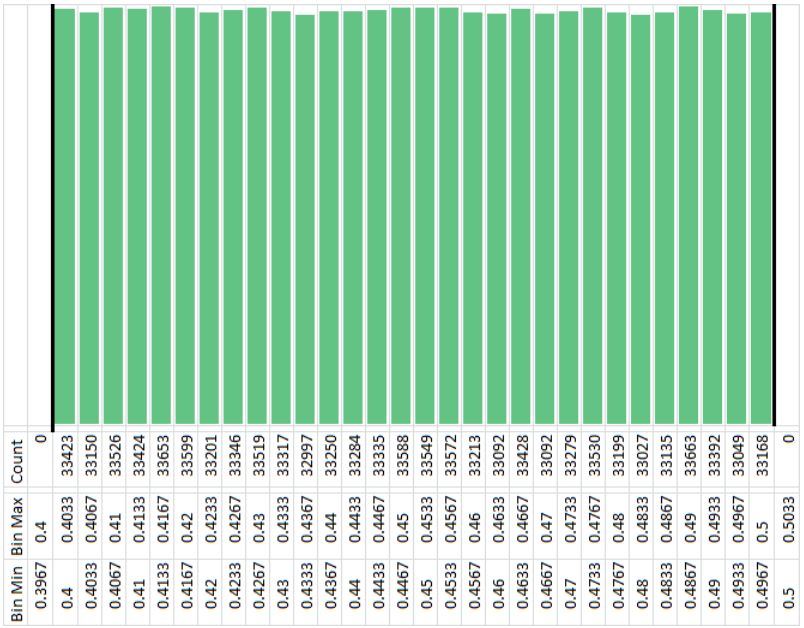

Bin Min	Bin Max	Count
0.3967	0.4	0
0.4	0.4033	33423
0.4033	0.4067	33150
0.4067	0.41	33526
0.41	0.4133	33424
0.4133	0.4167	33653
0.4167	0.42	33599
0.42	0.4233	33201
0.4233	0.4267	33346
0.4267	0.43	33519
0.43	0.4333	33317
0.4333	0.4367	32997
0.4367	0.44	33250
0.44	0.4433	33284
0.4433	0.4467	33335
0.4467	0.45	33588
0.45	0.4533	33549
0.4533	0.4567	33572
0.4567	0.46	33213
0.46	0.4633	33092
0.4633	0.4667	33428
0.4667	0.47	33092
0.47	0.4733	33279
0.4733	0.4767	33530
0.4767	0.48	33199
0.48	0.4833	33027
0.4833	0.4867	33135
0.4867	0.49	33663
0.49	0.4933	33392
0.4933	0.4967	33049
0.4967	0.5	33168
0.5	0.5033	0

Figure 10: Histogram of 1,000,000 run Monte Carlo simulation of equation (24) with uniformly distributed interval inputs.

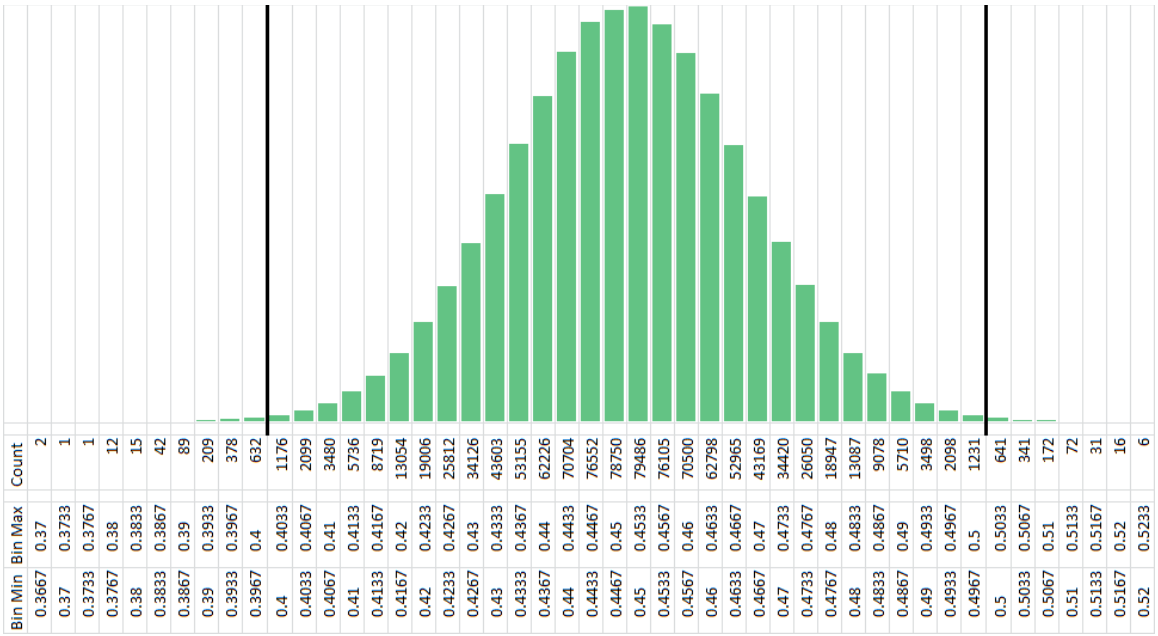

Bin Min	Bin Max	Count
0.3667	0.37	2
0.37	0.3733	1
0.3733	0.3767	1
0.3767	0.38	12
0.38	0.3833	15
0.3833	0.3867	42
0.3867	0.39	89
0.39	0.3933	209
0.3933	0.3967	378
0.3967	0.4	632
0.4	0.4033	1176
0.4033	0.4067	2099
0.4067	0.41	3480
0.41	0.4133	5736
0.4133	0.4167	8719
0.4167	0.42	13054
0.42	0.4233	19006
0.4233	0.4267	25812
0.4267	0.43	34126
0.43	0.4333	43603
0.4333	0.4367	53155
0.4367	0.44	62226
0.44	0.4433	70704
0.4433	0.4467	76552
0.4467	0.45	78750
0.45	0.4533	79486
0.4533	0.4567	76105
0.4567	0.46	70500
0.46	0.4633	62798
0.4633	0.4667	52965
0.4667	0.47	43169
0.47	0.4733	34420
0.4733	0.4767	26050
0.4767	0.48	18947
0.48	0.4833	13087
0.4833	0.4867	9078
0.4867	0.49	5710
0.49	0.4933	3498
0.4933	0.4967	2098
0.4967	0.5	1231
0.5	0.5033	641
0.5033	0.5067	341
0.5067	0.51	172
0.51	0.5133	72
0.5133	0.5167	31
0.5167	0.52	16
0.52	0.5233	6

Figure 11: Histogram of 1,000,000 run Monte Carlo simulation of equation (24) with normally distributed interval inputs. Each input interval was assumed to represent the ±3σ limits of a centered normal distribution. The result is perfectly normal and centered because the posterior probability shows no update from the prior, and because representation of complete ignorance used causes every input distribution to cancel out except for the prior probability.

4.5: Formulation of a Modified Generalized Interval Bayes' Rule

The Logic Coherence Constraint forces the appearance of the interval [0,0] whenever more than two mutually disjoint events representing complete ignorance occur.

In addition, when only two mutually disjoint events representing complete ignorance appear in the equation, the assignment of the intervals [0,1] or [1,0] to one or the other of them is entirely subjective, but it can have a major impact on the calculated posterior probability. For instance, using the values from Table 7 in equation (12) gives the posterior probability [0.4,0.5]. It should be noted that in Table 7, Td_{θ^c} and $Td_{\theta^c}^{C}$ are given the respective values of [0,1] and [1,0]; the two probability assignments could easily be reversed with no change in the meaning of the equation. However, in the first case the posterior probability $\boldsymbol{P}\left(\theta\middle|\frac{\Delta\rho}{\mathrm{n}}\right)$ is [0.4,0.5], while in the second case it is [0.4,1.0].

To address these problems and to add consistency to the analysis, a modification of the Generalized Interval Bayes' Rule is proposed: *when expressing complete ignorance, always use the interval [0,1], and do not use the Logic Coherence Constraint for that set of intervals*. With this modified rule, equation (12) becomes:

$$\boldsymbol{P}\left(\theta\middle|\frac{\Delta\rho}{\mathrm{n}}\right)=\frac{[[0.5,0.5]\quad[0,0]\quad[0.6665,0.6672]]\begin{bmatrix}[0,1] & [0,1]\\ [0,1] & [0,1]\\ [0,1] & [0,1]\end{bmatrix}\begin{bmatrix}[0.7923,1]\\ [0.2077,0]\end{bmatrix}[0.4,0.5]}{dual\left([[0.5,0.5]\quad[0,0]\quad[0.6665,0.6672]]\begin{bmatrix}[0,1] & [0,1]\\ [0,1] & [0,1]\\ [0,1] & [0,1]\end{bmatrix}\begin{bmatrix}[0.7923,1] & [0,1]\\ [0.2077,0] & [0,1]\end{bmatrix}\begin{bmatrix}[0.4,0.5]\\ [0.6,0.5]\end{bmatrix}\right)} \qquad (25)$$

The upper bound of the new posterior probability interval is easily calculated:

$$\overline{\boldsymbol{P}}\left(\theta\middle|\frac{\Delta\rho}{\mathrm{n}}\right)=\frac{[0.5\quad 0\quad 0.6672]\begin{bmatrix}1 & 1\\ 1 & 1\\ 1 & 1\end{bmatrix}\begin{bmatrix}1\\ 0\end{bmatrix}\cdot 0.5}{[0.5\quad 0\quad 0.6672]\begin{bmatrix}1 & 1\\ 1 & 1\\ 1 & 1\end{bmatrix}\begin{bmatrix}1 & 1\\ 0 & 1\end{bmatrix}\begin{bmatrix}0.5\\ 0.5\end{bmatrix}}=0.3333 \qquad (26)$$

However, the lower bound calculation suffers from the introduction of so many zeroes, and quickly leads to a 0/0 division problem.

$$\underline{\boldsymbol{P}}\left(\theta\middle|\frac{\Delta\rho}{\mathrm{n}}\right)=\frac{[0.5\quad 0\quad 0.6665]\begin{bmatrix}0 & 0\\ 0 & 0\\ 0 & 0\end{bmatrix}\begin{bmatrix}0.7923\\ 0.2077\end{bmatrix}\cdot 0.4}{[0.5\quad 0\quad 0.6665]\begin{bmatrix}0 & 0\\ 0 & 0\\ 0 & 0\end{bmatrix}\begin{bmatrix}0.7923 & 0\\ 0.2077 & 0\end{bmatrix}\begin{bmatrix}0.4\\ 0.6\end{bmatrix}} \qquad (27)$$

If calculated as a limit, however, a useful numerical value can be obtained:

$$\underline{\boldsymbol{P}}\left(\theta\middle|\frac{\Delta\rho}{n}\right)=\lim_{x\to 0}\frac{[0.5\quad 0\quad 0.6665]\begin{bmatrix}x & x\\ x & x\\ x & x\end{bmatrix}\begin{bmatrix}0.7923\\ 0.2077\end{bmatrix}\cdot 0.4}{[0.5\quad 0\quad 0.6665]\begin{bmatrix}x & x\\ x & x\\ x & x\end{bmatrix}\begin{bmatrix}0.7923 & x\\ 0.2077 & x\end{bmatrix}\begin{bmatrix}0.4\\ 0.6\end{bmatrix}}$$

Completing the first matrix multiplications allows the value 1.6665 x to be factored out and cancelled:

$$\underline{\boldsymbol{P}}\left(\theta\middle|\frac{\Delta\rho}{n}\right)=\lim_{x\to 0}\frac{[1.1665\cdot x\quad 1.1665\cdot x]\begin{bmatrix}0.7923\\ 0.2077\end{bmatrix}\cdot 0.4}{[1.1665\cdot x\quad 1.1665\cdot x]\begin{bmatrix}0.7923 & x\\ 0.2077 & x\end{bmatrix}\begin{bmatrix}0.4\\ 0.6\end{bmatrix}}$$

$$\underline{\boldsymbol{P}}\left(\theta\middle|\frac{\Delta\rho}{n}\right)=\lim_{x\to 0}\frac{1.1665\cdot x\cdot[1\quad 1]\begin{bmatrix}0.7923\\ 0.2077\end{bmatrix}\cdot 0.4}{1.1665\cdot x\cdot[1\quad 1]\begin{bmatrix}0.7923 & x\\ 0.2077 & x\end{bmatrix}\begin{bmatrix}0.4\\ 0.6\end{bmatrix}}$$

With this done, the limit can be executed and the numerical solution can be quickly reached:

$$\underline{\boldsymbol{P}}\left(\theta\middle|\frac{\Delta\rho}{n}\right)=\frac{[1\quad 1]\begin{bmatrix}0.7923\\ 0.2077\end{bmatrix}\cdot 0.4}{[1\quad 1]\begin{bmatrix}0.7923 & 0\\ 0.2077 & 0\end{bmatrix}\begin{bmatrix}0.4\\ 0.6\end{bmatrix}}$$

$$\underline{\boldsymbol{P}}\left(\theta\middle|\frac{\Delta\rho}{n}\right)=\frac{1\cdot 0.4}{[1\quad 0]\begin{bmatrix}0.4\\ 0.6\end{bmatrix}}$$

$$\underline{\boldsymbol{P}}\left(\theta\middle|\frac{\Delta\rho}{n}\right)=1$$

Thus, with eight probabilities represented as complete ignorance, the new posterior probability is calculated as $\boldsymbol{P}\left(\theta\middle|\frac{\Delta\rho}{n}\right)=[1,0.3333]$.

4.5.1: Verifying the New Rule through Monte Carlo Simulation

Because the input intervals have been changed, this interval cannot be compared to the previous Monte Carlo simulations, and new simulations are necessary. While the Logic Coherence Constraint is not maintained for the input intervals, it must be obeyed

within the Monte Carlo simulations. This adds a level of difficulty to the Monte Carlo simulations: in a group of three or more mutually disjoint events, if the probability of one variable is randomly selected with some distribution between zero and one, then the probability distribution for the other events will be altered. For instance, for three events A, B, and C, if A has a randomly selected probability of 0.75, then event B can only be randomly selected between 0 and 0.25. In order to mitigate this, the order in which the probabilities are determined must be randomized, thus making the Monte Carlo simulation a double-sampling process.

4.5.1.1: Monte Carlo Simulations with a Uniform Distribution

The first Monte Carlo simulation to verify equation (25) was run using uniformly distributed values for the input intervals. The results of one million calculations are shown in Figure 12.

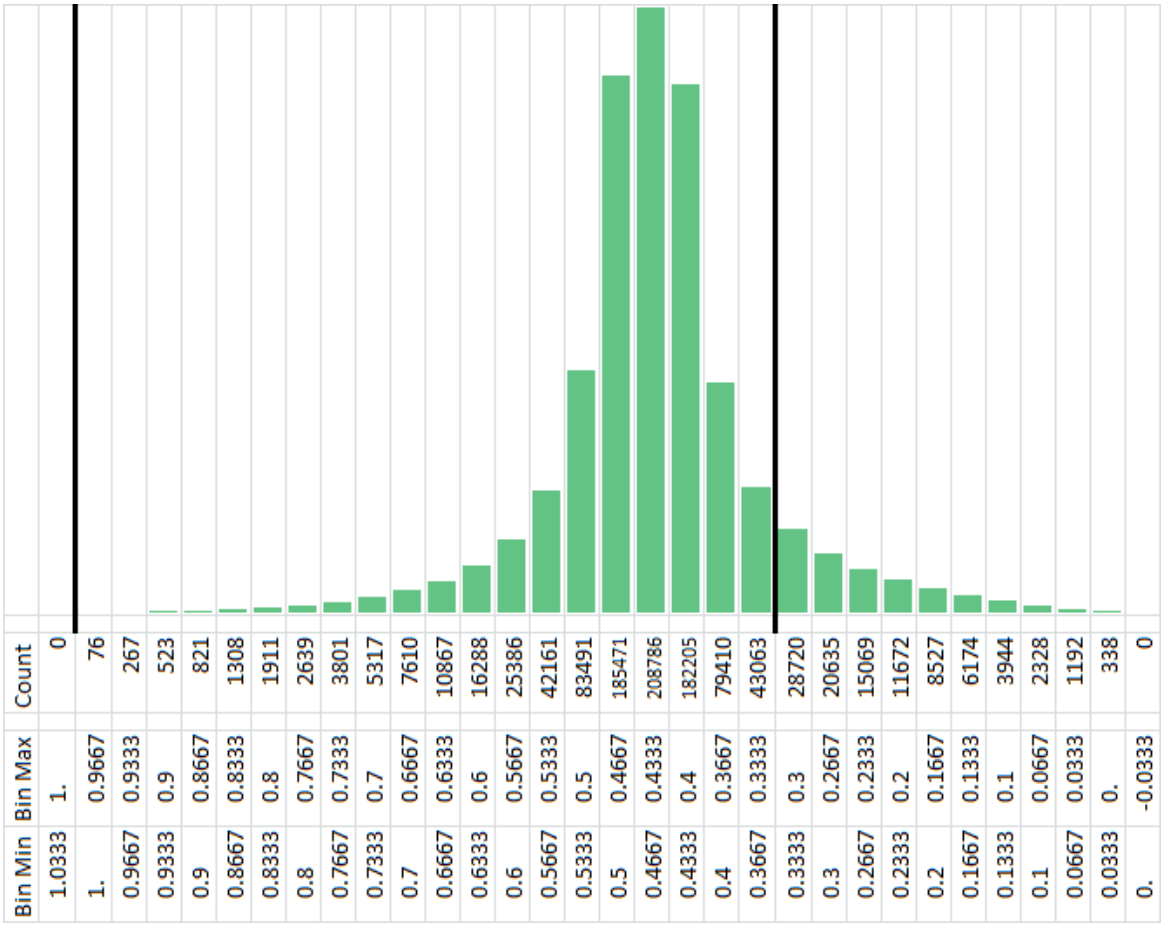

Bin Min	Bin Max	Count
1.0333	1.	0
1.	0.9667	76
0.9667	0.9333	267
0.9333	0.9	523
0.9	0.8667	821
0.8667	0.8333	1308
0.8333	0.8	1911
0.8	0.7667	2639
0.7667	0.7333	3801
0.7333	0.7	5317
0.7	0.6667	7610
0.6667	0.6333	10867
0.6333	0.6	16288
0.6	0.5667	25386
0.5667	0.5333	42161
0.5333	0.5	83491
0.5	0.4667	185471
0.4667	0.4333	208786
0.4333	0.4	182205
0.4	0.3667	79410
0.3667	0.3333	43063
0.3333	0.3	28720
0.3	0.2667	20635
0.2667	0.2333	15069
0.2333	0.2	11672
0.2	0.1667	8527
0.1667	0.1333	6174
0.1333	0.1	3944
0.1	0.0667	2328
0.0667	0.0333	1192
0.0333	0.	338
0.	-0.0333	0

Figure 12: One million run Monte Carlo simulation of interval equation (25) with uniformly distributed inputs.

90.14% of the one million runs were contained within the posterior probability interval limits [1,0.3333]. The posterior probability was only 67.07% of the range of the Monte Carlo simulation results, which stretched from 0.0011 to 0.9952.

4.5.1.2: Monte Carlo Simulations with a Normal Distribution

The second Monte Carlo simulation to verify equation (25) was run using normally distributed values for the input intervals, assuming that each input interval represented the ±3σ limits of a centered normal distribution. The results of one million calculations are shown visually in Figure 13, and numerically in Table 10.

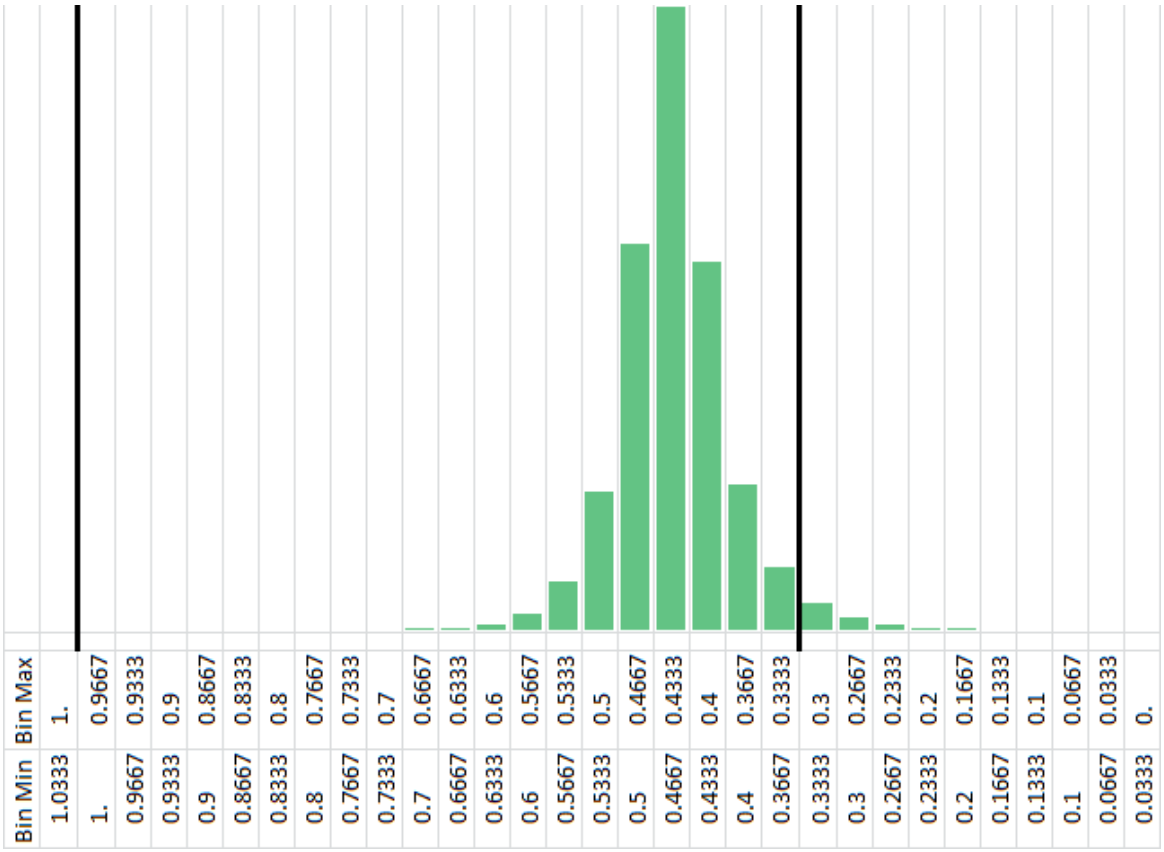

Figure 13: One million run Monte Carlo simulation of interval equation (25) with normally distributed inputs.

Table 11: Count of posterior probability calculations that fell within each bin for the 1,000,000 run Monte Carlo simulation with normally distributed inputs. Bins denoted with italics are wider than other bins due to the huge spread of the simulation results.

Bin	Count
7.00 ≤ P < 8.00	*1*
3.00 ≤ P < 7.00	*0*
2.00 ≤ P < 3.00	*2*
1.00 ≤ P < 2.00	*7*
0.97 ≤ P < 1.00	2
0.93 ≤ P < 0.97	4
0.90 ≤ P < 0.93	3
0.87 ≤ P < 0.90	6
0.83 ≤ P < 0.87	11
0.80 ≤ P < 0.83	24
0.77 ≤ P < 0.80	68
0.73 ≤ P < 0.77	113
0.70 ≤ P < 0.73	208
0.67 ≤ P < 0.70	495

Bin	Count
0.50 ≤ P < 0.53	74630
0.47 ≤ P < 0.50	208679
0.43 ≤ P < 0.47	336857
0.40 ≤ P < 0.43	198729
0.37 ≤ P < 0.40	78559
0.33 ≤ P < 0.37	33913
0.30 ≤ P < 0.33	15038
0.27 ≤ P < 0.30	6831
0.23 ≤ P < 0.27	3107
0.20 ≤ P < 0.23	1411
0.17 ≤ P < 0.20	703
0.13 ≤ P < 0.17	338
0.10 ≤ P < 0.13	199
0.07 ≤ P < 0.10	99

Bin	Count
-0.10 ≤ P < -0.07	10
-0.13 ≤ P < -0.10	9
-0.17 ≤ P < -0.13	8
-0.20 ≤ P < -0.17	7
-0.23 ≤ P < -0.20	4
-0.27 ≤ P < -0.23	1
-0.30 ≤ P < -0.27	2
-0.33 ≤ P < -0.30	5
-0.37 ≤ P < -0.33	1
-0.40 ≤ P < -0.37	3
-0.50 ≤ P < -0.40	*3*
-1.00 ≤ P < -0.50	*8*
-2.00 ≤ P < -1.00	*5*
-3.00 ≤ P < -2.00	*1*

Bin	Count
0.63 ≤ P < 0.67	1318
0.60 ≤ P < 0.63	3356
0.57 ≤ P < 0.60	9070
0.53 ≤ P < 0.57	26004

Bin	Count
0.03 ≤ P < 0.07	49
0.00 ≤ P < 0.03	55
-0.03 ≤ P < 0.00	27
-0.07 ≤ P < -0.03	15

Bin	Count
-4.00 ≤ P < -3.00	*1*
-5.00 ≤ P < -4.00	*0*
-6.00 ≤ P < -5.00	*1*

97.21% of the one million runs were contained within the posterior probability interval limits [1,0.3333]. The posterior probability was only 5.00% of the range of the Monte Carlo simulation results, which had an impossibly wide range of -5.7873 to 7.542. When simulation results greater than 1 or less than 0 were replaced with 1 and 0, respectively, the posterior probability was 66.67% of the range of the MC simulation results.

4.5.2: Cross-Checking the Treatment of Complete Ignorance

In order to verify the modified rule for more than just one case, equation (8) from Chapter 3 was again employed as a purely numerical example. The equation is repeated here as a reminder:

$$\boldsymbol{P}(\gamma|\alpha) = \frac{[\alpha_{\beta 1} \quad \alpha_{\beta 2} \quad \alpha_{\beta 3} \quad \alpha_{\beta 4}] \begin{bmatrix} \beta 1_\gamma \\ \beta 2_\gamma \\ \beta 3_\gamma \\ \beta 4_\gamma \end{bmatrix} \cdot \gamma}{dual\left([\alpha_{\beta 1} \quad \alpha_{\beta 2} \quad \alpha_{\beta 3} \quad \alpha_{\beta 4}] \begin{bmatrix} \beta 1_\gamma & \beta 1_{\gamma^C} \\ \beta 2_\gamma & \beta 2_{\gamma^C} \\ \beta 3_\gamma & \beta 3_{\gamma^C} \\ \beta 4_\gamma & \beta 4_{\gamma^C} \end{bmatrix} \begin{bmatrix} \gamma \\ \gamma^C \end{bmatrix} \right)} \qquad (8)$$

The values of the $\boldsymbol{P}(\beta|\gamma)$ terms in equation (8) are modified to represent complete ignorance as follows:

In the case of "complete ignorance with the Logic Coherence Constraint," the first $(\beta|\gamma)$ probability is given the obvious interval of complete ignorance, and thus $\boldsymbol{P}(\beta 1|\gamma) = [0,1]$. The second interval is given the only other interval that can represent complete ignorance, so $\boldsymbol{P}(\beta 2|\gamma) = [1,0]$. With these two intervals chosen, the Logic Coherence Constraint forces the choice of the other two values, and so $\boldsymbol{P}(\beta 3|\gamma) =$

$\boldsymbol{P}(\beta 4|\gamma) = [0,0]$. The values of the $(\beta|\gamma^C)$ intervals are similarly chosen, so that $\boldsymbol{P}(\beta 1|\gamma^C) = [0,1]$, $\boldsymbol{P}(\beta 2|\gamma^C) = [1,0]$, and $\boldsymbol{P}(\beta 3|\gamma^C) = \boldsymbol{P}(\beta 4|\gamma^C) = [0,0]$.

In the second case, all four intervals are given equal values in order to represent equal weighting of all cases. Due to the Logic Coherence Constraint, intervals with width greater than zero cannot be used, and so all four intervals $\boldsymbol{P}(\beta 1|\gamma) = \boldsymbol{P}(\beta 2|\gamma) = \boldsymbol{P}(\beta 3|\gamma) = \boldsymbol{P}(\beta 4|\gamma) = [¼, ¼]$. Likewise, $\boldsymbol{P}(\beta 1|\gamma^C) = \boldsymbol{P}(\beta 2|\gamma^C) = \boldsymbol{P}(\beta 3|\gamma^C) = \boldsymbol{P}(\beta 4|\gamma^C) = [¼, ¼]$.

In the third case, the Logic Coherence Constraint is ignored where complete ignorance is present, allowing the use of the interval $[0,1]$ for all four probabilities. The results of these calculations are shown in Table 12.

Table 12: The effect of complete ignorance occupying a link in the probability chain, with three different methods for representing complete ignorance.

Symbol	Probability	Original Interval	Complete Ignorance		
			Case 1: Forced zeros due to the LCC	Case 2: Equal Weights following the LCC	Case 3: Equal Weights without LCC
$\alpha_{\beta 1}$	$\boldsymbol{P}(\alpha\|\beta 1)$	[0.3880,0.9973]	Same as original		
$\alpha_{\beta 2}$	$\boldsymbol{P}(\alpha\|\beta 2)$	[0.7415,0.9024]	Same as original		
$\alpha_{\beta 3}$	$\boldsymbol{P}(\alpha\|\beta 3)$	[0.3667,0.8688]	Same as original		
$\alpha_{\beta 4}$	$\boldsymbol{P}(\alpha\|\beta 4)$	[0.1655,0.4140]	Same as original		
$\beta 1_{\gamma}$	$\boldsymbol{P}(\beta 1\|\gamma)$	[0.1197,0.1826]	[0,1]	[¼,¼]	[0,1]
$\beta 2_{\gamma}$	$\boldsymbol{P}(\beta 2\|\gamma)$	[0.1662,0.3080]	[1,0]	[¼,¼]	[0,1]
$\beta 3_{\gamma}$	$\boldsymbol{P}(\beta 3\|\gamma)$	[0.3587,0.4603]	[0,0]	[¼,¼]	[0,1]
$\beta 4_{\gamma}$	$\boldsymbol{P}(\beta 4\|\gamma)$	[0.3554,0.0491]	[0,0]	[¼,¼]	[0,1]
$\beta 1_{\gamma^C}$	$\boldsymbol{P}(\beta 1\|\gamma^C)$	[0.0410,0.1930]	[0,1]	[¼,¼]	[0,1]
$\beta 2_{\gamma^C}$	$\boldsymbol{P}(\beta 2\|\gamma^C)$	[0.1527,0.1772]	[1,0]	[¼,¼]	[0,1]
$\beta 3_{\gamma^C}$	$\boldsymbol{P}(\beta 3\|\gamma^C)$	[0.3683,0.4682]	[0,0]	[¼,¼]	[0,1]
$\beta 4_{\gamma^C}$	$\boldsymbol{P}(\beta 4\|\gamma^C)$	[0.4380,0.1616]	[0,0]	[¼,¼]	[0,1]
γ	$\boldsymbol{P}(\gamma)$	[0.3000,0.4500]	Same as original		
γ^C	$\boldsymbol{P}(\gamma^C)$	[0.7000,0.5500]	Same as original		
Posterior: $\boldsymbol{P}(\gamma\|\alpha)$		[0.3143,0.4658]	[0.30,0.45]	[0.30,0.45]	[0.30,0.45]

Interestingly enough, all three cases show the exact same thing: no update from the prior probability $\boldsymbol{P}(\gamma)$. In Case 2 and Case 3, the reason for this is identical to that given in §4.4.2.1: when all of the values in a matrix are identical, the effects of all other matrices are cancelled out except for the prior probability. This is true for 0 (when a limit is taken), ¼, 1, and any other number. Case 1 also cancels out the effects of all matrices, but it does so by eliminating all but one input at a time, which is then equal in both the numerator and the denominator of the matrix.

This lack of an update is actually encouraging. Evidence that cannot be linked to a prior probability should not be allowed to update that posterior probability. In essence, the examples of Table 12 illustrate that the GIBR equation automatically excludes irrelevant information. This also leads to one significant and positive conclusion: if GIBR is used when one of the links in the equation's chain is occupied by complete ignorance, it will provide no update. However, this provides no advantage over classical (non-interval) Bayes' Rule, which will also give no update when equal weighting is used to represent complete ignorance. This is illustrated in equation (28), below, where the $P(\beta|\gamma)$ and the $P(\beta|\gamma^C)$ terms have been replaced with equally weighted probabilities in order to represent complete ignorance, and the other terms have been replaced with real values centered on the intervals used elsewhere in this section:

$$P(\gamma|\alpha) = \frac{[0.6927 \quad 0.8220 \quad 0.6178 \quad 0.2898]\begin{bmatrix}0.2500\\0.2500\\0.2500\\0.2500\end{bmatrix} \cdot 0.3750}{[0.6927 \quad 0.8220 \quad 0.6178 \quad 0.2898]\begin{bmatrix}0.2500 & 0.2500\\0.2500 & 0.2500\\0.2500 & 0.2500\\0.2500 & 0.2500\end{bmatrix}\begin{bmatrix}0.3750\\0.6250\end{bmatrix}} = 0.3750 \qquad (28)$$

Perhaps a more common situation involves a link in the chain that is partially occupied by ignorance. This is illustrated in Table 13, where the values of the $\boldsymbol{P}(\beta|\gamma)$ terms are known, but the values of the $\boldsymbol{P}(\beta|\gamma^C)$ terms are representations of complete ignorance. This may occur when γ is used to represent a model, while γ^C is used to

represent "not the model." "Not the model" could be interpreted as *anything* else, and so complete ignorance in that case makes sense.

Table 13: The effect of complete ignorance occupying part of a link in the probability chain, with three different methods for representing complete ignorance. Note that the negative percentage for ($\boldsymbol{P}(\gamma|\alpha)$ range)/ (MC range) in Case 3 reflects the improper posterior interval $\boldsymbol{P}(\gamma|\alpha)$, and the large absolute value of that percentage reflects the fact that the posterior interval was wider than the range of the Monte Carlo simulation results.

Symbol	Probability	Original Interval	Complete Ignorance		
			Case 1: Forced zeros due to the LCC	Case 2: Equal Weights following the LCC	Case 3: Equal Weights without LCC
$\alpha_{\beta 1}$	$\boldsymbol{P}(\alpha\|\beta 1)$	[0.3880,0.9973]	Same as original		
$\alpha_{\beta 2}$	$\boldsymbol{P}(\alpha\|\beta 2)$	[0.7415,0.9024]	Same as original		
$\alpha_{\beta 3}$	$\boldsymbol{P}(\alpha\|\beta 3)$	[0.3667,0.8688]	Same as original		
$\alpha_{\beta 4}$	$\boldsymbol{P}(\alpha\|\beta 4)$	[0.1655,0.4140]	Same as original		
$\beta 1_{\gamma}$	$\boldsymbol{P}(\beta 1\|\gamma)$	[0.1197,0.1826]	Same as original		
$\beta 2_{\gamma}$	$\boldsymbol{P}(\beta 2\|\gamma)$	[0.1662,0.3080]	Same as original		
$\beta 3_{\gamma}$	$\boldsymbol{P}(\beta 3\|\gamma)$	[0.3587,0.4603]	Same as original		
$\beta 4_{\gamma}$	$\boldsymbol{P}(\beta 4\|\gamma)$	[0.3554,0.0491]	Same as original		
$\beta 1_{\gamma^c}$	$\boldsymbol{P}(\beta 1\|\gamma^C)$	[0.0410,0.1930]	[0,1]	[¼,¼]	[0,1]
$\beta 2_{\gamma^c}$	$\boldsymbol{P}(\beta 2\|\gamma^C)$	[0.1527,0.1772]	[1,0]	[¼,¼]	[0,1]
$\beta 3_{\gamma^c}$	$\boldsymbol{P}(\beta 3\|\gamma^C)$	[0.3683,0.4682]	[0,0]	[¼,¼]	[0,1]
$\beta 4_{\gamma^c}$	$\boldsymbol{P}(\beta 4\|\gamma^C)$	[0.4380,0.1616]	[0,0]	[¼,¼]	[0,1]
γ	$\boldsymbol{P}(\gamma)$	[0.3000,0.4500]	Same as original		
γ^C	$\boldsymbol{P}(\gamma^C)$	[0.7000,0.5500]	Same as original		
Posterior: $\boldsymbol{P}(\gamma\|\alpha)$		[0.3143,0.4658]	[0.1722,0.4193]	[0.2708,0.4751]	[1,0.1845]
% of MC simulation results contained (uniform inputs)		91.73%	94.41%	99.68%	100%
($\boldsymbol{P}(\gamma\|\alpha)$ range)/ (MC range)		57.19%	60.29%	82.56%	-136.64%

The calculations for these three cases representing complete ignorance unfortunately result in very different posterior probabilities. The point intervals used in Case 1 and Case 2 incorrectly imply that only one value is acceptable for the $\boldsymbol{P}(\beta|\gamma)$ terms in equation (8). From that perspective, Case 3 is the best representation of

complete ignorance. It has the added advantage of providing the widest posterior probability interval, although the interval is improper.

Although all three cases are intended to represent the same thing, their input intervals are different, and so all three require different Monte Carlo simulations for verification. All three are scaled such that the posterior probability intervals are represented by twenty bins. The results of these simulations are shown in Figure 14, Figure 15, and Figure 16.

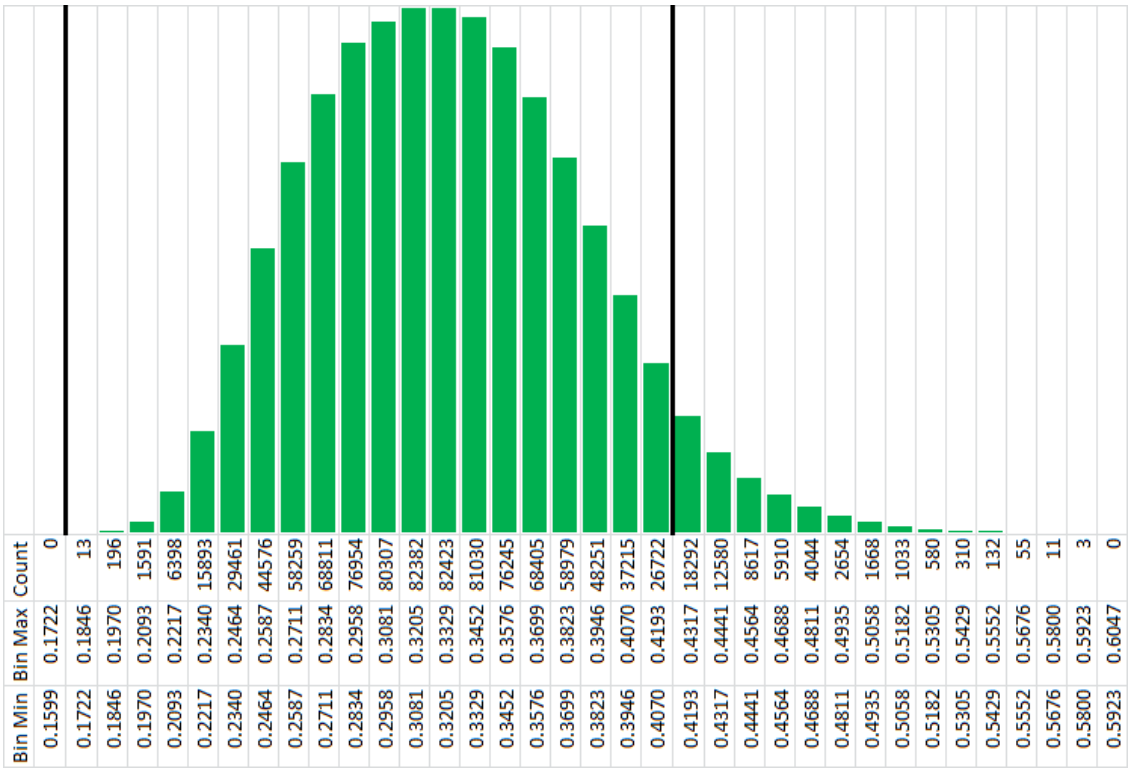

Bin Min	Bin Max	Count
0.1599	0.1722	0
0.1722	0.1846	13
0.1846	0.1970	196
0.1970	0.2093	1591
0.2093	0.2217	6398
0.2217	0.2340	15893
0.2340	0.2464	29461
0.2464	0.2587	44576
0.2587	0.2711	58259
0.2711	0.2834	68811
0.2834	0.2958	76954
0.2958	0.3081	80307
0.3081	0.3205	82382
0.3205	0.3329	82423
0.3329	0.3452	81030
0.3452	0.3576	76245
0.3576	0.3699	68405
0.3699	0.3823	58979
0.3823	0.3946	48251
0.3946	0.4070	37215
0.4070	0.4193	26722
0.4193	0.4317	18292
0.4317	0.4441	12580
0.4441	0.4564	8617
0.4564	0.4688	5910
0.4688	0.4811	4044
0.4811	0.4935	2654
0.4935	0.5058	1668
0.5058	0.5182	1033
0.5182	0.5305	580
0.5305	0.5429	310
0.5429	0.5552	132
0.5552	0.5676	55
0.5676	0.5800	11
0.5800	0.5923	3
0.5923	0.6047	0

Figure 14: 1,000,000 sample Monte Carlo simulation of Case 1 from Table 13, with uniform input intervals.

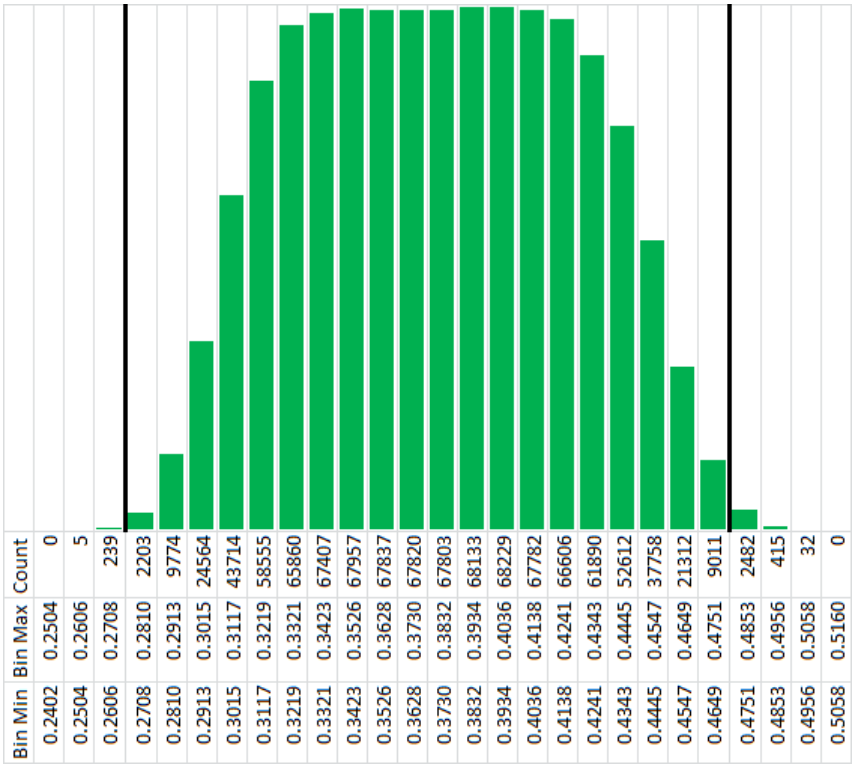

Bin Min	Bin Max	Count
0.2402	0.2504	0
0.2504	0.2606	5
0.2606	0.2708	239
0.2708	0.2810	2203
0.2810	0.2913	9774
0.2913	0.3015	24564
0.3015	0.3117	43714
0.3117	0.3219	58555
0.3219	0.3321	65860
0.3321	0.3423	67407
0.3423	0.3526	67957
0.3526	0.3628	67837
0.3628	0.3730	67820
0.3730	0.3832	67803
0.3832	0.3934	68133
0.3934	0.4036	68229
0.4036	0.4138	67782
0.4138	0.4241	66606
0.4241	0.4343	61890
0.4343	0.4445	52612
0.4445	0.4547	37758
0.4547	0.4649	21312
0.4649	0.4751	9011
0.4751	0.4853	2482
0.4853	0.4956	415
0.4956	0.5058	32
0.5058	0.5160	0

Figure 15: 1,000,000 sample Monte Carlo simulation of Case 2 from Table 13, with uniform input intervals.

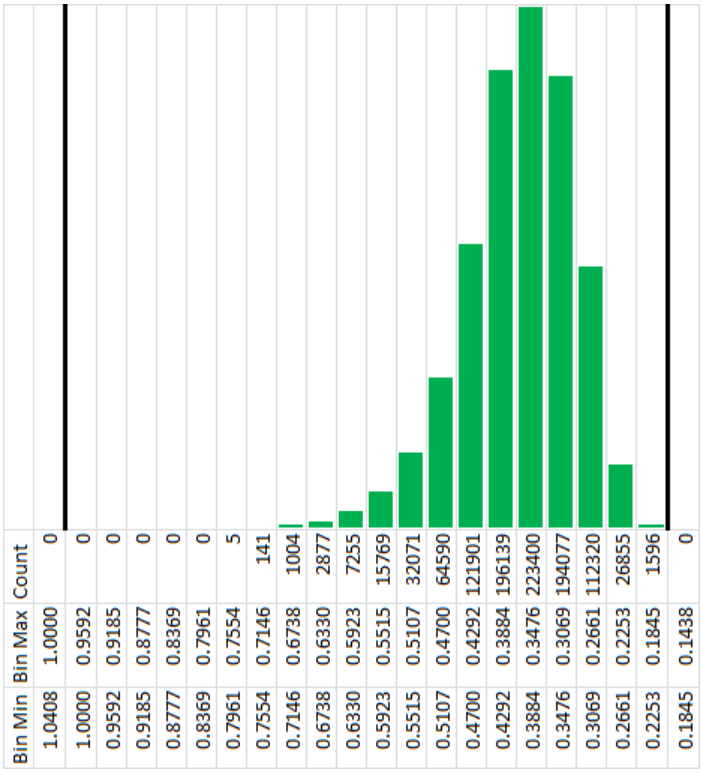

Bin Min	Bin Max	Count
1.0408	1.0000	0
1.0000	0.9592	0
0.9592	0.9185	0
0.9185	0.8777	0
0.8777	0.8369	0
0.8369	0.7961	0
0.7961	0.7554	5
0.7554	0.7146	141
0.7146	0.6738	1004
0.6738	0.6330	2877
0.6330	0.5923	7255
0.5923	0.5515	15769
0.5515	0.5107	32071
0.5107	0.4700	64590
0.4700	0.4292	121901
0.4292	0.3884	196139
0.3884	0.3476	223400
0.3476	0.3069	194077
0.3069	0.2661	112320
0.2661	0.2253	26855
0.2253	0.1845	1596
0.1845	0.1438	0

Figure 16: 1,000,000 sample Monte Carlo simulation of Case 3 from Table 13, with uniform input intervals.

It can be observed from these figures that the posterior probability interval in Case 1 is sound, but it is not centered on the sample output distribution. Case 3 is likewise not centered, but it provides a complete rather than a sound solution. The Case 2 sample output is centered and almost complete—its posterior probability gives perhaps the best estimate of its Monte Carlo simulation results out of all three. However, Case 2 suffers conceptually from the incorrect implication of certainty where equally weighted point intervals are applied. In this respect it is no worse than the traditional real-valued equation, though, which does give an update when part of a link is occupied by complete ignorance. This is illustrated below in equation (29), where the $P(\beta|\gamma^C)$ terms have been replaced with equally weighted probabilities that represent complete ignorance, and the other terms have been replaced with real values centered on the intervals used elsewhere in this section:

$$P(\gamma|\alpha) = \frac{\begin{bmatrix}0.6927 & 0.8220 & 0.6178 & 0.2898\end{bmatrix}\begin{bmatrix}0.1512\\0.2371\\0.4095\\0.2023\end{bmatrix}\cdot 0.3750}{\begin{bmatrix}0.6927 & 0.8220 & 0.6178 & 0.2898\end{bmatrix}\begin{bmatrix}0.1512 & 0.2500\\0.2371 & 0.2500\\0.4095 & 0.2500\\0.2023 & 0.2500\end{bmatrix}\begin{bmatrix}0.3750\\0.6250\end{bmatrix}} = 0.3772 \qquad (29)$$

This equation likewise provides an update in the face of a link partially occupied by complete ignorance, and likewise uses a potentially misleading impression that the values of the four $P(\beta|\gamma^C)$ terms are actually known.

4.6: Summary of Calculations

To ease review of this work, a summary of the equations used in Chapter 4 along with and their inputs and outputs is given in Table 15. Posterior probabilities were calculated for two main equation forms: equation (12) and equation (16), calculating the posterior probabilities $\boldsymbol{P}\left(\theta\middle|\frac{\Delta\rho}{\mathrm{n}}\right)$ and $\boldsymbol{P}\left(\theta\middle|\frac{\Delta\rho}{\mathrm{n}}\cap\frac{\Delta\ell/\ell}{n}\right)$, respectively. Equation (12) was calculated with several sets of inputs, represented by equations (13), (19), (20)(19), (21), (22), (23), (24), and (25). A posterior probability for equation

(16) was calculated only once, as shown in equation (17) in §4.2, and its results are not repeated here. A basic explanation for each of these equations is given in Table 14.

Table 14: Summary of the methods used to calculate a posterior probability using for equations (12) and (16). Equation (17) represents the interval values used in place of the symbolic equation (16); all others represent interval values used in place of the symbolic equation (12).

(13)	Intervals as originally interpreted. This includes a representation of complete ignorance that forces a zero-width [0,0] interval due to the LCC.
(19)	Reversed the bounds of the prior probability intervals.
(20)	Reversed the bounds of the Td_θ and Td_θ^c intervals.
(21)	Reversed the bounds of the Td_{θ^c} and $Td_{\theta^c}^c$ complete ignorance intervals.
(22)	Reversed the bounds of the Tm_{Td} complete ignorance intervals.
(23)	Reversed the bounds of the Tm_{Td^c} complete ignorance intervals.
(24)	Replaced the complete ignorance intervals with equally-weighted point intervals.
(25),	Replaced the complete ignorance intervals with full-width intervals ([0,1]) that are not subject to the LCC.
(17)	Intervals as originally interpreted, with added experimental information related to $\frac{\Delta\ell/\ell}{n}$. This gave a result identical to equation (13), as discussed in §4.2.

Table 15: Summary of interval input values and calculated posterior probabilities for equation (12).

Symbol	Value							
Equation:	(13)	(19)	(20)	(21)	(22)	(23)	(24)	(25)
Inputs								
ρ_{Tm1}	[0.5, 0.5]	[0.5, 0.5]	[0.5, 0.5]	[0.5, 0.5]	[0.5, 0.5]	[0.5, 0.5]	[0.5, 0.5]	[0.5, 0.5]
ρ_{Tm2}	[0,0]	[0,0]	[0,0]	[0,0]	[0,0]	[0,0]	[0,0]	[0,0]
ρ_{Tm3}	[0.6665, 0.6672]	[0.6665, 0.6672]	[0.6665, 0.6672]	[0.6665, 0.6672]	[0.6665, 0.6672]	[0.6665, 0.6672]	[0.6665, 0.6672]	[0.6665, 0.6672]
$Tm1_{Td}$	[0,1]	[0,1]	[0,1]	[0,1]	**[1,0]**	[0,1]	**[⅓,⅓]**	**[0,1]**
$Tm2_{Td}$	[0,0]	[0,0]	[0,0]	[0,0]	[0,0]	[0,0]	**[⅓,⅓]**	**[0,1]**
$Tm3_{Td}$	[1,0]	[1,0]	[1,0]	[1,0]	**[0,1]**	[1,0]	**[⅓,⅓]**	**[0,1]**
$Tm1_{Td^c}$	[0,0]	[0,0]	[0,0]	[0,0]	[0,0]	[0,0]	**[⅓,⅓]**	**[0,1]**
$Tm2_{Td^c}$	[0,1]	[0,1]	[0,1]	[0,1]	[0,1]	**[1,0]**	**[⅓,⅓]**	**[0,1]**
$Tm3_{Td^c}$	[1,0]	[1,0]	[1,0]	[1,0]	[1,0]	**[0,1]**	**[⅓,⅓]**	**[0,1]**
Td_θ	[0.7923, 1]	[0.7923, 1]	**[1, 0.7923]**	[0.7923, 1]	[0.7923, 1]	[0.7923, 1]	[0.7923, 1]	[0.7923, 1]
Td_θ^c	[0.2077, 0]	[0.2077, 0]	**[0, 0.2077]**	[0.2077, 0]	[0.2077, 0]	[0.2077, 0]	[0.2077, 0]	[0.2077, 0]
Td_{θ^c}	[0,1]	[0,1]	[0,1]	**[1,0]**	[0,1]	[0,1]	**[½,½]**	**[0,1]**
$Td_{\theta^c}^c$	[1,0]	[1,0]	[1,0]	**[0,1]**	[1,0]	[1,0]	**[½,½]**	**[0,1]**
θ	[0.4, 0.5]	**[0.5, 0.4]**	[0.4, 0.5]	[0.4, 0.5]	[0.4, 0.5]	[0.4, 0.5]	[0.4, 0.5]	[0.4, 0.5]
θ^c	[0.6, 0.5]	**[0.5, 0.6]**	[0.6, 0.5]	[0.6, 0.5]	[0.6, 0.5]	[0.6, 0.5]	[0.6, 0.5]	[0.6, 0.5]
Results								
$\boldsymbol{P}\left(\theta\middle\vert\frac{\Delta\rho}{n}\right)$	[0.4, 0.5]	[0.5, 0.4]	[0.4, 0.4421]	[0.4, 1]	[0.3484, 0.5]	[1, 0.5]	[0.4, 0.5]	[1, 0.3333]

Because the values of the interval bounds are identical for equations (13), (19), (20), (21), (22), and (23), each can be subject to the same Monte Carlo simulation results for verification—the results are simply viewed through a different posterior probability lens. This is illustrated in Figure 17. The drastic difference between these posterior probability intervals is a dramatic example of the huge effect that a small change can have on result of a GIBR equation, particularly in the case of equations (13)

and (21), where the difference between the inputs is the result of a completely subjective choice.

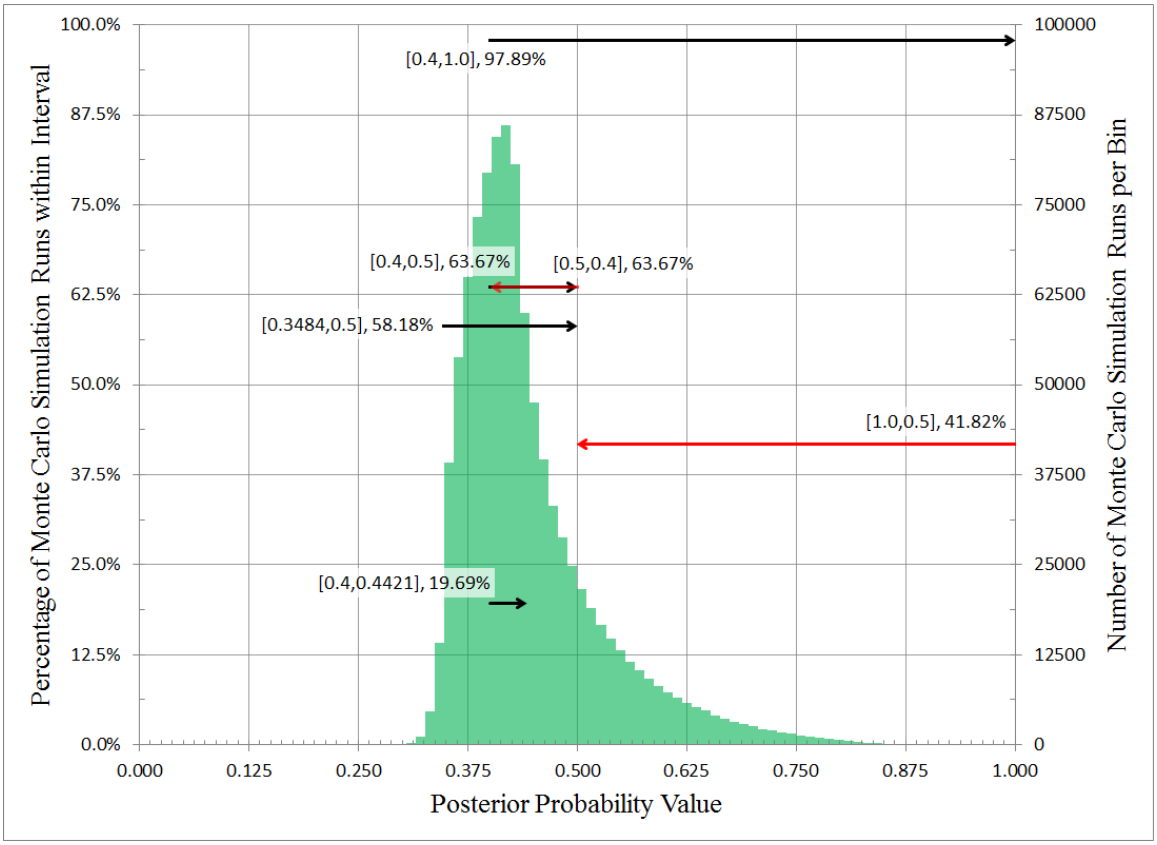

Figure 17: Visual comparison of the posterior probability intervals of six equations following the form of equation (12) versus a one million run Monte Carlo simulation of the equations. The Monte Carlo simulation uses uniform input intervals. The green vertical bars represent the Monte Carlo simulation results, while the horizontal lines represent each equation's posterior probability interval. The width of the line represents the width of the interval, and the vertical location of the line represents the percentage of the Monte Carlo simulation results that fell within the interval. Proper intervals are represented by black lines, and improper intervals by red lines. Each equation shares the same input intervals save for the order of the interval bounds.

Monte Carlo simulations to verify equations (24) and (25) are given in §4.4.2.1 and §4.5.1, respectively, and are not repeated here.

4.6.1: The complete solution

Of the fifteen input intervals used in equations (13), (19), (20), (21), (22), and (23), four are zero-width, and only six of the remaining eleven are independent when the Logic Coherence Constraint is obeyed. In order to determine the possible extremes of the real-valued solutions to these equations, only 64 (or 2^6) real-valued calculations are necessary, each one representing a different combination of the upper or

lower bounds of the independent input intervals. This set of calculations reveals that the extreme values possible using the intervals from equation (13), etc. are $\underline{\underline{\boldsymbol{P}}}\left(\theta \left| \frac{\Delta \rho}{\mathrm{n}} \right. \right) = 0.3332$ and $\overline{\overline{\boldsymbol{P}}}\left(\theta \left| \frac{\Delta \rho}{\mathrm{n}} \right. \right) = 1$, where the double underbars or double overbars represent the extreme lower and upper bounds, respectively. The values that lead to these posterior probabilities are shown in Table 16.

Table 16: Summary of the extreme values possible with real values within the bounds of the intervals used in equations (13), (19), (20), (21), (22), and (23).

	Eq. (13)	Type	Minimum	Maximum
ρ_{Tm1}	[0.5,0.5]	Point	0.5	0.5
ρ_{Tm2}	[0,0]	Point	0	0
ρ_{Tm3}	[0.6665,0.6672]	Independent	Either Bound	Either Bound
$Tm1_{Td}$	[0,1]	Independent	**1**	Either Bound
$Tm2_{Td}$	[0,0]	Point	0	0
$Tm3_{Td}$	[1,0]	Dependent	$= 1 - Tm1_{Td}$	
$Tm1_{Td^c}$	[0,0]	Point	0	0
$Tm2_{Td^c}$	[0,1]	Independent	**0**	**1**
$Tm3_{Td^c}$	[1,0]	Dependent	$= 1 - Tm2_{Td^c}$	
Td_θ	[0.7923,1]	Independent	**1**	Either Bound
Td_θ^c	[0.2077,0]	Dependent	$= 1 - Td_\theta$	
Td_{θ^c}	[0,1]	Independent	**0**	**0**
$Td_{\theta^c}^c$	[1,0]	Dependent	$= 1 - Td_{\theta^c}$	
θ	[0.4,0.5]	Independent	**0.4**	Either Bound
θ^c	[0.6,0.5]	Dependent	$= 1 - \theta$	
$\boldsymbol{P}\left(\theta \left\| \frac{\Delta\rho}{\mathrm{n}} \right.\right)$	[0.4,0.5]	Result	0.3332	1

No obvious formulation of GIBR leads to the complete interval, but the GIBR equation does assist the analyst in organizing the information, recognizing dependencies between intervals, and identifying point intervals in order to decrease the required number of calculations. While not as simple as a single interval-valued calculation (or two decoupled real-valued calculations), 64 calculations is still a great improvement over the one million calculations used in each of the Monte Carlo simulations.

4.7: Conclusions

This chapter has dealt with an example that contains instances of complete ignorance. Perhaps the most important conclusion is that interval probability mirrors other probability theories in cases of complete ignorance. In the best case scenario, intervals that are intended to represent complete ignorance may simply prevent the passage of information and deliver a posterior probability identical to the prior—making the analysis of no help other than to identify the existence of a missing link. In the worst case, intervals that represent complete ignorance can lead to the presence of subjective choices in bound limits. These choices can cause huge changes in the resulting posterior probability, despite ostensibly representing the exact same information. Between the best and the worst case, a "hybrid" of classical ignorance representation and interval ignorance may be used by employing equally weighted point intervals, but misleadingly implies certainty of input where there is none, and it may prevent information passage as well. If generalized interval Bayes' rule is desired for use in an instance where data are not available, the next best option would still be to consult a domain expert for an estimation of the input interval based on his or her best intuition and experience, since the application of complete ignorance by interval probability may result in non-deterministic update. The underlying reasons should be further investigated in the future.

CHAPTER 5: USING GIBR TO COMPARE MODELS

This chapter examines two methods to update belief in simulation results using Generalized Interval Bayes' Rule. The first method uses the results of physical experiments for an update, and thus is an example of model validation. The second updates the model's results with the evidence provided by a second model, and thus may be thought of as model verification or even model aggregation.

In the context of this chapter, Model 1 refers to a finite element simulation (Patra, Zhu, & McDowell, Constitutive equations, 2014) that predicts the yield strength of bcc iron based on a combination of six input parameters at varying levels. It is based on a dislocation density crystal plasticity model, and assumes that non-Schmid effects are heavily manifested in both the orientation dependence of a material and in the tension-compression asymmetry at initial yield. Model 2 in this chapter (Patra, Modeling mechanical behavior, 2013) uses the same set of parameters and predicts the same basic phenomena. It is similarly a crystal viscoplasticity model, but its formulation accounts for temperature-dependence in the non-Schmid parameters.

A third model was also investigated for this analysis. Models 1 and 2 may be thought of as "top-down" models—that is, their formulation and parameters are based primarily on larger-scale measurements. Like these models, Model 3 employs crystal plasticity flow rule. However, unlike the previous models, Model 3 is a "bottom-up" model: it employs atomistically informed parameters to predict the behavior of the BCC iron crystals, including dependencies on temperature, orientation, and strain rate (Narayanan, McDowell, & Zhu, 2014). The results are of the same type for each model: each temperature and orientation will predict values for the yield strength of the material. Combining or comparing Model 3 with either of the other models would thus be cross-scale model validation, as each model is based on a different scale of operation. The

results currently available for Model 3 are much more limited than for the other two models, and so only a limited analysis was performed using that model. Nevertheless, because of the similar form of the results of the models, the method for combining models 1 and 2 is identical to the method for combining models 1 and 3. Thus, even though Model 1 and Model 2 are of the same scale, the demonstrations with these two models can also serve as examples of how to complete cross-scale model validation.

GIBR is first used as a comparative tool between the two main simulations, with the updating experimental results acting as a standard. GIBR is then used to combine the results of the two simulations, with a prior probability intervals supplied by the simulations and an update coming from the experimental results. Model aggregation is a novel application of Bayes' Rule, and need not be confined to generalized interval applications—if the intervals are degenerated "point" intervals (i.e. real rather than interval values), then the application still may be used and is still novel.

5.1: Equation formulation for updating individual model probabilities

In an engineering application, it may be useful to know whether or not a material will yield under a given level of stress. In this example, a stress of 150 MPa is arbitrarily selected, and the probability that the model predicts yielding given that physical experiments predict yielding ($\boldsymbol{P}(y_m|y_e)$) is calculated with GIBR. In order to provide some consistent basis for comparing the results, the temperature of the simulation and of the experiment is used as a link in the GIBR. Under these conditions, the relevant equation is:

$$\boldsymbol{P}(y_m|y_e) = \frac{\int \boldsymbol{P}(y_e|t) \cdot \boldsymbol{P}(t|y_m)dt \cdot \boldsymbol{P}(y_m)}{dual(\int\int \boldsymbol{P}(y_e|t) \cdot \boldsymbol{P}(t|y_m) \cdot \boldsymbol{P}(y_m)dt\, dy_m)} \quad (30)$$

In this equation, y_m means "the model predicts yielding," y_e means "the experimental results demonstrate yielding," and t means "temperature." Using the conventions already established in this thesis, an integration over three possible

temperatures (143 K, 195 K, and 250 K) and two possible states of y_m (for "the model predicts yielding" and "the model does not predict yielding") looks like this:

$$\boldsymbol{P}(y_m|y_e) = \frac{[\boldsymbol{P}(y_e|t_1) \quad \boldsymbol{P}(y_e|t_2) \quad \boldsymbol{P}(y_e|t_3)] \begin{bmatrix} \boldsymbol{P}(t_1|y_m) \\ \boldsymbol{P}(t_2|y_m) \\ \boldsymbol{P}(t_3|y_m) \end{bmatrix} \boldsymbol{P}(y_m)}{dual\left([\boldsymbol{P}(y_e|t_1) \quad \boldsymbol{P}(y_e|t_2) \quad \boldsymbol{P}(y_e|t_3)] \begin{bmatrix} \boldsymbol{P}(t_1|y_m) & \boldsymbol{P}(t_1|y_m^C) \\ \boldsymbol{P}(t_2|y_m) & \boldsymbol{P}(t_2|y_m^C) \\ \boldsymbol{P}(t_3|y_m) & \boldsymbol{P}(t_3|y_m^C) \end{bmatrix} \begin{bmatrix} \boldsymbol{P}(y_m) \\ \boldsymbol{P}(y_m^C) \end{bmatrix} \right)} \quad (31)$$

In each finite element model, six input parameters (temperature, orientation, *p*, *q*, $\dot{\gamma}_0$, and ΔG) were combined at three levels each, resulting in 3^6 (or 729) total simulations—243 at each of the three orientations. The orientations are numbered 4, 5, and 6, which is a relic of some earlier simulations that were not included in this study. Yield behavior can vary significantly based on orientation, and the behaviors of different orientations cannot be averaged or otherwise combined: combining different orientations requires a polycrystalline model, which introduces the effects of grain boundaries and other slip mechanisms. Hence, for the single crystal models used here, the orientation of the material is the primary form of epistemic uncertainty. Given a specific orientation, the intervals would each collapse to a single real value.

5.1.1: Calculation of relevant probabilities from Model 1 results

In order to calculate a posterior probability $\boldsymbol{P}(y_{m1}|y_e)$ using equation (31), Model 1 results must be used to calculate $\boldsymbol{P}(t_1|y_{m1})$, $\boldsymbol{P}(t_2|y_{m1})$, $\boldsymbol{P}(t_3|y_{m1})$, $\boldsymbol{P}(t_1|y_{m1}^C)$, $\boldsymbol{P}(t_2|y_{m1}^C)$, $\boldsymbol{P}(t_3|y_{m1}^C)$, $\boldsymbol{P}(y_{m1})$, and $\boldsymbol{P}(y_{m1}^C)$. The calculation of the probabilities $\boldsymbol{P}(y_{m1})$ and $\boldsymbol{P}(y_{m1}^C)$ is examined first.

Using Model 1, 243 finite element simulations were run at each of three orientations. The mean and standard deviation of the resulting yield strengths is easily calculated and a CDF is generated for each orientation assuming a normal distribution of yield strengths. An example of the approximated CDF is shown in Figure 18 along with a

discretized CDF based on the actual values of predicted yield strength for Model 1, Orientation #4.

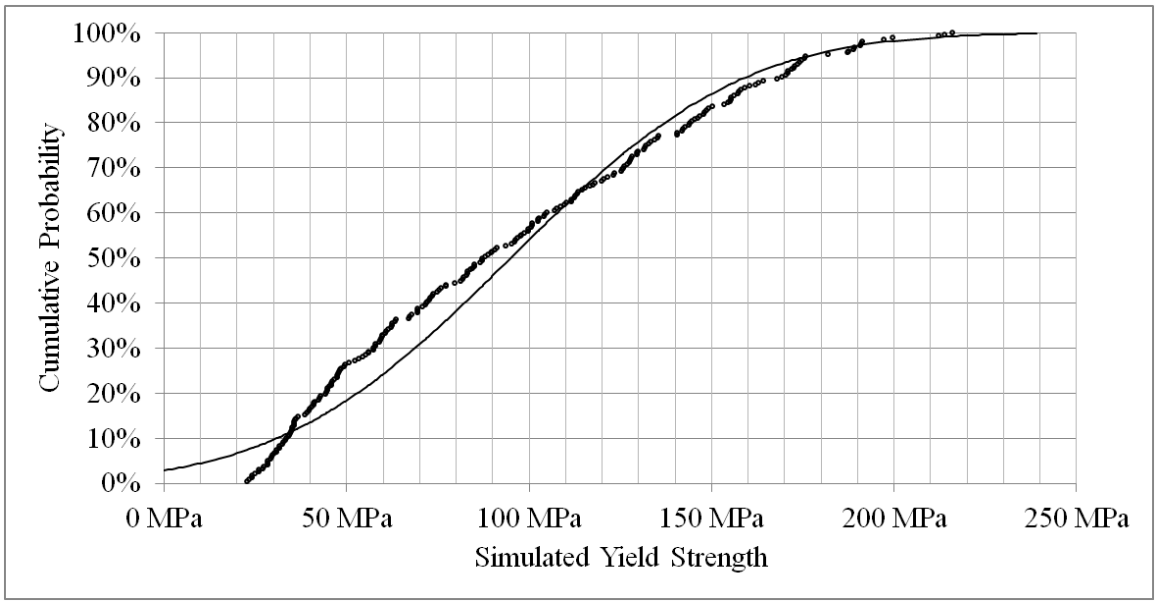

Figure 18: Discretized CDF made from the simulated yield strengths for each of the parameters used in Model 1, Orientation #4 plotted along with the smoothed CDF approximation, which assumes a normal distribution of simulated yield strengths.

By comparing the chosen stress of 150 MPa with these approximated CDFs, the probability that the model will predict yielding at each orientation can be determined. Then, because the orientation represents the epistemic uncertainty, the highest and lowest probabilities from among these three orientations then represent $\overline{\boldsymbol{P}}(y_{m1})$ and $\underline{\boldsymbol{P}}(y_{m1})$, respectively. These calculations are summarized in Table 17.

Table 17: Calculation of the interval probability that Model 1 predicts yielding.

Orientation	Average Yield Strength, Model 1	Standard Deviation of Yield Strength, Model 1	$P(y_{m1}\|orient.)$	$\boldsymbol{P}(y_{m1})$	
#4	94.9 MPa	50.0 MPa	86.47%	$\underline{\boldsymbol{P}}(y_{m1})$	$\overline{\boldsymbol{P}}(y_{m1})$
#5	101.5 MPa	52.9 MPa	82.02%	0.5523	0.8647
#6	140.0 MPa	76.4 MPa	55.23%		

Armed with the interval value of $\boldsymbol{P}(y_{m1})$, $\boldsymbol{P}(y_{m1}^{C})$ is easily calculated. The probability that Model 1 does not predict yielding is simply $1 - dual\big(\boldsymbol{P}(y_{m1})\big)$. Thus, $\boldsymbol{P}(y_{m1}^{C}) = [0.4477, 0.1353]$.

Next, the calculation of probabilities of the form $\boldsymbol{P}(t|y_m)$ is examined. Because these probabilities are based on a binary condition (the model did or did not predict yielding), and because the temperatures have been discretized, using a distribution to describe the conditional probabilities does not make sense. Instead, a simple proportion will be used to generate the probabilities of each temperature given yielding. Using orientation #4 as an example, 202 simulations exhibited a yield strength below 150 MPa. Of these 202 simulations, 41 used a temperature of 143K (or t_1), 80 used $t_2 = 195K$, and 81 used $t_3 = 250K$. This is interpreted to mean that, for Model 1, orientation #4, the probability that the temperature is 143K given that the model predicted yielding was $\frac{41}{202}$ or 20.30%. This probability changes with orientation. For orientation #5, $\boldsymbol{P}(t_1|y_{m1}) = \frac{30}{191}$ or 15.71%. For orientation #6, $\boldsymbol{P}(t_1|y_{m1}) = \frac{3}{142}$ or 2.11%. If the lack of knowledge about which orientation to use is taken to be the epistemic uncertainty, then the minimum and maximum of these three probabilities give the bounds for the interval, and thus $\boldsymbol{P}(t_1|y_{m1}) = [0.0211,0.2030]$. Following this method, the intervals $\boldsymbol{P}(t_2|y_{m1})$ and $\boldsymbol{P}(t_3|y_{m1})$ were calculated as [0.3960,0.4188] and [0.4010,0.5704], respectively. The results of these calculations are given in Table 18. It is important to note that, while each orientation individually adheres to the Logic Coherence Constraint, the intervals based on all three orientations do not adhere to the LCC. As such, it is necessary to choose one of the temperatures to be a non-focal event for the purposes of this GIBR, thus allowing its probability to be determined by the values of the probabilities of the other two temperatures. This will be discussed further in §5.1.4.

Table 18: Summary of the calculation of $P(t|y_{m1})$. Note that the row exhibiting information for "All Temperatures" is the sum of the rows above it. In the case of the "Quantity of Simulations" columns, this row exhibits the normalizing factor that the other quantities were divided by in order to reach a probability. In the probability columns, this row exhibits the behavior of the Logic Coherence Constraint.

	Quantity of Simulations Exhibiting Yield in Model 1			$\boldsymbol{P}(t\|y_{m1})$			
Orientation No.	#4	#5	#6	#4	#5	#6	Interval
T=143 K	41	30	3	0.2030	0.1571	0.0211	[0.0211,0.2030]
T=195 K	80	80	58	0.3960	0.4188	0.4085	[0.3960,0.4188]
T=250 K	81	81	81	0.4010	0.4241	0.5704	[0.4010,0.5704]
All Temps.	202	191	142	1.0000	1.0000	1.0000	[0.8182,1.1922]

A similar process was carried out in the calculation of $\boldsymbol{P}(t|y_{m1}^{C})$, except that the number of simulations not exhibiting yield (y^{C}) was examined rather than the number of simulations exhibiting yield (y). The results of these calculations, as well as the supporting values, are shown in Table 19.

Table 19: Summary of the calculation of $\boldsymbol{P}(t|y_{m1}^{C})$.

	Quantity of Simulations NOT Exhibiting Yield in Model 1			$\boldsymbol{P}(t\|y_{m1}^{C})$			
Orientation No.	#4	#5	#6	#4	#5	#6	Interval
T=143 K	40	51	78	0.9756	0.9808	0.7723	[0.7723,0.9808]
T=195 K	1	1	23	0.0244	0.0192	0.2277	[0.0192,0.2277]
T=250 K	0	0	0	0.0000	0.0000	0.0000	[0.0000,0.0000]
All Temps.	41	52	101	1.0000	1.0000	1.0000	[0.7915,1.2085]

5.1.2: Calculation of relevant probabilities from Model 2 results

While the underlying mechanisms for Model 1 and Model 2 are different, their results are of the same form. Thus, in order to calculate the probabilities $\boldsymbol{P}(t_1|y_{m2})$, $\boldsymbol{P}(t_2|y_{m2})$, $\boldsymbol{P}(t_3|y_{m2})$, $\boldsymbol{P}(t_1|y_{m2}^{C})$, $\boldsymbol{P}(t_2|y_{m2}^{C})$, $\boldsymbol{P}(t_3|y_{m2}^{C})$, $\boldsymbol{P}(y_{m2})$, and $\boldsymbol{P}(y_{m2}^{C})$, the exact same process is followed for Model 2 as for Model 1. The only difference is in the values used to generate the results. These are summarized in tabular form in the remainder of this section.

Table 20: Calculation of the interval probability that Model 2 predicts yielding.

Orientation	Average Yield Strength, Model 2	Standard Deviation of Yield Strength, Model 2	$P(y_{m2}\|orient.)$	$\boldsymbol{P}(y_{m2})$	
#4	135.0 MPa	64.0 MPa	59.24%	$\underline{\boldsymbol{P}}(y_{m2})$	$\overline{\boldsymbol{P}}(y_{m2})$
#5	135.6 MPa	68.2 MPa	58.34%	0.3417	0.5924
#6	190.5 MPa	99.3 MPa	34.17%		

By the Logic Coherence Constraint, $\boldsymbol{P}(y_{m2}^{C}) = [0.6583, 0.4076]$

Table 21: Summary of the calculation of $\boldsymbol{P}(\boldsymbol{t}|\boldsymbol{y_{m2}})$.

Orientation No.	Quantity of Simulations Exhibiting Yield in Model 2			$\boldsymbol{P}(t\|y_{m2})$			
	#4	#5	#6	#4	#5	#6	Interval
T=143 K	0	0	0	0.0000	0.0000	0.0000	[0.0000,0.0000]
T=195 K	81	81	0	0.5000	0.5000	0.0000	[0.0000,0.5000]
T=250 K	81	81	81	0.5000	0.5000	1.0000	[0.5000,1.0000]
All Temps.	162	162	81	1.0000	1.0000	1.0000	[0.5000,1.5000]

Table 22: Summary of the calculation of $\boldsymbol{P}(\boldsymbol{t}|\boldsymbol{y_{m2}^{C}})$.

Orientation No.	Quantity of Simulations NOT Exhibiting Yield in Model 2			$\boldsymbol{P}(t\|y_{m2}^{C})$			
	#4	#5	#6	#4	#5	#6	Interval
T=143 K	81	81	81	1.0000	1.0000	0.5000	[0.5000,1.0000]
T=195 K	0	0	81	0.0000	0.0000	0.5000	[0.0000,0.5000]
T=250 K	0	0	0	0.0000	0.0000	0.0000	[0.0000,0.0000]
All Temps.	81	81	162	1.0000	1.0000	1.0000	[0.5000,1.5000]

5.1.3: Calculation of relevant probabilities from the experimental results

Once the prior probabilities and the linking probabilities from the model are calculated, only the updating probabilities remain. These are based on experimental results. As with most of the probabilities in this document, there are potentially many ways to calculate each of these probabilities. For the limited experimental data available for use as a benchmark, a single yield strength is related to each combination of temperature and orientation. These are shown in Table 23. There is no randomness associated with this, and so the aleatory uncertainty of $\boldsymbol{P}(y_e|t_1)$, $\boldsymbol{P}(y_e|t_2)$, and $\boldsymbol{P}(y_e|t_3)$

should be zero. However, epistemic uncertainty will be present as long as a certain orientation has not been specified. For instance, at 195 K there are three experimental yield strengths that range from 148 MPa to 153 MPa, each one corresponding to a specific orientation. If the stress state for which information is desired is below 148 MPa, then according to that limited data set, the probability of yielding is zero. If the stress state in question is above 153 MPa, then the probability of yielding is one. If, however, the stress state is between 148 MPa and 153 MPa and the orientation has not been specified, then the probability is $[0,1]$. As soon as an orientation is specified, then a zero-width interval or a single valued probability should be used to indicate the elimination of epistemic uncertainty. For the chosen stress of 150 MPa, the three probability intervals are $\boldsymbol{P}(y_e|t_1 = 143K) = [0,0]$, $\boldsymbol{P}(y_e|t_2 = 195K) = [0,1]$, and $\boldsymbol{P}(y_e|t_3 = 250K) = [1,1]$.

Table 23: Experimental yield strengths and yield probability for each temperature and orientation. As with other probabilities in this section, a stress of 150 MPa is an implied condition for each probability.

Orientation	Experimental Yield Strengths			$P(y_e\|t)$		
	#4	#5	#6	#4	#5	#6
T=143 K	251.0 MPa	250.0 MPa	295.0 MPa	0.0000	0.0000	0.0000
T=195 K	151.0 MPa	148.0 MPa	153.0 MPa	0.0000	1.0000	0.0000
T=250 K	72.0 MPa	58.0 MPa	66.0 MPa	1.0000	1.0000	1.0000

Unfortunately, the interval $[0,1]$ used to represent $\boldsymbol{P}(y_e|t = 195K)$ provides the same information as complete ignorance. Because the detrimental effects of including complete ignorance intervals in the GIBR equations have been so thoroughly demonstrated in Chapter 4, a different calculation method will be employed to eliminate this overly wide interval. At 195 K, one of the three orientations yielded below 150 MPa, and the other two yielded above 150 MPa. In a more classical sense, this can be viewed as a one-in-three chance of yielding. Using this method, $\boldsymbol{P}(y_e|t = 195K)$ is expressed as a point interval: $[⅓, ⅓]$. The probabilities at 143K and 250K are unchanged when using

this method, and so the probabilities associated with the experimental results are $\boldsymbol{P}(y_e|t_1) = [0,0]$, $\boldsymbol{P}(y_e|t_2) = [⅓, ⅓]$, and $\boldsymbol{P}(y_e|t_3) = [1,1]$.

5.1.4: Calculating posterior probabilities for each model.

5.1.4.1: Model 1

With the relevant intervals in place of the symbolic representations for Model 1, equation (31) becomes equation (32):

$$\boldsymbol{P}(y_{m1}|y_e) = \frac{\begin{bmatrix}[0.0000,0.0000]\\[0.3333,0.3333]\\[1.0000,1.0000]\end{bmatrix}^T \begin{bmatrix}[0.0211,0.2030]\\[0.3960,0.4188]\\[0.4010,0.5704]\end{bmatrix} [0.5523,0.8647]}{dual\left(\begin{bmatrix}[0.0000,0.0000]\\[0.3333,0.3333]\\[1.0000,1.0000]\end{bmatrix}^T \begin{bmatrix}[0.0211,0.2030] & [0.7723,0.9808]\\[0.3960,0.4188] & [0.0192,0.2277]\\[0.4010,0.5704] & [0.0000,0.0000]\end{bmatrix} \begin{bmatrix}[0.5523,0.8647]\\[0.4477,0.1353]\end{bmatrix}\right)} \quad (32)$$

With the interval values in place, some of the choices as to which events should be focal or non-focal become clearer. From a mathematical standpoint, because $\boldsymbol{P}(y_e|t_1) = [0,0]$, none of the information from $\boldsymbol{P}(t_1|y_{m1})$ or $\boldsymbol{P}(t_1|y_{m1}^C)$ will have an effect on the final updated interval, because they will be multiplied by the zero value. From a logical standpoint, too, the updating equation is supposed to inform the prior probability in the instances where the experiment predicts yielding. Since the experiment does not ever predict yielding at 150 MPa for t_1, it is only logical that simulations at temperature $t_1$should be non-focal events, because they do not conform to the condition.

From a mathematical standpoint, the interval $\boldsymbol{P}(t_3|y_m^C) = [0,0]$ is both proper and improper, both focal and non-focal. Trying to force it to be strictly non-focal requires the subtraction $1 - dual\Big(\boldsymbol{P}(t_1|y_{m1}^C) + \boldsymbol{P}(t_2|y_{m1}^C)\Big)$, which gives the interval probability $[0.2085, -0.2085]$ for $\boldsymbol{P}(t_3|y_m^C)$. Negative probabilities have no logical meaning in this case, thus acting as a reminder that the simulations at temperature t_3 should be not be forced into a strictly non-focal status. Again, logically this fits as well. All of the experiments at temperature t_3 exhibited yielding below 150 MPa, and so the results of

the model at the same temperature should be very significant in determining the behavior of the model given that the experiment predicts yielding.

Temperature t_2 obviously falls somewhere in the middle. Making it a focal event could be logical since only one of the three temperatures needs to be non-focal in order to satisfy the Logic Coherence Constraint. However, since the effects of the t_1 simulations are already cancelled due to the [0,0] value of $\boldsymbol{P}(y_e|t_1)$, making t_2 non-focal would essentially put more significance on the only remaining focal event, t_3. These two potential paths bear further examination in the form of a verifying Monte Carlo simulation.

5.1.4.2: Model 2

With the relevant intervals in place of the symbolic representations for Model 2, equation (31) becomes equation (33):

$$\boldsymbol{P}(y_{m2}|y_e) = \frac{\begin{bmatrix}[0.0000,0.0000]\\[0.3333,0.3333]\\[1.0000,1.0000]\end{bmatrix}^T \begin{bmatrix}[0.0000,0.0000]\\[0.0000,0.5000]\\[0.5000,1.0000]\end{bmatrix} [0.3417,0.5924]}{dual\left(\begin{bmatrix}[0.0000,0.0000]\\[0.3333,0.3333]\\[1.0000,1.0000]\end{bmatrix}^T \begin{bmatrix}[0.0000,0.0000] & [0.5000,1.0000]\\[0.0000,0.5000] & [0.0000,0.5000]\\[0.5000,1.0000] & [0.0000,0.0000]\end{bmatrix} \begin{bmatrix}[0.3417,0.5924]\\[0.6583,0.4076]\end{bmatrix}\right)} \quad (33)$$

Some discussion is again warranted as to which events should be focal or non-focal. For the $\boldsymbol{P}(t|y_{m2})$ terms, $\boldsymbol{P}(t_1|y_{m2})$ is already both focal and non-focal and should not be forced to take on a strictly non-focal role. $\boldsymbol{P}(t_3|y_{m2}^C)$ exhibits the same characteristic among the $\boldsymbol{P}(t|y_{m2}^C)$ terms. This leaves two possibilities: either make the simulations at temperature t_2 non-focal, or choose different sets of simulations to be non-focal depending on whether the model did or did not predict yielding (y_m versus y_m^C). Again, these different paths bear further examination through Monte Carlo simulations.

5.1.5: Monte Carlo verification of Model 1 and Model 2 GIBR update.

The intervals used to generate the posterior probabilities $\boldsymbol{P}(y_m|y_e)$ are summarized in Table 24. The non-focal events, i.e. the intervals with values determined

by subtraction from other intervals, are italicized. In both models, the original intervals are not verified through Monte Carlo simulation because they do not conform to the Logic Coherence Constraint.

Table 24: Summary of the interval valued inputs and Monte Carlo simulation results for both Models 1 and 2 in the GIBR equation (31).

	Model 1			Model 2		
	Original Intervals	Case 1: Nonfocal T1	Case 2: Nonfocal T2	Original Intervals	Case 3: Nonfocal T2	Case 4: Nonfocal T1,T3
$\boldsymbol{P}(y_e\|t_1)$	[0.0000, 0.0000]	[0.0000, 0.0000]	[0.0000, 0.0000]	[0.0000, 0.0000]	[0.0000, 0.0000]	[0.0000, 0.0000]
$\boldsymbol{P}(y_e\|t_2)$	[0.3333, 0.3333]	[0.3333, 0.3333]	[0.3333, 0.3333]	[0.3333, 0.3333]	[0.3333, 0.3333]	[0.3333, 0.3333]
$\boldsymbol{P}(y_e\|t_3)$	[1.0000, 1.0000]	[1.0000, 1.0000]	[1.0000, 1.0000]	[1.0000, 1.0000]	[1.0000, 1.0000]	[1.0000, 1.0000]
$\boldsymbol{P}(t_1\|y_m)$	[0.0211, 0.2030]	*[0.2030, 0.0107]*	[0.0211, 0.2030]	[0.0000, 0.0000]	[0.0000, 0.0000]	[0.0000, 0.0000]
$\boldsymbol{P}(t_2\|y_m)$	[0.3960, 0.4188]	[0.3960, 0.4188]	*[0.5779, 0.2266]*	[0.0000, 0.5000]	*[0.5000, 0.0000]*	[0.0000, 0.5000]
$\boldsymbol{P}(t_3\|y_m)$	[0.4010, 0.5704]	[0.4010, 0.5704]	[0.4010, 0.5704]	[0.5000, 1.0000]	[0.5000, 1.0000]	*[1.0000, 0.5000]*
$\boldsymbol{P}(t_1\|y_m^C)$	[0.7723, 0.9808]	*[0.9808, 0.7723]*	[0.7723, 0.9808]	[0.5000, 1.0000]	[0.5000, 1.0000]	*[1.0000, 0.5000]*
$\boldsymbol{P}(t_2\|y_m^C)$	[0.0192, 0.2277]	[0.0192, 0.2277]	*[0.2277, 0.0192]*	[0.0000, 0.5000]	*[0.5000, 0.0000]*	[0.0000, 0.5000]
$\boldsymbol{P}(t_3\|y_m^C)$	[0.0000, 0.0000]	[0.0000, 0.0000]	[0.0000, 0.0000]	[0.0000, 0.0000]	[0.0000, 0.0000]	[0.0000, 0.0000]
$\boldsymbol{P}(y_m)$	[0.5523, 0.8647]	[0.5523, 0.8647]	[0.5523, 0.8647]	[0.3417, 0.5924]	[0.3417, 0.5924]	[0.3417, 0.5924]
$\boldsymbol{P}(y_m^C)$	*[0.4477, 0.1353]*	*[0.4477, 0.1353]*	*[0.4477, 0.1353]*	*[0.6583, 0.4076]*	*[0.6583, 0.4076]*	*[0.6583, 0.4076]*
Results						
$\boldsymbol{P}(y_m\|y_e)$	[0.9903, 0.9835]	[0.9903, 0.9835]	[0.9061, 0.9984]	[1.0000, .9105]	[0.6750, 1.0000]	[1.0000, 0.8532]
% of uniform MC simulation results contained by posterior interval	N/A	17.61%	99.98%	N/A	100.00%	75.11%
Range of MC results	N/A	0.8972 to 0.9985	0.8977 to 0.9985	N/A	0.6786 to 1.0000	
($\boldsymbol{P}(y_m\|y_e)$ range)/ (MC range), %	N/A	-6.71%	91.64%	N/A	101.15%	-45.67%

Some interesting things should be noted about the results. For Model 1, both the original intervals and Case 1 give the same posterior probability interval. This is due to the value of $\boldsymbol{P}(y_e|t_1) = [0,0]$—the values of any intervals that are multiplied by [0,0] will have no effect on the posterior probability. The only differences between Case 1 and the original equation are the values of $\boldsymbol{P}(t_1|y_{m1})$ and $\boldsymbol{P}(t_1|y_{m1}^C)$, and these are multiplied by $\boldsymbol{P}(y_e|t_1)$ in the probability chain. The result of the original equation should be ignored because it has not been subjected to the LCC, but Case 1 encompasses a disappointingly small proportion of the MC simulation results. On the other hand, Case 2 gives a posterior probability interval that excellently predicts the Monte Carlo simulation results.

For Model 2, the unique intervals used in Case 3 and Case 4 were determined by subtraction with the Logic Coherence Constraint. However, Case 3 can be converted to Case 4 by using the *dual* operator on the intervals $\boldsymbol{P}(t_2|y_m)$, $\boldsymbol{P}(t_3|y_m)$, $\boldsymbol{P}(t_1|y_m^C)$, and $\boldsymbol{P}(t_2|y_m^C)$. Thus both Case 3 and Case 4 can be subject to the exact same Monte Carlo simulation for verification. The graphical results of the applicable Monte Carlo simulations are shown in Figure 19, Figure 20, Figure 21, and Figure 22.

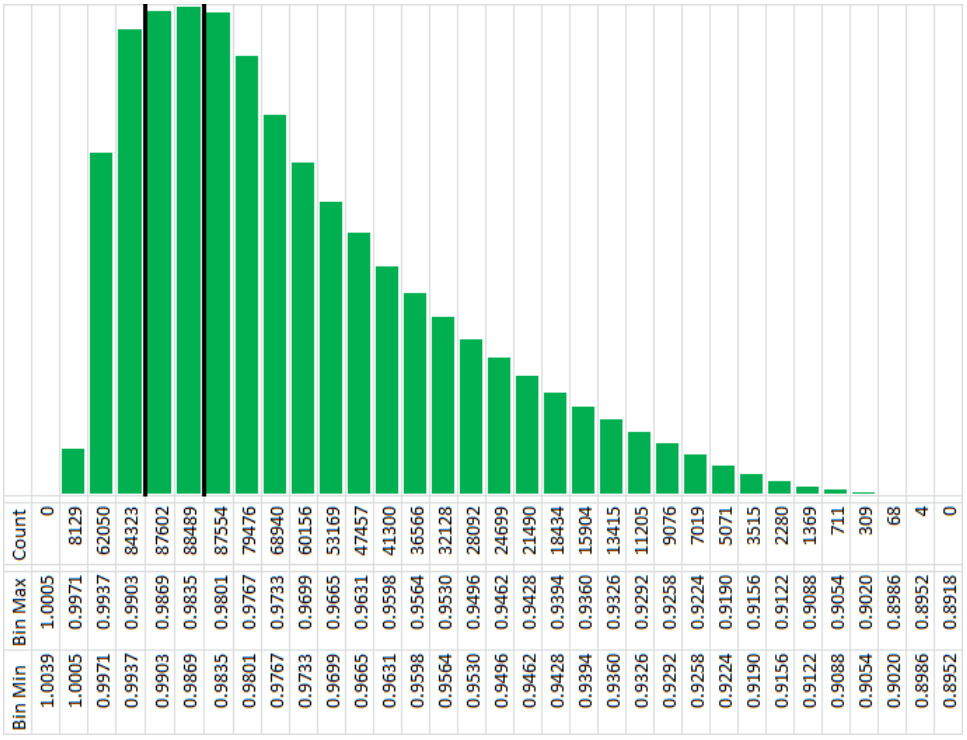

Bin Min	Bin Max	Count
1.0039	1.0005	0
1.0005	0.9971	8129
0.9971	0.9937	62050
0.9937	0.9903	84323
0.9903	0.9869	87602
0.9869	0.9835	88489
0.9835	0.9801	87554
0.9801	0.9767	79476
0.9767	0.9733	68940
0.9733	0.9699	60156
0.9699	0.9665	53169
0.9665	0.9631	47457
0.9631	0.9598	41300
0.9598	0.9564	36566
0.9564	0.9530	32128
0.9530	0.9496	28092
0.9496	0.9462	24699
0.9462	0.9428	21490
0.9428	0.9394	18434
0.9394	0.9360	15904
0.9360	0.9326	13415
0.9326	0.9292	11205
0.9292	0.9258	9076
0.9258	0.9224	7019
0.9224	0.9190	5071
0.9190	0.9156	3515
0.9156	0.9122	2280
0.9122	0.9088	1369
0.9088	0.9054	711
0.9054	0.9020	309
0.9020	0.8986	68
0.8986	0.8952	4
0.8952	0.8918	0

Figure 19:A histogram of the results of a 1,000,000 run Monte Carlo simulation of $P(y_m|y_e)$, Case 1, Model 1, with uniformly distributed input probabilities. Note that the bins are in decreasing order, because the Case 1 posterior probability interval $P(y_{m1}|y_e)$ is improper.

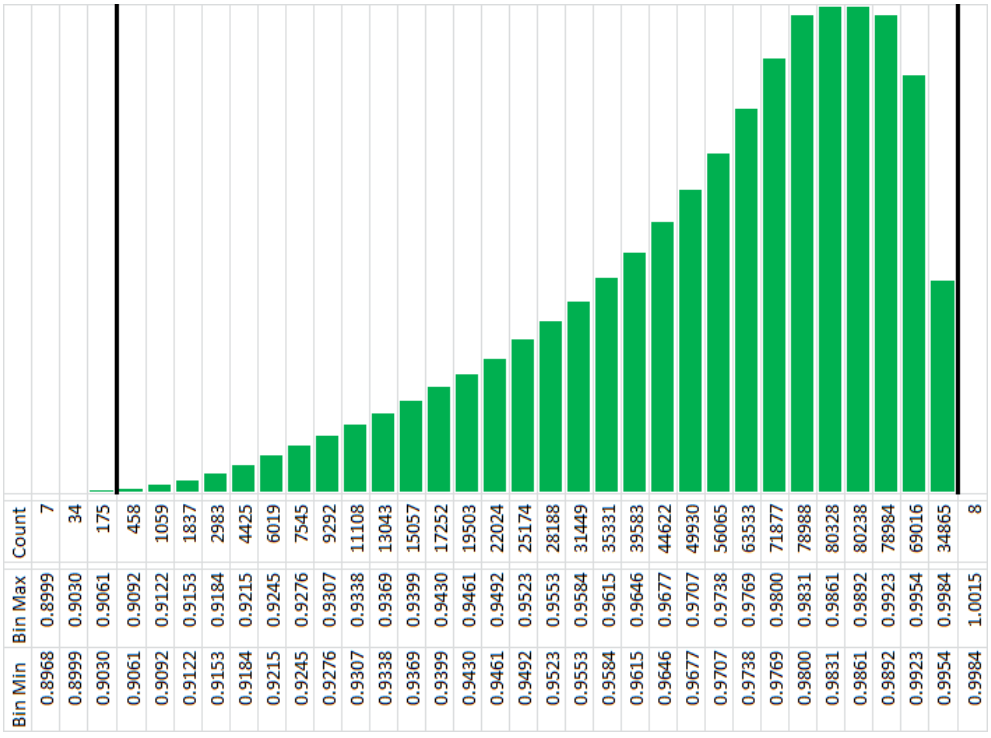

Bin Min	Bin Max	Count
0.8968	0.8999	7
0.8999	0.9030	34
0.9030	0.9061	175
0.9061	0.9092	458
0.9092	0.9122	1059
0.9122	0.9153	1837
0.9153	0.9184	2983
0.9184	0.9215	4425
0.9215	0.9245	6019
0.9245	0.9276	7545
0.9276	0.9307	9292
0.9307	0.9338	11108
0.9338	0.9369	13043
0.9369	0.9399	15057
0.9399	0.9430	17252
0.9430	0.9461	19503
0.9461	0.9492	22024
0.9492	0.9523	25174
0.9523	0.9553	28188
0.9553	0.9584	31449
0.9584	0.9615	35331
0.9615	0.9646	39583
0.9646	0.9677	44622
0.9677	0.9707	49930
0.9707	0.9738	56065
0.9738	0.9769	63533
0.9769	0.9800	71877
0.9800	0.9831	78988
0.9831	0.9861	80328
0.9861	0.9892	80238
0.9892	0.9923	78984
0.9923	0.9954	69016
0.9954	0.9984	34865
0.9984	1.0015	8

Figure 20: A histogram of the results of a 1,000,000 run Monte Carlo simulation of $P(y_m|y_e)$, Case 2, Model 1, with uniformly distributed input probabilities.

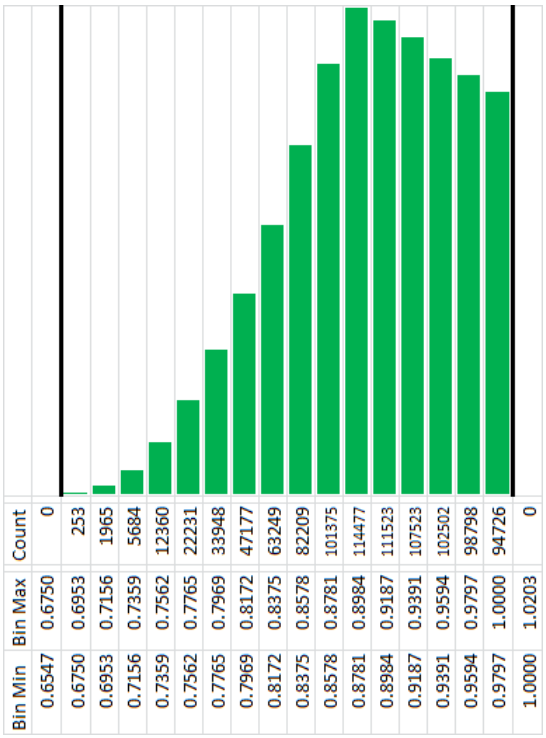

Bin Min	Bin Max	Count
0.6547	0.6750	0
0.6750	0.6953	253
0.6953	0.7156	1965
0.7156	0.7359	5684
0.7359	0.7562	12360
0.7562	0.7765	22231
0.7765	0.7969	33948
0.7969	0.8172	47177
0.8172	0.8375	63249
0.8375	0.8578	82209
0.8578	0.8781	101375
0.8781	0.8984	114477
0.8984	0.9187	111523
0.9187	0.9391	107523
0.9391	0.9594	102502
0.9594	0.9797	98798
0.9797	1.0000	94726
1.0000	1.0203	0

Figure 21: A histogram of the results of a 1,000,000 run Monte Carlo simulation of $P(y_m|y_e)$, Case 3, Model 2, with uniformly distributed input probabilities. The same MC simulation is also used in Figure 22, although it is binned differently to reflect the different posterior probability interval.

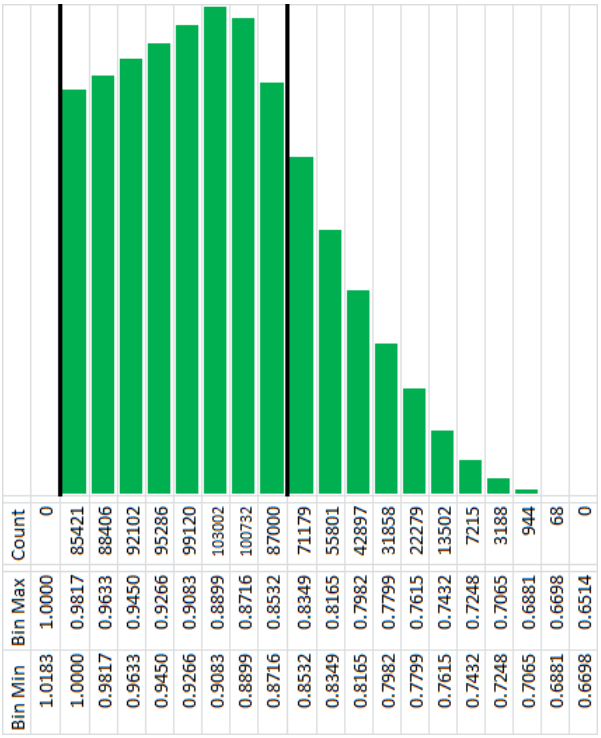

Bin Min	Bin Max	Count
1.0183	1.0000	0
1.0000	0.9817	85421
0.9817	0.9633	88406
0.9633	0.9450	92102
0.9450	0.9266	95286
0.9266	0.9083	99120
0.9083	0.8899	103002
0.8899	0.8716	100732
0.8716	0.8532	87000
0.8532	0.8349	71179
0.8349	0.8165	55801
0.8165	0.7982	42897
0.7982	0.7799	31858
0.7799	0.7615	22279
0.7615	0.7432	13502
0.7432	0.7248	7215
0.7248	0.7065	3188
0.7065	0.6881	944
0.6881	0.6698	68
0.6698	0.6514	0

Figure 22: A histogram of the results of a 1,000,000 run Monte Carlo simulation of $P(y_m|y_e)$, Case 4, Model 2, with uniformly distributed input probabilities. Note that the bins are in decreasing order, because the Case 4 posterior probability interval $P(y_{m2}|y_e)$ is improper.

The results of these Monte Carlo simulations are not particularly intuitive. The distributions of the Monte Carlo simulations for Model 1 (Case 1 and Case 2) have an almost identical shape and range—only the predicted range of the posterior probability interval was significantly different. The posterior probability interval for Case 2 was sound, as so many other predictions have been, but it was also nearly complete. This almost perfect prediction was the result of a seemingly subtle decision as to whether to consider simulations at temperature t_1 or t_2 non focal—and the better prediction came when t_2 was non-focal, even though t_2 should have a greater importance in the analysis than t_1.

In a similar fashion, the Monte Carlo simulation was identical for Case 3 and Case 4. The prediction of posterior probability for Case 3 was complete and nearly sound—it likely would prove entirely sound if enough simulations were run. Case 4, on

the other hand, contained far fewer of the MC simulation results. Again, it is non-intuitive that making t_2 into a non-focal event would result in an almost perfect prediction of the posterior probability.

5.1.6: Comparing models by comparing GIBR results

If Case 2 is taken as the best representation of Model 1 and Case 3 is taken as the best representation of Model 2, then some conclusions can be drawn about the relative behavior of each model. Recall that for Model 1, $\boldsymbol{P}(y_{m1}|y_e) = [0.9061, 0.9984]$, and for Model 2 $\boldsymbol{P}(y_{m2}|y_e) = [0.6750, 1.0000]$. Model 2 exhibits a far greater epistemic uncertainty than Model 1; it apparently predicts a wider range of results between the orientations, and so the lack of knowledge about which orientation is in use leads to greater uncertainty about yielding behavior. This conclusion, drawn from the posterior probability intervals alone, can be corroborated by comparing Table 17 with Table 20—the range of average yield strengths for Model 1 is about 45 MPa, to Model 2's 55 MPa, and Model 2 exhibits a larger standard deviation for yield strengths at all orientations.

Although $\overline{\boldsymbol{P}}(y_{m2}|y_e)$ is slightly larger than $\overline{\boldsymbol{P}}(y_{m1}|y_e)$, $\underline{\boldsymbol{P}}(y_{m1}|y_e)$ is much higher than $\underline{\boldsymbol{P}}(y_{m2}|y_e)$. From this it can be concluded that Model 1 has a much higher likelihood than Model 2 of predicting yield when the experiments exhibit yielding. This can be corroborated by again comparing Table 17 with Table 20—the yield strengths found by Model 1 are much lower than those found by Model 2.

These observations are not intended to show that one model is necessarily better or worse than the other. For instance, if a model m_0 showed yield strengths close to zero, then it would predict yielding for almost any stress, and $\boldsymbol{P}(y_{m0}|y_e)$ would be very close to $[1,1]$. This would not mean the model was good, but rather that the model was almost certain to predict yielding at or below the stress at which the experiments show yielding. Similarly, a model m_∞ with a nearly infinite yield strength would seldom predict yielding, and $\boldsymbol{P}(y_{m\infty}|y_e)$ would be very close to $[0,0]$, showing only that the model was

almost certain to not predict yielding where experiments demonstrate it should occur. Neither m_0 nor m_∞ is particularly accurate or useful, but their behavior exhibits very little uncertainty. For a measure of which model should be considered better, see §5.3: Model validation with Kullback-Leibler divergence.

5.2: GIBR as a combinatory tool.

5.2.1: Combining models of the same scale with Model 1 and Model 2

If two simulations arrive at different results and there is no experimental evidence available, it is helpful to have some method to combine the evidence of the simulations—to use one simulation to update the other. In this section, both $\boldsymbol{P}(y_{m1}|y_{m2})$ and $\boldsymbol{P}(y_{m2}|y_{m1})$ are calculated and then verified through Monte Carlo simulation. The equations necessary for this update are simple modifications of equation (31): the updating evidence y_e is replaced with the updating model y_{m^c}, where y_m is the primary model and y_{m^c} is the updating model. This is shown in equations (34) and (35).

$$\boldsymbol{P}(y_{m1}|y_{m2}) = \frac{[\boldsymbol{P}(y_{m2}|t_1) \quad \boldsymbol{P}(y_{m2}|t_2) \quad \boldsymbol{P}(y_{m2}|t_3)] \begin{bmatrix} \boldsymbol{P}(t_1|y_{m1}) \\ \boldsymbol{P}(t_2|y_{m1}) \\ \boldsymbol{P}(t_3|y_{m1}) \end{bmatrix} \boldsymbol{P}(y_{m1})}{dual\left([\boldsymbol{P}(y_{m2}|t_1) \quad \boldsymbol{P}(y_{m2}|t_2) \quad \boldsymbol{P}(y_{m2}|t_3)] \begin{bmatrix} \boldsymbol{P}(t_1|y_{m1}) & \boldsymbol{P}(t_1|y_{m1}^C) \\ \boldsymbol{P}(t_2|y_{m1}) & \boldsymbol{P}(t_2|y_{m1}^C) \\ \boldsymbol{P}(t_3|y_{m1}) & \boldsymbol{P}(t_3|y_{m1}^C) \end{bmatrix} \begin{bmatrix} \boldsymbol{P}(y_{m1}) \\ \boldsymbol{P}(y_{m1}^C) \end{bmatrix} \right)} \quad (34)$$

$$\boldsymbol{P}(y_{m2}|y_{m1}) = \frac{[\boldsymbol{P}(y_{m1}|t_1) \quad \boldsymbol{P}(y_{m1}|t_2) \quad \boldsymbol{P}(y_{m1}|t_3)] \begin{bmatrix} \boldsymbol{P}(t_1|y_{m2}) \\ \boldsymbol{P}(t_2|y_{m2}) \\ \boldsymbol{P}(t_3|y_{m2}) \end{bmatrix} \boldsymbol{P}(y_{m2})}{dual\left([\boldsymbol{P}(y_{m1}|t_1) \quad \boldsymbol{P}(y_{m1}|t_2) \quad \boldsymbol{P}(y_{m1}|t_3)] \begin{bmatrix} \boldsymbol{P}(t_1|y_{m2}) & \boldsymbol{P}(t_1|y_{m2}^C) \\ \boldsymbol{P}(t_2|y_{m2}) & \boldsymbol{P}(t_2|y_{m2}^C) \\ \boldsymbol{P}(t_3|y_{m2}) & \boldsymbol{P}(t_3|y_{m2}^C) \end{bmatrix} \begin{bmatrix} \boldsymbol{P}(y_{m2}) \\ \boldsymbol{P}(y_{m2}^C) \end{bmatrix} \right)} \quad (35)$$

5.2.1.1: Calculation of the relevant probabilities from the complementary model

The only interval inputs that have yet to be determined in the construction of these equations are $\boldsymbol{P}(y_{m1}|t_1)$, $\boldsymbol{P}(y_{m1}|t_2)$, $\boldsymbol{P}(y_{m1}|t_3)$, $\boldsymbol{P}(y_{m2}|t_1)$, $\boldsymbol{P}(y_{m2}|t_2)$, and $\boldsymbol{P}(y_{m2}|t_3)$. For each model, each temperature and orientation have 243 different predicted yield strengths. The mean and standard deviation of these yield strengths is easily calculated,

and the CDF of that distribution can then be compared to the test stress of 150 MPa, giving the probability that the model predicts yielding for that temperature and orientation. Then for each temperature, the highest and lowest probabilities from the three orientations are used as the bounds of the interval probability. These calculations are summarized for Model 1 in Table 25 and for Model 2 in Table 26.

Table 25: Calculation of $\boldsymbol{P(y_{m1}|t)}$for Model 1.

Temperature	t_1=143 K			t_2=195 K			t_3=250 K		
Orientation Number	#4	#5	#6	#4	#5	#6	#4	#5	#6
Average Yield Strength (MPa)	151.6	162.1	228.9	90.9	96.8	131.2	42.3	45.7	59.8
Standard Deviation of Yield Strength (MPa)	28.1	29.0	41.9	23.2	23.6	32.3	13.0	14.0	18.0
$P(y_{m1}\|t, orient.)$	47.74%	33.84%	2.97%	99.46%	98.81%	72.02%	100%	100%	100%
$\boldsymbol{P}(y_{m1}\|t)$	[0.0297,0.4774]			[0.7202,0.9946]			[1.0000,1.0000]		

Table 26: Calculation of $\boldsymbol{P(y_{m2}|t)}$for Model 2.

Temperature	t_1=143 K			t_2=195 K			t_3=250 K		
Orientation Number	#4	#5	#6	#4	#5	#6	#4	#5	#6
Average Yield Strength (MPa)	215.2	222.5	318.1	130.0	127.5	175.7	59.9	57.0	77.6
Standard Deviation of Yield Strength (MPa)	10.4	11.2	15.5	5.6	5.9	8.1	7.1	2.4	2.6
$P(y_{m2}\|t, orient.)$	0.00%	0.00%	0.00%	99.98%	99.99%	0.08%	100%	100%	100%
$\boldsymbol{P}(y_{m2}\|t)$	[0.0000,0.0000]			[0.0008,0.9999]			[1.0000,1.0000]		

Immediately the extreme width of the interval $\boldsymbol{P}(y_{m2}|t_2)$ incites caution. However, because it is not complete ignorance, and because eliminating it would also lead to eliminating much information from $\boldsymbol{P}(y_{m2}|t_1)$ and $\boldsymbol{P}(y_{m2}|t_3)$, it will remain in use for equation (34). It should be noted, however, that the results of equation (35) should be viewed with greater confidence than those of equation (34).

5.2.1.2: Calculating the posterior probabilities for each model, and verifying with Monte Carlo simulation

Calculating the posterior probabilities is a simple matter; the relevant intervals are simply substituted into equations (34) and (35). The input values and the resulting posterior probability intervals are shown along with the results of verifying Monte Carlo simulations in Table 27.

Table 27: Summary of the interval valued inputs and Monte Carlo simulation results for both Models 1 and 2 in the GIBR equation (31). For equation (34), y_{m^C} refers to Model 2 and y_m refers to Model 1. For equation (35) the reverse is true.

	Model 1, equation (34)			Model 2, equation (35)		
	Original Intervals	Case 1: Nonfocal T1	Case 2: Nonfocal T2	Original Intervals	Case 3: Nonfocal T2	Case 4: Nonfocal T1,T3
$\boldsymbol{P}(y_{m^C}\|t_1)$	[0.0000, 0.0000]	[0.0000, 0.0000]	[0.0000, 0.0000]	[0.0297, 0.4774	[0.0297, 0.4774	[0.0297, 0.4774
$\boldsymbol{P}(y_{m^C}\|t_2)$	[0.0008, 0.9999]	[0.0008, 0.9999]	[0.0008, 0.9999]	[0.7202, 0.9946]	[0.7202, 0.9946]	[0.7202, 0.9946]
$\boldsymbol{P}(y_{m^C}\|t_3)$	[1.0000, 1.0000]	[1.0000, 1.0000]	[1.0000, 1.0000]	[1.0000, 1.0000]	[1.0000, 1.0000]	[1.0000, 1.0000]
$\boldsymbol{P}(t_1\|y_m)$	[0.0211, 0.2030]	*[0.2030, 0.0107]*	[0.0211, 0.2030]	[0.0000, 0.0000]	[0.0000, 0.0000]	[0.0000, 0.0000]
$\boldsymbol{P}(t_2\|y_m)$	[0.3960, 0.4188]	[0.3960, 0.4188]	*[0.5779, 0.2266]*	[0.0000, 0.5000]	*[0.5000, 0.0000]*	[0.0000, 0.5000]
$\boldsymbol{P}(t_3\|y_m)$	[0.4010, 0.5704]	[0.4010, 0.5704]	[0.4010, 0.5704]	[0.5000, 1.0000]	[0.5000, 1.0000]	*[1.0000, 0.5000]*
$\boldsymbol{P}(t_1\|y_m^C)$	[0.7723, 0.9808]	*[0.9808, 0.7723]*	[0.7723, 0.9808]	[0.5000, 1.0000]	[0.5000, 1.0000]	*[1.0000, 0.5000]*
$\boldsymbol{P}(t_2\|y_m^C)$	[0.0192, 0.2277]	[0.0192, 0.2277]	*[0.2277, 0.0192]*	[0.0000, 0.5000]	*[0.5000, 0.0000]*	[0.0000, 0.5000]
$\boldsymbol{P}(t_3\|y_m^C)$	[0.0000, 0.0000]	[0.0000, 0.0000]	[0.0000, 0.0000]	[0.0000, 0.0000]	[0.0000, 0.0000]	[0.0000, 0.0000]
$\boldsymbol{P}(y_m)$	[0.5523, 0.8647]	[0.5523, 0.8647]	[0.5523, 0.8647]	[0.3417, 0.5924]	[0.3417, 0.5924]	[0.3417, 0.5924]
$\boldsymbol{P}(y_m^C)$	*[0.4477, 0.1353]*	*[0.4477, 0.1353]*	*[0.4477, 0.1353]*	*[0.6583, 0.4076]*	*[0.6583, 0.4076]*	*[0.6583, 0.4076]*

	Model 1, equation (34)			Model 2, equation (35)		
	Original Intervals	Case 1: Nonfocal T1	Case 2: Nonfocal T2	Original Intervals	Case 3: Nonfocal T2	Case 4: Nonfocal T1,T3
Results						
$\boldsymbol{P}(y_m \mid y_{m^c})$	[1.0000, 0.9652]	[1.0000, 0.9652]	[0.9996, 0.9962]	[0.9458, 0.6907]	[0.5408, 0.7527]	[0.9458, 0.6632
% of uniform MC simulation results contained by posterior interval	N/A	61.72%	6.37%	N/A	67.62%	56.47%
Range of MC results	N/A	0.8195 to 1.0000	0.8170 to 1.0000	N/A	0.4172 to 0.9774	
($\boldsymbol{P}(y_m \mid y_{m^c})$ range)/ (MC range), %	N/A	-19.24%	-1.86%	N/A	37.34%	-50.44%

As with the experimentally updated posterior probabilities from §5.1.5, both the original intervals and Case 1 for Model 1 give the same posterior probability interval when updated with the Model 2 results. Again, this is because $\boldsymbol{P}(y_{m2} \mid t_1)$, like $\boldsymbol{P}(y_e \mid t_1)$, is equal to $[0,0]$. Neither Case 1 nor Case 2, gives a posterior probability interval that predicts the range of the Monte Carlo simulation results very well. This is likely due to the already-mentioned width of the interval $\boldsymbol{P}(y_{m2} \mid t_2)$.

In another parallel to the experimentally updated posterior probabilities of §5.1.5, Case 3 and Case 4 of the two-model updates differ only by the use of the *dual* operator, despite being determined by choosing non-focal events and subjecting those events to the Logic Coherence Constraint. Case 3 and Case 4 thus share the same Monte Carlo simulation for verification, and once again Case 3 performs the best in terms of predicting where the greatest concentration of MC simulation results will be found. In fact, even though the Case 3 posterior probability interval is narrower than that of Case 4, it contains more of the simulation results due to better positioning. The results of the applicable Monte Carlo simulations are shown in Figure 23, Figure 24, Figure 25, and Figure 26.

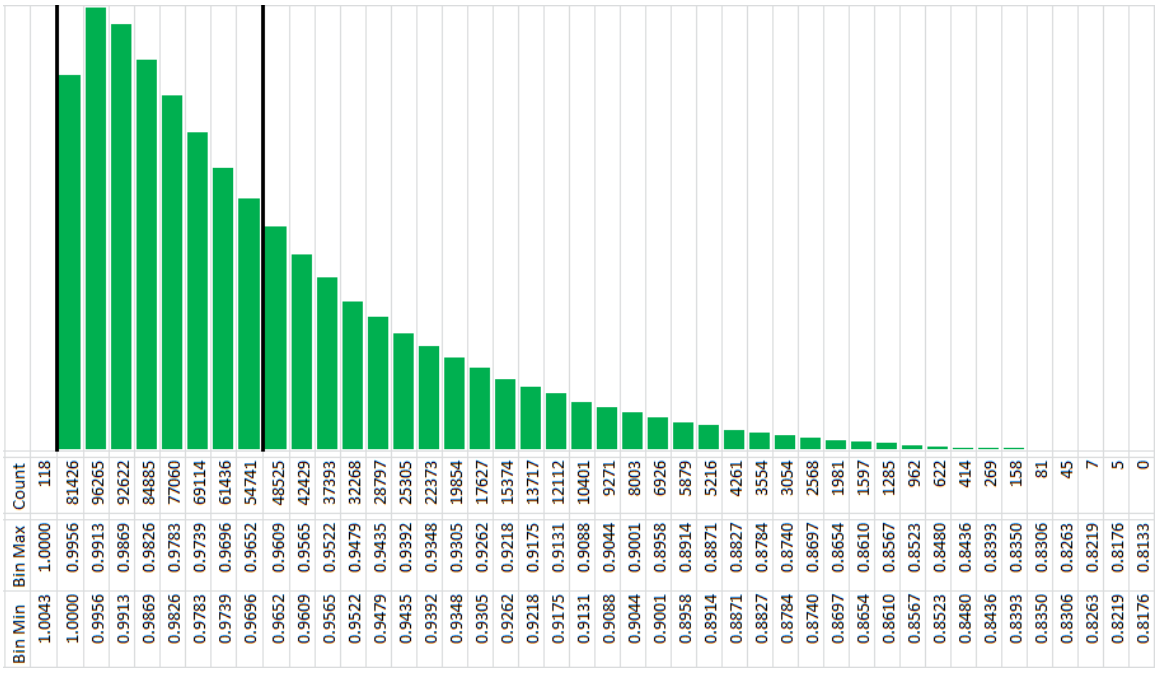

Bin Min	Bin Max	Count
1.0043	1.0000	118
1.0000	0.9956	81426
0.9956	0.9913	96265
0.9913	0.9869	92622
0.9869	0.9826	84885
0.9826	0.9783	77060
0.9783	0.9739	69114
0.9739	0.9696	61436
0.9696	0.9652	54741
0.9652	0.9609	48525
0.9609	0.9565	42429
0.9565	0.9522	37393
0.9522	0.9479	32268
0.9479	0.9435	28797
0.9435	0.9392	25305
0.9392	0.9348	22373
0.9348	0.9305	19854
0.9305	0.9262	17627
0.9262	0.9218	15374
0.9218	0.9175	13717
0.9175	0.9131	12112
0.9131	0.9088	10401
0.9088	0.9044	9271
0.9044	0.9001	8003
0.9001	0.8958	6926
0.8958	0.8914	5879
0.8914	0.8871	5216
0.8871	0.8827	4261
0.8827	0.8784	3554
0.8784	0.8740	3054
0.8740	0.8697	2568
0.8697	0.8654	1981
0.8654	0.8610	1597
0.8610	0.8567	1285
0.8567	0.8523	962
0.8523	0.8480	622
0.8480	0.8436	414
0.8436	0.8393	269
0.8393	0.8350	158
0.8350	0.8306	81
0.8306	0.8263	45
0.8263	0.8219	7
0.8219	0.8176	5
0.8176	0.8133	0

Figure 23: A histogram of the results of a 1,000,000 run Monte Carlo simulation of $P(y_{m1}|y_{m2})$ (equation (34)), Case 1, Model 1, with uniformly distributed input probabilities. Note that the bins are in decreasing order, because the Case 1 posterior probability interval $P(y_{m1}|y_{m2})$ is improper.

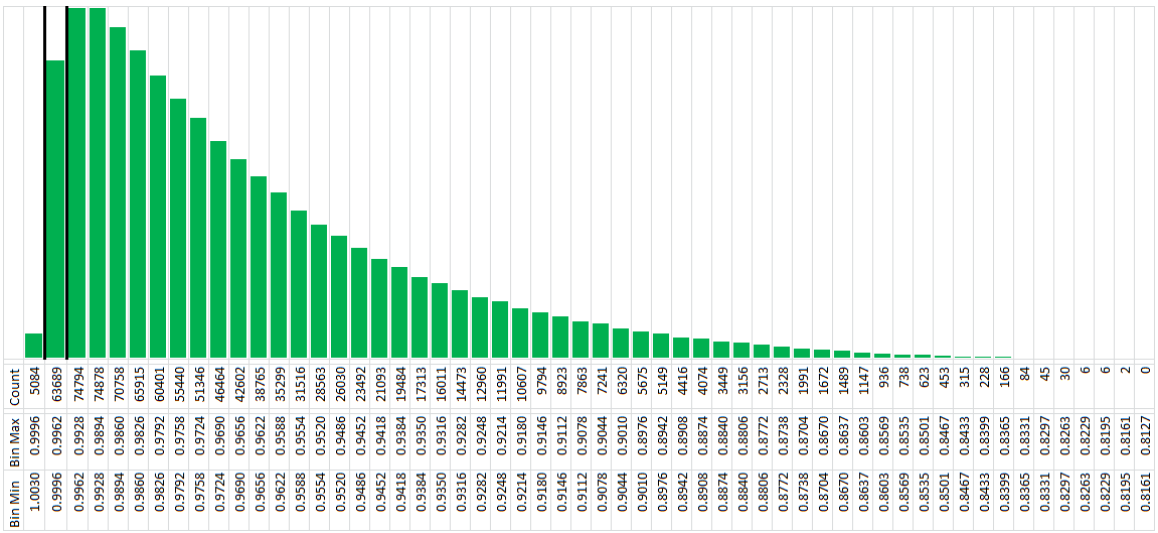

Bin Min	Bin Max	Count
1.0030	0.9996	5084
0.9996	0.9962	63689
0.9962	0.9928	74794
0.9928	0.9894	74878
0.9894	0.9860	70758
0.9860	0.9826	65915
0.9826	0.9792	60401
0.9792	0.9758	55440
0.9758	0.9724	51346
0.9724	0.9690	46464
0.9690	0.9656	42602
0.9656	0.9622	38765
0.9622	0.9588	35299
0.9588	0.9554	31516
0.9554	0.9520	28563
0.9520	0.9486	26030
0.9486	0.9452	23492
0.9452	0.9418	21093
0.9418	0.9384	19484
0.9384	0.9350	17313
0.9350	0.9316	16011
0.9316	0.9282	14473
0.9282	0.9248	12960
0.9248	0.9214	11991
0.9214	0.9180	10607
0.9180	0.9146	9794
0.9146	0.9112	8923
0.9112	0.9078	7863
0.9078	0.9044	7241
0.9044	0.9010	6320
0.9010	0.8976	5675
0.8976	0.8942	5149
0.8942	0.8908	4416
0.8908	0.8874	4074
0.8874	0.8840	3449
0.8840	0.8806	3156
0.8806	0.8772	2713
0.8772	0.8738	2328
0.8738	0.8704	1991
0.8704	0.8670	1672
0.8670	0.8637	1489
0.8637	0.8603	1147
0.8603	0.8569	936
0.8569	0.8535	738
0.8535	0.8501	623
0.8501	0.8467	453
0.8467	0.8433	315
0.8433	0.8399	228
0.8399	0.8365	166
0.8365	0.8331	84
0.8331	0.8297	45
0.8297	0.8263	30
0.8263	0.8229	6
0.8229	0.8195	6
0.8195	0.8161	2
0.8161	0.8127	0

Figure 24: A histogram of the results of a 1,000,000 run Monte Carlo simulation of $P(y_{m1}|y_{m2})$ (equation (34)), Case 2, Model 1, with uniformly distributed input probabilities. The bins are again in decreasing order, because the Case 2 posterior probability interval $P(y_{m1}|y_{m2})$ is improper. In fact, the simulation results appear almost identical to those of Case 1, although the predicted posterior probability interval is much narrower and does not contain the peak of the simulation results.

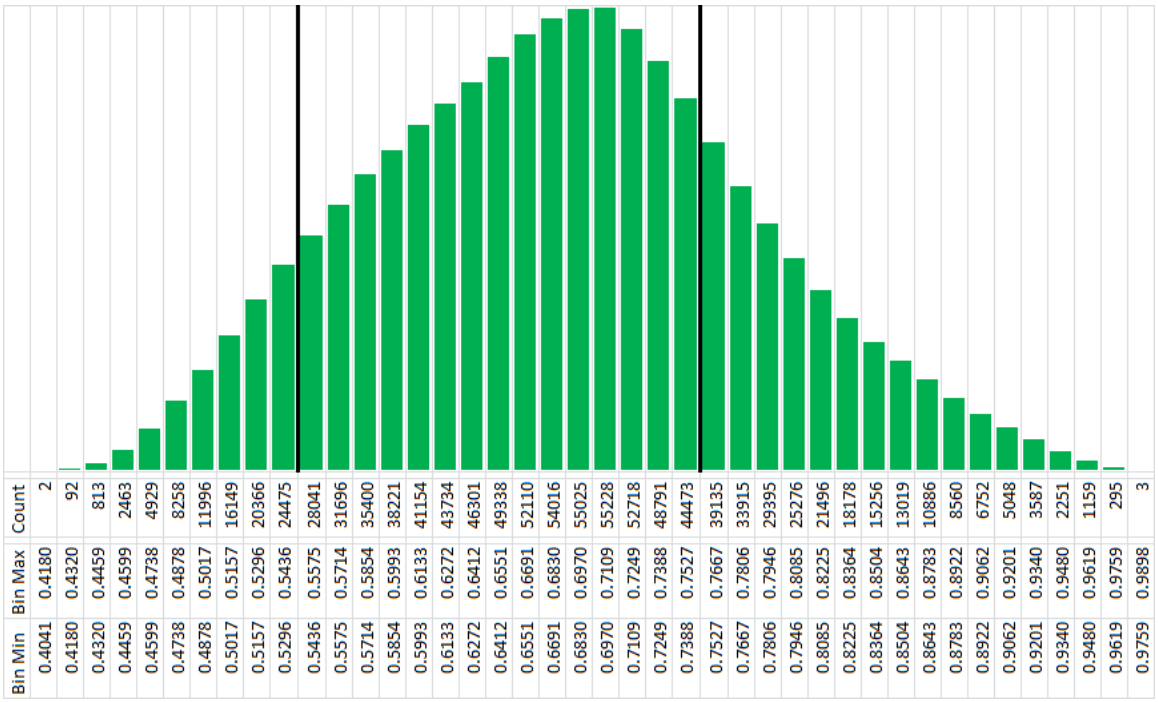

Bin Min	Bin Max	Count
0.4041	0.4180	2
0.4180	0.4320	92
0.4320	0.4459	813
0.4459	0.4599	2463
0.4599	0.4738	4929
0.4738	0.4878	8258
0.4878	0.5017	11996
0.5017	0.5157	16149
0.5157	0.5296	20366
0.5296	0.5436	24475
0.5436	0.5575	28041
0.5575	0.5714	31696
0.5714	0.5854	35400
0.5854	0.5993	38221
0.5993	0.6133	41154
0.6133	0.6272	43734
0.6272	0.6412	46301
0.6412	0.6551	49338
0.6551	0.6691	52110
0.6691	0.6830	54016
0.6830	0.6970	55025
0.6970	0.7109	55228
0.7109	0.7249	52718
0.7249	0.7388	48791
0.7388	0.7527	44473
0.7527	0.7667	39135
0.7667	0.7806	33915
0.7806	0.7946	29395
0.7946	0.8085	25276
0.8085	0.8225	21496
0.8225	0.8364	18178
0.8364	0.8504	15256
0.8504	0.8643	13019
0.8643	0.8783	10886
0.8783	0.8922	8560
0.8922	0.9062	6752
0.9062	0.9201	5048
0.9201	0.9340	3587
0.9340	0.9480	2251
0.9480	0.9619	1159
0.9619	0.9759	295
0.9759	0.9898	3

Figure 25: A histogram of the results of a 1,000,000 run Monte Carlo simulation of $P(y_{m2}|y_{m1})$ (equation (35)), Case 3, Model 2, with uniformly distributed input probabilities. The same MC simulation is also used in Figure 26, although it is binned differently to reflect the different posterior probability interval.

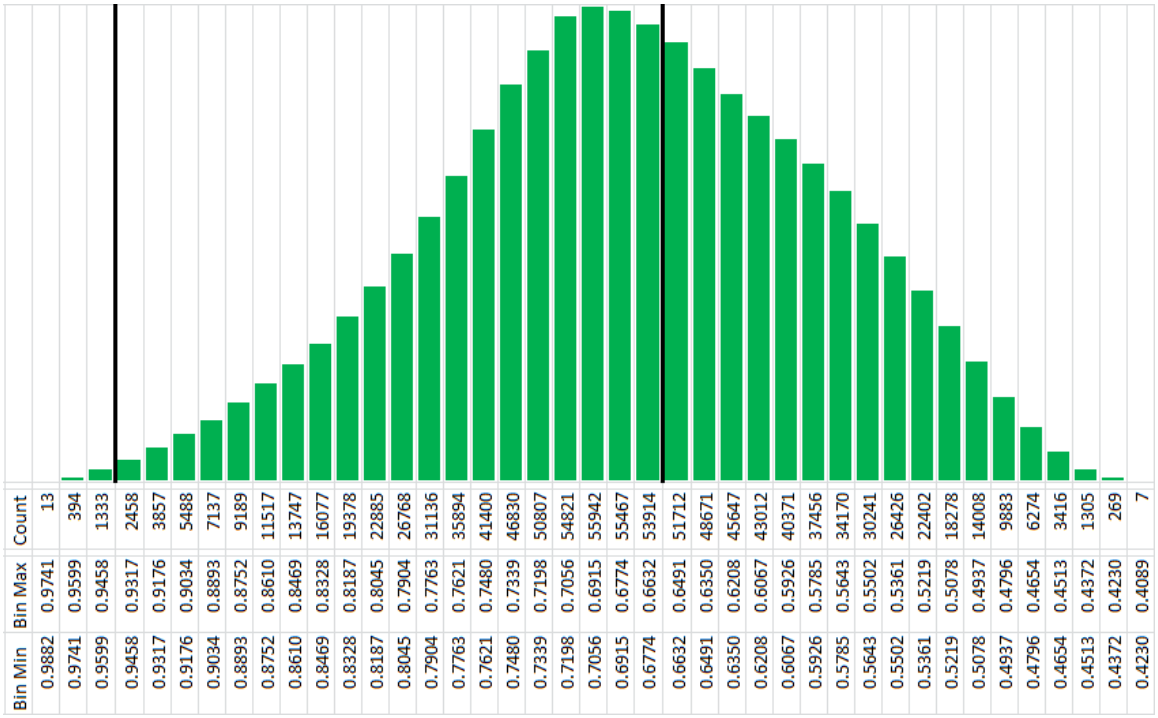

Bin Min	Bin Max	Count
0.9882	0.9741	13
0.9741	0.9599	394
0.9599	0.9458	1333
0.9458	0.9317	2458
0.9317	0.9176	3857
0.9176	0.9034	5488
0.9034	0.8893	7137
0.8893	0.8752	9189
0.8752	0.8610	11517
0.8610	0.8469	13747
0.8469	0.8328	16077
0.8328	0.8187	19378
0.8187	0.8045	22885
0.8045	0.7904	26768
0.7904	0.7763	31136
0.7763	0.7621	35894
0.7621	0.7480	41400
0.7480	0.7339	46830
0.7339	0.7198	50807
0.7198	0.7056	54821
0.7056	0.6915	55942
0.6915	0.6774	55467
0.6774	0.6632	53914
0.6632	0.6491	51712
0.6491	0.6350	48671
0.6350	0.6208	45647
0.6208	0.6067	43012
0.6067	0.5926	40371
0.5926	0.5785	37456
0.5785	0.5643	34170
0.5643	0.5502	30241
0.5502	0.5361	26426
0.5361	0.5219	22402
0.5219	0.5078	18278
0.5078	0.4937	14008
0.4937	0.4796	9883
0.4796	0.4654	6274
0.4654	0.4513	3416
0.4513	0.4372	1305
0.4372	0.4230	269
0.4230	0.4089	7

Figure 26: A histogram of the results of a 1,000,000 run Monte Carlo simulation of $P(y_{m2}|y_{m1})$ (equation (35)), Case 4, Model 2, with uniformly distributed input probabilities. Note that the bins are in decreasing order, because the Case 4 posterior probability interval $P(y_{m2}|y_{m1})$ is improper.

5.2.1.3: Comparing models using GIBR

Based on the results of the Monte Carlo simulations, Case 1 should be considered the best representation of $\boldsymbol{P}(y_{m1}|y_{m2})$, and Case 3 should be considered the best representation of $\boldsymbol{P}(y_{m2}|y_{m1})$. The results of Case 1 are suspect because of the wide interval for $\boldsymbol{P}(y_{m2}|t_2)$, but some general conclusions can be reached. Recall that for Case 1, $\boldsymbol{P}(y_{m1}|y_{m2}) = [1.0000, 0.9652]$. The high percentages of the aleatory uncertainty in this interval indicate that the updating model, Model 2, is much less likely to predict yielding than the updated model, Model 1—that Model 1 is almost certain to predict yielding whenever Model 2 does so. This reflects the higher yield strengths found by Model 2 (seen in Table 20) as compared to those found by Model 1 (Table 17).

Recall that for Case 3, $\boldsymbol{P}(y_{m2}|y_{m1}) = [0.5408, 0.7527]$. The aleatory uncertainty may be as low as an almost ambivalent 54.08%, indicating that Model 1's results do not greatly inform the user as to the likely result of Model 2. This makes sense, because Model 2 not only predicts higher yield strengths than Model 1, but it also has a much wider spread of yield strengths, reflected in its larger standard deviation. This may also be related to the fairly wide band of epistemic uncertainty present in the posterior probability—one that represents a significant lack of knowledge, but that by no means approaches complete ignorance.

5.2.2: Combining across scales with Model 1 and Model 3

While Model 3 has only limited data available, it is still possible to combine the limited evidence that is available with that of another model, in this case Model 1. Model 3 has no data available at temperature 3 (250 K), so the equations are simplified to only two discretized temperatures:

$$\boldsymbol{P}(y_{m1}|y_{m3}) = \frac{[\boldsymbol{P}(y_{m3}|t_1) \quad \boldsymbol{P}(y_{m3}|t_2)] \begin{bmatrix} \boldsymbol{P}(t_1|y_{m1}) \\ \boldsymbol{P}(t_2|y_{m1}) \end{bmatrix} \boldsymbol{P}(y_{m1})}{dual\left([\boldsymbol{P}(y_{m3}|t_1) \quad \boldsymbol{P}(y_{m3}|t_2)] \begin{bmatrix} \boldsymbol{P}(t_1|y_{m1}) & \boldsymbol{P}(t_1|y_{m1}^C) \\ \boldsymbol{P}(t_2|y_{m1}) & \boldsymbol{P}(t_2|y_{m1}^C) \end{bmatrix} \begin{bmatrix} \boldsymbol{P}(y_{m1}) \\ \boldsymbol{P}(y_{m1}^C) \end{bmatrix} \right)} \quad (36)$$

$$\boldsymbol{P}(y_{m3}|y_{m1}) = \frac{[\boldsymbol{P}(y_{m1}|t_1) \quad \boldsymbol{P}(y_{m1}|t_2)] \begin{bmatrix} \boldsymbol{P}(t_1|y_{m3}) \\ \boldsymbol{P}(t_2|y_{m3}) \end{bmatrix} \boldsymbol{P}(y_{m3})}{dual\left([\boldsymbol{P}(y_{m1}|t_1) \quad \boldsymbol{P}(y_{m1}|t_2)] \begin{bmatrix} \boldsymbol{P}(t_1|y_{m3}) & \boldsymbol{P}(t_1|y_{m3}^C) \\ \boldsymbol{P}(t_2|y_{m3}) & \boldsymbol{P}(t_2|y_{m3}^C) \end{bmatrix} \begin{bmatrix} \boldsymbol{P}(y_{m3}) \\ \boldsymbol{P}(y_{m3}^C) \end{bmatrix} \right)} \quad (37)$$

While some of the probabilities shown in these equations have been calculated previously, they included the data at 250 K for Model 1. Thus, all probabilities must be re-calculated for the sake of consistency within the equations. Because of the limited data available for Model 3 and the heavy effect of the prior probability on the posterior, using Model 3 to generate a prior and updating that with Model 1 is unlikely to have a useful result. However, the limited observations from Model 3 may be used to update Model 1. With this in mind, equation (36) will be investigated, while equation (37) will not be developed further. In order to avoid confusion with the other probabilities in this chapter, probabilities with potentially ambiguous labels will be denoted with a prime (e.g. y'), indicating that they are for use with this model combination only. Thus, the probabilities that must be calculated are $\boldsymbol{P}(y_{m3}|t_1)$, $\boldsymbol{P}(y_{m3}|t_2)$, $\boldsymbol{P}(t_1|y'_{m1})$, $\boldsymbol{P}(t_2|y'_{m1})$, $\boldsymbol{P}(t_1|y'^{C}_{m1})$, $\boldsymbol{P}(t_2|y'^{C}_{m1})$, $\boldsymbol{P}(y'_{m1})$, and $\boldsymbol{P}(y'^{C}_{m1})$, which will finally allow the calculation of $\boldsymbol{P}(y_{m1}|y_{m3})$.

5.2.2.1: Calculation of relevant probabilities from Model 1 results

By comparing the chosen stress of 150 MPa with the approximated CDFs mentioned in §5.1.1, the probability that the model will predict yielding at each orientation can be determined. In this case only the simulations at $t_1 = 143\ K$ and $t_2 = 195\ K$ are examined; this means that there are now 162 simulations at each orientation (81 simulations for each of two temperatures). These calculations are summarized in Table 28.

Table 28: Calculation of the interval probability that Model 1 predicts yielding, without the data from temperature 3.

Orientation	Average Yield Strength, Model 1	Standard Deviation of Yield Strength, Model 1	$P(y_{m1}\|orient.)$	$\boldsymbol{P}(y'_{m1})$	
#4	121.3 MPa	39.8 MPa	76.49%	$\underline{\boldsymbol{P}}(y'_{m1})$	$\overline{\boldsymbol{P}}(y'_{m1})$
#5	129.4 MPa	42.0 MPa	68.78%	0.3128	0.7649
#6	180.0 MPa	61.5 MPa	31.28%		

By the Logic Coherence Constraint, $\boldsymbol{P}\left(y'^{C}_{m1}\right) = [0.6872, 0.2351]$

The calculations for $\boldsymbol{P}(t_1|y'_{m1})$, $\boldsymbol{P}(t_2|y'_{m1})$, $\boldsymbol{P}(t_1|y'^{C}_{m1})$, and $\boldsymbol{P}(t_2|y'^{C}_{m1})$ are given in Table 29 and Table 30. It is worth noting that the values for $\boldsymbol{P}(t|y'^{C}_{m1})$ are identical to the values for $\boldsymbol{P}(t|y^{C}_{m1})$. This is due to the fact that all simulations at 250 K had exhibited yield strengths below 150 MPa.

Table 29: Summary of the calculation of $\boldsymbol{P}(t|y'_{m1})$.

	Quantity of Simulations Exhibiting Yield in Model 1			$\boldsymbol{P}(t\|y'_{m1})$			
Orientation No.	#4	#5	#6	#4	#5	#6	Interval
T=143 K	41	30	3	0.3388	0.2727	0.0492	[0.0492,0.3388]
T=195 K	80	80	58	0.6612	0.7273	0.9508	[0.6612,0.9508]
All Temps.	121	110	61	1.0000	1.0000	1.0000	[0.7915,1.2085]

Table 30: Summary of the calculation of $\boldsymbol{P}(t|y'^{C}_{m1})$.

	Quantity of Simulations NOT Exhibiting Yield in Model 1			$\boldsymbol{P}(t\|y'^{C}_{m1})$			
Orientation No.	#4	#5	#6	#4	#5	#6	Interval
T=143 K	40	51	78	0.9756	0.9808	0.7723	[0.7723,0.9808]
T=195 K	1	1	23	0.0244	0.0192	0.2277	[0.0192,0.2277]
All Temps.	41	52	101	1.0000	1.0000	1.0000	[0.7915,1.2085]

5.2.2.2: Calculation of the relevant probabilities from the Model 3 results

One set of simulations was run using Model 3 for each temperature and orientation. In order to calculate $\boldsymbol{P}(y_{m3}|t_1)$ and $\boldsymbol{P}(y_{m3}|t_2)$, it is only necessary to know

whether or not each simulation predicted yield at or below 150 MPa. The graphs of stress and strain for these simulations are shown in Figure 27 through Figure 32:

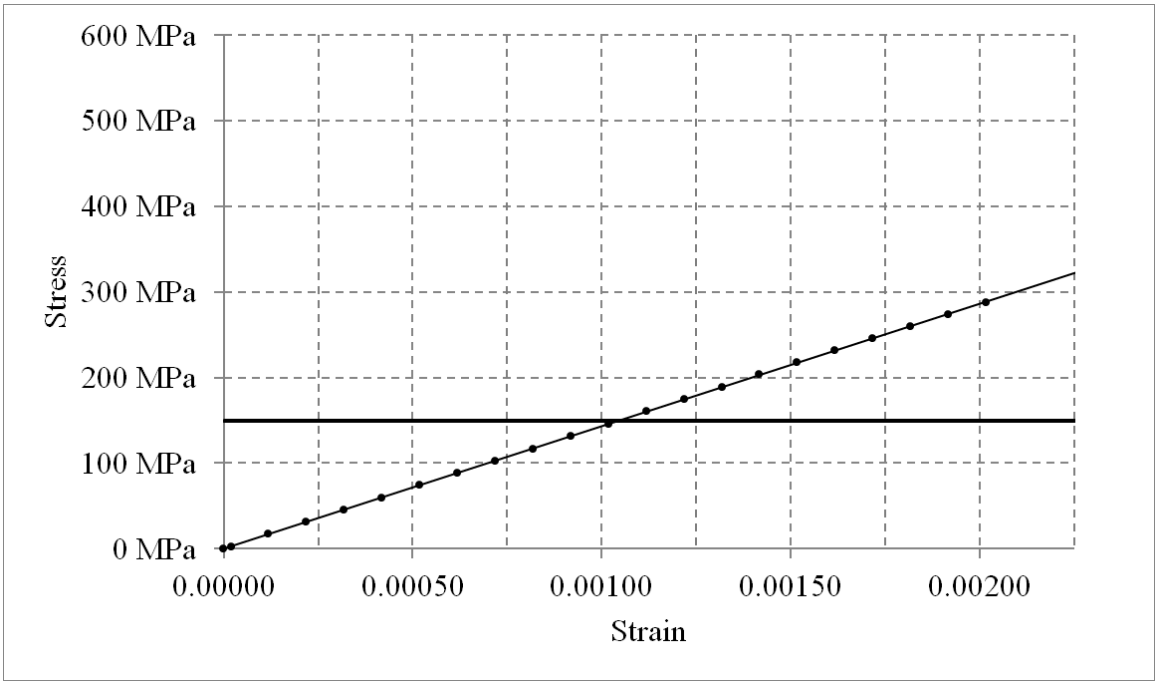

Figure 27: Stress-strain data for Model 3 at 143 K, Orientation #4. The sloped line shown is a linear regression of all the data points.

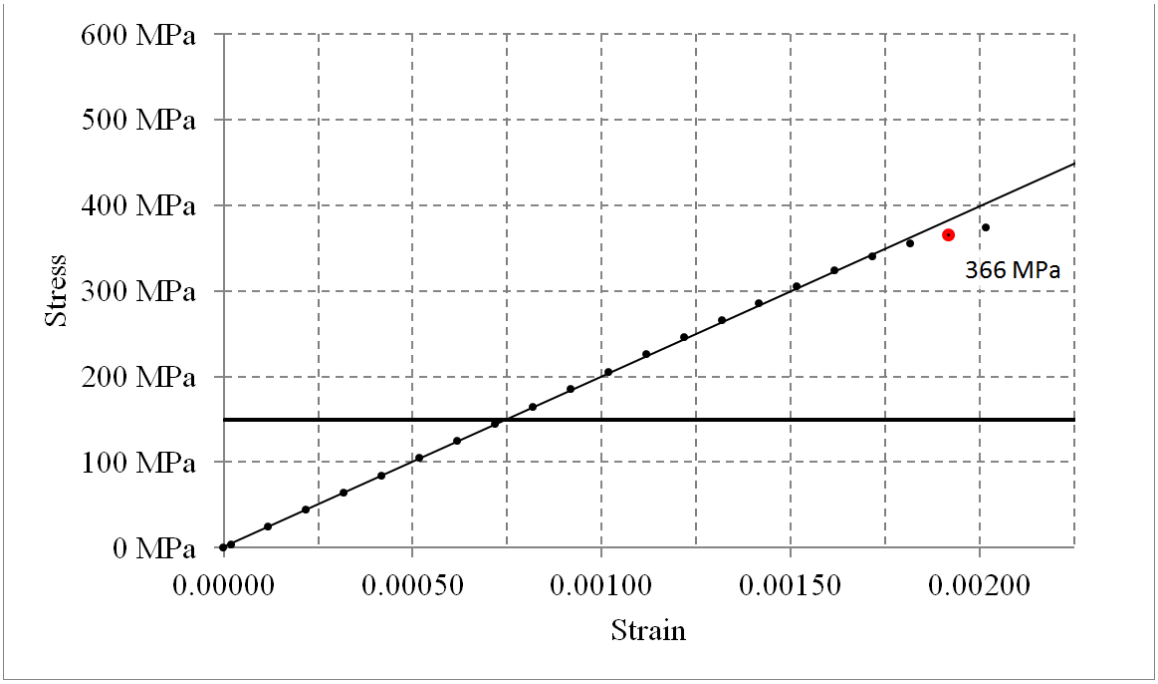

Figure 28: Stress-strain data for Model 3 at 143 K, Orientation #5. The sloped line shown is a linear regression of the first 20 data points, which does not include the labeled point at 366 MPa.

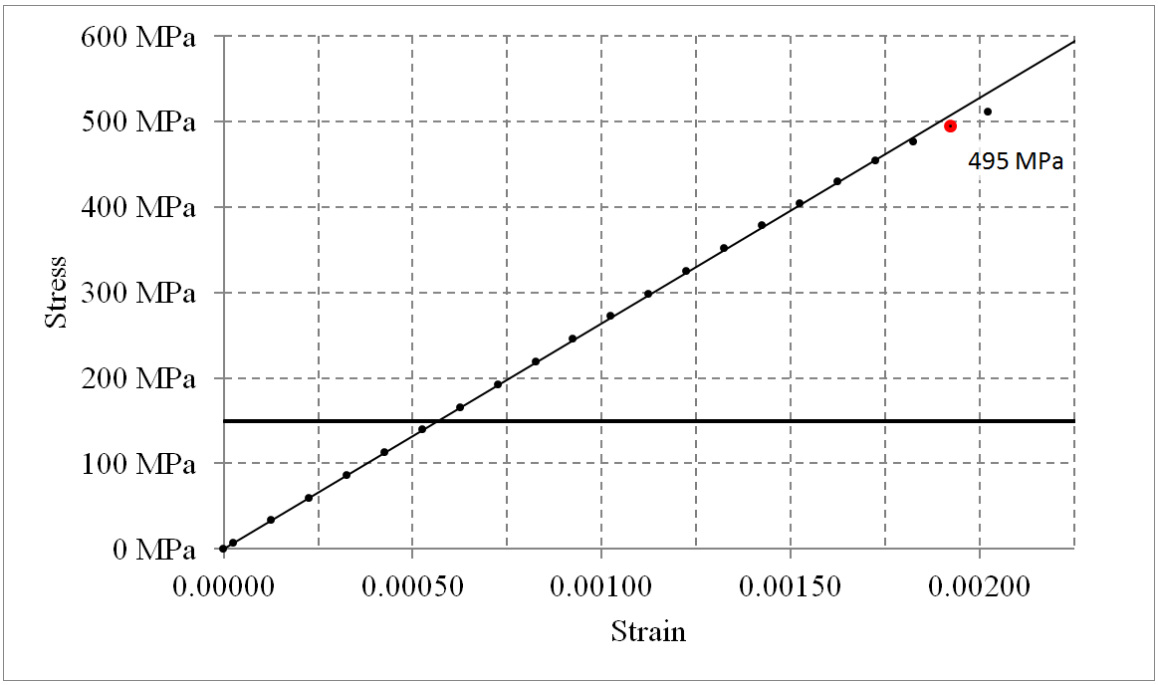

Figure 29: Stress-strain data for Model 3 at 143 K, Orientation #6. The sloped line shown is a linear regression of the first 20 data points, which does not include the labeled point at 495 MPa.

As seen in Figure 27, Figure 28, and Figure 29, all of the simulations at 143 K exhibited yield far above 150 MPa. The yield stresses for orientations #5 and #6 were estimated as 366 MPa and 495 MPa, respectively, by visually checking for inelastic behavior in the curves. While the actual yield stress for orientation #4 at this temperature was not determined, it is enough to know that it had not yet yielded by 150 MPa. This analysis results in the interval $\boldsymbol{P}(y_{m3}|t_1) = [0,0]$.

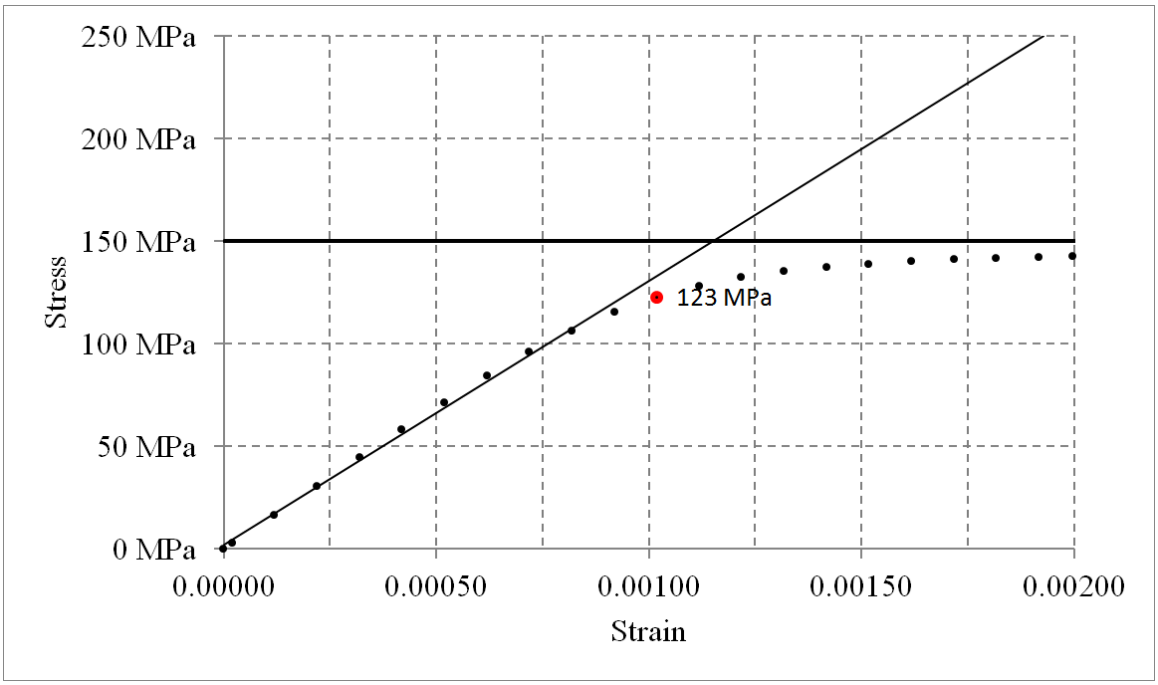

Figure 30: Stress-strain data for Model 3 at 195 K, Orientation #4. The sloped line shown is a linear regression of the first eleven data points, which does not include the labeled point at 123 MPa.

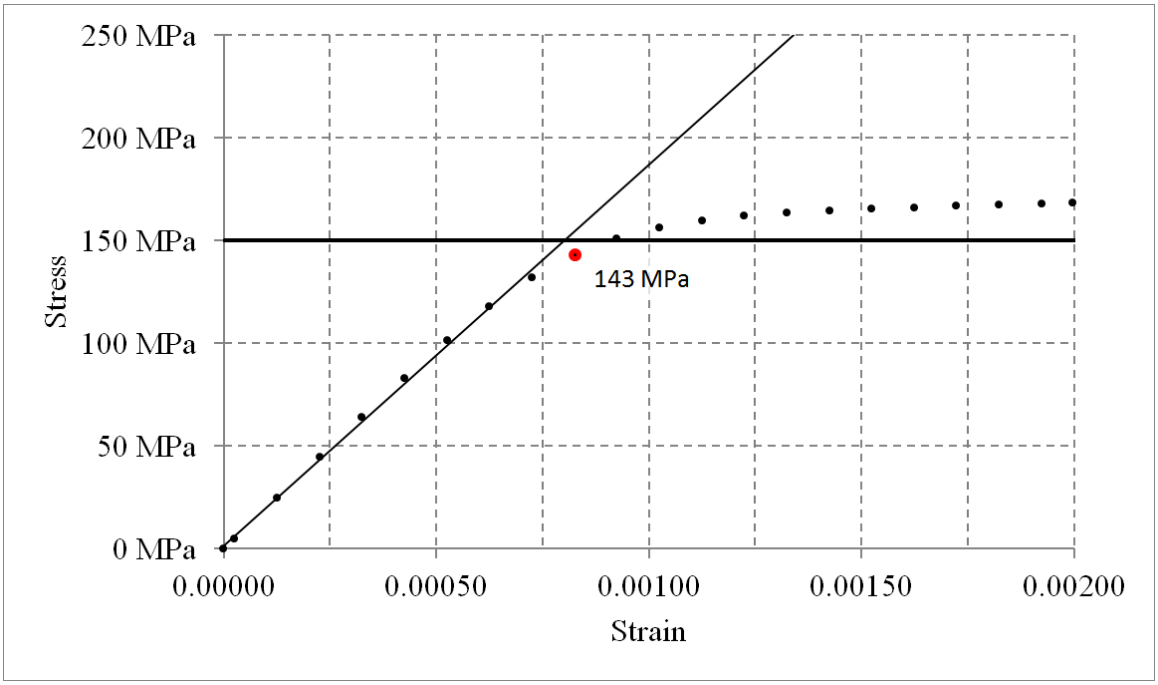

Figure 31: Stress-strain data for Model 3 at 195 K, Orientation #5. The sloped line shown is a linear regression of the first nine data points, which does not include the labeled point at 143 MPa.

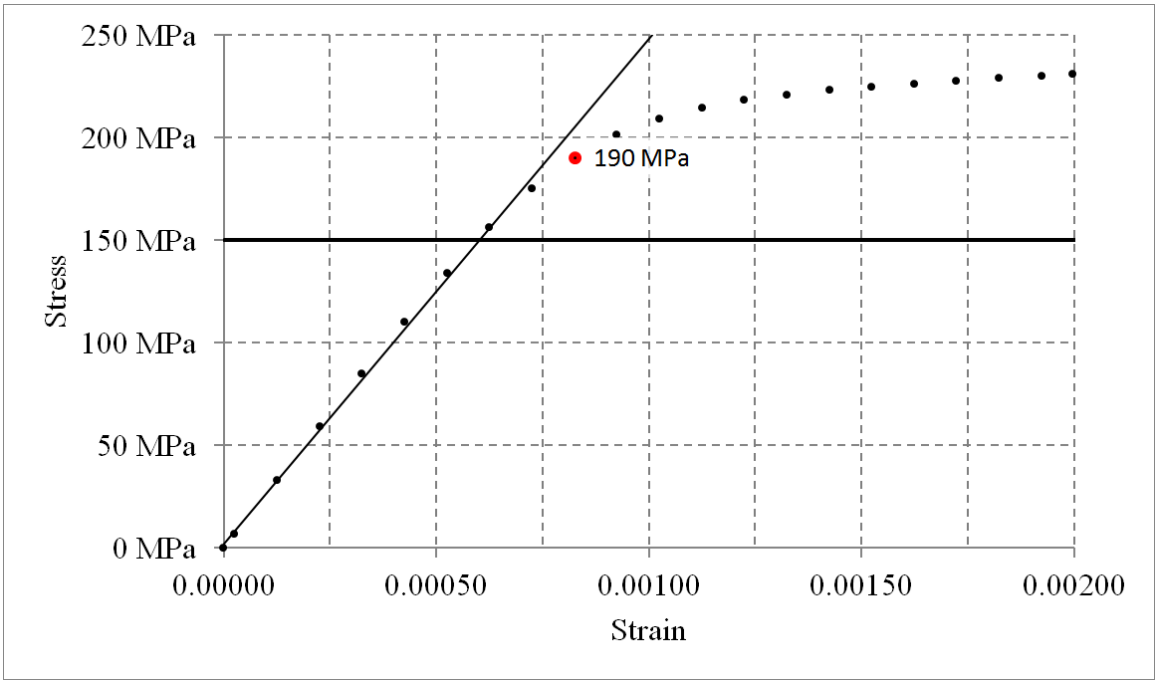

Figure 32: Stress-strain data for Model 3 at 195 K, Orientation #6. The sloped line shown is a linear regression of the first nine data points, which does not include the labeled point at 190 MPa.

When the stress-strain behavior of the material was simulated at 195 K, the yield strengths of orientations #4 through #6 were estimated as 123 MPa, 143 MPa, and 190 MPa, respectively. These values encompass the stress of interest, 150 MPa, and so the value of $\boldsymbol{P}(y_{m3}|t_2)$ is [0,1].

5.2.2.3: Calculating the update of Model 1 by Model 3

With all of the relevant values in place, equation (36) becomes:

$$\boldsymbol{P}(y_{m1}|y_{m3}) = \frac{[[0,0] \quad [0,1]] \begin{bmatrix}[0.0492,0.3388]\\[0.6612,0.9508]\end{bmatrix} [0.3128,0.7649]}{dual\left([[0,0] \quad [0,1]] \begin{bmatrix}[0.0492,0.3388] & [0.7723,0.9808]\\[0.6612,0.9508] & [0.0192,0.2277]\end{bmatrix} \begin{bmatrix}[0.3128,0.7649]\\[0.6872,0.2351]\end{bmatrix}\right)} \quad (38)$$

Note that the mutually disjoint events $\boldsymbol{P}(t_1|y'_{m1})$ and $\boldsymbol{P}(t_2|y'_{m1})$ do not comply with the Logic Coherence Constraint, nor do events $\boldsymbol{P}(t_1|y'^{C}_{m1})$ and $\boldsymbol{P}(t_2|y'^{C}_{m1})$. However, due to the nature of the discretization used, selecting a non-focal event simply switches the bounds of the associated intervals. Thus, if temperature 1 is considered non-focal, then equation (38) becomes equation (39), and if temperature 2 is considered non-focal, then equation (38) becomes equation (40):

$$\boldsymbol{P}(y_{m1}|y_{m3}) = \frac{[[0,0] \quad [0,1]] \begin{bmatrix} [\mathbf{0.3388, 0.0492}] \\ [0.6612,0.9508] \end{bmatrix} [0.3128,0.7649]}{dual\left([[0,0] \quad [0,1]] \begin{bmatrix} [\mathbf{0.3388, 0.0492}] & [\mathbf{0.9808, 0.7723}] \\ [0.6612,0.9508] & [0.0192,0.2277] \end{bmatrix} \begin{bmatrix} [0.3128,0.7649] \\ [0.6872,0.2351] \end{bmatrix}\right)} \quad (39)$$

$$\boldsymbol{P}(y_{m1}|y_{m3}) = \frac{[[0,0] \quad [0,1]] \begin{bmatrix} [0.0492,0.3388] \\ [\mathbf{0.9508, 0.6612}] \end{bmatrix} [0.3128,0.7649]}{dual\left([[0,0] \quad [0,1]] \begin{bmatrix} [0.0492,0.3388] & [0.7723,0.9808] \\ [\mathbf{0.9508, 0.6612}] & [\mathbf{0.2277, 0.0192}] \end{bmatrix} \begin{bmatrix} [0.3128,0.7649] \\ [0.6872,0.2351] \end{bmatrix}\right)} \quad (40)$$

In addition, because of the zeros in the lower bounds of the $\boldsymbol{P}(y_{m3}|t)$ terms, the limit of each equation must be taken in order to calculate the lower bound of the posterior probability. The results of these equations are given in Table 31:

Table 31: Summary of the interval valued inputs and Monte Carlo simulation results for updating Model 1 with Model 3 in GIBR equation (36). The Monte Carlo simulation utilized uniform inputs, and consisted of one million runs. Also included are the real values from the intervals that give the extreme possible values for the posterior probability. Italics denote values determined by subtraction from a complementary event.

	Original, equation (38)	Nonfocal T1, equation (39)	Nonfocal T2, equation (40)	Lower Extreme	Upper Extreme
$\boldsymbol{P}(y_{m3}\|t_1)$	[0.0000,0.0000]	[0.0000,0.0000]	[0.0000,0.0000]	0.0000	0.0000
$\boldsymbol{P}(y_{m3}\|t_2)$	[0.0000,1.0000]	[0.0000,1.0000]	[0.0000,1.0000]	0.0000	1.0000
$\boldsymbol{P}(t_1\|y'_{m1})$	[0.0492,0.3388]	*[0.3388,0.0492]*	[0.0492,0.3388]	0.0492	0.0492
$\boldsymbol{P}(t_2\|y'_{m1})$	[0.6612,0.9508]	[0.6612,0.9508]	*[0.9508,0.6612]*	*0.9508*	*0.9508*
$\boldsymbol{P}(t_1\|y'^{C}_{m1})$	[0.7723,0.9808]	*[0.9808,0.7723]*	[0.7723,0.9808]	0.9808	0.9808
$\boldsymbol{P}(t_2\|y'^{C}_{m1})$	[0.0192,0.2277]	[0.0192,0.2277]	*[0.2277,0.0192]*	*0.0192*	*0.0192*
$\boldsymbol{P}(y'_{m1})$	[0.3128,0.7649]	[0.3128,0.7649]	[0.3128,0.7649]	0.3128	0.7649
$\boldsymbol{P}(y'^{C}_{m1})$	*[0.6872,0.2351]*	*[0.6872,0.2351]*	*[0.6872,0.2351]*	*0.6872*	*0.2351*
$\boldsymbol{P}(y_{m1}\|y_{m3})$	[0.2900,0.9314]	[0.3128,0.9314]	[0.3128,0.9911]	0.0223	0.9938
% of uniform MC simulation results contained by posterior interval	70.15%	70.15%	99.90%	N/A	N/A
Range of MC results	0.5753 to 0.9935			N/A	N/A
($\boldsymbol{P}(y_{m1}\|y_{m3})$ range)/ (MC range), %	153.4%	147.9%	162.2%	N/A	N/A

The updates provided by these three formulations of equation (36) are each very similar. While all three updates raise the upper bound, possibly indicating an increase in the probability of Model 1 predicting yield, they also lower the lower bound. Ultimately,

the uncertainty contained in the added evidence from Model 3 is the dominant characteristic of the update, which shows an increase in uncertainty.

Monte Carlo simulation was performed to verify the soundness and completeness of each of these equations. This included the original interval equation despite its lack of compliance with the Logic Coherence Constraint. As with some of the earlier examples, because the intervals have the same bounds with different modality for all three cases of this equation, they can be verified using the exact same Monte Carlo simulation. The results of these Monte Carlo simulations are provided visually in Figure 33, Figure 34, and Figure 35.

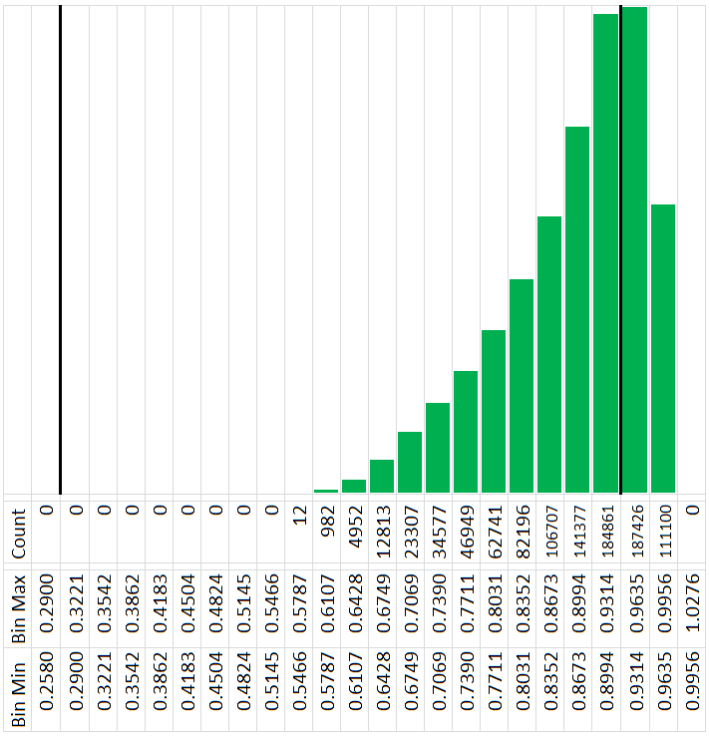

Bin Min	Bin Max	Count
0.2580	0.2900	0
0.2900	0.3221	0
0.3221	0.3542	0
0.3542	0.3862	0
0.3862	0.4183	0
0.4183	0.4504	0
0.4504	0.4824	0
0.4824	0.5145	0
0.5145	0.5466	0
0.5466	0.5787	12
0.5787	0.6107	982
0.6107	0.6428	4952
0.6428	0.6749	12813
0.6749	0.7069	23307
0.7069	0.7390	34577
0.7390	0.7711	46949
0.7711	0.8031	62741
0.8031	0.8352	82196
0.8352	0.8673	106707
0.8673	0.8994	141377
0.8994	0.9314	184861
0.9314	0.9635	187426
0.9635	0.9956	111100
0.9956	1.0276	0

Figure 33: Histogram of a one million run Monte Carlo simulation of equation (38), with uniform inputs.

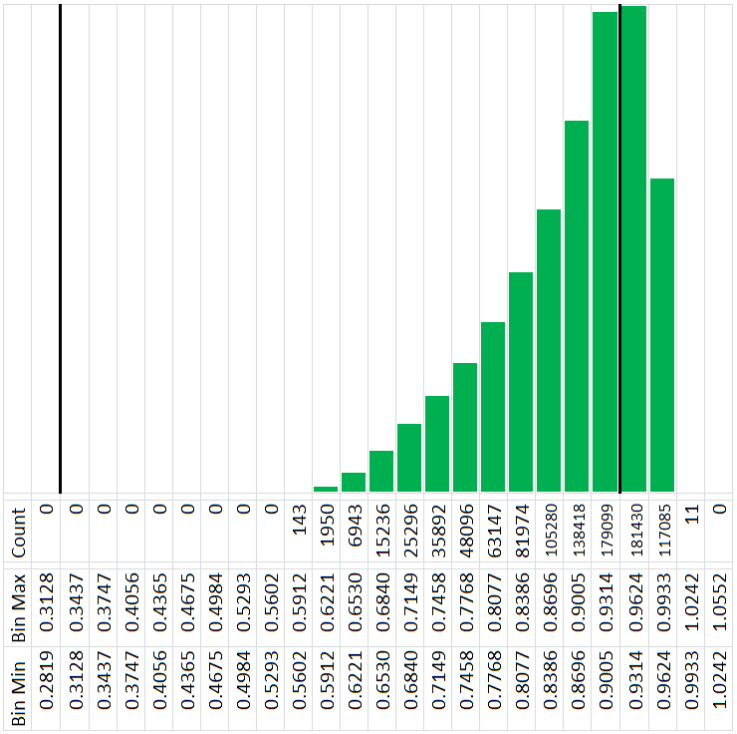

Bin Min	Bin Max	Count
0.2819	0.3128	0
0.3128	0.3437	0
0.3437	0.3747	0
0.3747	0.4056	0
0.4056	0.4365	0
0.4365	0.4675	0
0.4675	0.4984	0
0.4984	0.5293	0
0.5293	0.5602	0
0.5602	0.5912	143
0.5912	0.6221	1950
0.6221	0.6530	6943
0.6530	0.6840	15236
0.6840	0.7149	25296
0.7149	0.7458	35892
0.7458	0.7768	48096
0.7768	0.8077	63147
0.8077	0.8386	81974
0.8386	0.8696	105280
0.8696	0.9005	138418
0.9005	0.9314	179099
0.9314	0.9624	181430
0.9624	0.9933	117085
0.9933	1.0242	11
1.0242	1.0552	0

Figure 34: Histogram of a one million run Monte Carlo simulation of equation (39), with uniform inputs.

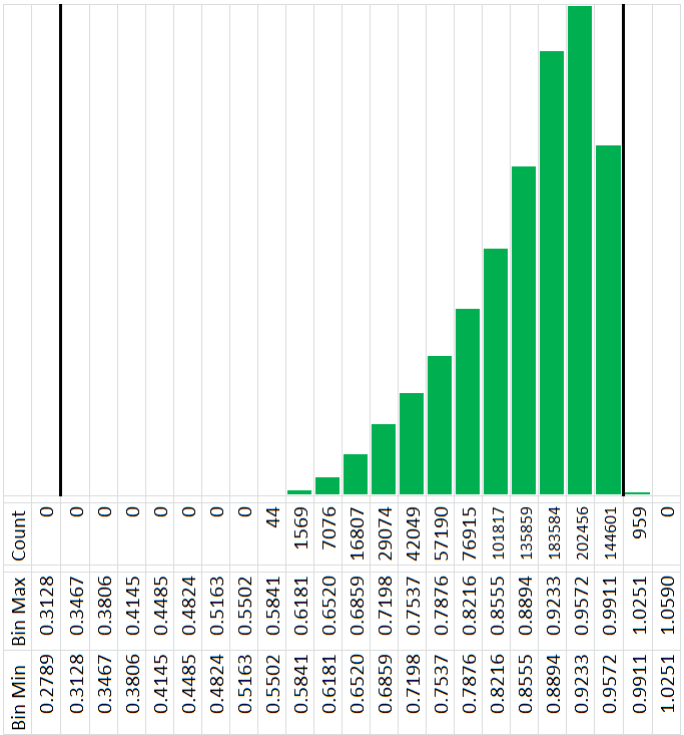

Bin Min	Bin Max	Count
0.2789	0.3128	0
0.3128	0.3467	0
0.3467	0.3806	0
0.3806	0.4145	0
0.4145	0.4485	0
0.4485	0.4824	0
0.4824	0.5163	0
0.5163	0.5502	0
0.5502	0.5841	44
0.5841	0.6181	1569
0.6181	0.6520	7076
0.6520	0.6859	16807
0.6859	0.7198	29074
0.7198	0.7537	42049
0.7537	0.7876	57190
0.7876	0.8216	76915
0.8216	0.8555	101817
0.8555	0.8894	135859
0.8894	0.9233	183584
0.9233	0.9572	202456
0.9572	0.9911	144601
0.9911	1.0251	959
1.0251	1.0590	0

Figure 35: Histogram of a one million run Monte Carlo simulation of equation (40), with uniform inputs.

Each of these histograms reveals that the Monte Carlo simulation results leave a large portion of the posterior probability interval un-used, which may give the impression

that the predicted interval is not sound. However, Table 31 also contains the upper and lower extreme real values that are possible using the intervals. These extreme values were found by completing sixteen real-valued calculations, which allowed for every combination of extremes in the four independent intervals. The extreme values encompass both the Monte Carlo simulation results and the posterior probability intervals, illustrating that the predicted intervals are indeed sound.

5.3 : Model validation with Kullback-Leibler divergence

Model validation (or invalidation) may be based on the distance between a model and its Bayesian update (Babuška, Nobile, & Tempone, 2008) (Mahadevan & Rebba, 2005). The Kullback-Leibler divergence (Kullback & Leibler, 1951) (Kullback S. , 1997) provides information about the divergence between two probability distributions. In the strictest sense, its lack of symmetry means that it is not a distance, but it is often used in a similar way in the validation process (Burnham & Anderson, 1998) (Cheung & Beck, 2008). Where P and Q are discretized probability distributions, the K-L divergence of P from Q is given by:

$$D_{KL}(P|Q) = \sum_i P_i \ln \frac{P_i}{Q_i}$$

For the special case of only two probabilities for each distribution (e.g. $P(y_m)$ and $P(y_m^C)$), this is written as:

$$D_{KL}(P|Q) = P_1 \ln \frac{P_1}{Q_1} + P_2 \ln \frac{P_2}{Q_2}$$

And, because $\sum_i P_i = \sum_i Q_i = 1$, this can be written as:

$$D_{KL}(P|Q) = P_1 \ln \frac{P_1}{Q_1} + (1 - P_1) \ln \frac{1 - P_1}{1 - Q_1}$$

If either P_1 or $Q_1$is equal to either zero or one, the above equation is defined as equal to zero.

The K-L divergence is not symmetric—that is, typically $D_{KL}(P|Q) \neq D_{KL}(Q|P)$. A symmetric measurement of the divergence between two probabilities P and Q can be obtained by adding $D_{KL}(P|Q)$ and $D_{KL}(Q|P)$. The sum of these is herein denoted as $D_{KLS}(P,Q)$. For any of these three measures of divergence, the closer the result is to zero, the less the two distributions diverge from one another, and the better each one approximates the other.

5.3.1: Interval-valued K-L divergence

When generalized interval valued-probabilities are used, the modality of the intervals must be considered. D_{KL} may take on any value greater than or equal to zero, and it is useful to know the largest possible range of values that the divergence may take. For this reason the interval-valued K-L divergence is formulated to provide a worst-case analysis. For the generalized interval valued probabilities $\boldsymbol{p}_1$ and $\boldsymbol{q}_1$, the following equations are used to calculate $\boldsymbol{D}_{KLS}$:

$$\begin{gathered}
\boldsymbol{P}_1 = pro(\boldsymbol{p}_1), \qquad \boldsymbol{P}_2 = 1 - dual(\boldsymbol{P}_1) \\
\boldsymbol{Q}_1 = pro(\boldsymbol{q}_1), \qquad \boldsymbol{Q}_2 = 1 - dual(\boldsymbol{Q}_1) \\
\boldsymbol{D}_{KL}(\boldsymbol{P}|\boldsymbol{Q}) = \boldsymbol{P}_1 \ln\frac{\boldsymbol{P}_1}{\boldsymbol{Q}_1} + \boldsymbol{P}_2 \ln\frac{\boldsymbol{P}_2}{\boldsymbol{Q}_2} \\
\boldsymbol{D}_{KL}(\boldsymbol{Q}|\boldsymbol{P}) = \boldsymbol{Q}_1 \ln\frac{\boldsymbol{Q}_1}{\boldsymbol{P}_1} + \boldsymbol{Q}_2 \ln\frac{\boldsymbol{Q}_2}{\boldsymbol{P}_2} \\
\boldsymbol{D}_{KLS}(\boldsymbol{p},\boldsymbol{q}) = pro\big(\boldsymbol{D}_{KL}(\boldsymbol{P}|\boldsymbol{Q})\big) + pro\big(\boldsymbol{D}_{KL}(\boldsymbol{Q}|\boldsymbol{P})\big)
\end{gathered} \tag{41}$$

The divergence between $\boldsymbol{P}(y_m)$ and $\boldsymbol{P}(y_m|y_e)$ provides an idea of the validity of the model. The results of these divergence calculations are given below in Table 32:

Table 32: K-L divergence validation of updating Models 1 and 2 with experimental results.

	Model 1		Model 2	
	Case 1: Nonfocal T1	Case 2: Nonfocal T2	Case 3: Nonfocal T2	Case 4: Nonfocal T1,T3
$pro\big(\boldsymbol{P}(y_m)\big)$	[0.5523,0.8647]	[0.5523,0.8647]	[0.3417,0.5924]	[0.3417,0.5924]
$pro\big(\boldsymbol{P}(y_m\|y_e)\big)$	[0.9835,0.9903]	[0.9061,0.9984]	[0.6750,1.0000]	[0.8532,1.0000]
$\boldsymbol{D}_{KL}(\boldsymbol{P}(y_m)\|\boldsymbol{P}(y_m\|y_e))$	[1.3931,0.1734]	[2.1954,0.0090]	[0.0000,0.0150]	[0.0000,0.2001]
$\boldsymbol{D}_{KL}(\boldsymbol{P}(y_m\|y_e)\|\boldsymbol{P}(y_m))$	[0.0919,0.5411]	[0.0081,0.5821]	[0.0145,1.0738]	[0.1613,1.0738]
$\boldsymbol{D}_{KLS}(\boldsymbol{P}(y_m),\boldsymbol{P}(y_m\|y_e))$	[0.2653,1.9342]	[0.0171,2.7775]	[0.0145,1.0888]	[0.1613,1.2740]

In general, the divergence values for Model 2 are lower than those for Model 1, indicating that Model 2 is more valid than Model 1 when compared to the available experimental results. For Model 2, the symmetric K-L divergence for Case 3 is partially less than that of Case 4 ($C_3\boldsymbol{D}_{KLS} \prec C_4\boldsymbol{D}_{KLS}$), indicating that Case 3 is generally more valid than Case 4. For Model 1, no such conclusion can be made as $C_1\boldsymbol{D}_{KLS} \subset C_2\boldsymbol{D}_{KLS}$, although it can be seen that Case 1 exhibits less epistemic uncertainty than Case 2 in terms of its validity.

Because each model involved is based upon a certain amount of experimental data, the update of one model with another model still represents a branch of model validation. The divergence between $\boldsymbol{P}(y_m)$ and $\boldsymbol{P}\big(y_m\big|y_{m^c}\big)$ thus serves to validate the result of each two-model update. The results of these divergence calculations are given below in Table 33:

Table 33: K-L divergence validation of updating Models 1 and 2 with the other (complementary) model.

	Model 1		Model 2	
	Case 1: Nonfocal T1	Case 2: Nonfocal T2	Case 3: Nonfocal T2	Case 4: Nonfocal T1,T3
$pro\big(\boldsymbol{P}(y_m)\big)$	[0.5523,0.8647]	[0.5523,0.8647]	[0.3417,0.5924]	[0.3417,0.5924]
$pro\left(\boldsymbol{P}\big(y_m\big|y_{m^c}\big)\right)$	[0.9652,1.0000]	[0.9962,0.9996]	[0.5408,0.7527]	[0.6632,0.9458]
$\boldsymbol{D}_{KL}\left(\boldsymbol{P}(y_m)\middle\|\boldsymbol{P}\big(y_m\big|y_{m^c}\big)\right)$	[0.0000,0.0886]	[2.8154,0.3609]	[0.3747,0.0054]	[1.2959,0.0109]
$\boldsymbol{D}_{KL}\left(\boldsymbol{P}\big(y_m\big|y_{m^c}\big)\middle\|\boldsymbol{P}(y_m)\right)$	[0.0589,0.5937]	[0.1275,0.5902]	[0.0055,0.3523]	[0.0106,0.8276]
$\boldsymbol{D}_{KLS}\left(\boldsymbol{P}(y_m),\boldsymbol{P}\big(y_m\big|y_{m^c}\big)\right)$	[0.0589,0.6823]	[0.4884,3.4056]	[0.0109,0.7270]	[0.0215,2.1235]

For Model 1, $C_1\boldsymbol{D}_{KLS} \prec C_2\boldsymbol{D}_{KLS}$, indicating that Case 1 may be more valid than Case 2. Similarly, for Model 2, $C_3\boldsymbol{D}_{KLS} \prec C_4\boldsymbol{D}_{KLS}$, indicating that Case 3 may be more valid than Case 4 when Model 1 is allowed to update Model 2.

5.3.2: Verification versus validation

The "better" case as determined by the K-L divergence need not correspond with the "better" case as determined by the Monte Carlo simulations; the two methods measure different things. Monte Carlo simulations serve as verification—a purely mathematical check of how well the posterior probability interval represents the range of outputs that may be produced by real values within the input intervals (the prior and likelihoods). K-L divergence, on the other hand, serves as validation—a comparison of the updated model with the experimental results to determine how well the model represents reality.

5.4: Model updates with real-valued Bayes' Rule

The difficulties encountered in making the applications of equations (31), (34), and (35) comply with the Logic Coherence Constraint were largely due to the fact that the epistemic uncertainty of the application included three possible orientations, whereas an interval only has two bounds. For the sake of comparison, the real-valued posterior probabilities are also calculated here for each of the three orientations individually and independently.

5.4.1: Updating with experimental results

The relevant real-valued equation for updating a model with experimental results is:

$$P(y_m|y_e) = \frac{[P(y_e|t_1) \quad P(y_e|t_2) \quad P(y_e|t_3)] \begin{bmatrix} P(t_1|y_m) \\ P(t_2|y_m) \\ P(t_3|y_m) \end{bmatrix} P(y_m)}{[P(y_e|t_1) \quad P(y_e|t_2) \quad P(y_e|t_3)] \begin{bmatrix} P(t_1|y_m) & P(t_1|y_m^C) \\ P(t_2|y_m) & P(t_2|y_m^C) \\ P(t_3|y_m) & P(t_3|y_m^C) \end{bmatrix} \begin{bmatrix} P(y_m) \\ P(y_m^C) \end{bmatrix}}$$

The values used in this equation for each orientation have been determined previously, and are summarized for each orientation and equation here:

Table 34: Values used to update Models 1 and 2 according to experimental results.

Orientation	Model 1			Model 2		
	#4	#5	#6	#4	#5	#6
$P(y_e\|t_1)$	0.0000	0.0000	0.0000	0.0000	0.0000	0.0000
$P(y_e\|t_2)$	0.0000	1.0000	0.0000	0.0000	1.0000	0.0000
$P(y_e\|t_3)$	1.0000	1.0000	1.0000	1.0000	1.0000	1.0000
$P(t_1\|y_m)$	0.2030	0.1571	0.0211	0.0000	0.0000	0.0000
$P(t_2\|y_m)$	0.3960	0.4188	0.4085	0.5000	0.5000	0.0000
$P(t_3\|y_m)$	0.4010	0.4241	0.5704	0.5000	0.5000	1.0000
$P(t_1\|y_m^C)$	0.9756	0.9808	0.7723	1.0000	1.0000	0.5000
$P(t_2\|y_m^C)$	0.0244	0.0192	0.2277	0.0000	0.0000	0.5000
$P(t_3\|y_m^C)$	0.0000	0.0000	0.0000	0.0000	0.0000	0.0000
$P(y_m)$	0.8647	0.8202	0.5523	0.5924	0.5834	0.3417
$P(y_m^C)$	0.1353	0.1798	0.4477	0.4076	0.4166	0.6583
$P(y_m\|y_e)$	1.0000	0.9950	1.0000	1.0000	1.0000	1.0000

For both models, the posterior probabilities are extremely high—100% in five out of six cases. This is because the experimental results showed yield strengths that were, in general, much higher than the yield strengths predicted by the models. When stresses are high enough to cause yielding in the experiments, they are almost certainly high enough to predict yielding in the models.

For Model 1, GIBR Case 2 (with non-focal T2) gave a posterior probability interval of $\boldsymbol{P}(y_{m1}|y_e) = [0.9061, 0.9984]$. $P(y_{m1}|y_e)$ is above the upper end of this interval for both orientation #4 and #6, and is just inside the upper end of the interval for orientation #5. All three orientations' posterior probabilities are above the peak of the Monte Carlo simulation. If an interval is made of the posterior probabilities for the three

orientations as calculated separately, $\boldsymbol{P}(y_{m1}|y_e) = [0.9950,1.0000]$. By this measure, GIBR has underestimated the posterior probability's value and overestimated its epistemic uncertainty. A similar case can be made for Model 2, where GIBR (Case 3) predicts $\boldsymbol{P}(y_{m2}|y_e) = [0.6750,1.0000]$, and creating an interval from the individual orientations predicts the point interval $\boldsymbol{P}(y_{m2}|y_e) = [1.0000,1.0000]$.

5.4.2: Updating one model with another model

The real-valued equation for updating one model with the complementary model is as follows:

$$P(y_m|y_{m^c}) = \frac{\begin{bmatrix} P(y_{m^c}|t_1) & P(y_{m^c 2}|t_2) & P(y_{m^c}|t_3) \end{bmatrix} \begin{bmatrix} P(t_1|y_m) \\ P(t_2|y_m) \\ P(t_3|y_m) \end{bmatrix} P(y_m)}{\begin{bmatrix} P(y_{m^c}|t_1) & P(y_{m^c 2}|t_2) & P(y_{m^c}|t_3) \end{bmatrix} \begin{bmatrix} P(t_1|y_m) & P(t_1|y_m^C) \\ P(t_2|y_m) & P(t_2|y_m^C) \\ P(t_3|y_m) & P(t_3|y_m^C) \end{bmatrix} \begin{bmatrix} P(y_m) \\ P(y_m^C) \end{bmatrix}}$$

The values used to inform this model for each individual orientation are given below:

Table 35: Values used to update Models 1 and 2 according to the other (complementary) model.

Orientation	Model 1			Model 2		
	#4	#5	#6	#4	#5	#6
$P(y_{m^c}\|t_1)$	0.0000	0.0000	0.0000	0.4774	0.3384	0.0297
$P(y_{m^c}\|t_2)$	0.9998	0.9999	0.0008	0.9946	0.9881	0.7202
$P(y_{m^c}\|t_3)$	1.0000	1.0000	1.0000	1.0000	1.0000	1.0000
$P(t_1\|y_m)$	0.2030	0.1571	0.0211	0.0000	0.0000	0.0000
$P(t_2\|y_m)$	0.3960	0.4188	0.4085	0.5000	0.5000	0.0000
$P(t_3\|y_m)$	0.4010	0.4241	0.5704	0.5000	0.5000	1.0000
$P(t_1\|y_m^C)$	0.9756	0.9808	0.7723	1.0000	1.0000	0.5000
$P(t_2\|y_m^C)$	0.0244	0.0192	0.2277	0.0000	0.0000	0.5000
$P(t_3\|y_m^C)$	0.0000	0.0000	0.0000	0.0000	0.0000	0.0000
$P(y_m)$	0.8647	0.8202	0.5523	0.5924	0.5834	0.3417
$P(y_m^C)$	0.1353	0.1798	0.4477	0.4076	0.4166	0.6583
$P(y_m\|y_{m^c})$	0.9952	0.9950	0.9997	0.7522	0.8044	0.5806

When Model 1 is updated by Model 2, the posterior probabilities are very high and very tightly grouped—once again indicating the Model 2 predicts higher yield strengths than does Model 1, and does so consistently. An interval created by examining the individual orientations is $\boldsymbol{P}(y_{m1}|y_{m2})$=[0.9950,0.9997]. GIBR Case 1 predicts a posterior probability interval of $\boldsymbol{P}(y_{m1}|y_{m2})$=[1.0000,0.9652], which fully encompasses the independent orientations' interval, but is much wider and so implies more epistemic uncertainty than actually exists. While GIBR Case 2 did not contain its MC results as Case 1, it gave a posterior probability interval of $\boldsymbol{P}(y_{m1}|y_{m2})$=[0.9996,0.9962]. Although this is an improper interval, it is only slightly narrower than the interval predicted by examining the orientations independently, and it is in nearly the same location.

When Model 2 is updated by Model 1, the independent orientations combine to give a posterior probability interval of $\boldsymbol{P}(y_{m2}|y_{m1})$=[0.5806,0.8044]. This only slightly wider and slightly higher than the GIBR result of Model 2, Case 3, for which $\boldsymbol{P}(y_{m2}|y_{m1})$=[0.5408,0.7527]. In this instance, GIBR closely predicted the actual range of the results for each of the three orientations.

5.5: Conclusions

Within this chapter, GIBR was used to update the belief in a model's results by using either experimental results for validation, or by using another model for verification and model aggregation. It was demonstrated that the selection of certain probabilities as focal or non-focal must be done on an application-by-application basis; when Model 1 was updated by experimental results, Case 2 better contained the MC simulation results, but when Model 1 was updated by Model 2, Case 1 did a better job. For Model 2, however, Case 3 did better than Case 4 whether the model was updated by the experiment or by the other model. With the current level of understanding, the degree of

soundness/completeness of the posterior probability interval still cannot be anticipated without verification by Monte Carlo simulation or some other verification tool.

In this chapter, the orientation of the specimen represented the epistemic uncertainty of each interval, where the three orientations considered were defined as the only possible orientations for the specimen. Out of the four GIBR examples $\boldsymbol{P}(y_{m1}|y_e)$, $\boldsymbol{P}(y_{m2}|y_e)$, $\boldsymbol{P}(y_{m1}|y_{m2})$, and $\boldsymbol{P}(y_{m2}|y_{m1})$, only one gave a good estimate of the actual interval of posterior probabilities as determined by looking at the orientations individually. While this result was promising, arriving at the GIBR result involved some subjective decisions and more computations and comparisons than did examining the orientations individually. From this it can be concluded that, at least when the number of configurations represented by epistemic uncertainty is small, it is both more efficient and more reliable to examine each configuration and update it independently of the others, and then look at the range of results in order to determine a posterior probability interval.

Some of the intervals used in this were surprisingly wide, exhibiting high amounts of epistemic uncertainty even though they were based on data rather than ignorance. Examples include four of the $\boldsymbol{P}(t|y_{m2})$ intervals, with a width of 0.5, the initial calculation of $\boldsymbol{P}(y_e|t = 195K)$, with a width of 1, and $\boldsymbol{P}(y_{m2}|t = 195K)$, with a width of 0.9991. The width of these intervals was due to the differences in behavior among the three orientations analyzed. If more orientations were included in the analysis, the intervals could only be made wider as long as the actual orientation of interest remained unknown—the epistemic uncertainty would actually increase because more orientations would be considered as possibilities. Similarly, increasing the number of temperatures examined in the discretization of the likelihoods would not change the variation among orientations already included at each temperature. It is possible that, with a larger number of mutually disjoint events involved, two or more probabilities would need to be designated as non-focal in order to ensure compliance with the Logic Coherence Constraint in the face of a few very wide focal probabilities.

CHAPTER 6: CONCLUSIONS AND FUTURE WORK

6.1: Conclusions

Early discussions of Generalized Interval Bayes' Rule have included the hope that it could be used as a basic estimator of a range of outcomes in the face of large amounts of uncertainty. However, the research detailed in this thesis has revealed that GIBR has some of the same problems dealing with complete ignorance as do other probability theories. Complete ignorance is difficult to represent. The worst-case scenario is that the GIBR equation gives an update in the face of complete ignorance, shifting the posterior probability when no actual information has been added. Initial attempts to represent unknown probabilities with the total ignorance interval of [0,1] quickly run afoul of the Logic Coherence Constraint, which specifies that the probabilities of mutually disjoint events must sum to [1,1]. Alternatives include switching to equally-weighted point intervals, or ignoring the LCC and using all intervals of [0,1]. The best case scenario is that these representations of complete ignorance give no probability update. This is as it should be—if the evidence cannot be linked to the prior probability, then the probability should not be updated. In this case, simply filling out the links in the GIBR equation may be helpful in that it shows the analyst where the missing link is, and thus where they need to focus more effort in order to discover the value of that link. If further data cannot be obtained, the analyst may instead opt for an expert elicitation of a probability interval. If these options are not viable and a link of complete ignorance cannot be eliminated, then users of GIBR should not expect an update from it.

Caution is also required when determining which probabilities are considered focal or non-focal in a GIBR equation. When all of the probabilities within an equation can be determined from the evidence at hand, it is easy to end up with an equation that does not conform to the Logic Coherence Constraint. In that case care must be exercised

in choosing which intervals should be considered non-focal and thus calculated by subtracting the sum of the other intervals from $[1,1]$—an incorrect choice may lead to results that are clearly impossible. Even when this is not the case, a subjective decision as to which event should be focal or non-focal can lead to large differences in not only the posterior probability interval, but also the range of possible results and the degree to which the posterior probability interval contains those results, both of which can be illustrated by Monte Carlo simulations. Where evidence is available for all events in a mutually disjoint group and the choice of focality is not obvious, analysts would be wise to calculate the results of each possible choice of non-focal event in order to make the best decision.

GIBR gives a solution that is sound but typically not complete. As such, it is primarily a tool for very early investigations into a problem—a brief calculation that provides a general idea of where to focus further effort. It is a tool that can provide economical preliminary decision support analysis for modeling and simulation applications. When necessary, the complete solution can be determined by examining the range of results of 2^n real-valued Bayes' Rule calculations, where *n* is the number of independent intervals with nonzero width in the GIBR equation. In this case, GIBR is useful primarily as a way to organize data and to identify events for which information may be missing. If the actual distribution of the posterior probabilities is needed and so Monte Carlo sampling is required, then GIBR does not offer any great advantage over other sampling-based techniques.

The proposed Bayesian approach for model validation based on K-L divergence incorporates interval probability. The example is the simplest case where only two possible event outcomes are available. These two probabilities are not independent. A underestimation of a posterior will lead to an overestimation of its complementary. In this case, the calculated K-L divergence is likely to be a compromise between completeness and soundness. This observation needs further investigation.

6.2: Future Work

Because the posterior intervals predicted by GIBR can change significantly with the modality choices of the priors and likelihoods, it is still advisable to verify any GIBR update with a Monte Carlo simulation or sensitivity analysis by variation as a much cheaper alternative. The ultimate goal is to make this verification step unnecessary. This requires a better understanding of the conditions under which certain probabilities should be focal or non-focal are better understood. Further research may reveal a more consistent procedure or rules for determining focality of events, rendering further verification unnecessary. This would in turn render GIBR as a computationally inexpensive method for predicting sound, reasonable posterior probability intervals.

This thesis has served to confirm the presence of certain drawbacks to GIBR—drawbacks that are common to many types of probability analysis. However, Bayes' Rule is only one of many different probability analysis tools available to a savvy researcher. Generalized Interval Probability Theory should encompass all of these tools, and these have yet to be explored. This thesis has also demonstrated the de-coupled nature of the interval bounds within the GIBR equations. Other options for analyzing probabilities within GIPT have yet to be fully explored.

Several of the challenges that have arisen with GIBR have been related to enforcing the Logic Coherence Constraint. However, the Logic Coherence Constraint represents one of the most restrictive constraints possible. Weaker constraints, such as avoiding sure loss or avoiding partial loss, have yet to be examined in the context of GIBR. Employing another constraint system may allow analysts to circumvent some of the subjective choices of GIBR and thus make it into a more easily applicable method.

This thesis has largely focused on using GIBR in the face of large unknowns, even approaching complete ignorance. However, some of the results examined suggest that GIBR may be more reliable when used with relatively narrow intervals. This in turn leads to the possibility that GIPT may provide a viable method of sensitivity analysis.

Current sensitivity analysis techniques can be computationally expensive, requiring simulations similar to the Monte Carlo simulations used to verify GIBR here. Further refinement of the rules of GIPT, and further analysis of its behavior with narrower intervals should eliminate the need of verifying simulations, in which case it would provide a much simpler method of sensitivity analysis than is currently available.

APPENDIX A: MODEL 1 DATA

The following abbreviations for orientations are used: O#4 is [1,1,16], O#5 is [-1,3,7], and O#6 is [-4,9,9].

Temp	Case	ΔG (eV)	$\dot{\gamma}_0$ (s^{-1})	p	q	O#	Simulated Yield, MPa	Experimental Yield, MPa
143 K	1	0.725	10000000	0.37	1	4	132	251
143 K	2	0.725	10000000	0.37	1.1	4	115	251
143 K	3	0.725	10000000	0.37	1.2	4	100	251
143 K	4	0.725	10000000	0.42	1	4	158	251
143 K	5	0.725	10000000	0.42	1.1	4	135	251
143 K	6	0.725	10000000	0.42	1.2	4	120	251
143 K	7	0.725	10000000	0.47	1	4	182	251
143 K	8	0.725	10000000	0.47	1.1	4	159	251
143 K	9	0.725	10000000	0.47	1.2	4	143	251
143 K	10	0.725	13333333	0.37	1	4	130	251
143 K	11	0.725	13333333	0.37	1.1	4	113	251
143 K	12	0.725	13333333	0.37	1.2	4	98	251
143 K	13	0.725	13333333	0.42	1	4	155	251
143 K	14	0.725	13333333	0.42	1.1	4	134	251
143 K	15	0.725	13333333	0.42	1.2	4	118	251
143 K	16	0.725	13333333	0.47	1	4	176	251
143 K	17	0.725	13333333	0.47	1.1	4	157	251
143 K	18	0.725	13333333	0.47	1.2	4	141	251
143 K	19	0.725	16666667	0.37	1	4	128	251
143 K	20	0.725	16666667	0.37	1.1	4	108	251
143 K	21	0.725	16666667	0.37	1.2	4	94	251
143 K	22	0.725	16666667	0.42	1	4	154	251
143 K	23	0.725	16666667	0.42	1.1	4	132	251
143 K	24	0.725	16666667	0.42	1.2	4	117	251
143 K	25	0.725	16666667	0.47	1	4	174	251
143 K	26	0.725	16666667	0.47	1.1	4	156	251
143 K	27	0.725	16666667	0.47	1.2	4	136	251
143 K	28	0.775	10000000	0.37	1	4	148	251
143 K	29	0.775	10000000	0.37	1.1	4	130	251
143 K	30	0.775	10000000	0.37	1.2	4	114	251
143 K	31	0.775	10000000	0.42	1	4	175	251
143 K	32	0.775	10000000	0.42	1.1	4	155	251
143 K	33	0.775	10000000	0.42	1.2	4	135	251
143 K	34	0.775	10000000	0.47	1	4	200	251
143 K	35	0.775	10000000	0.47	1.1	4	176	251

Temp	Case	ΔG (eV)	$\dot{\gamma}_0$ (s^{-1})	p	q	O#	Simulated Yield, MPa	Experimental Yield, MPa
143 K	36	0.775	10000000	0.47	1.2	4	158	251
143 K	37	0.775	13333333	0.37	1	4	146	251
143 K	38	0.775	13333333	0.37	1.1	4	128	251
143 K	39	0.775	13333333	0.37	1.2	4	112	251
143 K	40	0.775	13333333	0.42	1	4	173	251
143 K	41	0.775	13333333	0.42	1.1	4	149	251
143 K	42	0.775	13333333	0.42	1.2	4	133	251
143 K	43	0.775	13333333	0.47	1	4	197	251
143 K	44	0.775	13333333	0.47	1.1	4	174	251
143 K	45	0.775	13333333	0.47	1.2	4	156	251
143 K	46	0.775	16666667	0.37	1	4	145	251
143 K	47	0.775	16666667	0.37	1.1	4	126	251
143 K	48	0.775	16666667	0.37	1.2	4	107	251
143 K	49	0.775	16666667	0.42	1	4	171	251
143 K	50	0.775	16666667	0.42	1.1	4	148	251
143 K	51	0.775	16666667	0.42	1.2	4	131	251
143 K	52	0.775	16666667	0.47	1	4	191	251
143 K	53	0.775	16666667	0.47	1.1	4	172	251
143 K	54	0.775	16666667	0.47	1.2	4	155	251
143 K	55	0.825	10000000	0.37	1	4	168	251
143 K	56	0.825	10000000	0.37	1.1	4	144	251
143 K	57	0.825	10000000	0.37	1.2	4	127	251
143 K	58	0.825	10000000	0.42	1	4	191	251
143 K	59	0.825	10000000	0.42	1.1	4	170	251
143 K	60	0.825	10000000	0.42	1.2	4	149	251
143 K	61	0.825	10000000	0.47	1	4	216	251
143 K	62	0.825	10000000	0.47	1.1	4	191	251
143 K	63	0.825	10000000	0.47	1.2	4	173	251
143 K	64	0.825	13333333	0.37	1	4	162	251
143 K	65	0.825	13333333	0.37	1.1	4	142	251
143 K	66	0.825	13333333	0.37	1.2	4	122	251
143 K	67	0.825	13333333	0.42	1	4	189	251
143 K	68	0.825	13333333	0.42	1.1	4	164	251
143 K	69	0.825	13333333	0.42	1.2	4	147	251
143 K	70	0.825	13333333	0.47	1	4	214	251
143 K	71	0.825	13333333	0.47	1.1	4	189	251
143 K	72	0.825	13333333	0.47	1.2	4	171	251
143 K	73	0.825	16666667	0.37	1	4	161	251
143 K	74	0.825	16666667	0.37	1.1	4	141	251
143 K	75	0.825	16666667	0.37	1.2	4	120	251
143 K	76	0.825	16666667	0.42	1	4	187	251
143 K	77	0.825	16666667	0.42	1.1	4	163	251
143 K	78	0.825	16666667	0.42	1.2	4	146	251

Temp	Case	ΔG (eV)	$\dot{\gamma}_0$ (s^{-1})	p	q	O#	Simulated Yield, MPa	Experimental Yield, MPa
143 K	79	0.825	16666667	0.47	1	4	212	251
143 K	80	0.825	16666667	0.47	1.1	4	188	251
143 K	81	0.825	16666667	0.47	1.2	4	169	251
143 K	1	0.725	10000000	0.37	1	5	144	250
143 K	2	0.725	10000000	0.37	1.1	5	124	250
143 K	3	0.725	10000000	0.37	1.2	5	107	250
143 K	4	0.725	10000000	0.42	1	5	168	250
143 K	5	0.725	10000000	0.42	1.1	5	147	250
143 K	6	0.725	10000000	0.42	1.2	5	130	250
143 K	7	0.725	10000000	0.47	1	5	191	250
143 K	8	0.725	10000000	0.47	1.1	5	169	250
143 K	9	0.725	10000000	0.47	1.2	5	151	250
143 K	10	0.725	13333333	0.37	1	5	141	250
143 K	11	0.725	13333333	0.37	1.1	5	121	250
143 K	12	0.725	13333333	0.37	1.2	5	105	250
143 K	13	0.725	13333333	0.42	1	5	166	250
143 K	14	0.725	13333333	0.42	1.1	5	145	250
143 K	15	0.725	13333333	0.42	1.2	5	127	250
143 K	16	0.725	13333333	0.47	1	5	188	250
143 K	17	0.725	13333333	0.47	1.1	5	167	250
143 K	18	0.725	13333333	0.47	1.2	5	149	250
143 K	19	0.725	16666667	0.37	1	5	139	250
143 K	20	0.725	16666667	0.37	1.1	5	120	250
143 K	21	0.725	16666667	0.37	1.2	5	104	250
143 K	22	0.725	16666667	0.42	1	5	164	250
143 K	23	0.725	16666667	0.42	1.1	5	143	250
143 K	24	0.725	16666667	0.42	1.2	5	126	250
143 K	25	0.725	16666667	0.47	1	5	186	250
143 K	26	0.725	16666667	0.47	1.1	5	165	250
143 K	27	0.725	16666667	0.47	1.2	5	147	250
143 K	28	0.775	10000000	0.37	1	5	162	250
143 K	29	0.775	10000000	0.37	1.1	5	140	250
143 K	30	0.775	10000000	0.37	1.2	5	122	250
143 K	31	0.775	10000000	0.42	1	5	187	250
143 K	32	0.775	10000000	0.42	1.1	5	165	250
143 K	33	0.775	10000000	0.42	1.2	5	145	250
143 K	34	0.775	10000000	0.47	1	5	210	250
143 K	35	0.775	10000000	0.47	1.1	5	187	250
143 K	36	0.775	10000000	0.47	1.2	5	168	250
143 K	37	0.775	13333333	0.37	1	5	159	250
143 K	38	0.775	13333333	0.37	1.1	5	138	250
143 K	39	0.775	13333333	0.37	1.2	5	120	250
143 K	40	0.775	13333333	0.42	1	5	184	250

Temp	Case	ΔG (eV)	$\dot{\gamma}_0$ (s^{-1})	p	q	O#	Simulated Yield, MPa	Experimental Yield, MPa
143 K	41	0.775	13333333	0.42	1.1	5	162	250
143 K	42	0.775	13333333	0.42	1.2	5	143	250
143 K	43	0.775	13333333	0.47	1	5	207	250
143 K	44	0.775	13333333	0.47	1.1	5	185	250
143 K	45	0.775	13333333	0.47	1.2	5	165	250
143 K	46	0.775	16666667	0.37	1	5	157	250
143 K	47	0.775	16666667	0.37	1.1	5	133	250
143 K	48	0.775	16666667	0.37	1.2	5	118	250
143 K	49	0.775	16666667	0.42	1	5	182	250
143 K	50	0.775	16666667	0.42	1.1	5	160	250
143 K	51	0.775	16666667	0.42	1.2	5	141	250
143 K	52	0.775	16666667	0.47	1	5	206	250
143 K	53	0.775	16666667	0.47	1.1	5	183	250
143 K	54	0.775	16666667	0.47	1.2	5	164	250
143 K	55	0.825	10000000	0.37	1	5	179	250
143 K	56	0.825	10000000	0.37	1.1	5	152	250
143 K	57	0.825	10000000	0.37	1.2	5	133	250
143 K	58	0.825	10000000	0.42	1	5	205	250
143 K	59	0.825	10000000	0.42	1.1	5	181	250
143 K	60	0.825	10000000	0.42	1.2	5	160	250
143 K	61	0.825	10000000	0.47	1	5	228	250
143 K	62	0.825	10000000	0.47	1.1	5	204	250
143 K	63	0.825	10000000	0.47	1.2	5	183	250
143 K	64	0.825	13333333	0.37	1	5	173	250
143 K	65	0.825	13333333	0.37	1.1	5	150	250
143 K	66	0.825	13333333	0.37	1.2	5	131	250
143 K	67	0.825	13333333	0.42	1	5	202	250
143 K	68	0.825	13333333	0.42	1.1	5	178	250
143 K	69	0.825	13333333	0.42	1.2	5	158	250
143 K	70	0.825	13333333	0.47	1	5	225	250
143 K	71	0.825	13333333	0.47	1.1	5	202	250
143 K	72	0.825	13333333	0.47	1.2	5	181	250
143 K	73	0.825	16666667	0.37	1	5	171	250
143 K	74	0.825	16666667	0.37	1.1	5	149	250
143 K	75	0.825	16666667	0.37	1.2	5	130	250
143 K	76	0.825	16666667	0.42	1	5	200	250
143 K	77	0.825	16666667	0.42	1.1	5	173	250
143 K	78	0.825	16666667	0.42	1.2	5	153	250
143 K	79	0.825	16666667	0.47	1	5	223	250
143 K	80	0.825	16666667	0.47	1.1	5	200	250
143 K	81	0.825	16666667	0.47	1.2	5	179	250
143 K	1	0.725	10000000	0.37	1	6	199	295
143 K	2	0.725	10000000	0.37	1.1	6	172	295

Temp	Case	ΔG (eV)	$\dot{\gamma}_0$ (s^{-1})	p	q	O#	Simulated Yield, MPa	Experimental Yield, MPa
143 K	3	0.725	10000000	0.37	1.2	6	149	295
143 K	4	0.725	10000000	0.42	1	6	239	295
143 K	5	0.725	10000000	0.42	1.1	6	210	295
143 K	6	0.725	10000000	0.42	1.2	6	185	295
143 K	7	0.725	10000000	0.47	1	6	271	295
143 K	8	0.725	10000000	0.47	1.1	6	241	295
143 K	9	0.725	10000000	0.47	1.2	6	215	295
143 K	10	0.725	13333333	0.37	1	6	196	295
143 K	11	0.725	13333333	0.37	1.1	6	169	295
143 K	12	0.725	13333333	0.37	1.2	6	146	295
143 K	13	0.725	13333333	0.42	1	6	235	295
143 K	14	0.725	13333333	0.42	1.1	6	201	295
143 K	15	0.725	13333333	0.42	1.2	6	182	295
143 K	16	0.725	13333333	0.47	1	6	268	295
143 K	17	0.725	13333333	0.47	1.1	6	238	295
143 K	18	0.725	13333333	0.47	1.2	6	212	295
143 K	19	0.725	16666667	0.37	1	6	194	295
143 K	20	0.725	16666667	0.37	1.1	6	167	295
143 K	21	0.725	16666667	0.37	1.2	6	144	295
143 K	22	0.725	16666667	0.42	1	6	232	295
143 K	23	0.725	16666667	0.42	1.1	6	199	295
143 K	24	0.725	16666667	0.42	1.2	6	175	295
143 K	25	0.725	16666667	0.47	1	6	265	295
143 K	26	0.725	16666667	0.47	1.1	6	235	295
143 K	27	0.725	16666667	0.47	1.2	6	209	295
143 K	28	0.775	10000000	0.37	1	6	225	295
143 K	29	0.775	10000000	0.37	1.1	6	195	295
143 K	30	0.775	10000000	0.37	1.2	6	170	295
143 K	31	0.775	10000000	0.42	1	6	266	295
143 K	32	0.775	10000000	0.42	1.1	6	234	295
143 K	33	0.775	10000000	0.42	1.2	6	207	295
143 K	34	0.775	10000000	0.47	1	6	298	295
143 K	35	0.775	10000000	0.47	1.1	6	266	295
143 K	36	0.775	10000000	0.47	1.2	6	239	295
143 K	37	0.775	13333333	0.37	1	6	222	295
143 K	38	0.775	13333333	0.37	1.1	6	192	295
143 K	39	0.775	13333333	0.37	1.2	6	167	295
143 K	40	0.775	13333333	0.42	1	6	262	295
143 K	41	0.775	13333333	0.42	1.1	6	226	295
143 K	42	0.775	13333333	0.42	1.2	6	200	295
143 K	43	0.775	13333333	0.47	1	6	295	295
143 K	44	0.775	13333333	0.47	1.1	6	263	295
143 K	45	0.775	13333333	0.47	1.2	6	235	295

Temp	Case	ΔG (eV)	$\dot{\gamma}_0$ (s^{-1})	p	q	O#	Simulated Yield, MPa	Experimental Yield, MPa
143 K	46	0.775	16666667	0.37	1	6	219	295
143 K	47	0.775	16666667	0.37	1.1	6	190	295
143 K	48	0.775	16666667	0.37	1.2	6	165	295
143 K	49	0.775	16666667	0.42	1	6	259	295
143 K	50	0.775	16666667	0.42	1.1	6	223	295
143 K	51	0.775	16666667	0.42	1.2	6	197	295
143 K	52	0.775	16666667	0.47	1	6	292	295
143 K	53	0.775	16666667	0.47	1.1	6	260	295
143 K	54	0.775	16666667	0.47	1.2	6	228	295
143 K	55	0.825	10000000	0.37	1	6	249	295
143 K	56	0.825	10000000	0.37	1.1	6	218	295
143 K	57	0.825	10000000	0.37	1.2	6	190	295
143 K	58	0.825	10000000	0.42	1	6	291	295
143 K	59	0.825	10000000	0.42	1.1	6	252	295
143 K	60	0.825	10000000	0.42	1.2	6	224	295
143 K	61	0.825	10000000	0.47	1	6	324	295
143 K	62	0.825	10000000	0.47	1.1	6	290	295
143 K	63	0.825	10000000	0.47	1.2	6	261	295
143 K	64	0.825	13333333	0.37	1	6	246	295
143 K	65	0.825	13333333	0.37	1.1	6	214	295
143 K	66	0.825	13333333	0.37	1.2	6	187	295
143 K	67	0.825	13333333	0.42	1	6	287	295
143 K	68	0.825	13333333	0.42	1.1	6	249	295
143 K	69	0.825	13333333	0.42	1.2	6	221	295
143 K	70	0.825	13333333	0.47	1	6	320	295
143 K	71	0.825	13333333	0.47	1.1	6	287	295
143 K	72	0.825	13333333	0.47	1.2	6	253	295
143 K	73	0.825	16666667	0.37	1	6	243	295
143 K	74	0.825	16666667	0.37	1.1	6	212	295
143 K	75	0.825	16666667	0.37	1.2	6	185	295
143 K	76	0.825	16666667	0.42	1	6	279	295
143 K	77	0.825	16666667	0.42	1.1	6	247	295
143 K	78	0.825	16666667	0.42	1.2	6	219	295
143 K	79	0.825	16666667	0.47	1	6	317	295
143 K	80	0.825	16666667	0.47	1.1	6	279	295
143 K	81	0.825	16666667	0.47	1.2	6	251	295
195 K	1	0.725	10000000	0.37	1	4	69	151
195 K	2	0.725	10000000	0.37	1.1	4	59	151
195 K	3	0.725	10000000	0.37	1.2	4	51	151
195 K	4	0.725	10000000	0.42	1	4	87	151
195 K	5	0.725	10000000	0.42	1.1	4	75	151
195 K	6	0.725	10000000	0.42	1.2	4	68	151
195 K	7	0.725	10000000	0.47	1	4	109	151

Temp	Case	ΔG (eV)	$\dot{\gamma}_0$ (s^{-1})	p	q	O#	Simulated Yield, MPa	Experimental Yield, MPa
195 K	8	0.725	10000000	0.47	1.1	4	95	151
195 K	9	0.725	10000000	0.47	1.2	4	84	151
195 K	10	0.725	13333333	0.37	1	4	67	151
195 K	11	0.725	13333333	0.37	1.1	4	57	151
195 K	12	0.725	13333333	0.37	1.2	4	49	151
195 K	13	0.725	13333333	0.42	1	4	85	151
195 K	14	0.725	13333333	0.42	1.1	4	73	151
195 K	15	0.725	13333333	0.42	1.2	4	64	151
195 K	16	0.725	13333333	0.47	1	4	103	151
195 K	17	0.725	13333333	0.47	1.1	4	90	151
195 K	18	0.725	13333333	0.47	1.2	4	82	151
195 K	19	0.725	16666667	0.37	1	4	63	151
195 K	20	0.725	16666667	0.37	1.1	4	56	151
195 K	21	0.725	16666667	0.37	1.2	4	48	151
195 K	22	0.725	16666667	0.42	1	4	83	151
195 K	23	0.725	16666667	0.42	1.1	4	72	151
195 K	24	0.725	16666667	0.42	1.2	4	62	151
195 K	25	0.725	16666667	0.47	1	4	101	151
195 K	26	0.725	16666667	0.47	1.1	4	88	151
195 K	27	0.725	16666667	0.47	1.2	4	77	151
195 K	28	0.775	10000000	0.37	1	4	85	151
195 K	29	0.775	10000000	0.37	1.1	4	73	151
195 K	30	0.775	10000000	0.37	1.2	4	63	151
195 K	31	0.775	10000000	0.42	1	4	104	151
195 K	32	0.775	10000000	0.42	1.1	4	91	151
195 K	33	0.775	10000000	0.42	1.2	4	82	151
195 K	34	0.775	10000000	0.47	1	4	128	151
195 K	35	0.775	10000000	0.47	1.1	4	113	151
195 K	36	0.775	10000000	0.47	1.2	4	100	151
195 K	37	0.775	13333333	0.37	1	4	83	151
195 K	38	0.775	13333333	0.37	1.1	4	71	151
195 K	39	0.775	13333333	0.37	1.2	4	61	151
195 K	40	0.775	13333333	0.42	1	4	102	151
195 K	41	0.775	13333333	0.42	1.1	4	89	151
195 K	42	0.775	13333333	0.42	1.2	4	77	151
195 K	43	0.775	13333333	0.47	1	4	125	151
195 K	44	0.775	13333333	0.47	1.1	4	110	151
195 K	45	0.775	13333333	0.47	1.2	4	98	151
195 K	46	0.775	16666667	0.37	1	4	81	151
195 K	47	0.775	16666667	0.37	1.1	4	69	151
195 K	48	0.775	16666667	0.37	1.2	4	60	151
195 K	49	0.775	16666667	0.42	1	4	101	151
195 K	50	0.775	16666667	0.42	1.1	4	87	151

Temp	Case	ΔG (eV)	$\dot{\gamma}_0$ (s^{-1})	p	q	O#	Simulated Yield, MPa	Experimental Yield, MPa
195 K	51	0.775	16666667	0.42	1.2	4	76	151
195 K	52	0.775	16666667	0.47	1	4	123	151
195 K	53	0.775	16666667	0.47	1.1	4	105	151
195 K	54	0.775	16666667	0.47	1.2	4	96	151
195 K	55	0.825	10000000	0.37	1	4	101	151
195 K	56	0.825	10000000	0.37	1.1	4	87	151
195 K	57	0.825	10000000	0.37	1.2	4	75	151
195 K	58	0.825	10000000	0.42	1	4	126	151
195 K	59	0.825	10000000	0.42	1.1	4	110	151
195 K	60	0.825	10000000	0.42	1.2	4	96	151
195 K	61	0.825	10000000	0.47	1	4	150	151
195 K	62	0.825	10000000	0.47	1.1	4	130	151
195 K	63	0.825	10000000	0.47	1.2	4	115	151
195 K	64	0.825	13333333	0.37	1	4	99	151
195 K	65	0.825	13333333	0.37	1.1	4	85	151
195 K	66	0.825	13333333	0.37	1.2	4	73	151
195 K	67	0.825	13333333	0.42	1	4	123	151
195 K	68	0.825	13333333	0.42	1.1	4	104	151
195 K	69	0.825	13333333	0.42	1.2	4	91	151
195 K	70	0.825	13333333	0.47	1	4	144	151
195 K	71	0.825	13333333	0.47	1.1	4	127	151
195 K	72	0.825	13333333	0.47	1.2	4	113	151
195 K	73	0.825	16666667	0.37	1	4	97	151
195 K	74	0.825	16666667	0.37	1.1	4	83	151
195 K	75	0.825	16666667	0.37	1.2	4	72	151
195 K	76	0.825	16666667	0.42	1	4	118	151
195 K	77	0.825	16666667	0.42	1.1	4	103	151
195 K	78	0.825	16666667	0.42	1.2	4	90	151
195 K	79	0.825	16666667	0.47	1	4	142	151
195 K	80	0.825	16666667	0.47	1.1	4	126	151
195 K	81	0.825	16666667	0.47	1.2	4	112	151
195 K	1	0.725	10000000	0.37	1	5	76	148
195 K	2	0.725	10000000	0.37	1.1	5	65	148
195 K	3	0.725	10000000	0.37	1.2	5	57	148
195 K	4	0.725	10000000	0.42	1	5	96	148
195 K	5	0.725	10000000	0.42	1.1	5	83	148
195 K	6	0.725	10000000	0.42	1.2	5	71	148
195 K	7	0.725	10000000	0.47	1	5	116	148
195 K	8	0.725	10000000	0.47	1.1	5	101	148
195 K	9	0.725	10000000	0.47	1.2	5	89	148
195 K	10	0.725	13333333	0.37	1	5	71	148
195 K	11	0.725	13333333	0.37	1.1	5	63	148
195 K	12	0.725	13333333	0.37	1.2	5	53	148

Temp	Case	ΔG (eV)	$\dot{\gamma}_0$ (s^{-1})	p	q	O#	Simulated Yield, MPa	Experimental Yield, MPa
195 K	13	0.725	13333333	0.42	1	5	90	148
195 K	14	0.725	13333333	0.42	1.1	5	80	148
195 K	15	0.725	13333333	0.42	1.2	5	69	148
195 K	16	0.725	13333333	0.47	1	5	110	148
195 K	17	0.725	13333333	0.47	1.1	5	99	148
195 K	18	0.725	13333333	0.47	1.2	5	86	148
195 K	19	0.725	16666667	0.37	1	5	70	148
195 K	20	0.725	16666667	0.37	1.1	5	61	148
195 K	21	0.725	16666667	0.37	1.2	5	52	148
195 K	22	0.725	16666667	0.42	1	5	89	148
195 K	23	0.725	16666667	0.42	1.1	5	78	148
195 K	24	0.725	16666667	0.42	1.2	5	68	148
195 K	25	0.725	16666667	0.47	1	5	108	148
195 K	26	0.725	16666667	0.47	1.1	5	97	148
195 K	27	0.725	16666667	0.47	1.2	5	85	148
195 K	28	0.775	10000000	0.37	1	5	90	148
195 K	29	0.775	10000000	0.37	1.1	5	79	148
195 K	30	0.775	10000000	0.37	1.2	5	68	148
195 K	31	0.775	10000000	0.42	1	5	115	148
195 K	32	0.775	10000000	0.42	1.1	5	99	148
195 K	33	0.775	10000000	0.42	1.2	5	86	148
195 K	34	0.775	10000000	0.47	1	5	137	148
195 K	35	0.775	10000000	0.47	1.1	5	120	148
195 K	36	0.775	10000000	0.47	1.2	5	105	148
195 K	37	0.775	13333333	0.37	1	5	88	148
195 K	38	0.775	13333333	0.37	1.1	5	77	148
195 K	39	0.775	13333333	0.37	1.2	5	66	148
195 K	40	0.775	13333333	0.42	1	5	109	148
195 K	41	0.775	13333333	0.42	1.1	5	97	148
195 K	42	0.775	13333333	0.42	1.2	5	84	148
195 K	43	0.775	13333333	0.47	1	5	130	148
195 K	44	0.775	13333333	0.47	1.1	5	117	148
195 K	45	0.775	13333333	0.47	1.2	5	103	148
195 K	46	0.775	16666667	0.37	1	5	86	148
195 K	47	0.775	16666667	0.37	1.1	5	73	148
195 K	48	0.775	16666667	0.37	1.2	5	64	148
195 K	49	0.775	16666667	0.42	1	5	107	148
195 K	50	0.775	16666667	0.42	1.1	5	92	148
195 K	51	0.775	16666667	0.42	1.2	5	82	148
195 K	52	0.775	16666667	0.47	1	5	128	148
195 K	53	0.775	16666667	0.47	1.1	5	111	148
195 K	54	0.775	16666667	0.47	1.2	5	101	148
195 K	55	0.825	10000000	0.37	1	5	107	148

Temp	Case	ΔG (eV)	$\dot{\gamma}_0$ (s^{-1})	p	q	O#	Simulated Yield, MPa	Experimental Yield, MPa
195 K	56	0.825	10000000	0.37	1.1	5	91	148
195 K	57	0.825	10000000	0.37	1.2	5	80	148
195 K	58	0.825	10000000	0.42	1	5	130	148
195 K	59	0.825	10000000	0.42	1.1	5	116	148
195 K	60	0.825	10000000	0.42	1.2	5	101	148
195 K	61	0.825	10000000	0.47	1	5	156	148
195 K	62	0.825	10000000	0.47	1.1	5	137	148
195 K	63	0.825	10000000	0.47	1.2	5	121	148
195 K	64	0.825	13333333	0.37	1	5	105	148
195 K	65	0.825	13333333	0.37	1.1	5	89	148
195 K	66	0.825	13333333	0.37	1.2	5	78	148
195 K	67	0.825	13333333	0.42	1	5	127	148
195 K	68	0.825	13333333	0.42	1.1	5	110	148
195 K	69	0.825	13333333	0.42	1.2	5	99	148
195 K	70	0.825	13333333	0.47	1	5	150	148
195 K	71	0.825	13333333	0.47	1.1	5	135	148
195 K	72	0.825	13333333	0.47	1.2	5	119	148
195 K	73	0.825	16666667	0.37	1	5	103	148
195 K	74	0.825	16666667	0.37	1.1	5	87	148
195 K	75	0.825	16666667	0.37	1.2	5	77	148
195 K	76	0.825	16666667	0.42	1	5	126	148
195 K	77	0.825	16666667	0.42	1.1	5	108	148
195 K	78	0.825	16666667	0.42	1.2	5	97	148
195 K	79	0.825	16666667	0.47	1	5	148	148
195 K	80	0.825	16666667	0.47	1.1	5	129	148
195 K	81	0.825	16666667	0.47	1.2	5	117	148
195 K	1	0.725	10000000	0.37	1	6	103	153
195 K	2	0.725	10000000	0.37	1.1	6	87	153
195 K	3	0.725	10000000	0.37	1.2	6	77	153
195 K	4	0.725	10000000	0.42	1	6	130	153
195 K	5	0.725	10000000	0.42	1.1	6	111	153
195 K	6	0.725	10000000	0.42	1.2	6	96	153
195 K	7	0.725	10000000	0.47	1	6	157	153
195 K	8	0.725	10000000	0.47	1.1	6	136	153
195 K	9	0.725	10000000	0.47	1.2	6	119	153
195 K	10	0.725	13333333	0.37	1	6	95	153
195 K	11	0.725	13333333	0.37	1.1	6	84	153
195 K	12	0.725	13333333	0.37	1.2	6	75	153
195 K	13	0.725	13333333	0.42	1	6	126	153
195 K	14	0.725	13333333	0.42	1.1	6	108	153
195 K	15	0.725	13333333	0.42	1.2	6	93	153
195 K	16	0.725	13333333	0.47	1	6	153	153
195 K	17	0.725	13333333	0.47	1.1	6	133	153

Temp	Case	ΔG (eV)	$\dot{\gamma}_0$ (s^{-1})	p	q	O#	Simulated Yield, MPa	Experimental Yield, MPa
195 K	18	0.725	13333333	0.47	1.2	6	116	153
195 K	19	0.725	16666667	0.37	1	6	94	153
195 K	20	0.725	16666667	0.37	1.1	6	83	153
195 K	21	0.725	16666667	0.37	1.2	6	70	153
195 K	22	0.725	16666667	0.42	1	6	119	153
195 K	23	0.725	16666667	0.42	1.1	6	106	153
195 K	24	0.725	16666667	0.42	1.2	6	91	153
195 K	25	0.725	16666667	0.47	1	6	145	153
195 K	26	0.725	16666667	0.47	1.1	6	130	153
195 K	27	0.725	16666667	0.47	1.2	6	114	153
195 K	28	0.775	10000000	0.37	1	6	121	153
195 K	29	0.775	10000000	0.37	1.1	6	107	153
195 K	30	0.775	10000000	0.37	1.2	6	91	153
195 K	31	0.775	10000000	0.42	1	6	155	153
195 K	32	0.775	10000000	0.42	1.1	6	134	153
195 K	33	0.775	10000000	0.42	1.2	6	116	153
195 K	34	0.775	10000000	0.47	1	6	184	153
195 K	35	0.775	10000000	0.47	1.1	6	161	153
195 K	36	0.775	10000000	0.47	1.2	6	142	153
195 K	37	0.775	13333333	0.37	1	6	118	153
195 K	38	0.775	13333333	0.37	1.1	6	104	153
195 K	39	0.775	13333333	0.37	1.2	6	89	153
195 K	40	0.775	13333333	0.42	1	6	146	153
195 K	41	0.775	13333333	0.42	1.1	6	131	153
195 K	42	0.775	13333333	0.42	1.2	6	113	153
195 K	43	0.775	13333333	0.47	1	6	181	153
195 K	44	0.775	13333333	0.47	1.1	6	158	153
195 K	45	0.775	13333333	0.47	1.2	6	139	153
195 K	46	0.775	16666667	0.37	1	6	116	153
195 K	47	0.775	16666667	0.37	1.1	6	102	153
195 K	48	0.775	16666667	0.37	1.2	6	87	153
195 K	49	0.775	16666667	0.42	1	6	144	153
195 K	50	0.775	16666667	0.42	1.1	6	128	153
195 K	51	0.775	16666667	0.42	1.2	6	111	153
195 K	52	0.775	16666667	0.47	1	6	172	153
195 K	53	0.775	16666667	0.47	1.1	6	155	153
195 K	54	0.775	16666667	0.47	1.2	6	136	153
195 K	55	0.825	10000000	0.37	1	6	144	153
195 K	56	0.825	10000000	0.37	1.1	6	127	153
195 K	57	0.825	10000000	0.37	1.2	6	109	153
195 K	58	0.825	10000000	0.42	1	6	180	153
195 K	59	0.825	10000000	0.42	1.1	6	156	153
195 K	60	0.825	10000000	0.42	1.2	6	136	153

Temp	Case	ΔG (eV)	$\dot{\gamma}_0$ (s^{-1})	p	q	O#	Simulated Yield, MPa	Experimental Yield, MPa
195 K	61	0.825	10000000	0.47	1	6	211	153
195 K	62	0.825	10000000	0.47	1.1	6	186	153
195 K	63	0.825	10000000	0.47	1.2	6	164	153
195 K	64	0.825	13333333	0.37	1	6	141	153
195 K	65	0.825	13333333	0.37	1.1	6	119	153
195 K	66	0.825	13333333	0.37	1.2	6	106	153
195 K	67	0.825	13333333	0.42	1	6	171	153
195 K	68	0.825	13333333	0.42	1.1	6	153	153
195 K	69	0.825	13333333	0.42	1.2	6	133	153
195 K	70	0.825	13333333	0.47	1	6	207	153
195 K	71	0.825	13333333	0.47	1.1	6	182	153
195 K	72	0.825	13333333	0.47	1.2	6	161	153
195 K	73	0.825	16666667	0.37	1	6	138	153
195 K	74	0.825	16666667	0.37	1.1	6	117	153
195 K	75	0.825	16666667	0.37	1.2	6	104	153
195 K	76	0.825	16666667	0.42	1	6	169	153
195 K	77	0.825	16666667	0.42	1.1	6	146	153
195 K	78	0.825	16666667	0.42	1.2	6	131	153
195 K	79	0.825	16666667	0.47	1	6	204	153
195 K	80	0.825	16666667	0.47	1.1	6	179	153
195 K	81	0.825	16666667	0.47	1.2	6	158	153
250 K	1	0.725	10000000	0.37	1	4	28	72
250 K	2	0.725	10000000	0.37	1.1	4	26	72
250 K	3	0.725	10000000	0.37	1.2	4	24	72
250 K	4	0.725	10000000	0.42	1	4	35	72
250 K	5	0.725	10000000	0.42	1.1	4	32	72
250 K	6	0.725	10000000	0.42	1.2	4	30	72
250 K	7	0.725	10000000	0.47	1	4	44	72
250 K	8	0.725	10000000	0.47	1.1	4	41	72
250 K	9	0.725	10000000	0.47	1.2	4	36	72
250 K	10	0.725	13333333	0.37	1	4	27	72
250 K	11	0.725	13333333	0.37	1.1	4	25	72
250 K	12	0.725	13333333	0.37	1.2	4	23	72
250 K	13	0.725	13333333	0.42	1	4	33	72
250 K	14	0.725	13333333	0.42	1.1	4	31	72
250 K	15	0.725	13333333	0.42	1.2	4	28	72
250 K	16	0.725	13333333	0.47	1	4	43	72
250 K	17	0.725	13333333	0.47	1.1	4	39	72
250 K	18	0.725	13333333	0.47	1.2	4	34	72
250 K	19	0.725	16666667	0.37	1	4	26	72
250 K	20	0.725	16666667	0.37	1.1	4	24	72
250 K	21	0.725	16666667	0.37	1.2	4	23	72
250 K	22	0.725	16666667	0.42	1	4	32	72

Temp	Case	ΔG (eV)	$\dot{\gamma}_0$ (s^{-1})	p	q	O#	Simulated Yield, MPa	Experimental Yield, MPa
250 K	23	0.725	16666667	0.42	1.1	4	30	72
250 K	24	0.725	16666667	0.42	1.2	4	27	72
250 K	25	0.725	16666667	0.47	1	4	41	72
250 K	26	0.725	16666667	0.47	1.1	4	36	72
250 K	27	0.725	16666667	0.47	1.2	4	33	72
250 K	28	0.775	10000000	0.37	1	4	36	72
250 K	29	0.775	10000000	0.37	1.1	4	33	72
250 K	30	0.775	10000000	0.37	1.2	4	30	72
250 K	31	0.775	10000000	0.42	1	4	47	72
250 K	32	0.775	10000000	0.42	1.1	4	43	72
250 K	33	0.775	10000000	0.42	1.2	4	39	72
250 K	34	0.775	10000000	0.47	1	4	60	72
250 K	35	0.775	10000000	0.47	1.1	4	55	72
250 K	36	0.775	10000000	0.47	1.2	4	48	72
250 K	37	0.775	13333333	0.37	1	4	35	72
250 K	38	0.775	13333333	0.37	1.1	4	32	72
250 K	39	0.775	13333333	0.37	1.2	4	29	72
250 K	40	0.775	13333333	0.42	1	4	46	72
250 K	41	0.775	13333333	0.42	1.1	4	41	72
250 K	42	0.775	13333333	0.42	1.2	4	36	72
250 K	43	0.775	13333333	0.47	1	4	58	72
250 K	44	0.775	13333333	0.47	1.1	4	52	72
250 K	45	0.775	13333333	0.47	1.2	4	46	72
250 K	46	0.775	16666667	0.37	1	4	34	72
250 K	47	0.775	16666667	0.37	1.1	4	31	72
250 K	48	0.775	16666667	0.37	1.2	4	28	72
250 K	49	0.775	16666667	0.42	1	4	44	72
250 K	50	0.775	16666667	0.42	1.1	4	40	72
250 K	51	0.775	16666667	0.42	1.2	4	35	72
250 K	52	0.775	16666667	0.47	1	4	56	72
250 K	53	0.775	16666667	0.47	1.1	4	49	72
250 K	54	0.775	16666667	0.47	1.2	4	45	72
250 K	55	0.825	10000000	0.37	1	4	48	72
250 K	56	0.825	10000000	0.37	1.1	4	43	72
250 K	57	0.825	10000000	0.37	1.2	4	37	72
250 K	58	0.825	10000000	0.42	1	4	61	72
250 K	59	0.825	10000000	0.42	1.1	4	55	72
250 K	60	0.825	10000000	0.42	1.2	4	48	72
250 K	61	0.825	10000000	0.47	1	4	80	72
250 K	62	0.825	10000000	0.47	1.1	4	69	72
250 K	63	0.825	10000000	0.47	1.2	4	61	72
250 K	64	0.825	13333333	0.37	1	4	46	72
250 K	65	0.825	13333333	0.37	1.1	4	41	72

Temp	Case	ΔG (eV)	$\dot{\gamma}_0$ (s^{-1})	p	q	O#	Simulated Yield, MPa	Experimental Yield, MPa
250 K	66	0.825	13333333	0.37	1.2	4	36	72
250 K	67	0.825	13333333	0.42	1	4	59	72
250 K	68	0.825	13333333	0.42	1.1	4	53	72
250 K	69	0.825	13333333	0.42	1.2	4	47	72
250 K	70	0.825	13333333	0.47	1	4	74	72
250 K	71	0.825	13333333	0.47	1.1	4	67	72
250 K	72	0.825	13333333	0.47	1.2	4	59	72
250 K	73	0.825	16666667	0.37	1	4	45	72
250 K	74	0.825	16666667	0.37	1.1	4	40	72
250 K	75	0.825	16666667	0.37	1.2	4	35	72
250 K	76	0.825	16666667	0.42	1	4	58	72
250 K	77	0.825	16666667	0.42	1.1	4	50	72
250 K	78	0.825	16666667	0.42	1.2	4	45	72
250 K	79	0.825	16666667	0.47	1	4	72	72
250 K	80	0.825	16666667	0.47	1.1	4	62	72
250 K	81	0.825	16666667	0.47	1.2	4	58	72
250 K	1	0.725	10000000	0.37	1	5	31	58
250 K	2	0.725	10000000	0.37	1.1	5	28	58
250 K	3	0.725	10000000	0.37	1.2	5	25	58
250 K	4	0.725	10000000	0.42	1	5	40	58
250 K	5	0.725	10000000	0.42	1.1	5	35	58
250 K	6	0.725	10000000	0.42	1.2	5	32	58
250 K	7	0.725	10000000	0.47	1	5	51	58
250 K	8	0.725	10000000	0.47	1.1	5	44	58
250 K	9	0.725	10000000	0.47	1.2	5	40	58
250 K	10	0.725	13333333	0.37	1	5	29	58
250 K	11	0.725	13333333	0.37	1.1	5	26	58
250 K	12	0.725	13333333	0.37	1.2	5	24	58
250 K	13	0.725	13333333	0.42	1	5	38	58
250 K	14	0.725	13333333	0.42	1.1	5	34	58
250 K	15	0.725	13333333	0.42	1.2	5	31	58
250 K	16	0.725	13333333	0.47	1	5	47	58
250 K	17	0.725	13333333	0.47	1.1	5	42	58
250 K	18	0.725	13333333	0.47	1.2	5	38	58
250 K	19	0.725	16666667	0.37	1	5	28	58
250 K	20	0.725	16666667	0.37	1.1	5	25	58
250 K	21	0.725	16666667	0.37	1.2	5	23	58
250 K	22	0.725	16666667	0.42	1	5	36	58
250 K	23	0.725	16666667	0.42	1.1	5	32	58
250 K	24	0.725	16666667	0.42	1.2	5	30	58
250 K	25	0.725	16666667	0.47	1	5	44	58
250 K	26	0.725	16666667	0.47	1.1	5	40	58
250 K	27	0.725	16666667	0.47	1.2	5	37	58

Temp	Case	ΔG (eV)	$\dot{\gamma}_0$ (s^{-1})	p	q	O#	Simulated Yield, MPa	Experimental Yield, MPa
250 K	28	0.775	10000000	0.37	1	5	41	58
250 K	29	0.775	10000000	0.37	1.1	5	36	58
250 K	30	0.775	10000000	0.37	1.2	5	32	58
250 K	31	0.775	10000000	0.42	1	5	51	58
250 K	32	0.775	10000000	0.42	1.1	5	46	58
250 K	33	0.775	10000000	0.42	1.2	5	41	58
250 K	34	0.775	10000000	0.47	1	5	66	58
250 K	35	0.775	10000000	0.47	1.1	5	59	58
250 K	36	0.775	10000000	0.47	1.2	5	51	58
250 K	37	0.775	13333333	0.37	1	5	39	58
250 K	38	0.775	13333333	0.37	1.1	5	34	58
250 K	39	0.775	13333333	0.37	1.2	5	31	58
250 K	40	0.775	13333333	0.42	1	5	50	58
250 K	41	0.775	13333333	0.42	1.1	5	44	58
250 K	42	0.775	13333333	0.42	1.2	5	40	58
250 K	43	0.775	13333333	0.47	1	5	63	58
250 K	44	0.775	13333333	0.47	1.1	5	56	58
250 K	45	0.775	13333333	0.47	1.2	5	49	58
250 K	46	0.775	16666667	0.37	1	5	37	58
250 K	47	0.775	16666667	0.37	1.1	5	33	58
250 K	48	0.775	16666667	0.37	1.2	5	30	58
250 K	49	0.775	16666667	0.42	1	5	47	58
250 K	50	0.775	16666667	0.42	1.1	5	43	58
250 K	51	0.775	16666667	0.42	1.2	5	38	58
250 K	52	0.775	16666667	0.47	1	5	61	58
250 K	53	0.775	16666667	0.47	1.1	5	55	58
250 K	54	0.775	16666667	0.47	1.2	5	48	58
250 K	55	0.825	10000000	0.37	1	5	51	58
250 K	56	0.825	10000000	0.37	1.1	5	45	58
250 K	57	0.825	10000000	0.37	1.2	5	40	58
250 K	58	0.825	10000000	0.42	1	5	67	58
250 K	59	0.825	10000000	0.42	1.1	5	59	58
250 K	60	0.825	10000000	0.42	1.2	5	51	58
250 K	61	0.825	10000000	0.47	1	5	83	58
250 K	62	0.825	10000000	0.47	1.1	5	74	58
250 K	63	0.825	10000000	0.47	1.2	5	65	58
250 K	64	0.825	13333333	0.37	1	5	49	58
250 K	65	0.825	13333333	0.37	1.1	5	43	58
250 K	66	0.825	13333333	0.37	1.2	5	38	58
250 K	67	0.825	13333333	0.42	1	5	64	58
250 K	68	0.825	13333333	0.42	1.1	5	57	58
250 K	69	0.825	13333333	0.42	1.2	5	49	58
250 K	70	0.825	13333333	0.47	1	5	81	58

Temp	Case	ΔG (eV)	$\dot{\gamma}_0$ (s^{-1})	p	q	O#	Simulated Yield, MPa	Experimental Yield, MPa
250 K	71	0.825	13333333	0.47	1.1	5	69	58
250 K	72	0.825	13333333	0.47	1.2	5	63	58
250 K	73	0.825	16666667	0.37	1	5	48	58
250 K	74	0.825	16666667	0.37	1.1	5	42	58
250 K	75	0.825	16666667	0.37	1.2	5	37	58
250 K	76	0.825	16666667	0.42	1	5	63	58
250 K	77	0.825	16666667	0.42	1.1	5	55	58
250 K	78	0.825	16666667	0.42	1.2	5	48	58
250 K	79	0.825	16666667	0.47	1	5	78	58
250 K	80	0.825	16666667	0.47	1.1	5	68	58
250 K	81	0.825	16666667	0.47	1.2	5	61	58
250 K	1	0.725	10000000	0.37	1	6	41	66
250 K	2	0.725	10000000	0.37	1.1	6	36	66
250 K	3	0.725	10000000	0.37	1.2	6	33	66
250 K	4	0.725	10000000	0.42	1	6	52	66
250 K	5	0.725	10000000	0.42	1.1	6	47	66
250 K	6	0.725	10000000	0.42	1.2	6	43	66
250 K	7	0.725	10000000	0.47	1	6	64	66
250 K	8	0.725	10000000	0.47	1.1	6	57	66
250 K	9	0.725	10000000	0.47	1.2	6	52	66
250 K	10	0.725	13333333	0.37	1	6	38	66
250 K	11	0.725	13333333	0.37	1.1	6	35	66
250 K	12	0.725	13333333	0.37	1.2	6	32	66
250 K	13	0.725	13333333	0.42	1	6	50	66
250 K	14	0.725	13333333	0.42	1.1	6	45	66
250 K	15	0.725	13333333	0.42	1.2	6	39	66
250 K	16	0.725	13333333	0.47	1	6	61	66
250 K	17	0.725	13333333	0.47	1.1	6	55	66
250 K	18	0.725	13333333	0.47	1.2	6	50	66
250 K	19	0.725	16666667	0.37	1	6	37	66
250 K	20	0.725	16666667	0.37	1.1	6	34	66
250 K	21	0.725	16666667	0.37	1.2	6	31	66
250 K	22	0.725	16666667	0.42	1	6	48	66
250 K	23	0.725	16666667	0.42	1.1	6	43	66
250 K	24	0.725	16666667	0.42	1.2	6	38	66
250 K	25	0.725	16666667	0.47	1	6	59	66
250 K	26	0.725	16666667	0.47	1.1	6	54	66
250 K	27	0.725	16666667	0.47	1.2	6	49	66
250 K	28	0.775	10000000	0.37	1	6	53	66
250 K	29	0.775	10000000	0.37	1.1	6	48	66
250 K	30	0.775	10000000	0.37	1.2	6	43	66
250 K	31	0.775	10000000	0.42	1	6	67	66
250 K	32	0.775	10000000	0.42	1.1	6	60	66

Temp	Case	ΔG (eV)	$\dot{\gamma}_0$ (s^{-1})	p	q	O#	Simulated Yield, MPa	Experimental Yield, MPa
250 K	33	0.775	10000000	0.42	1.2	6	55	66
250 K	34	0.775	10000000	0.47	1	6	86	66
250 K	35	0.775	10000000	0.47	1.1	6	77	66
250 K	36	0.775	10000000	0.47	1.2	6	67	66
250 K	37	0.775	13333333	0.37	1	6	51	66
250 K	38	0.775	13333333	0.37	1.1	6	45	66
250 K	39	0.775	13333333	0.37	1.2	6	40	66
250 K	40	0.775	13333333	0.42	1	6	65	66
250 K	41	0.775	13333333	0.42	1.1	6	58	66
250 K	42	0.775	13333333	0.42	1.2	6	52	66
250 K	43	0.775	13333333	0.47	1	6	83	66
250 K	44	0.775	13333333	0.47	1.1	6	74	66
250 K	45	0.775	13333333	0.47	1.2	6	65	66
250 K	46	0.775	16666667	0.37	1	6	50	66
250 K	47	0.775	16666667	0.37	1.1	6	44	66
250 K	48	0.775	16666667	0.37	1.2	6	39	66
250 K	49	0.775	16666667	0.42	1	6	63	66
250 K	50	0.775	16666667	0.42	1.1	6	56	66
250 K	51	0.775	16666667	0.42	1.2	6	50	66
250 K	52	0.775	16666667	0.47	1	6	80	66
250 K	53	0.775	16666667	0.47	1.1	6	68	66
250 K	54	0.775	16666667	0.47	1.2	6	63	66
250 K	55	0.825	10000000	0.37	1	6	67	66
250 K	56	0.825	10000000	0.37	1.1	6	59	66
250 K	57	0.825	10000000	0.37	1.2	6	53	66
250 K	58	0.825	10000000	0.42	1	6	87	66
250 K	59	0.825	10000000	0.42	1.1	6	77	66
250 K	60	0.825	10000000	0.42	1.2	6	67	66
250 K	61	0.825	10000000	0.47	1	6	109	66
250 K	62	0.825	10000000	0.47	1.1	6	93	66
250 K	63	0.825	10000000	0.47	1.2	6	85	66
250 K	64	0.825	13333333	0.37	1	6	64	66
250 K	65	0.825	13333333	0.37	1.1	6	57	66
250 K	66	0.825	13333333	0.37	1.2	6	51	66
250 K	67	0.825	13333333	0.42	1	6	84	66
250 K	68	0.825	13333333	0.42	1.1	6	75	66
250 K	69	0.825	13333333	0.42	1.2	6	64	66
250 K	70	0.825	13333333	0.47	1	6	106	66
250 K	71	0.825	13333333	0.47	1.1	6	91	66
250 K	72	0.825	13333333	0.47	1.2	6	82	66
250 K	73	0.825	16666667	0.37	1	6	62	66
250 K	74	0.825	16666667	0.37	1.1	6	55	66
250 K	75	0.825	16666667	0.37	1.2	6	49	66

Temp	Case	ΔG (eV)	$\dot{\gamma}_0$ (s^{-1})	p	q	O#	Simulated Yield, MPa	Experimental Yield, MPa
250 K	76	0.825	16666667	0.42	1	6	82	66
250 K	77	0.825	16666667	0.42	1.1	6	69	66
250 K	78	0.825	16666667	0.42	1.2	6	63	66
250 K	79	0.825	16666667	0.47	1	6	103	66
250 K	80	0.825	16666667	0.47	1.1	6	88	66
250 K	81	0.825	16666667	0.47	1.2	6	80	66

APPENDIX B: MODEL 2 DATA

The following abbreviations for orientations are used: O#4 is [1,1,16], O#5 is [-1,3,7], and O#6 is [-4,9,9].

Temp	Case	ΔG (eV)	$\dot{\gamma}_0$ (s^{-1})	p	q	O#	Simulated Yield, MPa	Experimental Yield, MPa
143 K	1	0.65	50000	0.23	1.34	4	208	251
143 K	2	0.65	50000	0.23	1.44	4	204	251
143 K	3	0.65	50000	0.23	1.54	4	200	251
143 K	4	0.65	50000	0.255	1.34	4	219	251
143 K	5	0.65	50000	0.255	1.44	4	210	251
143 K	6	0.65	50000	0.255	1.54	4	206	251
143 K	7	0.65	50000	0.28	1.34	4	231	251
143 K	8	0.65	50000	0.28	1.44	4	221	251
143 K	9	0.65	50000	0.28	1.54	4	216	251
143 K	10	0.65	66667	0.23	1.34	4	207	251
143 K	11	0.65	66667	0.23	1.44	4	203	251
143 K	12	0.65	66667	0.23	1.54	4	196	251
143 K	13	0.65	66667	0.255	1.34	4	218	251
143 K	14	0.65	66667	0.255	1.44	4	209	251
143 K	15	0.65	66667	0.255	1.54	4	205	251
143 K	16	0.65	66667	0.28	1.34	4	229	251
143 K	17	0.65	66667	0.28	1.44	4	220	251
143 K	18	0.65	66667	0.28	1.54	4	215	251
143 K	19	0.65	83333	0.23	1.34	4	206	251
143 K	20	0.65	83333	0.23	1.44	4	202	251
143 K	21	0.65	83333	0.23	1.54	4	195	251
143 K	22	0.65	83333	0.255	1.34	4	217	251
143 K	23	0.65	83333	0.255	1.44	4	208	251
143 K	24	0.65	83333	0.255	1.54	4	204	251
143 K	25	0.65	83333	0.28	1.34	4	228	251
143 K	26	0.65	83333	0.28	1.44	4	219	251
143 K	27	0.65	83333	0.28	1.54	4	214	251
143 K	28	0.675	50000	0.23	1.34	4	214	251
143 K	29	0.675	50000	0.23	1.44	4	206	251
143 K	30	0.675	50000	0.23	1.54	4	202	251
143 K	31	0.675	50000	0.255	1.34	4	222	251
143 K	32	0.675	50000	0.255	1.44	4	217	251
143 K	33	0.675	50000	0.255	1.54	4	208	251
143 K	34	0.675	50000	0.28	1.34	4	234	251
143 K	35	0.675	50000	0.28	1.44	4	228	251

Temp	Case	ΔG (eV)	$\dot{\gamma}_0$ (s^{-1})	p	q	O#	Simulated Yield, MPa	Experimental Yield, MPa
143 K	36	0.675	50000	0.28	1.54	4	219	251
143 K	37	0.675	66667	0.23	1.34	4	209	251
143 K	38	0.675	66667	0.23	1.44	4	205	251
143 K	39	0.675	66667	0.23	1.54	4	201	251
143 K	40	0.675	66667	0.255	1.34	4	221	251
143 K	41	0.675	66667	0.255	1.44	4	216	251
143 K	42	0.675	66667	0.255	1.54	4	207	251
143 K	43	0.675	66667	0.28	1.34	4	233	251
143 K	44	0.675	66667	0.28	1.44	4	223	251
143 K	45	0.675	66667	0.28	1.54	4	218	251
143 K	46	0.675	83333	0.23	1.34	4	209	251
143 K	47	0.675	83333	0.23	1.44	4	204	251
143 K	48	0.675	83333	0.23	1.54	4	201	251
143 K	49	0.675	83333	0.255	1.34	4	220	251
143 K	50	0.675	83333	0.255	1.44	4	215	251
143 K	51	0.675	83333	0.255	1.54	4	207	251
143 K	52	0.675	83333	0.28	1.34	4	232	251
143 K	53	0.675	83333	0.28	1.44	4	222	251
143 K	54	0.675	83333	0.28	1.54	4	217	251
143 K	55	0.7	50000	0.23	1.34	4	217	251
143 K	56	0.7	50000	0.23	1.44	4	208	251
143 K	57	0.7	50000	0.23	1.54	4	204	251
143 K	58	0.7	50000	0.255	1.34	4	229	251
143 K	59	0.7	50000	0.255	1.44	4	219	251
143 K	60	0.7	50000	0.255	1.54	4	214	251
143 K	61	0.7	50000	0.28	1.34	4	242	251
143 K	62	0.7	50000	0.28	1.44	4	231	251
143 K	63	0.7	50000	0.28	1.54	4	221	251
143 K	64	0.7	66667	0.23	1.34	4	216	251
143 K	65	0.7	66667	0.23	1.44	4	207	251
143 K	66	0.7	66667	0.23	1.54	4	203	251
143 K	67	0.7	66667	0.255	1.34	4	228	251
143 K	68	0.7	66667	0.255	1.44	4	218	251
143 K	69	0.7	66667	0.255	1.54	4	209	251
143 K	70	0.7	66667	0.28	1.34	4	236	251
143 K	71	0.7	66667	0.28	1.44	4	230	251
143 K	72	0.7	66667	0.28	1.54	4	220	251
143 K	73	0.7	83333	0.23	1.34	4	215	251
143 K	74	0.7	83333	0.23	1.44	4	207	251
143 K	75	0.7	83333	0.23	1.54	4	203	251
143 K	76	0.7	83333	0.255	1.34	4	223	251
143 K	77	0.7	83333	0.255	1.44	4	217	251
143 K	78	0.7	83333	0.255	1.54	4	209	251

Temp	Case	ΔG (eV)	$\dot{\gamma}_0$ (s^{-1})	p	q	O#	Simulated Yield, MPa	Experimental Yield, MPa
143 K	79	0.7	83333	0.28	1.34	4	235	251
143 K	80	0.7	83333	0.28	1.44	4	229	251
143 K	81	0.7	83333	0.28	1.54	4	220	251
143 K	1	0.65	50000	0.23	1.34	5	215	250
143 K	2	0.65	50000	0.23	1.44	5	209	250
143 K	3	0.65	50000	0.23	1.54	5	205	250
143 K	4	0.65	50000	0.255	1.34	5	227	250
143 K	5	0.65	50000	0.255	1.44	5	220	250
143 K	6	0.65	50000	0.255	1.54	5	212	250
143 K	7	0.65	50000	0.28	1.34	5	240	250
143 K	8	0.65	50000	0.28	1.44	5	229	250
143 K	9	0.65	50000	0.28	1.54	5	223	250
143 K	10	0.65	66667	0.23	1.34	5	214	250
143 K	11	0.65	66667	0.23	1.44	5	208	250
143 K	12	0.65	66667	0.23	1.54	5	204	250
143 K	13	0.65	66667	0.255	1.34	5	226	250
143 K	14	0.65	66667	0.255	1.44	5	219	250
143 K	15	0.65	66667	0.255	1.54	5	211	250
143 K	16	0.65	66667	0.28	1.34	5	235	250
143 K	17	0.65	66667	0.28	1.44	5	228	250
143 K	18	0.65	66667	0.28	1.54	5	221	250
143 K	19	0.65	83333	0.23	1.34	5	213	250
143 K	20	0.65	83333	0.23	1.44	5	207	250
143 K	21	0.65	83333	0.23	1.54	5	203	250
143 K	22	0.65	83333	0.255	1.34	5	225	250
143 K	23	0.65	83333	0.255	1.44	5	215	250
143 K	24	0.65	83333	0.255	1.54	5	210	250
143 K	25	0.65	83333	0.28	1.34	5	234	250
143 K	26	0.65	83333	0.28	1.44	5	227	250
143 K	27	0.65	83333	0.28	1.54	5	220	250
143 K	28	0.675	50000	0.23	1.34	5	221	250
143 K	29	0.675	50000	0.23	1.44	5	212	250
143 K	30	0.675	50000	0.23	1.54	5	207	250
143 K	31	0.675	50000	0.255	1.34	5	231	250
143 K	32	0.675	50000	0.255	1.44	5	224	250
143 K	33	0.675	50000	0.255	1.54	5	215	250
143 K	34	0.675	50000	0.28	1.34	5	245	250
143 K	35	0.675	50000	0.28	1.44	5	233	250
143 K	36	0.675	50000	0.28	1.54	5	226	250
143 K	37	0.675	66667	0.23	1.34	5	220	250
143 K	38	0.675	66667	0.23	1.44	5	211	250
143 K	39	0.675	66667	0.23	1.54	5	206	250
143 K	40	0.675	66667	0.255	1.34	5	230	250

Temp	Case	ΔG (eV)	$\dot{\gamma}_0$ (s^{-1})	p	q	O#	Simulated Yield, MPa	Experimental Yield, MPa
143 K	41	0.675	66667	0.255	1.44	5	222	250
143 K	42	0.675	66667	0.255	1.54	5	214	250
143 K	43	0.675	66667	0.28	1.34	5	243	250
143 K	44	0.675	66667	0.28	1.44	5	232	250
143 K	45	0.675	66667	0.28	1.54	5	225	250
143 K	46	0.675	83333	0.23	1.34	5	218	250
143 K	47	0.675	83333	0.23	1.44	5	210	250
143 K	48	0.675	83333	0.23	1.54	5	205	250
143 K	49	0.675	83333	0.255	1.34	5	229	250
143 K	50	0.675	83333	0.255	1.44	5	221	250
143 K	51	0.675	83333	0.255	1.54	5	213	250
143 K	52	0.675	83333	0.28	1.34	5	241	250
143 K	53	0.675	83333	0.28	1.44	5	231	250
143 K	54	0.675	83333	0.28	1.54	5	224	250
143 K	55	0.7	50000	0.23	1.34	5	225	250
143 K	56	0.7	50000	0.23	1.44	5	215	250
143 K	57	0.7	50000	0.23	1.54	5	210	250
143 K	58	0.7	50000	0.255	1.34	5	235	250
143 K	59	0.7	50000	0.255	1.44	5	227	250
143 K	60	0.7	50000	0.255	1.54	5	221	250
143 K	61	0.7	50000	0.28	1.34	5	249	250
143 K	62	0.7	50000	0.28	1.44	5	240	250
143 K	63	0.7	50000	0.28	1.54	5	230	250
143 K	64	0.7	66667	0.23	1.34	5	223	250
143 K	65	0.7	66667	0.23	1.44	5	214	250
143 K	66	0.7	66667	0.23	1.54	5	209	250
143 K	67	0.7	66667	0.255	1.34	5	234	250
143 K	68	0.7	66667	0.255	1.44	5	226	250
143 K	69	0.7	66667	0.255	1.54	5	219	250
143 K	70	0.7	66667	0.28	1.34	5	247	250
143 K	71	0.7	66667	0.28	1.44	5	235	250
143 K	72	0.7	66667	0.28	1.54	5	228	250
143 K	73	0.7	83333	0.23	1.34	5	222	250
143 K	74	0.7	83333	0.23	1.44	5	213	250
143 K	75	0.7	83333	0.23	1.54	5	208	250
143 K	76	0.7	83333	0.255	1.34	5	232	250
143 K	77	0.7	83333	0.255	1.44	5	225	250
143 K	78	0.7	83333	0.255	1.54	5	216	250
143 K	79	0.7	83333	0.28	1.34	5	246	250
143 K	80	0.7	83333	0.28	1.44	5	234	250
143 K	81	0.7	83333	0.28	1.54	5	227	250
143 K	1	0.65	50000	0.23	1.34	6	307	295
143 K	2	0.65	50000	0.23	1.44	6	300	295

Temp	Case	ΔG (eV)	$\dot{\gamma}_0$ (s^{-1})	p	q	O#	Simulated Yield, MPa	Experimental Yield, MPa
143 K	3	0.65	50000	0.23	1.54	6	294	295
143 K	4	0.65	50000	0.255	1.34	6	325	295
143 K	5	0.65	50000	0.255	1.44	6	315	295
143 K	6	0.65	50000	0.255	1.54	6	304	295
143 K	7	0.65	50000	0.28	1.34	6	343	295
143 K	8	0.65	50000	0.28	1.44	6	328	295
143 K	9	0.65	50000	0.28	1.54	6	319	295
143 K	10	0.65	66667	0.23	1.34	6	306	295
143 K	11	0.65	66667	0.23	1.44	6	299	295
143 K	12	0.65	66667	0.23	1.54	6	293	295
143 K	13	0.65	66667	0.255	1.34	6	323	295
143 K	14	0.65	66667	0.255	1.44	6	309	295
143 K	15	0.65	66667	0.255	1.54	6	302	295
143 K	16	0.65	66667	0.28	1.34	6	335	295
143 K	17	0.65	66667	0.28	1.44	6	326	295
143 K	18	0.65	66667	0.28	1.54	6	317	295
143 K	19	0.65	83333	0.23	1.34	6	305	295
143 K	20	0.65	83333	0.23	1.44	6	298	295
143 K	21	0.65	83333	0.23	1.54	6	292	295
143 K	22	0.65	83333	0.255	1.34	6	321	295
143 K	23	0.65	83333	0.255	1.44	6	308	295
143 K	24	0.65	83333	0.255	1.54	6	301	295
143 K	25	0.65	83333	0.28	1.34	6	334	295
143 K	26	0.65	83333	0.28	1.44	6	324	295
143 K	27	0.65	83333	0.28	1.54	6	316	295
143 K	28	0.675	50000	0.23	1.34	6	317	295
143 K	29	0.675	50000	0.23	1.44	6	304	295
143 K	30	0.675	50000	0.23	1.54	6	297	295
143 K	31	0.675	50000	0.255	1.34	6	330	295
143 K	32	0.675	50000	0.255	1.44	6	320	295
143 K	33	0.675	50000	0.255	1.54	6	308	295
143 K	34	0.675	50000	0.28	1.34	6	349	295
143 K	35	0.675	50000	0.28	1.44	6	333	295
143 K	36	0.675	50000	0.28	1.54	6	324	295
143 K	37	0.675	66667	0.23	1.34	6	310	295
143 K	38	0.675	66667	0.23	1.44	6	302	295
143 K	39	0.675	66667	0.23	1.54	6	296	295
143 K	40	0.675	66667	0.255	1.34	6	328	295
143 K	41	0.675	66667	0.255	1.44	6	318	295
143 K	42	0.675	66667	0.255	1.54	6	306	295
143 K	43	0.675	66667	0.28	1.34	6	347	295
143 K	44	0.675	66667	0.28	1.44	6	331	295
143 K	45	0.675	66667	0.28	1.54	6	322	295

Temp	Case	ΔG (eV)	$\dot{\gamma}_0$ (s^{-1})	p	q	O#	Simulated Yield, MPa	Experimental Yield, MPa
143 K	46	0.675	83333	0.23	1.34	6	309	295
143 K	47	0.675	83333	0.23	1.44	6	301	295
143 K	48	0.675	83333	0.23	1.54	6	295	295
143 K	49	0.675	83333	0.255	1.34	6	327	295
143 K	50	0.675	83333	0.255	1.44	6	317	295
143 K	51	0.675	83333	0.255	1.54	6	305	295
143 K	52	0.675	83333	0.28	1.34	6	345	295
143 K	53	0.675	83333	0.28	1.44	6	329	295
143 K	54	0.675	83333	0.28	1.54	6	321	295
143 K	55	0.7	50000	0.23	1.34	6	321	295
143 K	56	0.7	50000	0.23	1.44	6	308	295
143 K	57	0.7	50000	0.23	1.54	6	301	295
143 K	58	0.7	50000	0.255	1.34	6	335	295
143 K	59	0.7	50000	0.255	1.44	6	325	295
143 K	60	0.7	50000	0.255	1.54	6	316	295
143 K	61	0.7	50000	0.28	1.34	6	355	295
143 K	62	0.7	50000	0.28	1.44	6	343	295
143 K	63	0.7	50000	0.28	1.54	6	329	295
143 K	64	0.7	66667	0.23	1.34	6	319	295
143 K	65	0.7	66667	0.23	1.44	6	306	295
143 K	66	0.7	66667	0.23	1.54	6	299	295
143 K	67	0.7	66667	0.255	1.34	6	333	295
143 K	68	0.7	66667	0.255	1.44	6	323	295
143 K	69	0.7	66667	0.255	1.54	6	310	295
143 K	70	0.7	66667	0.28	1.34	6	353	295
143 K	71	0.7	66667	0.28	1.44	6	336	295
143 K	72	0.7	66667	0.28	1.54	6	327	295
143 K	73	0.7	83333	0.23	1.34	6	318	295
143 K	74	0.7	83333	0.23	1.44	6	305	295
143 K	75	0.7	83333	0.23	1.54	6	298	295
143 K	76	0.7	83333	0.255	1.34	6	332	295
143 K	77	0.7	83333	0.255	1.44	6	322	295
143 K	78	0.7	83333	0.255	1.54	6	309	295
143 K	79	0.7	83333	0.28	1.34	6	351	295
143 K	80	0.7	83333	0.28	1.44	6	334	295
143 K	81	0.7	83333	0.28	1.54	6	325	295
195 K	1	0.65	50000	0.23	1.34	4	127	151
195 K	2	0.65	50000	0.23	1.44	4	122	151
195 K	3	0.65	50000	0.23	1.54	4	120	151
195 K	4	0.65	50000	0.255	1.34	4	131	151
195 K	5	0.65	50000	0.255	1.44	4	129	151
195 K	6	0.65	50000	0.255	1.54	4	127	151
195 K	7	0.65	50000	0.28	1.34	4	136	151

Temp	Case	ΔG (eV)	$\dot{\gamma}_0$ (s^{-1})	p	q	O#	Simulated Yield, MPa	Experimental Yield, MPa
195 K	8	0.65	50000	0.28	1.44	4	133	151
195 K	9	0.65	50000	0.28	1.54	4	131	151
195 K	10	0.65	66667	0.23	1.34	4	127	151
195 K	11	0.65	66667	0.23	1.44	4	122	151
195 K	12	0.65	66667	0.23	1.54	4	120	151
195 K	13	0.65	66667	0.255	1.34	4	130	151
195 K	14	0.65	66667	0.255	1.44	4	128	151
195 K	15	0.65	66667	0.255	1.54	4	127	151
195 K	16	0.65	66667	0.28	1.34	4	135	151
195 K	17	0.65	66667	0.28	1.44	4	132	151
195 K	18	0.65	66667	0.28	1.54	4	130	151
195 K	19	0.65	83333	0.23	1.34	4	123	151
195 K	20	0.65	83333	0.23	1.44	4	121	151
195 K	21	0.65	83333	0.23	1.54	4	120	151
195 K	22	0.65	83333	0.255	1.34	4	130	151
195 K	23	0.65	83333	0.255	1.44	4	128	151
195 K	24	0.65	83333	0.255	1.54	4	123	151
195 K	25	0.65	83333	0.28	1.34	4	134	151
195 K	26	0.65	83333	0.28	1.44	4	131	151
195 K	27	0.65	83333	0.28	1.54	4	129	151
195 K	28	0.675	50000	0.23	1.34	4	129	151
195 K	29	0.675	50000	0.23	1.44	4	127	151
195 K	30	0.675	50000	0.23	1.54	4	122	151
195 K	31	0.675	50000	0.255	1.34	4	133	151
195 K	32	0.675	50000	0.255	1.44	4	131	151
195 K	33	0.675	50000	0.255	1.54	4	129	151
195 K	34	0.675	50000	0.28	1.34	4	142	151
195 K	35	0.675	50000	0.28	1.44	4	135	151
195 K	36	0.675	50000	0.28	1.54	4	132	151
195 K	37	0.675	66667	0.23	1.34	4	128	151
195 K	38	0.675	66667	0.23	1.44	4	123	151
195 K	39	0.675	66667	0.23	1.54	4	121	151
195 K	40	0.675	66667	0.255	1.34	4	132	151
195 K	41	0.675	66667	0.255	1.44	4	130	151
195 K	42	0.675	66667	0.255	1.54	4	127	151
195 K	43	0.675	66667	0.28	1.34	4	141	151
195 K	44	0.675	66667	0.28	1.44	4	134	151
195 K	45	0.675	66667	0.28	1.54	4	132	151
195 K	46	0.675	83333	0.23	1.34	4	128	151
195 K	47	0.675	83333	0.23	1.44	4	123	151
195 K	48	0.675	83333	0.23	1.54	4	121	151
195 K	49	0.675	83333	0.255	1.34	4	132	151
195 K	50	0.675	83333	0.255	1.44	4	129	151

Temp	Case	ΔG (eV)	$\dot{\gamma}_0$ (s^{-1})	p	q	O#	Simulated Yield, MPa	Experimental Yield, MPa
195 K	51	0.675	83333	0.255	1.54	4	128	151
195 K	52	0.675	83333	0.28	1.34	4	136	151
195 K	53	0.675	83333	0.28	1.44	4	134	151
195 K	54	0.675	83333	0.28	1.54	4	131	151
195 K	55	0.7	50000	0.23	1.34	4	131	151
195 K	56	0.7	50000	0.23	1.44	4	128	151
195 K	57	0.7	50000	0.23	1.54	4	123	151
195 K	58	0.7	50000	0.255	1.34	4	135	151
195 K	59	0.7	50000	0.255	1.44	4	133	151
195 K	60	0.7	50000	0.255	1.54	4	130	151
195 K	61	0.7	50000	0.28	1.34	4	145	151
195 K	62	0.7	50000	0.28	1.44	4	141	151
195 K	63	0.7	50000	0.28	1.54	4	134	151
195 K	64	0.7	66667	0.23	1.34	4	130	151
195 K	65	0.7	66667	0.23	1.44	4	128	151
195 K	66	0.7	66667	0.23	1.54	4	123	151
195 K	67	0.7	66667	0.255	1.34	4	135	151
195 K	68	0.7	66667	0.255	1.44	4	132	151
195 K	69	0.7	66667	0.255	1.54	4	130	151
195 K	70	0.7	66667	0.28	1.34	4	143	151
195 K	71	0.7	66667	0.28	1.44	4	136	151
195 K	72	0.7	66667	0.28	1.54	4	134	151
195 K	73	0.7	83333	0.23	1.34	4	129	151
195 K	74	0.7	83333	0.23	1.44	4	127	151
195 K	75	0.7	83333	0.23	1.54	4	122	151
195 K	76	0.7	83333	0.255	1.34	4	134	151
195 K	77	0.7	83333	0.255	1.44	4	131	151
195 K	78	0.7	83333	0.255	1.54	4	129	151
195 K	79	0.7	83333	0.28	1.34	4	143	151
195 K	80	0.7	83333	0.28	1.44	4	136	151
195 K	81	0.7	83333	0.28	1.54	4	133	151
195 K	1	0.65	50000	0.23	1.34	5	123	148
195 K	2	0.65	50000	0.23	1.44	5	121	148
195 K	3	0.65	50000	0.23	1.54	5	119	148
195 K	4	0.65	50000	0.255	1.34	5	129	148
195 K	5	0.65	50000	0.255	1.44	5	125	148
195 K	6	0.65	50000	0.255	1.54	5	123	148
195 K	7	0.65	50000	0.28	1.34	5	136	148
195 K	8	0.65	50000	0.28	1.44	5	131	148
195 K	9	0.65	50000	0.28	1.54	5	127	148
195 K	10	0.65	66667	0.23	1.34	5	122	148
195 K	11	0.65	66667	0.23	1.44	5	120	148
195 K	12	0.65	66667	0.23	1.54	5	118	148

Temp	Case	ΔG (eV)	$\dot{\gamma}_0$ (s^{-1})	p	q	O#	Simulated Yield, MPa	Experimental Yield, MPa
195 K	13	0.65	66667	0.255	1.34	5	127	148
195 K	14	0.65	66667	0.255	1.44	5	124	148
195 K	15	0.65	66667	0.255	1.54	5	122	148
195 K	16	0.65	66667	0.28	1.34	5	133	148
195 K	17	0.65	66667	0.28	1.44	5	130	148
195 K	18	0.65	66667	0.28	1.54	5	127	148
195 K	19	0.65	83333	0.23	1.34	5	122	148
195 K	20	0.65	83333	0.23	1.44	5	119	148
195 K	21	0.65	83333	0.23	1.54	5	118	148
195 K	22	0.65	83333	0.255	1.34	5	127	148
195 K	23	0.65	83333	0.255	1.44	5	124	148
195 K	24	0.65	83333	0.255	1.54	5	121	148
195 K	25	0.65	83333	0.28	1.34	5	132	148
195 K	26	0.65	83333	0.28	1.44	5	129	148
195 K	27	0.65	83333	0.28	1.54	5	126	148
195 K	28	0.675	50000	0.23	1.34	5	125	148
195 K	29	0.675	50000	0.23	1.44	5	122	148
195 K	30	0.675	50000	0.23	1.54	5	120	148
195 K	31	0.675	50000	0.255	1.34	5	131	148
195 K	32	0.675	50000	0.255	1.44	5	128	148
195 K	33	0.675	50000	0.255	1.54	5	125	148
195 K	34	0.675	50000	0.28	1.34	5	140	148
195 K	35	0.675	50000	0.28	1.44	5	133	148
195 K	36	0.675	50000	0.28	1.54	5	130	148
195 K	37	0.675	66667	0.23	1.34	5	124	148
195 K	38	0.675	66667	0.23	1.44	5	122	148
195 K	39	0.675	66667	0.23	1.54	5	120	148
195 K	40	0.675	66667	0.255	1.34	5	130	148
195 K	41	0.675	66667	0.255	1.44	5	127	148
195 K	42	0.675	66667	0.255	1.54	5	124	148
195 K	43	0.675	66667	0.28	1.34	5	138	148
195 K	44	0.675	66667	0.28	1.44	5	132	148
195 K	45	0.675	66667	0.28	1.54	5	129	148
195 K	46	0.675	83333	0.23	1.34	5	124	148
195 K	47	0.675	83333	0.23	1.44	5	121	148
195 K	48	0.675	83333	0.23	1.54	5	119	148
195 K	49	0.675	83333	0.255	1.34	5	129	148
195 K	50	0.675	83333	0.255	1.44	5	126	148
195 K	51	0.675	83333	0.255	1.54	5	123	148
195 K	52	0.675	83333	0.28	1.34	5	137	148
195 K	53	0.675	83333	0.28	1.44	5	132	148
195 K	54	0.675	83333	0.28	1.54	5	128	148
195 K	55	0.7	50000	0.23	1.34	5	128	148

Temp	Case	ΔG (eV)	$\dot{\gamma}_0$ (s^{-1})	p	q	O#	Simulated Yield, MPa	Experimental Yield, MPa
195 K	56	0.7	50000	0.23	1.44	5	124	148
195 K	57	0.7	50000	0.23	1.54	5	122	148
195 K	58	0.7	50000	0.255	1.34	5	134	148
195 K	59	0.7	50000	0.255	1.44	5	130	148
195 K	60	0.7	50000	0.255	1.54	5	127	148
195 K	61	0.7	50000	0.28	1.34	5	143	148
195 K	62	0.7	50000	0.28	1.44	5	138	148
195 K	63	0.7	50000	0.28	1.54	5	132	148
195 K	64	0.7	66667	0.23	1.34	5	127	148
195 K	65	0.7	66667	0.23	1.44	5	124	148
195 K	66	0.7	66667	0.23	1.54	5	121	148
195 K	67	0.7	66667	0.255	1.34	5	133	148
195 K	68	0.7	66667	0.255	1.44	5	129	148
195 K	69	0.7	66667	0.255	1.54	5	126	148
195 K	70	0.7	66667	0.28	1.34	5	142	148
195 K	71	0.7	66667	0.28	1.44	5	137	148
195 K	72	0.7	66667	0.28	1.54	5	131	148
195 K	73	0.7	83333	0.23	1.34	5	126	148
195 K	74	0.7	83333	0.23	1.44	5	123	148
195 K	75	0.7	83333	0.23	1.54	5	121	148
195 K	76	0.7	83333	0.255	1.34	5	132	148
195 K	77	0.7	83333	0.255	1.44	5	128	148
195 K	78	0.7	83333	0.255	1.54	5	125	148
195 K	79	0.7	83333	0.28	1.34	5	141	148
195 K	80	0.7	83333	0.28	1.44	5	136	148
195 K	81	0.7	83333	0.28	1.54	5	131	148
195 K	1	0.65	50000	0.23	1.34	6	169	153
195 K	2	0.65	50000	0.23	1.44	6	167	153
195 K	3	0.65	50000	0.23	1.54	6	164	153
195 K	4	0.65	50000	0.255	1.34	6	176	153
195 K	5	0.65	50000	0.255	1.44	6	172	153
195 K	6	0.65	50000	0.255	1.54	6	169	153
195 K	7	0.65	50000	0.28	1.34	6	187	153
195 K	8	0.65	50000	0.28	1.44	6	182	153
195 K	9	0.65	50000	0.28	1.54	6	175	153
195 K	10	0.65	66667	0.23	1.34	6	169	153
195 K	11	0.65	66667	0.23	1.44	6	166	153
195 K	12	0.65	66667	0.23	1.54	6	164	153
195 K	13	0.65	66667	0.255	1.34	6	175	153
195 K	14	0.65	66667	0.255	1.44	6	171	153
195 K	15	0.65	66667	0.255	1.54	6	168	153
195 K	16	0.65	66667	0.28	1.34	6	185	153
195 K	17	0.65	66667	0.28	1.44	6	177	153

Temp	Case	ΔG (eV)	$\dot{\gamma}_0$ (s^{-1})	p	q	O#	Simulated Yield, MPa	Experimental Yield, MPa
195 K	18	0.65	66667	0.28	1.54	6	174	153
195 K	19	0.65	83333	0.23	1.34	6	168	153
195 K	20	0.65	83333	0.23	1.44	6	165	153
195 K	21	0.65	83333	0.23	1.54	6	163	153
195 K	22	0.65	83333	0.255	1.34	6	174	153
195 K	23	0.65	83333	0.255	1.44	6	170	153
195 K	24	0.65	83333	0.255	1.54	6	168	153
195 K	25	0.65	83333	0.28	1.34	6	184	153
195 K	26	0.65	83333	0.28	1.44	6	176	153
195 K	27	0.65	83333	0.28	1.54	6	173	153
195 K	28	0.675	50000	0.23	1.34	6	172	153
195 K	29	0.675	50000	0.23	1.44	6	169	153
195 K	30	0.675	50000	0.23	1.54	6	166	153
195 K	31	0.675	50000	0.255	1.34	6	183	153
195 K	32	0.675	50000	0.255	1.44	6	175	153
195 K	33	0.675	50000	0.255	1.54	6	171	153
195 K	34	0.675	50000	0.28	1.34	6	191	153
195 K	35	0.675	50000	0.28	1.44	6	186	153
195 K	36	0.675	50000	0.28	1.54	6	181	153
195 K	37	0.675	66667	0.23	1.34	6	171	153
195 K	38	0.675	66667	0.23	1.44	6	168	153
195 K	39	0.675	66667	0.23	1.54	6	165	153
195 K	40	0.675	66667	0.255	1.34	6	181	153
195 K	41	0.675	66667	0.255	1.44	6	174	153
195 K	42	0.675	66667	0.255	1.54	6	170	153
195 K	43	0.675	66667	0.28	1.34	6	190	153
195 K	44	0.675	66667	0.28	1.44	6	184	153
195 K	45	0.675	66667	0.28	1.54	6	176	153
195 K	46	0.675	83333	0.23	1.34	6	170	153
195 K	47	0.675	83333	0.23	1.44	6	167	153
195 K	48	0.675	83333	0.23	1.54	6	165	153
195 K	49	0.675	83333	0.255	1.34	6	177	153
195 K	50	0.675	83333	0.255	1.44	6	173	153
195 K	51	0.675	83333	0.255	1.54	6	170	153
195 K	52	0.675	83333	0.28	1.34	6	188	153
195 K	53	0.675	83333	0.28	1.44	6	183	153
195 K	54	0.675	83333	0.28	1.54	6	176	153
195 K	55	0.7	50000	0.23	1.34	6	175	153
195 K	56	0.7	50000	0.23	1.44	6	171	153
195 K	57	0.7	50000	0.23	1.54	6	168	153
195 K	58	0.7	50000	0.255	1.34	6	187	153
195 K	59	0.7	50000	0.255	1.44	6	181	153
195 K	60	0.7	50000	0.255	1.54	6	174	153

Temp	Case	ΔG (eV)	$\dot{\gamma}_0$ (s^{-1})	p	q	O#	Simulated Yield, MPa	Experimental Yield, MPa
195 K	61	0.7	50000	0.28	1.34	6	196	153
195 K	62	0.7	50000	0.28	1.44	6	190	153
195 K	63	0.7	50000	0.28	1.54	6	185	153
195 K	64	0.7	66667	0.23	1.34	6	174	153
195 K	65	0.7	66667	0.23	1.44	6	170	153
195 K	66	0.7	66667	0.23	1.54	6	167	153
195 K	67	0.7	66667	0.255	1.34	6	185	153
195 K	68	0.7	66667	0.255	1.44	6	177	153
195 K	69	0.7	66667	0.255	1.54	6	173	153
195 K	70	0.7	66667	0.28	1.34	6	194	153
195 K	71	0.7	66667	0.28	1.44	6	188	153
195 K	72	0.7	66667	0.28	1.54	6	183	153
195 K	73	0.7	83333	0.23	1.34	6	173	153
195 K	74	0.7	83333	0.23	1.44	6	169	153
195 K	75	0.7	83333	0.23	1.54	6	167	153
195 K	76	0.7	83333	0.255	1.34	6	184	153
195 K	77	0.7	83333	0.255	1.44	6	176	153
195 K	78	0.7	83333	0.255	1.54	6	172	153
195 K	79	0.7	83333	0.28	1.34	6	193	153
195 K	80	0.7	83333	0.28	1.44	6	187	153
195 K	81	0.7	83333	0.28	1.54	6	182	153
250 K	1	0.65	50000	0.23	1.34	4	58	72
250 K	2	0.65	50000	0.23	1.44	4	57	72
250 K	3	0.65	50000	0.23	1.54	4	58	72
250 K	4	0.65	50000	0.255	1.34	4	60	72
250 K	5	0.65	50000	0.255	1.44	4	59	72
250 K	6	0.65	50000	0.255	1.54	4	58	72
250 K	7	0.65	50000	0.28	1.34	4	62	72
250 K	8	0.65	50000	0.28	1.44	4	62	72
250 K	9	0.65	50000	0.28	1.54	4	61	72
250 K	10	0.65	66667	0.23	1.34	4	57	72
250 K	11	0.65	66667	0.23	1.44	4	57	72
250 K	12	0.65	66667	0.23	1.54	4	57	72
250 K	13	0.65	66667	0.255	1.34	4	60	72
250 K	14	0.65	66667	0.255	1.44	4	61	72
250 K	15	0.65	66667	0.255	1.54	4	58	72
250 K	16	0.65	66667	0.28	1.34	4	63	72
250 K	17	0.65	66667	0.28	1.44	4	62	72
250 K	18	0.65	66667	0.28	1.54	4	61	72
250 K	19	0.65	83333	0.23	1.34	4	59	72
250 K	20	0.65	83333	0.23	1.44	4	59	72
250 K	21	0.65	83333	0.23	1.54	4	58	72
250 K	22	0.65	83333	0.255	1.34	4	59	72

Temp	Case	ΔG (eV)	$\dot{\gamma}_0$ (s^{-1})	p	q	O#	Simulated Yield, MPa	Experimental Yield, MPa
250 K	23	0.65	83333	0.255	1.44	4	61	72
250 K	24	0.65	83333	0.255	1.54	4	0	72
250 K	25	0.65	83333	0.28	1.34	4	62	72
250 K	26	0.65	83333	0.28	1.44	4	61	72
250 K	27	0.65	83333	0.28	1.54	4	60	72
250 K	28	0.675	50000	0.23	1.34	4	59	72
250 K	29	0.675	50000	0.23	1.44	4	59	72
250 K	30	0.675	50000	0.23	1.54	4	57	72
250 K	31	0.675	50000	0.255	1.34	4	62	72
250 K	32	0.675	50000	0.255	1.44	4	61	72
250 K	33	0.675	50000	0.255	1.54	4	59	72
250 K	34	0.675	50000	0.28	1.34	4	64	72
250 K	35	0.675	50000	0.28	1.44	4	63	72
250 K	36	0.675	50000	0.28	1.54	4	62	72
250 K	37	0.675	66667	0.23	1.34	4	59	72
250 K	38	0.675	66667	0.23	1.44	4	59	72
250 K	39	0.675	66667	0.23	1.54	4	58	72
250 K	40	0.675	66667	0.255	1.34	4	61	72
250 K	41	0.675	66667	0.255	1.44	4	60	72
250 K	42	0.675	66667	0.255	1.54	4	59	72
250 K	43	0.675	66667	0.28	1.34	4	64	72
250 K	44	0.675	66667	0.28	1.44	4	63	72
250 K	45	0.675	66667	0.28	1.54	4	62	72
250 K	46	0.675	83333	0.23	1.34	4	61	72
250 K	47	0.675	83333	0.23	1.44	4	59	72
250 K	48	0.675	83333	0.23	1.54	4	59	72
250 K	49	0.675	83333	0.255	1.34	4	61	72
250 K	50	0.675	83333	0.255	1.44	4	62	72
250 K	51	0.675	83333	0.255	1.54	4	59	72
250 K	52	0.675	83333	0.28	1.34	4	64	72
250 K	53	0.675	83333	0.28	1.44	4	61	72
250 K	54	0.675	83333	0.28	1.54	4	61	72
250 K	55	0.7	50000	0.23	1.34	4	60	72
250 K	56	0.7	50000	0.23	1.44	4	59	72
250 K	57	0.7	50000	0.23	1.54	4	58	72
250 K	58	0.7	50000	0.255	1.34	4	64	72
250 K	59	0.7	50000	0.255	1.44	4	63	72
250 K	60	0.7	50000	0.255	1.54	4	60	72
250 K	61	0.7	50000	0.28	1.34	4	68	72
250 K	62	0.7	50000	0.28	1.44	4	65	72
250 K	63	0.7	50000	0.28	1.54	4	64	72
250 K	64	0.7	66667	0.23	1.34	4	60	72
250 K	65	0.7	66667	0.23	1.44	4	59	72

Temp	Case	ΔG (eV)	$\dot{\gamma}_0$ (s^{-1})	p	q	O#	Simulated Yield, MPa	Experimental Yield, MPa
250 K	66	0.7	66667	0.23	1.54	4	58	72
250 K	67	0.7	66667	0.255	1.34	4	62	72
250 K	68	0.7	66667	0.255	1.44	4	61	72
250 K	69	0.7	66667	0.255	1.54	4	60	72
250 K	70	0.7	66667	0.28	1.34	4	65	72
250 K	71	0.7	66667	0.28	1.44	4	64	72
250 K	72	0.7	66667	0.28	1.54	4	63	72
250 K	73	0.7	83333	0.23	1.34	4	59	72
250 K	74	0.7	83333	0.23	1.44	4	61	72
250 K	75	0.7	83333	0.23	1.54	4	60	72
250 K	76	0.7	83333	0.255	1.34	4	63	72
250 K	77	0.7	83333	0.255	1.44	4	60	72
250 K	78	0.7	83333	0.255	1.54	4	60	72
250 K	79	0.7	83333	0.28	1.34	4	65	72
250 K	80	0.7	83333	0.28	1.44	4	64	72
250 K	81	0.7	83333	0.28	1.54	4	63	72
250 K	1	0.65	50000	0.23	1.34	5	55	58
250 K	2	0.65	50000	0.23	1.44	5	54	58
250 K	3	0.65	50000	0.23	1.54	5	53	58
250 K	4	0.65	50000	0.255	1.34	5	57	58
250 K	5	0.65	50000	0.255	1.44	5	56	58
250 K	6	0.65	50000	0.255	1.54	5	55	58
250 K	7	0.65	50000	0.28	1.34	5	59	58
250 K	8	0.65	50000	0.28	1.44	5	58	58
250 K	9	0.65	50000	0.28	1.54	5	57	58
250 K	10	0.65	66667	0.23	1.34	5	54	58
250 K	11	0.65	66667	0.23	1.44	5	54	58
250 K	12	0.65	66667	0.23	1.54	5	53	58
250 K	13	0.65	66667	0.255	1.34	5	57	58
250 K	14	0.65	66667	0.255	1.44	5	56	58
250 K	15	0.65	66667	0.255	1.54	5	55	58
250 K	16	0.65	66667	0.28	1.34	5	59	58
250 K	17	0.65	66667	0.28	1.44	5	58	58
250 K	18	0.65	66667	0.28	1.54	5	57	58
250 K	19	0.65	83333	0.23	1.34	5	54	58
250 K	20	0.65	83333	0.23	1.44	5	53	58
250 K	21	0.65	83333	0.23	1.54	5	53	58
250 K	22	0.65	83333	0.255	1.34	5	56	58
250 K	23	0.65	83333	0.255	1.44	5	55	58
250 K	24	0.65	83333	0.255	1.54	5	54	58
250 K	25	0.65	83333	0.28	1.34	5	58	58
250 K	26	0.65	83333	0.28	1.44	5	57	58
250 K	27	0.65	83333	0.28	1.54	5	56	58

Temp	Case	ΔG (eV)	$\dot{\gamma}_0$ (s^{-1})	p	q	O#	Simulated Yield, MPa	Experimental Yield, MPa
250 K	28	0.675	50000	0.23	1.34	5	56	58
250 K	29	0.675	50000	0.23	1.44	5	55	58
250 K	30	0.675	50000	0.23	1.54	5	54	58
250 K	31	0.675	50000	0.255	1.34	5	58	58
250 K	32	0.675	50000	0.255	1.44	5	57	58
250 K	33	0.675	50000	0.255	1.54	5	56	58
250 K	34	0.675	50000	0.28	1.34	5	61	58
250 K	35	0.675	50000	0.28	1.44	5	60	58
250 K	36	0.675	50000	0.28	1.54	5	58	58
250 K	37	0.675	66667	0.23	1.34	5	56	58
250 K	38	0.675	66667	0.23	1.44	5	55	58
250 K	39	0.675	66667	0.23	1.54	5	54	58
250 K	40	0.675	66667	0.255	1.34	5	58	58
250 K	41	0.675	66667	0.255	1.44	5	57	58
250 K	42	0.675	66667	0.255	1.54	5	56	58
250 K	43	0.675	66667	0.28	1.34	5	61	58
250 K	44	0.675	66667	0.28	1.44	5	59	58
250 K	45	0.675	66667	0.28	1.54	5	58	58
250 K	46	0.675	83333	0.23	1.34	5	55	58
250 K	47	0.675	83333	0.23	1.44	5	54	58
250 K	48	0.675	83333	0.23	1.54	5	53	58
250 K	49	0.675	83333	0.255	1.34	5	57	58
250 K	50	0.675	83333	0.255	1.44	5	56	58
250 K	51	0.675	83333	0.255	1.54	5	56	58
250 K	52	0.675	83333	0.28	1.34	5	60	58
250 K	53	0.675	83333	0.28	1.44	5	59	58
250 K	54	0.675	83333	0.28	1.54	5	58	58
250 K	55	0.7	50000	0.23	1.34	5	57	58
250 K	56	0.7	50000	0.23	1.44	5	56	58
250 K	57	0.7	50000	0.23	1.54	5	55	58
250 K	58	0.7	50000	0.255	1.34	5	60	58
250 K	59	0.7	50000	0.255	1.44	5	58	58
250 K	60	0.7	50000	0.255	1.54	5	57	58
250 K	61	0.7	50000	0.28	1.34	5	63	58
250 K	62	0.7	50000	0.28	1.44	5	61	58
250 K	63	0.7	50000	0.28	1.54	5	60	58
250 K	64	0.7	66667	0.23	1.34	5	57	58
250 K	65	0.7	66667	0.23	1.44	5	56	58
250 K	66	0.7	66667	0.23	1.54	5	55	58
250 K	67	0.7	66667	0.255	1.34	5	59	58
250 K	68	0.7	66667	0.255	1.44	5	58	58
250 K	69	0.7	66667	0.255	1.54	5	57	58
250 K	70	0.7	66667	0.28	1.34	5	63	58

Temp	Case	ΔG (eV)	$\dot{\gamma}_0$ (s^{-1})	p	q	O#	Simulated Yield, MPa	Experimental Yield, MPa
250 K	71	0.7	66667	0.28	1.44	5	61	58
250 K	72	0.7	66667	0.28	1.54	5	59	58
250 K	73	0.7	83333	0.23	1.34	5	56	58
250 K	74	0.7	83333	0.23	1.44	5	56	58
250 K	75	0.7	83333	0.23	1.54	5	54	58
250 K	76	0.7	83333	0.255	1.34	5	59	58
250 K	77	0.7	83333	0.255	1.44	5	58	58
250 K	78	0.7	83333	0.255	1.54	5	57	58
250 K	79	0.7	83333	0.28	1.34	5	62	58
250 K	80	0.7	83333	0.28	1.44	5	60	58
250 K	81	0.7	83333	0.28	1.54	5	59	58
250 K	1	0.65	50000	0.23	1.34	6	76	66
250 K	2	0.65	50000	0.23	1.44	6	75	66
250 K	3	0.65	50000	0.23	1.54	6	74	66
250 K	4	0.65	50000	0.255	1.34	6	78	66
250 K	5	0.65	50000	0.255	1.44	6	77	66
250 K	6	0.65	50000	0.255	1.54	6	76	66
250 K	7	0.65	50000	0.28	1.34	6	80	66
250 K	8	0.65	50000	0.28	1.44	6	79	66
250 K	9	0.65	50000	0.28	1.54	6	78	66
250 K	10	0.65	66667	0.23	1.34	6	75	66
250 K	11	0.65	66667	0.23	1.44	6	74	66
250 K	12	0.65	66667	0.23	1.54	6	72	66
250 K	13	0.65	66667	0.255	1.34	6	77	66
250 K	14	0.65	66667	0.255	1.44	6	76	66
250 K	15	0.65	66667	0.255	1.54	6	76	66
250 K	16	0.65	66667	0.28	1.34	6	80	66
250 K	17	0.65	66667	0.28	1.44	6	78	66
250 K	18	0.65	66667	0.28	1.54	6	77	66
250 K	19	0.65	83333	0.23	1.34	6	74	66
250 K	20	0.65	83333	0.23	1.44	6	73	66
250 K	21	0.65	83333	0.23	1.54	6	73	66
250 K	22	0.65	83333	0.255	1.34	6	77	66
250 K	23	0.65	83333	0.255	1.44	6	75	66
250 K	24	0.65	83333	0.255	1.54	6	75	66
250 K	25	0.65	83333	0.28	1.34	6	79	66
250 K	26	0.65	83333	0.28	1.44	6	78	66
250 K	27	0.65	83333	0.28	1.54	6	77	66
250 K	28	0.675	50000	0.23	1.34	6	77	66
250 K	29	0.675	50000	0.23	1.44	6	76	66
250 K	30	0.675	50000	0.23	1.54	6	74	66
250 K	31	0.675	50000	0.255	1.34	6	79	66
250 K	32	0.675	50000	0.255	1.44	6	78	66

Temp	Case	ΔG (eV)	$\dot{\gamma}_0$ (s^{-1})	p	q	O#	Simulated Yield, MPa	Experimental Yield, MPa
250 K	33	0.675	50000	0.255	1.54	6	76	66
250 K	34	0.675	50000	0.28	1.34	6	83	66
250 K	35	0.675	50000	0.28	1.44	6	81	66
250 K	36	0.675	50000	0.28	1.54	6	79	66
250 K	37	0.675	66667	0.23	1.34	6	76	66
250 K	38	0.675	66667	0.23	1.44	6	76	66
250 K	39	0.675	66667	0.23	1.54	6	75	66
250 K	40	0.675	66667	0.255	1.34	6	79	66
250 K	41	0.675	66667	0.255	1.44	6	77	66
250 K	42	0.675	66667	0.255	1.54	6	77	66
250 K	43	0.675	66667	0.28	1.34	6	82	66
250 K	44	0.675	66667	0.28	1.44	6	80	66
250 K	45	0.675	66667	0.28	1.54	6	79	66
250 K	46	0.675	83333	0.23	1.34	6	75	66
250 K	47	0.675	83333	0.23	1.44	6	75	66
250 K	48	0.675	83333	0.23	1.54	6	75	66
250 K	49	0.675	83333	0.255	1.34	6	78	66
250 K	50	0.675	83333	0.255	1.44	6	77	66
250 K	51	0.675	83333	0.255	1.54	6	76	66
250 K	52	0.675	83333	0.28	1.34	6	81	66
250 K	53	0.675	83333	0.28	1.44	6	79	66
250 K	54	0.675	83333	0.28	1.54	6	78	66
250 K	55	0.7	50000	0.23	1.34	6	78	66
250 K	56	0.7	50000	0.23	1.44	6	77	66
250 K	57	0.7	50000	0.23	1.54	6	76	66
250 K	58	0.7	50000	0.255	1.34	6	81	66
250 K	59	0.7	50000	0.255	1.44	6	79	66
250 K	60	0.7	50000	0.255	1.54	6	78	66
250 K	61	0.7	50000	0.28	1.34	6	84	66
250 K	62	0.7	50000	0.28	1.44	6	83	66
250 K	63	0.7	50000	0.28	1.54	6	81	66
250 K	64	0.7	66667	0.23	1.34	6	77	66
250 K	65	0.7	66667	0.23	1.44	6	76	66
250 K	66	0.7	66667	0.23	1.54	6	75	66
250 K	67	0.7	66667	0.255	1.34	6	80	66
250 K	68	0.7	66667	0.255	1.44	6	78	66
250 K	69	0.7	66667	0.255	1.54	6	78	66
250 K	70	0.7	66667	0.28	1.34	6	84	66
250 K	71	0.7	66667	0.28	1.44	6	82	66
250 K	72	0.7	66667	0.28	1.54	6	80	66
250 K	73	0.7	83333	0.23	1.34	6	77	66
250 K	74	0.7	83333	0.23	1.44	6	76	66
250 K	75	0.7	83333	0.23	1.54	6	75	66

Temp	Case	ΔG (eV)	$\dot{\gamma}_0$ (s^{-1})	p	q	O#	Simulated Yield, MPa	Experimental Yield, MPa
250 K	76	0.7	83333	0.255	1.34	6	80	66
250 K	77	0.7	83333	0.255	1.44	6	78	66
250 K	78	0.7	83333	0.255	1.54	6	77	66
250 K	79	0.7	83333	0.28	1.34	6	83	66
250 K	80	0.7	83333	0.28	1.44	6	81	66
250 K	81	0.7	83333	0.28	1.54	6	80	66

APPENDIX C: MODEL 3 DATA

143 K, Orientation #4		
Simulation Time, s	Strain	Stress, MPa
0.00E+00	0.00E+00	0.0
1.93E-01	1.93E-05	2.8
1.19E+00	1.19E-04	17.0
2.19E+00	2.19E-04	31.3
3.19E+00	3.19E-04	45.6
4.19E+00	4.19E-04	59.9
5.19E+00	5.19E-04	74.2
6.19E+00	6.19E-04	88.5
7.19E+00	7.19E-04	102.8
8.19E+00	8.19E-04	117.1
9.19E+00	9.19E-04	131.5
1.02E+01	1.02E-03	145.8
1.12E+01	1.12E-03	160.2
1.22E+01	1.22E-03	174.5
1.32E+01	1.32E-03	188.8
1.42E+01	1.42E-03	203.2
1.52E+01	1.52E-03	217.5
1.62E+01	1.62E-03	231.8
1.72E+01	1.72E-03	246.0
1.82E+01	1.82E-03	260.0
1.92E+01	1.92E-03	273.9
2.02E+01	2.02E-03	287.3

195 K, Orientation #4		
Simulation Time, s	Strain	Stress, MPa
0.00E+00	0.00E+00	0.0
1.93E-01	1.93E-05	2.7
1.19E+00	1.19E-04	16.7
2.19E+00	2.19E-04	30.7
3.19E+00	3.19E-04	44.6
4.19E+00	4.19E-04	58.2
5.19E+00	5.19E-04	71.5
6.19E+00	6.19E-04	84.2
7.19E+00	7.19E-04	95.9
8.19E+00	8.19E-04	106.4
9.19E+00	9.19E-04	115.4
1.02E+01	1.02E-03	122.6
1.12E+01	1.12E-03	128.2
1.22E+01	1.22E-03	132.3
1.32E+01	1.32E-03	135.3
1.42E+01	1.42E-03	137.4
1.52E+01	1.52E-03	138.9
1.62E+01	1.62E-03	140.1
1.72E+01	1.72E-03	141.0
1.82E+01	1.82E-03	141.7
1.92E+01	1.92E-03	142.3
2.00E+01	2.00E-03	142.7

143 K, Orientation #5		
Simulation Time, s	Strain	Stress, MPa
0.00E+00	0.00E+00	0.0
1.93E-01	1.93E-05	3.9
1.19E+00	1.19E-04	23.9
2.19E+00	2.19E-04	44.1
3.19E+00	3.19E-04	64.2
4.19E+00	4.19E-04	84.3
5.19E+00	5.19E-04	104.5
6.19E+00	6.19E-04	124.7
7.19E+00	7.19E-04	144.8
8.19E+00	8.19E-04	165.0
9.19E+00	9.19E-04	185.2
1.02E+01	1.02E-03	205.4
1.12E+01	1.12E-03	225.5
1.22E+01	1.22E-03	245.7
1.32E+01	1.32E-03	265.7
1.42E+01	1.42E-03	285.5
1.52E+01	1.52E-03	304.9
1.62E+01	1.62E-03	323.4
1.72E+01	1.72E-03	340.2
1.82E+01	1.82E-03	354.5
1.92E+01	1.92E-03	365.7
2.02E+01	2.02E-03	373.8

195 K, Orientation #5		
Simulation Time, s	Strain	Stress, MPa
0.00E+00	0.00E+00	0.0
2.56E-01	2.56E-05	5.1
1.26E+00	1.26E-04	24.9
2.26E+00	2.26E-04	44.6
3.26E+00	3.26E-04	64.0
4.26E+00	4.26E-04	83.1
5.26E+00	5.25E-04	101.2
6.26E+00	6.25E-04	117.8
7.26E+00	7.25E-04	131.9
8.26E+00	8.25E-04	143.0
9.26E+00	9.25E-04	150.9
1.03E+01	1.03E-03	156.2
1.13E+01	1.12E-03	159.6
1.23E+01	1.22E-03	161.8
1.33E+01	1.32E-03	163.3
1.43E+01	1.42E-03	164.4
1.53E+01	1.52E-03	165.3
1.63E+01	1.62E-03	166.0
1.73E+01	1.72E-03	166.6
1.83E+01	1.82E-03	167.2
1.93E+01	1.92E-03	167.8
2.00E+01	2.00E-03	168.2

143 K, Orientation #6		
Simulation Time, s	Strain	Stress, MPa
0.00E+00	0.00E+00	0.0
2.56E-01	2.56E-05	6.8
1.26E+00	1.26E-04	33.3
2.26E+00	2.26E-04	59.7
3.26E+00	3.26E-04	86.2
4.26E+00	4.26E-04	112.7
5.26E+00	5.25E-04	139.2
6.26E+00	6.25E-04	165.8
7.26E+00	7.25E-04	192.3
8.26E+00	8.25E-04	218.8
9.26E+00	9.25E-04	245.4
1.03E+01	1.03E-03	271.9
1.13E+01	1.12E-03	298.5
1.23E+01	1.22E-03	325.0
1.33E+01	1.32E-03	351.5
1.43E+01	1.42E-03	377.8
1.53E+01	1.52E-03	403.8
1.63E+01	1.62E-03	429.2
1.73E+01	1.72E-03	453.5
1.83E+01	1.82E-03	475.8
1.93E+01	1.92E-03	495.2
2.03E+01	2.02E-03	510.8

195 K, Orientation #6		
Simulation Time, s	Strain	Stress, MPa
0.00E+00	0.00E+00	0.0
2.56E-01	2.56E-05	6.7
1.26E+00	1.26E-04	32.9
2.26E+00	2.26E-04	58.9
3.26E+00	3.26E-04	84.7
4.26E+00	4.26E-04	110.0
5.26E+00	5.25E-04	134.1
6.26E+00	6.25E-04	156.1
7.26E+00	7.25E-04	175.1
8.26E+00	8.25E-04	190.2
9.26E+00	9.25E-04	201.4
1.03E+01	1.03E-03	209.1
1.13E+01	1.12E-03	214.4
1.23E+01	1.22E-03	218.0
1.33E+01	1.32E-03	220.8
1.43E+01	1.42E-03	222.9
1.53E+01	1.52E-03	224.7
1.63E+01	1.62E-03	226.2
1.73E+01	1.72E-03	227.6
1.83E+01	1.82E-03	228.8
1.93E+01	1.92E-03	229.9
2.00E+01	2.00E-03	230.7

APPENDIX D: EXAMPLE EXCEL FORMULAS

The Monte Carlo simulations in this thesis were complete using Microsoft Excel. Representative examples of the formulas used are given in this appendix. The following examples use equation (8), repeated here:

$$\boldsymbol{P}(\gamma|\alpha) = \frac{[\alpha_{\beta 1} \quad \alpha_{\beta 2} \quad \alpha_{\beta 3} \quad \alpha_{\beta 4}] \begin{bmatrix} \beta 1_\gamma \\ \beta 2_\gamma \\ \beta 3_\gamma \\ \beta 4_\gamma \end{bmatrix} \cdot \gamma}{dual\left([\alpha_{\beta 1} \quad \alpha_{\beta 2} \quad \alpha_{\beta 3} \quad \alpha_{\beta 4}] \begin{bmatrix} \beta 1_\gamma & \beta 1_{\gamma^C} \\ \beta 2_\gamma & \beta 2_{\gamma^C} \\ \beta 3_\gamma & \beta 3_{\gamma^C} \\ \beta 4_\gamma & \beta 4_{\gamma^C} \end{bmatrix} \begin{bmatrix} \gamma \\ \gamma^C \end{bmatrix} \right)} \quad (8)$$

Uniform inputs

When the intervals populating equation (8) needed to be simulated with uniform inputs, the following formulas were used:

	A	B	C	D	E	F	G	H	I
1		α|β1	α|β2	α|β3	α|β4	β1|γ	β2|γ	β3|γ	βC|γ
2	$\underline{X}$	0.3880	0.7415	0.3667	0.1655	0.1197	0.1662	0.3587	0.3554
3	$\overline{X}$	0.9973	0.9024	0.8688	0.4140	0.1826	0.3080	0.4603	0.0491
4									
5	Rand 1	=RAND()*(B$3-B$2)+B$2	=RAND()*(C$3-C$2)+C$2	=RAND()*(D$3-D$2)+D$2	=RAND()*(E$3-E$2)+E$2	=RAND()*(F$3-F$2)+F$2	=RAND()*(G$3-G$2)+G$2	=RAND()*(H$3-H$2)+H$2	=1-SUM(F5:H5)

	J	K	L	M	N	O	P	Q	R
1	β1|γC	β2|γC	β3|γC	βC|γC	γ	γC	Num	Denom	Posterior
2	0.0410	0.1527	0.3683	0.4380	0.3000	0.7000	0.1080	0.3437	0.3143
3	0.1930	0.1772	0.4682	0.1616	0.4500	0.5500	0.3961	0.8505	0.4658
4									
5	=RAND()*(J$3-J$2)+J$2	=RAND()*(K$3-K$2)+K$2	=RAND()*(L$3-L$2)+L$2	=1-SUM(J5:L5)	=RAND()*(N$3-N$2)+N$2	=1-N5	=B5*F5*N5 +C5*G5*N5 +D5*H5*N5 +E5*I5*N5	=B5*F5*N5 +B5*J5*O5 +C5*G5*N5 +C5*K5*O5 +D5*H5*N5 +D5*L5*O5 +E5*I5*N5 +E5*M5*O5	=P5/Q5

The "Rand()" function generates random numbers uniformly distributed between zero and one, and the values following "Rand" in each of the formulas simply scale the result according to the interval bounds. Variables whose value was determined by the LCC were calculated by subtraction from the randomly generated values. With these formulas in place, row 5 was repeated 100,000 times, and then the values from column R were re-generated and copied 10 times in order to generate a one million run simulation.

Normal Inputs

When the intervals populating equation (8) needed to be simulated with normal inputs, the following formulas were used:

	A	B	C	D	E	F	G	H	I
1		α|β1	α|β2	α|β3	α|β4	β1|γ	β2|γ	β3|γ	βC|γ
2	$\underline{X}$	0.3880	0.7415	0.3667	0.1655	0.1197	0.1662	0.3587	0.3554
3	$\overline{X}$	0.9973	0.9024	0.8688	0.4140	0.1826	0.3080	0.4603	0.0491
4									
5	Rand 1	=IFERROR(NORM.INV(RAND(),AVERAGE(B$2:B$3),ABS(B$3-B$2)/6), AVERAGE(B$2:B$3))	=IFERROR(NORM.INV(RAND(),AVERAGE(C$2:C$3),ABS(C$3-C$2)/6), AVERAGE(C$2:C$3))	NORM.INV(RAND(),AVERAGE(D$2:D$3),ABS(D$3-D$2)/6), AVERAGE(D$2:D$3))	=IFERROR(NORM.INV(RAND(),AVERAGE(E$2:E$3),ABS(E$3-E$2)/6), AVERAGE(E$2:E$3))	=IFERROR(NORM.INV(RAND(),AVERAGE(F$2:F$3),ABS(F$3-F$2)/6), AVERAGE(F$2:F$3))	NORM.INV(RAND(),AVERAGE(G$2:G$3),ABS(G$3-G$2)/6), AVERAGE(G$2:G$3))	NORM.INV(RAND(),AVERAGE(H$2:H$3),ABS(H$3-H$2)/6), AVERAGE(H$2:H$3))	*=1-SUM(F5:H5)*

	J	K	L	M	N	O	P	Q	R
1	β1|γC	β2|γC	β3|γC	βC|γC	γ	γC	Num	Denom	Posterior
2	0.0410	0.1527	0.3683	0.4380	0.3000	0.7000	0.1080	0.3437	0.3143
3	0.1930	0.1772	0.4682	0.1616	0.4500	0.5500	0.3961	0.8505	0.4658
4									
5	=IFERROR(NORM.INV(RAND(),AVERAGE(J$2:J$3),ABS(J$3-J$2)/6), AVERAGE(J$2:J$3))	=IFERROR(NORM.INV(RAND(),AVERAGE(K$2:K$3),ABS(K$3-K$2)/6), AVERAGE(K$2:K$3))	=IFERROR(NORM.INV(RAND(),AVERAGE(L$2:L$3),ABS(L$3-L$2)/6), AVERAGE(L$2:L$3))	*=1-SUM(J5:L5)*	NORM.INV(RAND(),AVERAGE(N$2:N$3),ABS(N$3-N$2)/6), AVERAGE(N$2:N$3))	*=1-N5*	=B5*F5*N5 +C5*G5*N5 +D5*H5*N5 +E5*I5*N5	=B5*F5*N5 +B5*J5*O5 +C5*G5*N5 +C5*K5*O5 +D5*H5*N5 +D5*L5*O5 +E5*I5*N5 +E5*M5*O5	=P5/Q5

The inverse normal function “Norm.Inv()” calculates the probability of a value within a normal distribution. The distribution was centered on each input interval, where the bounds of the input interval represented ±3σ limits of the distribution. The “IfError()” function replaces calculation errors with the mean of the interval bounds. With these formulas in place, row 5 was repeated 100,000 times, and then the values from column R were re-generated and copied 10 times in order to generate a one million run simulation.

Uniform Inputs without the LCC

When the intervals populating equation (8) needed to be simulated with uniform inputs, and the interval equation was not subject to the LCC, the following formulas were used to ensure that the real-valued calculations would still be properly normalized:

	A	B	C	D	E	F	G	H
1		Uniform	Uniform Remainder1	Uniform Remainder2	Final Remainder	Order	Order	Order
2	$\underline{X}$							
3	$\overline{X}$							
4								
5	Rand 1	=RAND()	=RAND()*(1-B5)	=RAND()*(1-SUM(B5:C5))	=1-SUM(B5:D5)	=RANDBETWEEN(1,4)	=RANDBETWEEN(1,3)	=RANDBETWEEN(1,2)

	I	J	K	L	M	N	O
1	Uniform	Uniform Remainder1	Uniform Remainder2	Final Remainder	Order	Order	Order
2							
3							
4							
5	=RAND()	=RAND()*(1-I5)	=RAND()*(1-SUM(I5:J5))	=1-SUM(I5:K5)	=RANDBETWEEN(1,4)	=RANDBETWEEN(1,3)	=RANDBETWEEN(1,2)

	P	Q	R	S	T	U	V	W
1	α|β1	α|β2	α|β3	α|β4	β1|γ	β2|γ	β3|γ	β4|γ
2	0.3880	0.7415	0.3667	0.1655	0.0000	0.0000	0.0000	0.0000
3	0.9973	0.9024	0.8688	0.4140	1.0000	1.0000	1.0000	1.0000
4								
5	=RAND()*(P$3-P$2)+P$2	=RAND()*(Q$3-Q$2)+Q$2	=RAND()*(R$3-R$2)+R$2	=RAND()*(S$3-S$2)+S$2	=IF(F5=1,B5, IF(G5=1,C5, IF(H5=1,D5, E5)))	=IF(F5=2,B5, IF(G5=2,C5, IF(H5=2,D5, E5)))	=IF(F5=3,B5, IF(G5=3,C5, IF(H5=G5,D5, E5)))	=IF(F5=4,B5, IF(F5=G5,C5, IF(OR(F5=H5,AND(F5=3,G5=H5)),D5, E5)))

	X	Y	Z	AA	AB	AC
1	β1|γC	β2|γC	β3|γC	β4|γC	γ	γC
2	0.0000	0.0000	0.0000	0.0000	0.3000	0.7000
3	1.0000	1.0000	1.0000	1.0000	0.4500	0.5500
4						
5	=IF(M5=1,J5, IF(N5=1,J5, IF(O5=1,K5, L5)))	=IF(M5=2,J5, IF(N5=2,J5, IF(O5=2,K5, L5)))	=IF(M5=3,J5, IF(N5=3,J5, IF(O5=N5,K5, L5)))	=IF(M5=4,J5, IF(M5=N5,J5, IF(OR(M5=O5,AND(M5=3,N5=O5)),K5, L5)))	=RAND()*(AB$3-AB$2)+AB$2	=1-AB5

	AD	AE	AF
1	Num	Denom	Posterior
2	0.0000	0.0000	0.3000
3	1.4321	3.1825	0.4500
4			
5	=P5*T5*AB5 +Q5*U5*AB5 +R5*V5*AB5 +S5*W5*AB5	=P5*T5*AB5 +P5*X5*AC5 +Q5*U5*AB5 +Q5*Y5*AC5 +R5*V5*AB5 +R5*Z5*AC5 +S5*W5*AB5 +S5*AA5*AC5	=AD5/AE5

	AD	AE	AF
1	Num	Denom	Posterior
2	0.0000	0.0000	0.3000
3	1.4321	3.1825	0.4500
4			
5	=P5*T5*AB5 +Q5*U5*AB5 +R5*V5*AB5 +S5*W5*AB5	=P5*T5*AB5 +P5*X5*AC5 +Q5*U5*AB5 +Q5*Y5*AC5 +R5*V5*AB5 +R5*Z5*AC5 +S5*W5*AB5 +S5*AA5*AC5	=AD5/AE5

Columns B through E and I through L generate uniformly distributed random numbers scaled to be complementary. Columns F through H and M through O serve to determine the order in which those random values with be inserted into the real-valued equation. The random values are ordered in columns T through W and X through AA. This double-sampling process avoids favoring any one variable over another when the intervals represent complete ignorance. With these formulas in place, row 5 was repeated 100,000 times, and then the values from column AF were re-generated and copied 10 times in order to generate a one million run simulation.

REFERENCES

Babu, G. J., & Rao, C. R. (1993). Bootstrap Methodology. In *Handbook of Statistics* (Vol. 9, pp. 627-659).

Babuška, I., Nobile, F., & Tempone, R. (2008). A systematic approach to model validation based on Bayesian updates and prediction related rejection criteria. *Computer Methods in Applied Mechanics and Engineering, 197*(29), 2517-2539.

Barton, R. R., & Schruben, L. W. (1993). Uniform and bootstrap resampling of empirical distributions. *Proceedings of the 25th conference on Winter simulation* (pp. 503-508). Piscataway, New Jersey: Institute of Electrical and Electronics Engineers.

Barton, R. R., & Schruben, L. W. (2001). Resampling methods for input modeling. In B. A. Peters, J. S. Smith, D. J. Medeiros, & M. W. Rohrer (Ed.), *Proceedings of the 2001 Winter Simulation Conference* (pp. 372-378). IEEE.

Batarseh, O. Y. (2010). An Interval based Approach to Model Input Uncertainty in Discrete-Event Simulation. *Ph.D. Dissertation.*

Bayes, & Price. (1763). An essay towards solving a problem in the doctrine of chance. by the late rev. mr. bayes, frs communicated by mr. price, in a letter to john canton, amfrs. *Philosophical Transactions*, 370-418.

Berger, J. O. (1994). An Overview of Robust Bayesian Analysis. *Test, 3*(1), 5-124.

Berger, J., & Berliner, L. M. (1986). Robust Bayes and empirical Bayes analysis with ϵ-contaminated priors. *The Annals of Statistics, 14*(2), 461-486.

Börner, F., Bulatov, A., Jeavons, P., & Krokhin, A. (2003). Quantified Constraints: Algorithms and Complexity. In *Computer Science Logic* (pp. 58-70). Berlin Heidelberg: Springer.

Burnham, K. P., & Anderson, D. R. (1998). *Model Selection and Inference.* New York: Springer-Verlag.

Cao, Y., Li, S., Petzold, L., & Serban, R. (2003). Adjoint sensitivity analysis for differential-algebraic equations: the adjoint DAE system and its numerical solution. *SIAM Journal on Scientific Computing, 24*(3), 1076-1089.

Cheung, S. H., & Beck, J. L. (2008). New Bayesian updating methodology for model validation and robust predictions based on data from hierarchical subsystems tests.

Chick, S. E. (1999). Steps to Implement Bayesian Input Distribution Selection. In P. A. Farrington, H. B. Nembhard, D. T. Sturrock, & G. W. Evans (Ed.), *Proceedings of the 31st conference on Winter simulation: Simulation---a bridge to the future, 1*, pp. 317-324.

Cozman, F. G. (2000). Credal Networks. *Artificial Intelligence, 120*, 199-233.

de Cooman, G., Hermans, F., Antonucci, A., & Zaffalon, M. (2010). Epistemic irrelevance in credal nets: The case of imprecise Markov trees. *International Journal of Approximate Reasoning, 51*, 1029-1052.

Dempster, A. P. (1967). Upper and lower probabilities induced by a multivalued mapping. *The annals of mathematical statistics*, 325-339.

Diaconis, P., & Zabell, S. (1986). Some alternatives to Bayes' Rule. *Proceedings of the Second University of California, Irvine, Conference on Political Economy*, (pp. 25-38).

Dimitrova, N. S., Markov, S. M., & Popova, E. D. (1992). Extended Interval Arithmetics: New Results and Applications. In L. Atanassova, & J. Herzberger (Ed.), *Computer Arithmetic and Enclosure Methods* (pp. 225-232). Oldenburg, Germany: Elsevier Science Publishers.

Dunlop, A., & Lesueur, D. (1989). Electrical resistivity and length variations of iron and nickel during low temperature electron irradiations. *Radiation Effects and Defects in Solids, 108*(2-4), 337-350.

Efron, B. (1982). *The Jackknife, the Bootstrap and Other Resampling Plans.* Philadelphia: Society for Industrial and Applied Mathematics.

Errico, R. M. (1997). What is an adjoint model. *Bulletin of the American Meteorological Society, 78*(11), 2577-2591.

Ferson, S., Kreinovich, V., Ginzburg, L., Myers, D. S., & Sentz, K. (2002). *Constructing Probability Boxes and Dempster-Shafer Structures.* Albuquerque: Sandia National Laboratories.

Gardeñes, E., Sainz, M. Á., Jorba, L., Calm, R., Estela, R., Mielgo, H., & Trepat, A. (2001, April). Modal Intervals. *Reliable Computing, 7*(2), 77-111.

Ghanem, R. G., & Spanos, P. D. (2003). *Stochastic Finite Elements: A Spectral Approach.* Courier Corporation.

Helton, J. C., Johnson, J. D., Sallaberry, C. J., & Storlie, C. B. (2006). Survey of Sampling-Based Methods for Uncertainty and Sensitivity Analysis. *Reliability Engineering & System Safety, 91*(10), 1175-1209.

Hoeting, J. A., Madigan, D., Raftery, A. E., & Volinsky, C. T. (1999, November). Bayesian Model Averaging: A Tutorial. *Statistical Science, 14*(4), 382-401.

Hu, J., & Wang, Y. (2013). Sensitivity analysis in quantified interval constraint satisfaction problems. *ASME 2013 International Design Engineering Technical Conferences and Computers and Information in Engineering Conference.* Portland, Oregon: American Society of Mechanical Engineers.

Hu, J., Aminzadeh, M., & Wang, Y. (2014). Searching Feasible Design Space by Solving Quantified Constraint Satisfaction Problems. *ASME Journal of Mechanical Design, 136*(3), 031002(1-11).

Kaucher, E. (1980). Interval Analysis in the Extended Space IR. *Computing, Supplement 2*, 33-49.

Kullback, S. (1997). *Information theory and statistics.* New York: John Wiley & Sons, Inc.

Kullback, S., & Leibler, R. A. (1951, March). On Information and Sufficiency. *The Annals of Mathematical Statistics, 22*(1), 79-86.

Lawson, J., & Erjavec, J. (2001). *Modern Statistics for Engineering and Quality Improvement.* Pacific Grove, CA: Duxbury.

MacDonald, I. L., & Zucchini, W. (1997). *Hidden Markov and other models for discrete-valued time series.* London: CRC Press.

Mahadevan, S., & Rebba, R. (2005). Validation of reliability computational models using Bayes networks. *Reliability Engineering and System Safety, 87*, 223-232.

Maury, F., Biget, M., Vajda, P., Lucasson, A., & Lucasson, P. (1976, December 15). Anisotropy of defect creation in electron-irradiated iron crytals. *Physical Review, 14*(12), 5303-5313.

Molchanov, I. (2005). *Theory of Random Sets.* London: Springer.

Möller, B., & Beer, M. (2004). *Fuzzy Randomness.* Berlin: Springer-Verlag.

Moore, R. E. (1966). *Interval Analysis.* Englewood Cliffs, New Jersey: Prentice Hall.

Moreno, E., & Pericchi, L. R. (1993). Bayesian robustnesss for hierarchical ϵ-contamination models. *Journal of Statistical Planning and Inference, 37*, 159-167.

Narayanan, S., McDowell, D. L., & Zhu, T. (2014). Crystal plasticity model for BCC iron atomistically informed by kinetics of correlated kinkpair nucleation on screw dislocation. *Journal of the Mechanics and Physics of Solids, 65*, 54-68.

Neumaier, A. (2004). Clouds, fuzzy sets, and probability intervals. *Reliable Computing, 10*(4), 249-272.

O'Hagan, A. (2013). Polynomial Chaos: A Tutorial and Critique from a Statistician's Perspective. *Submitted for publication*.

Patra, A. (2013, December). Modeling the Mechanical Behavior and Deformed Microstructure of Irradiated BCC Materials using Continuum Crystal Plasticity. *Doctoral Dissertation*. Georgia Institute of Technology.

Patra, A., Zhu, T., & McDowell, D. L. (2014, August). Constitutive equations for modeling non-Schmid effects in single crystal bcc-Fe at low and ambient temperatures. *International Journal of Plasticity, 59*, 1-14.

Pericchi, L. R., & Walley, P. (1991, April). Robust Bayesian Credible Intervals and Prior Ignorance. *International Statistical Review / Revue Internationale de Statistique, 59*(1), 1-23.

Sainz, M. A., Armengol, J., Calm, R., Herrero, P., Jorba, L., & Vehi, J. (2014). *Modal Interval Analysis.* New York: Springer.

Saltelli, A., Ratto, M., Andres, T., Campolongo, F., Cariboni, J., Gatelli, D., . . . Tarantola, S. (2008). *Global Sensitivity Analysis: The Primer*. West Sussex, England: John Wiley & Sons.

Sandu, A., Daescu, D. N., & Carmichael, G. R. (2003). Direct and adjoint sensitivity analysis of chemical kinetic systems with KPP: Part I—theory and software tools. *Atmospheric Environment, 37*, 5083-5096.

Shafer, G. (1976). *A mathematical theory of evidence.* Princeton: Princeton University Press.

Shanker, A., & Kelton, W. D. (1991). Empirical input distributions : an alternative to standard input distributions in simulation modeling. *Proceedings of the 23rd conference on Winter simulation* (pp. 978-985). Piscataway, New Jersey: Institute of Electrical and Electronics Engineers.

Shary, S. P. (1996). Algebraic approach to the interval linear static identification, tolerance, and control problems, or one more application of kaucher arithmetic. *Reliable Computing, 2*(1), 3-33.

Shary, S. P. (2002, October). A New Technique in Systems Analysis Under Interval Uncertainty and Ambiguity. *Reliable Computing, 8*(5), 321-418.

Swiler, L. P., Paez, T. L., Mayes, R. L., & Eldred, M. S. (2009). Epistemic Uncertainty in the Calculation of Margins. *AIAA Structures, Structural Dynamics, and Materials Conference.* Palm Springs, CA.

Tallman, A. E., Blumer, J. D., Wang, Y., & McDowell, D. L. (2014). Multiscale Model Validation Based On Generalized Interval Bayes' Rule and its Application in Molecular Dynamics Simulation. *Proceedings of ASME 2014 International Design Engineering Techincal Conferences & Computers and Information in Engineering Conference.* Buffalo, New York, USA.

Vajda, P. (1977, July). Anisotropy of electron radiation damage in metal crystals. *Reviews of Modern Physics, 49*(3), 481-521.

Walley, P. (1991). *Statistical Reasoning with Imprecise Probabilities.* London: Chapman and Hall.

Wang, Y. (2008). Imprecise Probabilities with a Generalized Interval Form. In R. Muhanna, & R. Mullen (Ed.), *International Workshop on Reliable Engineering Computing (REC '08).* Savannah, GA.

Wang, Y. (2010). Imprecise Probabilities based on Generalized Intervals for System Reliability Assessment. *International Journal of Reliability & Safety, 4*(4), 319-342.

Wang, Y. (2011). Multiscale Uncertainty Quantification based on A Generalized Hidden Markov Model. *ASME Journal of Mechanical Design, 133*(3), 031004(1-10).

Weichselberger, K. (2000). The Theory of Interval-Probability as a Unifying Concept for Uncertainty. *International Journal of Approximate Reasoning*, 149-170.

Weirs, V. G., Kamm, J. R., Swiler, L. P., Tarantola, S., Ratto, M., Adams, B. M., . . . Eldred, M. S. (2012). Sensitivity analysis techniques applied to a system of hyperbolic conservation laws. *Reliability Engineering and System Safety, 107*, 157-170.

Xiu, D., & Karniadakis, G. E. (2002). The Wiener--Askey polynomia chaos for stochastic differential equations. *SIAM Journal on Scientific Computing, 24*(2), 619-644.